Halo- and organogold(I) complexes as potential metallomesogens

A thesis submitted to the

University of Cape Town

in fulfilment of the requirements of the degree

Master of Science

by

Fiona Millicent Hess

Department of Chemistry

University of Cape Town

Rondebosch, 7700

South Africa

July 1999

Dedication

To see a world in a grain of sand

And a heaven in a wild flower,

Hold Infinity in the palm of your hand

And Eternity in an hour.

William Blake

Auguries if Innocence

Solitude is as needful to the imagination

as society is wholesome for the character.

James Russell Lowell

Dryden in *Literary Essays*

Yet Ah, that Spring should vanish with the rose!

That Youth's sweet-scented Manuscript should close!

The Nightingale that in the branches sang,

Ah whence, and whither flown again, who knows!

Edward FitzGerald

The Rubáiyát of Omar Khayyám

For Timothy, who could have.

Acknowledgements

Prof. J. R. Moss for advice and encouragement in more than just chemistry and Dr. A. T. Hutton in assistance with liquid crystal matters.

Prof. M. Cairo for assistance with X-ray crystallography, Dr S. Churms for advice on writing style and encouragement and Dr. C. Imrie and Prof. D. Bruce for assistance in identifying liquid crystal phases.

To all my friends and family, who have in small and large ways supported me during this thesis. Although unfair to single out a few, thank-you Shawn, Kalle and Ghalib. And to Julius, my good friend and confidant, special thanks for your patience and care.

Members of the organometallic research group at UCT for their advice on experimental techniques and companionship during the many hours spent in Lab A111.

Dr K. Dimitrova for ^{1}H-and ^{13}C-NMR analysis, Mr H. Spies for ^{19}F-NMR analysis, Miss A. Jacobs for DSC and TG analysis, Mr. P. Benincasa for elemental analysis and Dr. P. Boshoff for FAB and EI mass spectrometry analysis. Dr. C. Imrie and Dr. E. J. Starr are also gratefully acknowledged for providing some n-OST ligands and Johnson Matthey for loan of gold and palladium

DAAD and FRD for providing financial assistance.

Abstract

There is currently much interest in how the properties of liquid crystals may be altered by metal atoms. Gold(I) complexes of the type RAuL have recently been shown to exhibit interesting liquid crystal behaviour. As molecular structure and intermolecular forces play a major role in liquid crystal chemistry, changing the nature of the R and L groups result in changes mesomorphic properties.

The aim of the project was to synthesise RAuL complexes with stilbazole ligands and to investigate how different R groups influence the liquid crystal properties. ClAu(n-OST) complexes, n-OST = trans-4,4'-alkoxystilbazole with n = number of carbon atoms in the alkoxy chain, were synthesised from ClAu(tht) and n-OST. They were found to exhibit smectic A mesophases, melting between 135-153 °C and decomposing at the clearing point at 168-180 °C. The transition temperatures decreased as the chain length of the n-OST ligand increased.

RAu(7-OST) complexes, R = C_6F_5, 2-C_6F_4Br, 4-C_6F_4Br or μ-4,4'-$C_6F_4C_6F_4$, were synthesised by reacting the appropriate perhaloaryllithium reagent with ClAu(tht), followed by displacement of tht with 7-OST. These complexes formed predominantly nematic phases and also partially decomposed at the clearing points. Mononuclear complexes had similar melting (148-166 °C) and clearing (179-222 °C) temperatures to the analogous ClAu(7-OST) complex. The μ-4,4'-$C_6F_4C_6F_4$ group resulted in increased melting (206 °C) and clearing (246 °C) temperatures due to increased polarisability of the molecule. Conductivity, FAB mass spectrometry and a crystal structure of C_6F_5Au(7-OST) suggest that the RAuL complexes investigated in this study are neutral and monomeric in structure with no Au...Au bonding interactions or π-stacking affecting liquid crystalline properties. It was not possible to synthesis RAuL complexes were R = phenyl, methyl or iodo and alkylAuPPh_3 complexes did not have mesomorphic properties, due to the bulky PPh_3 group.

Table of contents

Glossary

Complex **1**

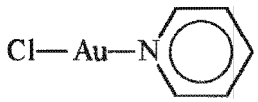

Complex **2**

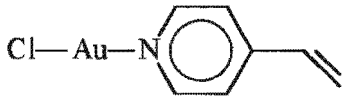

Complexes **3-9** (n = 4-10)

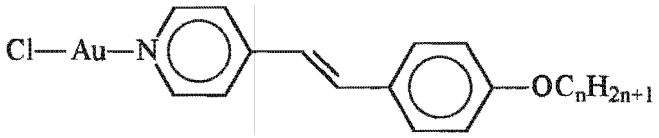

Complexes
3a (n = 4)
5a (n = 6)

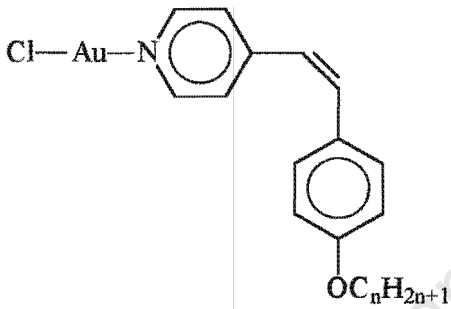

Complex **10**

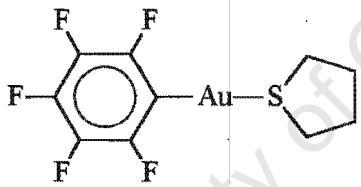

Complex **11**

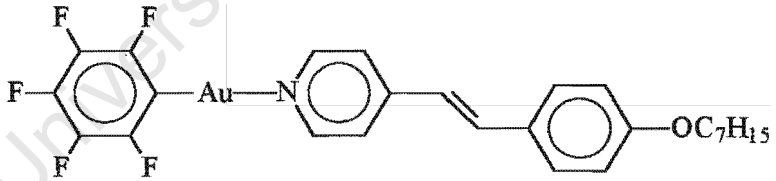

Complex **12**

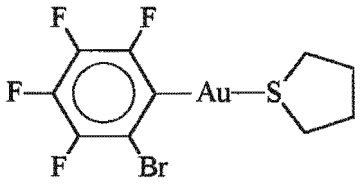

Complex **13**

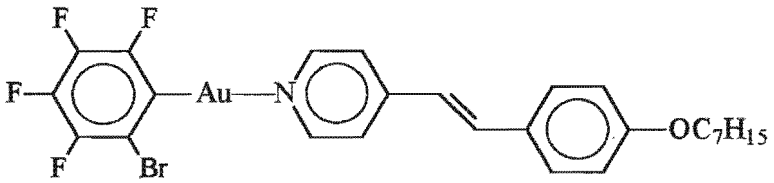

Complex **14**

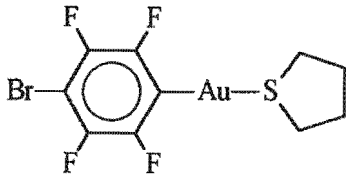

Complex **15**

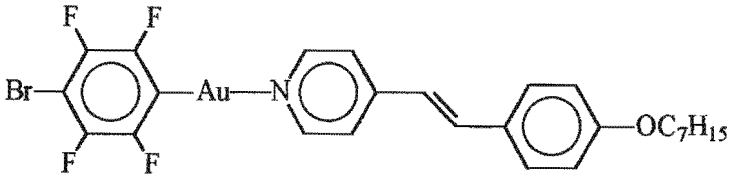

Complex **16**

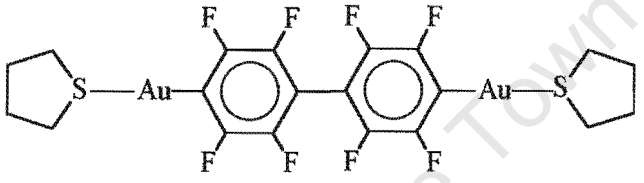

Complex **17**

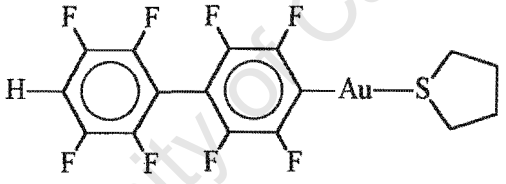

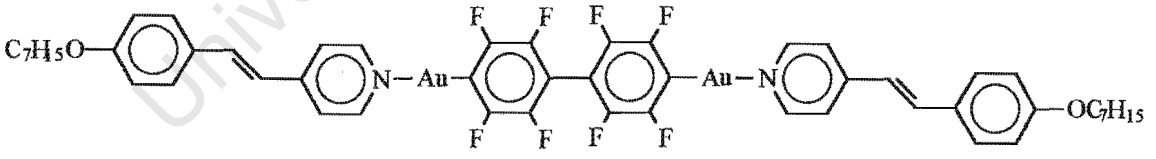

Complex **18**

Complexes
19-23 (n = 1-5)
24 (n = 7)

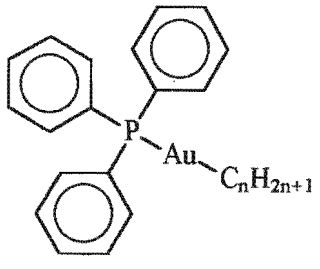

Labelling schemes for ^{1}H- ^{13}C and ^{19}F-NMR spectra

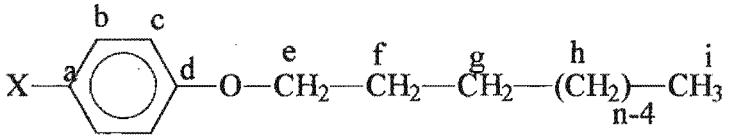

Labelling scheme for ^{1}H- and ^{13}C-NMR spectra of 4-haloalkoxybenzene compounds

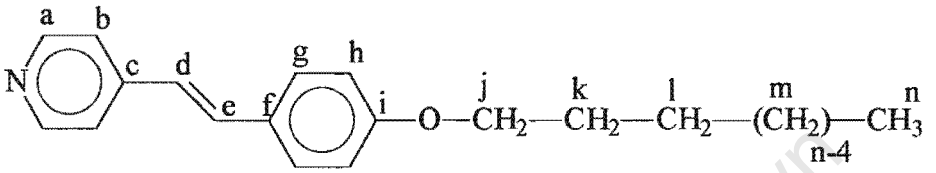

Labelling scheme for ^{1}H- and ^{13}C-NMR spectra of n-OST ligands,n = 4-10 and complexes **1-9, 11, 13, 15** and **18**

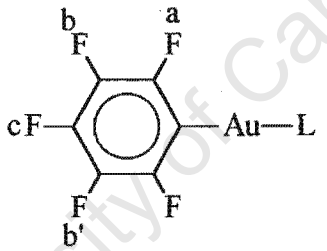

Labelling scheme for ^{19}F-NMR spectra of complexes **10-16**, **18**, L = tht, 7-OST

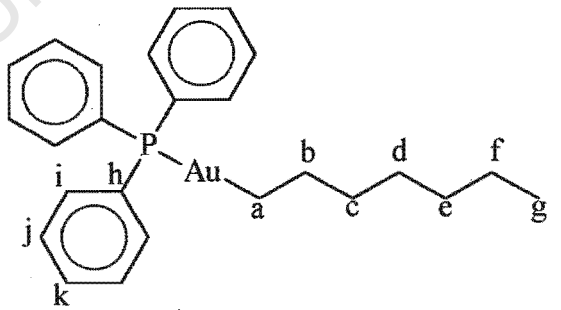

Labelling scheme for ^{1}H- and ^{13}C-NMR spectra of complexes **19-24**

List of Abbreviations

n-OST	trans-4,4'-alkoxystilbazole, n = nunber of carbon atoms in the alkoxy chain
py	pyridine
vnlpy	4-vinylpyridine
PPh_3	triphenylphosphine
tht	tetrahydrothiophene
PPR_3	tertiary substituted phosphines
-C(O)O-	carboxylic group linking two phenyl rings with the carbon atom nearer to gold(I)
-OC(O)-	carboxylic group linking two phenyl rings with the oxygen atom nearer to gold(I)
-C=C-	alkene group linking two phenyl rings
$-CH_2CH_2-$	ethylene group linking two phenyl rings
MeLi	methyl lithium
n-BuLi	*n*-butyl lithium
TLC	thin layer chromatography
DMSO	dimethyl sulfoxide
THF	tetrahydrofuran
e.s.d.	estimated standard deviation

CHAPTER 1. Introduction

The interest in materials which combine the properties of liquids (molecular mobility and fluidity) with properties normally associated with the crystalline phase (*e.g.* optical and electrical anisotropy) is the driving force behind the multidisciplinary field of liquid crystal research, involving overlap between chemistry, physics, biology, electronics and engineering.[1,2] Electro-optical liquid-crystal displays,[2-7] utilising mainly organic compounds, have in the past twenty-five years developed into a common feature of everyday life. Other major applications of organic liquid crystals include temperature-sensing devices (*e.g.* as biofeedback mechanisms in psychological therapy situations)[3] and ultra high strength fibres such as kevlar (*e.g.* bulletproof vests, mooring cables, etc.).[8] Organic liquid crystals also have interesting photoelectrical[9,10] and electrical[11,12] properties, are sensitive to changes in pressure, electrical and magnetic fields and could be used in the detection of ultrasonic waves and certain vapours.[3] Anisotropic solvents are also a good medium in which to conduct column chromatography[3,8] and certain chemical reactions (e.g. charge transfer reactions)[3,13] occur better in anisotropic environments.

1.1 First reports of metallomesogens

The discovery of metallomesogens is closely related to the discovery of organic mesogens,[14,15] but whereas development of organic mesogens as an independent branch of science flourished with the invention of liquid crystal displays in 1968,[16] the same was not case for metallomesogens. Interest in how metal atoms would affect mesomorphic properties only started developing rapidly after 1986[15] and has currently expanded into an active field of research, with many review articles, chapters in books

and at least one book devoted to the topic.[14,17-22] The reason for the such rapid development in interest is due to the possibility of combining the properties of liquid crystals with properties associated with metal atoms such as colour, polarisability, paramagnetism and a mobile electron density.[20,23]

The first observations of compounds exhibiting liquid crystalline behavior occurred at about 1850.[21] These compounds included nerve myelin,[21] natural fatty acids, eg stearin,[16] and various soaps.[15] Several of the soaps were alkali metal salts of naturally occurring fatty acids, *e.g.* magnesium tetradecanoate,[24] and are the first documented reports of metallomesogens.[14,15] It was however Reinitzer's work in 1888 on cholesterol derivatives[25] that was accepted as the first report of liquid crystalline phenomena and Vorländer's description of the thermotropic properties of alkali metal carboxylates[26] in 1910 as the first scientific paper discussing metallomesogens. The first organometallic metallomesogens were covalent diaryl mercury(II) Schiff base derivatives exhibiting smectic mesophases and were also reported by Vorländer in 1923.[27]

1.2 Future applications of metallomesogens

Given that the field of metallomesogens is a relatively young branch of the more established discipline of organic mesogens, the nature in which metals affect the physical properties of mesomorphic materials is still in the process of being rationalised. The exact role which metallomesogens may play as advanced materials based on liquid crystal technologies is as yet unknown. In order to be considered for advanced materials, metallomesogens should be thermally stable and inert. Disadvantages such as high transition temperatures (which affect the thermal stability)

and the fact that the metal centre can act as a reactive site towards moisture and/or air are problems that must be overcome and recent advances indicate that this is possible.[28]

Metallomesogens generally have higher viscosities and lower molecular mobility compared to organic mesogens, limiting their application to fast-switching device technologies such as liquid crystal displays but enhancing possibilities in fields such as non-linear optics or recording techniques in which glassy states are used.[28] As metals have a high density of polarisable electrons, the introduction of metal centres increases the overall molecular polarisability and also influences other important mesomorphic properties such as birefringence or dielectric constants.[20,28] Compounds with interesting magnetic (paramagnetism), electrical (one-dimensional conductors), optical (strong birefringence, dichroism, non-linear optical behaviour) and electro-optical (photo-electric behaviour, ferroelectric electro-optic responses) have already been achieved as well as improvements in the processing of high performance liquid crystal polymers.[15,20,28,29]

1.3 Basic concepts in liquid crystals[15]

Liquid crystals (or *mesogens*) are materials which exhibit liquid-crystalline (or *mesomorphic*) behaviour and under certain conditions, giving rise to *mesophases*. A mesophase is a phase in which the molecular order is intermediate between an ordered solid and a disordered liquid or solution and has been defined as an "orientationally ordered" liquid or a "positionally disordered" crystal. A mesomorphic molecule containing a metal atom is referred to as a metallomesogen.

There are two main classes of mesophases, based on two different ways in which the mesophase can be formed.

(i) *Thermotropic* liquid-crystals

Pure compounds (or mixtures of compounds) can form these under the influence of a variation in temperature. The melting point is then defined as the transition from the solid phase to the mesophase and the clearing point as the transition from the mesophase to the isotropic liquid phase. When the thermotropic mesophase appears in both the heating and cooling events, it is referred to as *enantiotropic* and is thermodynamically stable. When the thermotropic mesophase appears only while cooling, it is referred to as *monotropic*. The monotropic phase is thermodynamically unstable and occurs due to a hysteresis in the crystallisation point.

(ii) *Lyotropic* liquid-crystals

These are formed as a result of certain species (*e.g.* amphiphiles) forming anisotropic aggregates in the presence of a solvent (usually water). The temperature and concentration of the species in the solvent are important factors.

Some liquid crystalline compounds have been reported to exhibit both thermotropic and lyotropic mesophases and are referred to as *amphotropic* liquid crystals. Thermotropic liquid crystals can be further divided into two main groups depending on their structural features. These are either *calamitic* mesogens (with rod-shaped molecules) or *discotic* mesogens (with disc-shaped molecules). The calamitic compounds have a structure in which the axial component is larger than the radial components (Figure 1.1) and the discotic compounds vice-versa (Figure 1.2).

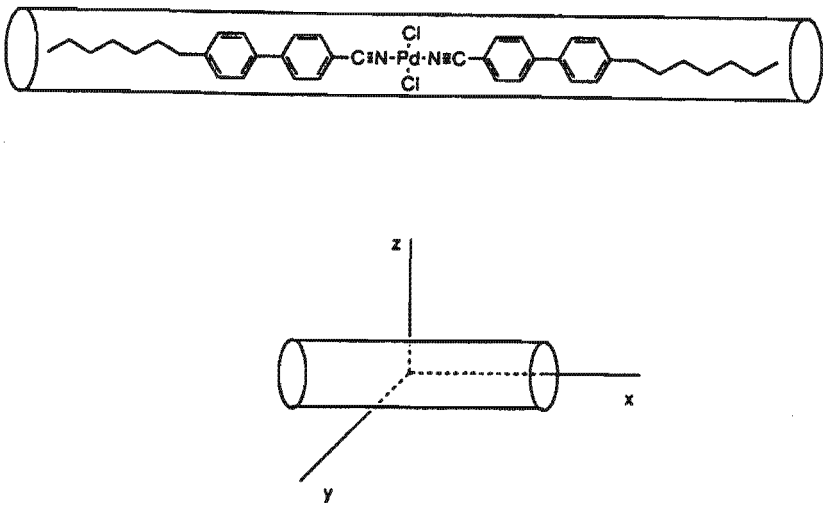

Figure 1.1: Calamitic mesogen with rod-shaped molecules[15]

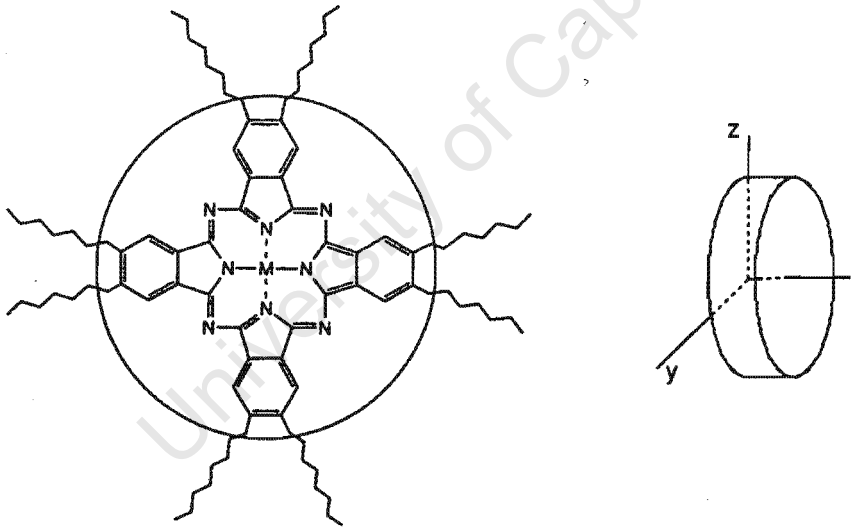

Figure 1.2: Discotic mesogen with disc-shaped molecules[15]

Calamitic compounds form *nematic* and/or *smectic* mesophases. The least ordered mesophase is the nematic (N) phase, where the molecules are not arranged in discrete layers, but are aligned parallel in a preferred direction (Figure 1.3). The smectic mesophase shows a higher degree of order, with the molecules organised into layers and the rod-like molecules within each layer tending to align parallel to each other

(Figure 1.3). Two types of smectic mesophases, namely smectic A (S_A) and smectic C (S_C) phases, commonly occur in calamitic mesogens.

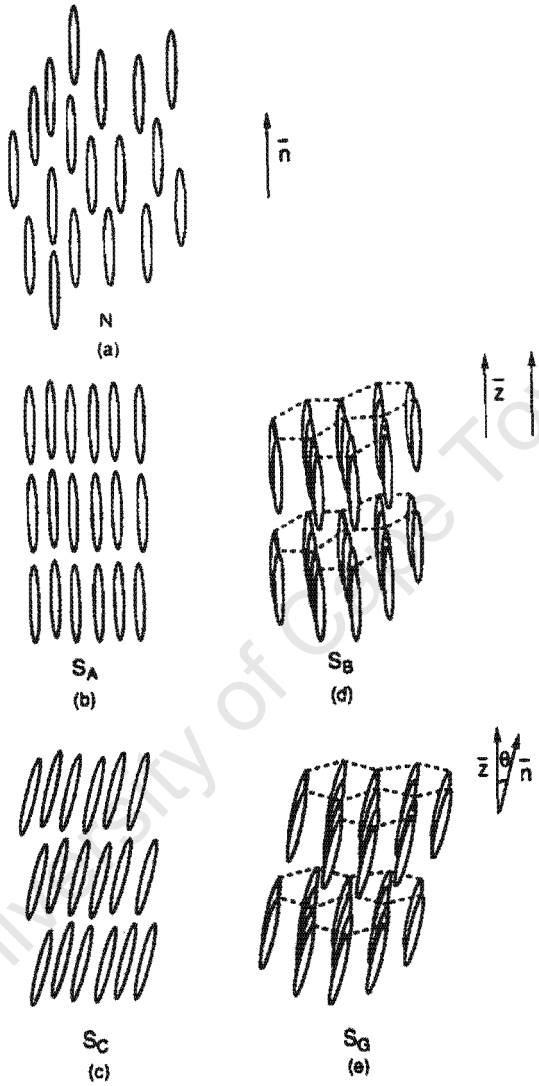

Figure 1.3: Schematic representation of calamitic mesophases[15]

The rod-like molecules are aligned orthogonally to the layers in the case of S_A phases and the average orientation of the rod-like molecules is tilted relative to the layers in the case of S_C phases (Figure 1.3). The molecular mobility inherent in the S_A and S_C mesophases results in their lower viscosities and they are termed fluid smectic phases.

Less commonly observed types of smectic mesophases (S_B, S_E, S_G, S_H, S_I, S_K) show intralayer as well as interlayer positional order, *e.g.* the molecules in the hexatic S_B and S_G phases adopt a hexagonal arrangement (Figure 1.3) The three-dimensional order restricts mobility, resulting in higher viscosities and these types of mesophases are termed the crystal smectic phases.

Discotic mesogens form nematic (N_D), lamellar (D_L) and columnar phases. In the columnar mesophases, the molecules tend to stack in columns to form the nematic columnar phase (N_c) or the columns are arranged parallel to one another to form hexagonal (D_h), rectangular (D_r) or tetragonal (D_{tet}) columnar phases (Figure 1.4).

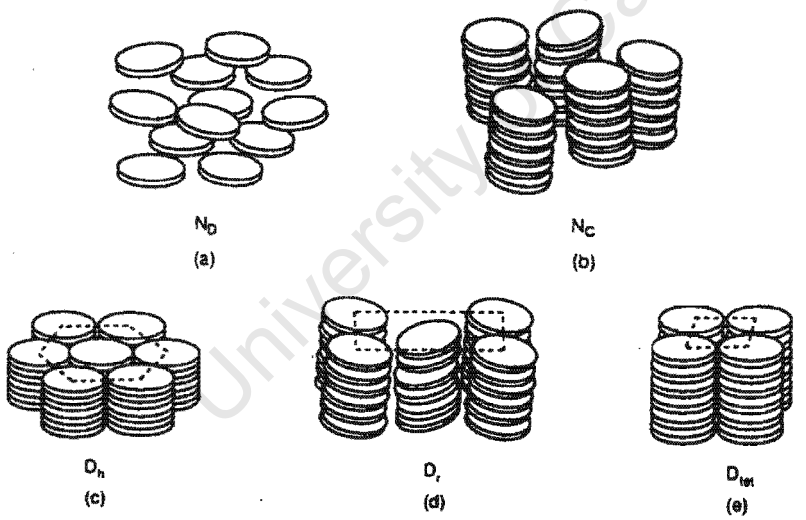

Figure 1.4: Schematic representation of discotic mesophases.[15]

Chirality introduces an additional property to the structure of the nematic and smectic mesophase. In the case of the chiral nematic N* phase, chiral molecules result in the twisted nematic (or *cholesteric*) phase, in which a helical rotation of the orientation of the aligned molecules is observed (Figure 1.5). Chiral mesophases show optical

activity with the N* phase forming the basis of liquid crystal display technologies[2,3,30] and the chiral smectic C* phase giving rise to ferro-, ferri-, or antiferroelectric properties.[15]

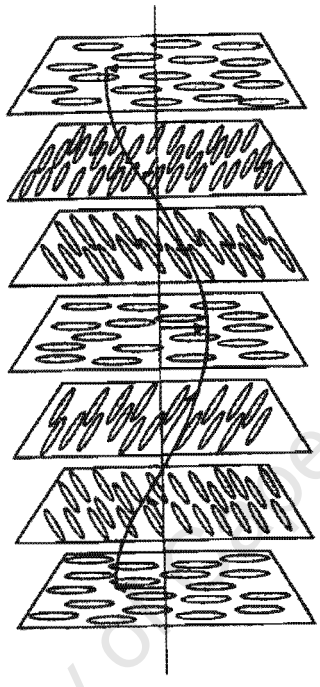

Figure 1.5: The N* phase where the direction of molecular orientation rotates in a helical fashion.

1.4 Molecular structure/property relationships for gold(I) mesogens

Chlorogold(heptyloxystilbazole), was the first mesomorphic gold(I) complex reported to form an unidentified mesophase between 120 and 200 °C before decomposition by Bruce *et al* in 1986.[31,32] Thereafter, in 1991, dihalo- and dimethylgold(4-alkoxydithiobenzoate) derivatives were reported by Bruce *et al*[33] to exhibit S_A mesophases. The methylgold(III) derivative (60 to 130 °C) formed mesophases at lower temperature ranges than the halogold(III) derivatives (145 to 200 °C), but was

also thermally less stable. These complexes were to the best of our knowledge the only reported examples of mesomorphic gold(III) complexes. Between 1994 and 1998, interest in the potential of linear gold(I) complexes to form liquid crystal phases increased dramatically. Within this period, gold(I) complexes with various isocyanide,[34-40] acetylide,[38,39] aryl,[40] carbene[41-43] and pyrazolate[44-46] ligands were reported to be mesomorphic. Some of the isocyanide[37] and pyrazolate[44,45] derivatives even form stable mesophases at room temperature, overcoming the disadvantage of higher transition temperatures (and associated decomposition) usually associated with the presence of metal atoms. The formation of stable hexagonal columnar mesophase for gold(I) compounds at room temperature might lead to a possible application for gold(I) metallomesogens, as there is currently much interest in columnar liquid crystals due to the possibility of generating one-dimensional molecular "pathways" for electron, photon, energy or ion migration.[48]

It is evident from the following discussion of gold(I) mesogens (Table 1.1) that molecular structures of the complexes are closely related to the formation and properties of the mesophases. Factors such as (i) changes in the number of polarisable phenyl rings in the rigid core, (ii) the length of the aliphatic chains, (iii) the nature and position of lateral substituents and (iv) the nature of linking groups between the polarisable rings are common to both metallomesogens and organic mesogens. Other factors such as (v) changes in the nature of the dipole moment of the gold-halogen bond, (vi) changes in the polarisability of the biphenylisocyanide ligand when complexed to gold and (vii) intermolecular Au...Au bonding interactions are due to the presence of the Au^{I} atom only and demonstrate that metal-ligand and metal-metal effects also influence mesomorphic properties.

Table 1.1: Mesomorphic properties of gold(I) complexes of the type RAuL, L = neutral ligand and R = sigma-bonded group.

No. of L groups	L group Type	No. of R groups	R group Type	Au(I) atoms	Character	Enantiotropic Phases	Enantiotropic Temp.[a]	Monotropic Phases	Monotropic Temp.[a]	Reference
			Halogold(isocyanides)							
1	4-alkoxyphenyl isocyanide	1	Cl, Br or I	1	covalent	S_A	94-175	S_A	97-94	36
1	4-alkoxyphenyl isocyanide with 2- or 3-fluoro substituents	1	Cl, Br or I	1	covalent	S_A, N	93-205	S_A	106-103	37
1	3,4,5-trialkoxyphenyl isocyanide	1	Cl, Br or I	1	covalent	D_h	0-80	Col_h	13-?	37
1	4-alkoxybiphenyl isocyanide	1	Cl, Br or I	1	covalent	S_A, N	121-300[d]			35
1	4-alkoxybiphenyl isocyanide with -C(O)O-linkage[b]	1	Cl	1	covalent	S_C, S_A, N	172-270[d]			34
1	4-alkoxybiphenyl isocyanide with -C(O)O-linkage with a lateral alkoxy substituent	1	Cl	1	covalent	S_A, N	87-190	S_A, N	118-? 99-? 87-? 81-?	34
			Acetylidegold(isocyanides)							
1	phenyl isocyanide	1	4-alkylphenyl acetylide	1	covalent	S_A	102-121[d]			38
1	4-alkoxyphenyl isocyanide	1	4-alkylphenyl acetylide	1	covalent	S_A	130-174[d]			38
1	4-alkoxybiphenyl isocyanide with -OC(O)-linkage	1	4-alkoxyphenyl acetylide	1	covalent	S_A	165-?[d]			39
1	4-alkoxybiphenyl isocyanide with -C(O)O-linkage and a lateral alkoxy substituent	1	4-alkoxyphenyl acetylide	1	covalent	S_A, N	87-130[d], 142-?[d]			39
1	"	1	alkyl acetylides	1	covalent	S_A, N	71-103[d]	S_A, N	74-?	39
1	4-alkoxybiphenyl isocyanide with -OC(O)-linkage and a lateral alkyl or alkoxy substituent	1	alkyl acetylides	1	covalent	N	78-108			39
1	alkyl isocyanide	1	4-alkoxybiphenyl acetylide with -OC(O)-linkage	1	covalent	N	87-164[d]	N	69-? 52-?	39
1	alkyl isocyanide	1	4-alkoxybiphenyl acetylide with -OC(O)-linkage and lateral Cl substituent	1	covalent	N	84-141			39
1	alkyl isocyanide	1	4-alkoxybiphenyl acetylide with -C(O)O-linkage	1	covalent	N	101-163[d]	N	48-?	39

No. of L groups	L group Type	No. of R groups	R goup Type	Au(I) atoms	Character	Enantiotropic Phases	Enantiotropic Temp.[a]	Monotropic Phases	Monotropic Temp.[a]	Reference
			Arylgold(isocyanides)							
2	4-alkoxyphenyl isocyanide	1	μ-4,4′-$C_6F_4C_6F_4$	2	covalent	N	150-275[d]			40
2	4- alkoxybiphenyl isocyanide	1	μ-4,4′-$C_6F_4C_6F_4$	2	covalent	N	161-278[d]			40
1	4- alkoxybiphenyl isocyanide	1	C_6F_5, 2-C_6F_3Br or 4-C_6F_3Br	1	covalent	S_A, N	75-220[d]			40
			Halogold(carbenes)							
1	(alkoxy)(4-alkoxybiphenylamino) carbene with -C(O)O-linkage	1	Cl or I	1	covalent	S_A	114-160[d]	S_A, M	118-? 104-? 96-? 91-? 77-? 60-?	41,42
1	(alkoxy)(4-alkoxytriphenylamino) carbene with -C(O)O-linkage	1	Cl	1	covalent	M[c]	186-?[d] 194-?[d]			42
1	(alkylamino)(4-alkoxybiphenylamino) carbene with -C(O)O-linkage	1	Cl	1	covalent	S_A	113-?[d] 133-?[d] 137-?[d]			42
1	(alkoxy)(4-alkoxybiphenylamino) carbene with -OC(O)-linkage	1	Cl	1	covalent			S_A, M	109-? 102-? 67-?	42
1	(alkoxy)(4-alkoxybiphenylamino) carbene with –C=C-linkage	1	Cl	1	covalent			S_A, M	132-? 125-?	42
1	(N,N′-dimethyl-1,6-diamino)(4-alkoxybiphenyl amino) carbene with -C(O)O-linkage	2	Cl	2	covalent	M	211-?[d]			42
2	1,3-dialkylbenzimidalozolium	1	Br	1	ionic	S_B	92-162			43

No. of L groups	L group Type	No. of R groups	R group Type			Enantiotropic		Monotropic		Reference
						Phases	Temp.[a]	Phases	Temp.[a]	
			(Nitrogen-donor)gold(I) complexes							
1	alkoxystilbazole	1	Cl	1	covalent	M	120-200[d]			31,32
		3	(alky)pyrazolate	3	covalent			D_h	112-61	46
		3	(di-,trialkoxyphenyl)pyrazolate	3	covalent	D_h	r.t.-64			44,45

a = The range represents the general temperature range of mesophase exsistence reported for the respective series of complexes with ? indicating unreported values and [d] indicating associated decomposition. b = -C(O)O-, -OC(O)- and –C=C- linking groups between the phenyl groups of the organic ligands and are further described in the list of abbreviations.
c = unidentified mesophases (M).

Many of the gold(I) liquid crystals have quite high transition temperatures (Table 1.1) and undergo decomposition at or close to their clearing points - a common problem for metallomesogens. Well-defined trends in the transition temperatures for the gold(I) liquid crystals (Table 1.1) have been observed and explained on the basis of steric and electronic effects and are summarised below:

(i) Aryl-[40] or acetylidegold(I)[39] complexes (Table 1.1) with 4-alkoxybiphenyl isocyanide ligands resulted in mesophase formation whereas the analogous complexes with 4-alkoxyphenyl ligands did not. Halogold(I) complexes with 4-alkoxybiphenyl isocyanide ligands[35] also had higher transition temperatures than the corresponding complexes with 4-alkoxyphenyl ligands.[36] These changes are due to the increased polarisability afforded by the addition of the second phenyl ring.

(ii) As observed in conventional organic and other metal-containing calamitic systems, an increase in the aliphatic chain length of isocyanide ligands resulted in a decrease in melting point for halo- and acetylidegold(I) complexes.[35,36,40]

(iii) Lateral alkoxy, alkyl or halogen substituents generally tend to lower the transition temperatures and form complexes that are thermally more stable and less prone to decomposition. These lateral substituents lower the transition temperatures by increasing the breadth of the molecules and thereby reducing intermolecular attractions and has especially been observed for lateral alkoxy derivatives of gold(I) mesogens (Table 1.1). It is also observed that longer lateral chains of isocyanide and acetylide ligands[34,39] favour the formation of the nematic phase at the expense of all other phases. This agrees with the general observations for lateral alkylation of calamitic mesomorphic compounds, due to suppression of lateral interactions between

the rigid cores.[23] In fact, the gold(I) complexes with isocyanide and pyrazolate ligands which form stable liquid-crystal phases at room temperature have such a large lateral component that hexagonal columnar[37,44,45] rather than nematic or smectic phases are formed. On the other hand, the electronegative halogen substituents may also result in increased polarisability and hence transition temperatures. Most notably, changes in transition temperatures and mesophases for gold(I) mesogens with fluorine and bromine substituents (Table 1.1) has been attributed to a delicate balance between steric and electronic effects.[37,40]

(iv) Linking groups (*e.g.* -C(O)O-, -OC(O)-, -C=C- and -CH_2CH_2-) between phenyl rings are often used in the molecular design of liquid crystals to alter their mesomorphic properties.[20,21] The groups tend to increase the length, while preserving the overall linearity, of the molecules and in most cases extends the conjugation of the system.[20,21] The biphenyisocyanide complex with a -C(O)O- linking group[34] between the phenyl rings compared to an analogous complex without the linking group[35] exhibits a 40 °C increase in melting point, due to an increase in polarisability, and the appearance of a S_C mesophase. Compared to the -C(O)O- linking group, the -OC(O)- group resulted in lower transition temperatures for the acetylide,[39] isocyanide[39] and carbene[42] derivatives and the formation of monotropic phases for the isocyanide[39] and carbene[42] derivatives (Table 1.1). For the carbene[42] derivatives, the –C=C- linking group resulted in the formation of some monotropic phases and some complexes which were not mesomorphic, but the -CH_2CH_2- linking group resulted in complete loss of mesomorphic properties, due to greatly reduced polarisability between the phenyl rings.

(v) The changes in transition temperatures for the halogold(isocyanide) complexes have been explained by considering that these molecules have several dipole moments along their length.[35-37] According to the electronegativities of the halogens, the dipole moment associated with the Au-X bond decreases in polarity in the order Cl > Br > I. This corresponds with the trend observed in transition temperatures, which decreases in the order Cl > Br > I for the alkoxyphenylisocyanide series.[36,37]

(vi) It has been shown using UV spectroscopy that the polarisability of the biphenyl system of the isocyanide ligand increases in the order NC << NCAuCl < NCAuBr < NCAuI.[35] The dipole moment associated with the polarisability of the isocyanide ligand can thus explain the increasing trend observed in the transition temperatures in the order Cl < Br < I for the alkoxybiphenylisocyanide series.[35]

(vii) It is commonly observed in linear gold(I) compounds that intra- or intermolecular distances between two gold atoms are shorter than would be expected considering the sum of their van der Waals radii.[47] The accepted range of these Au...Au bonding interactions is between 2.75-3.40 Å,[39,42] with repulsive forces expected to dominate below this range and the energy of these interactions are equivalent to the energy of hydrogen bonds. These interactions hardly ever disturb the linear co-ordination, are usually perpendicular to the ligand-gold bond axis and their formation is thought to be hindered by bulky ligands.[47]

Single crystal X-ray diffraction studies were conducted on mesomorphic chloro-gold(isocyanide),[34] acetylidegold(isocyanide)[39] and halogold(carbene/dicarbene)[41-43] complexes and Au...Au bonding interactions were not observed in any of the

complexes except for the chlorogold(isocyanide) complex, where the shortest Au...Au intermolecular distances was quoted to be 3.4 Å.[34] It was suggested that this interaction plays an important role in mesophase formation in halogold(isocyanide) complexes,[34,39] but not in acetylidegold(isocyanide) complexes.[39] It should, however, be noted that this value is at the upper limit of the accepted range for Au...Au bonding interactions.

X-ray diffraction studies were conducted in both the crystal and mesophase for discotic ClAu(trialkoxyphenylisocyanide)[37] and trinuclear gold(I) pyrazolate[44.45,46] complexes. Short intramolecular Au...Au distances occur between the three gold(I) atoms forming the nine-membered metallocycle cores of all the trinuclear gold(I) pyrazolate[44.45,46] complexes. An X-ray diffraction study of ClAu(trialkoxyphenylisocyanide) in the mesophase[37] suggests that two molecules form a disc by arranging in an antiparallel position and this paring of the partial disc shaped molecules to form discs is responsible for the formation of the discotic mesophase, but no Au...Au bonding interactions were reported. Similarly, the arrangement of two trinuclear gold(I) pyrazolate molecules with three alkyl side-chains to form dimeric discs with six alkyl side-chains has been reported to be responsible for the formation of the discotic mesophase.[46] Intermolecular Au...Au bonding interactions (3.255(2) Å) were responsible for dimer formation in the solid state[46] and would most likely be preserved in the mesophase. More bulky di- and trialkoxyphenyl substituents form discotic mesophases without the Au...Au, intermolecular, dimeric association.[44,45] The ability of gold(I) complexes to form Au...Au bonds is thus another factor which may affect the molecular structure and hence the mesomorphic properties of these types of complexes.

1.5 Focus of project

The main aim of this project was to synthesise gold(I) complexes of the type RAuL that may possess liquid crystalline properties. The molecular structure of these complexes affects the nature of the intermolecular interactions that would in turn determine whether these complexes exhibit liquid crystalline behaviour, as well as the type of mesophases formed. It would be particularly interesting to investigate how changing the nature of the R or L groups would affect the mesomorphic properties.

We decided to investigated gold(I) complexes with alkoxystilbazole ligands because although many transition metals with alkoxystilbazole ligands, such as Ag^{I}, Ir^{I}, Rh^{I}, Pt^{II}, Pd^{II} and cobaloxime derivatives, [48,52] have liquid crystalline properties, no systematic study for gold(I) complexes has yet to our knowledge been attempted. Theses types of complexes have interesting optical and electrical properties. The second order non-linear optical properties of some of the Ir^{I} and Rh^{I} complexes of alkoxystilbazoles were investigated,[49,50] and some of the Ir^{I} derivatives have also been shown to form Y-type Langmuir-Bladgett films of high quality.[51]

As a starting point, ClAuL complexes, L = py, vnlpy and n-OST, are investigated in chapter 2. The ClAu(py) and ClAu(vnlpy) complexes are model complexes and are not expected to have mesomorphic characteristics. The ClAu(n-OST) complexes with an additional polarisable phenyl ring, an aliphatic alkoxy chain and a –C=C- linking group which preserves the linearity of the molecule as well as the polarisability between the aromatic rings, are expected to form calamitic mesophase. The length of the alkoxy chain of the n-OST ligands will be varied, as transition temperatures are

usually lowered when the alkoxy chain lengths are increased. The free n-OST ligands are already mesomorphic[53] and have in fact been reported to form an unidentified mesophase when complexed to gold(I).[31,32] As with other metal systems, the complex reported had high transition temperatures and was thermally unstable. Similar to the ClAu(isocyanide) complexes,[34-37] ClAu(n-OST) molecules may have a multipolar structure along the rigid core, including a strong dipole associated with the Au-Cl bond as well as a dipole associated with the organic ligand. As transition temperatures have either increased or decreased in the order of Cl > Br > I as the Au-X dipolar interaction were varied for the isocyanide gold(I) complexes, BrAu(n-OST) or IAu(n-OST) complexes will synthesised in order to investigate how n-OST ligands are affected by the Au-X dipole.

Subsequent, in chapter 3, we will attempt to replace the halogen group with a more bulky organic phenyl group. This may result in increased transition temperatures as another polarisable aromatic ring is being added to the molecule. Conversely, the strong intermolecular attractions may be reduced as the strong dipole associated with the Au-X bond will no longer be present and phenyl ring is more bulky than the halogen atoms. This factor may also promote the formation of the less ordered nematic phase. Although more polarisable, fluorine substituents on the phenyl ring generally lower the transition temperatures and would increase the stability of the Au-C bond. Bromine substituents on the perfluorophenyl ring may increase transition temperatures, as the bromine atom is more polarisable than the fluorine atom. The bromine atoms are also more bulky and depending on their position, may result in reduced intermolecular interactions and lower transition temperatures.

As alkyl gold(I) liquid crystals have not yet been reported, we will be attempt to make RAuL complexes, R = alkyl, L = n-OST, PPh_3, in chapter 4. As with the Au^{III} alkoxydithiobenzoate[33] complexes, the RAu(n-OST) complexes will be expected to have lower transition temperatures compared to the ClAu(n-OST) complexes, but unfortunately the thermal stability is also expected to decrease. RAu(PPh_3) complexes would be more stable than RAu(n-OST) complexes and the linear alkyl groups may allow the molecules to align themselves to form liquid crystal phases, despite the bulky PPh_3 ligand.

RAuL complexes, R = X or organic fragment, may have neutral monomeric or ionic dimeric structures if no intermolecular Au...Au bonds occur. If intermolecular Au...Au bonds do form, then neutral polymeric or ionic tetrameric or polymeric structures may form. XAu(py) complexes have been reported to from such ionic structures and it would be interesting to establish if similar structures are formed by RAu(n-OST) complexes. As molecular structure and intermolecular attractions influence liquid crystal properties, it would be important to determine the molecular structure of the RAuL complexes to investigate their structure-property relationships.

1.6 References

1. J. W. Goodby, Liquid Crystals - An Introduction by Professor J. W. Goodby, *J. Mater. Chem.*, 1995, **5**, ix.
2. M. Freemantle, Polishing LCDs - Multidisciplinary research aims to improve viewing angle, response time, and brightness of liquid-crystal displays, *C&EN*, 1996, December 16, 33.
3. P. J. Collings, LCD Technology and Other Applications, in *Liquid Crystals, Nature's Delicate Phase of Matter*, ed. P. J. Collings, Adam Hilger, Bristol, 1990, ch. 7, pp. 121-146.
4. K. Siemensmeyer, G. Gesekus, V. Volkmar, *Ger. Offen.*, DE 19 640 618, 1998.
5. N. Demoli, U. Dahms, H. Gruber and G. Wernicke, *Applied Optics*, 1997, **36**, 8417.
6. K. Yamamoto, K. Kuriyama. M. Kimura and Y. Matsuki, *Jap. Pat.*, 10 218 992, 1997.
7. D. Coates, S. Greenfield, M. Goulding, J. Hanmer, S. Marden and O. L. Parri, *Merck Pat., PCT Int. Appl.*, WO 97 35 219, 1996.
8. P. J. Collings, Polymer Liquid Crystals, in *Liquid Crystals, Nature's Delicate Phase of Matter*, ed. P. J. Collings, Adam Hilger, Bristol, 1990, ch. 9, pp. 162-180.
9. H. Eichhorn, D. W. Bruce and D. Wöhtle, *Adv. Mater.*, 1998, **10**, 419.
10. T. Christ, B. Glüsen, A. Greiner, A. Kettner, R. Sander, V. Stümpflen, V. Tsukruk and J. Wendorff, *Adv. Mater.*, 1997, **9**, 48.
11. M. Grell, D. D. C. Bradley, M. Inbasekaran and E. P. Woo, *Adv. Mater.*, 1997, **9**, 798.
12. H. Tokuhisa, M. Era and T. Tsutsui, *Adv. Mater.*, 1998, **10**, 404.

13. G. P. Wiederrecht, W. A. Svec and M. R. Wasielewski, *J. Am. Chem. Soc.*, 1997, **119**, 6199.

14. B. Donnio and D. W. Bruce, *Struct. Bonding (Berlin)*, 1999, **95**, 193.

15. J. L. Serrano, Introduction, in *Metallomesogens: Synthesis, Properties, and Applications*, ed. J. L. Serrano, VCH, Weinheim, 1st edn.,1996, ch. 1, pp. 1-21.

16. P. J. Collings, The Story of Liquid Crystals, in *Liquid Crystals, Nature's Delicate Phase of Matter*, ed. P. J. Collings, Adam Hilger, Bristol, 1990, ch. 2, pp. 24-34.

17. A. Giroud-Godquin and P. M. Maitlis, *Angew. Chem., Int. Ed. Engl.*, 1991, **30**, 375.

18. P. Espinet, M. A. Esteruelas, L. A. Oro, J. L. Serrano and E. Sola, *Coord. Chem. Rev.*, 1992, **117**, 215.

19. S. Hudson and P. M. Maitlis, *Chem. Rev.*, 1993, **93**, 861.

20. D. W. Bruce, *J. Chem. Soc., Dalton Trans.*, 1993, 2983.

21. D. W. Bruce, Metal-containing Liquid Crystals, in *Inorganic Materials*, eds. D. W. Bruce and D. O'Hare, John Wiley & Sons Ltd, Chichester, 2nd edn., 1996, ch. 8, pp. 433-522.

22. *Metallomesogens: Synthesis, Properties, and Applications*, ed. J. L. Serrano, VCH, Weinheim, 1st edn.,1996, p. 483.

23. S. R. Collinson and D. W. Bruce, Metallomesogens-Supramolecular Organization of Metal Complexes in Fluid Phases, in *Transition Metals in Supramolecular Chemistry*, ed. J. P. Sauvage, John Wiley & Sons, Chichester, 1999, ch. 7, pp. 285-369.

24. W. Heintz, *J. Prakt. Chem.*, 1855, **66**, 1.

25. F. Reinitzer, *Monatsh. Chem.*, 1888, **9**, 421.

26. D. Vorländer, *Ber. Dtsch., Chem. Ges.*, 1910, **43**, 3120.

27. D. Vorländer, *Z. Phys., Chem. Stoechiom., Verwandschaftsl.*, 1923, **105**, 211.

28. M. B. Ros, Other Physical Properties and Possible Applications of Metallomesogens, in *Metallomesogens: Synthesis, Properties, and Applications*, ed. J.L. Serrano, VCH, Weinheim, 1st edn.,1996, ch. 11, pp. 419-480.

29. P. J. Alonso, Magnetic Properties of Metallomesogens, in *Metallomesogens: Synthesis, Properties, and Applications*, ed. J.L. Serrano, VCH, Weinheim, 1st edn.,1996, ch. 10, pp. 387-418.

30. R. Dagani, Molecules Flip with Chiral Light, *C&EN*, 1996, September 23, 17.

31. D.W. Bruce, E. Lalinde, P. Styring, D.A. Dunmur and P.M. Maitlis, *J. Chem. Soc., Chem. Commun.*, 1986, 581.

32. H. Adams, N.A. Bailey, D.W. Bruce, R. Dhillon, D.A. Dunmur, S.E. Hunt, E.Lalinde, A.A. Maggs, R. Orr, P. Styring, M.S. Wrag and P.M. Maitlis, *Polyhedron*, 1988, **7**, 1861.

33. H. Adams, A.C. Albeniz, N.A. Bailey, D.W. Bruce, A.S. Cherodia, R. Dhillon, D.A. Dunmur, R. Espinet, J.L. Feijoo, E. Lalinde, P.M. Maitlis, R.M. Richardson and G. Ungar, *J. Mater. Chem.*, 1991, **1**, 843.

34. T. Kaharu, R. Ishii and S. Takahashi, *J. Chem. Soc., Chem. Commun.*, 1994, 1349.

35. M. Benouazzane, S. Coco, P. Espinet and J.M. Martín-Alvarez, *J. Mater. Chem.*, 1995, **5**, 441.

36. S. Coco, P. Espinet, S. Falagán and J.M. Martín-Alvarez, *New. J. Chem.*, 1995, **19**, 959.

37. S. Coco, P. Espinet, J.M. Martín-Alvarez and A. Levelut, *J. Mater. Chem.*, 1997, **7**, 19.

38. P. Alejos, S. Coco and P. Espinet, *New J. Chem.*, 1995, **19**, 799.

39. T. Kaharu, R. Ishii, T. Adachi, T. Yoshida and S. Takahashi, *J. Mater. Chem.*,

1995, **5**, 687.

40. R. Bayón, S. Coco, P. Espinet, C. Fernández-Mayordomo and J.M. Martín-Alvarez, *Inorg. Chem.*, 1997, **36**, 2329.

41. R. Ishii, T. Kaharu, N. Pirio, S. Zhan and S. Takahashi, *J. Chem. Soc., Chem. Commun.*, 1995, 1215.

42. S. Zhang, R. Ishii and S. Takahashi, *Organometallics*, 1997, **16**, 20.

43. K. M. Lee, C. K. Lee and I. J. B. Lin, *Angew. Chem., Int. Ed. Engl.*, 1997, **36**, 1850.

44. J. Barberá, A. Elduque, R. Giménez, L.A. Oro and J.L. Serrano, *Angew. Chem., Int. Ed. Engl.*, 1996, **35**, 2832.

45. J. Barberá, A. Elduque, R. Giménez, F. J. Lahoz, J. A. López, L.A. Oro and J.L. Serrano, *Inorg. Chem.*, 1998, **37**, 2960.

46. S. J. Kim, S. H. Kang, K. Park, H. Kim, W. Zin, M. Choi and K. Kim, *Chem. Mater.*, 1998, **10**, 1889.

47. P. G. Jones, *Gold Bull.*, 1981, **14**, 102.

48. B. Donnio and D. W. Bruce, *J. Chem. Soc., Dalton Trans.*, 1997, 2745, and references therein.

49. C. Bertram, D. W. Bruce, D. A. Dunmur, S. E. Hunt, P. M. Maitlis and M. McCann, *J. Chem. Soc., Chem. Commun.*, 1991, 69.

50. D. W. Bruce and A. Thornton, *Mol. Cryst. Liq. Cryst.*, 1993, **231**, 253.

51. D. W. Bruce, D. A. Dunmur, M. A. Esteruelas, S. E. Hunt, R. Le Lagadec, P. M. Maitlis, R. J. Marsden, E. Sola and J. M. Stacey, *J. Mater. Chem.*, 1991, **1**, 251.

52. E. J. Starr, Ph.D. Thesis, University of Cape Town, 1997.

53. D. W. Bruce, D. A. Dunmur, E. Lalinde, P. M. Maitlis and P. Styring, *Liquid Crystals*, 1988, **3**, 385.

CHAPTER 2. Synthesis, cis-trans isomerisation and mesomorphic behaviour of XAuL complexes, X = Cl and L = py, vnlpy and n-OST (n = 4-10)

2.1 Introduction

Chapter 2 deals broadly with the synthesis and characterisation of complexes of the type XAuL where X = chloride and L = pyridine (py), vinylpyridine (vnlpy) and trans-4,4'-alkoxystilbazole (n-OST), where n = number of carbon atoms in the alkoxy chain. Complexes **1** (L = py) and **2** (L = vnlpy) were prepared as model systems in order to understand the more complicated L = n-OST system, which exhibits cis-trans isomerisation and liquid crystalline behaviour. The introduction of a metal atom to the already mesomorphic n-OST ligands[1] would result in different liquid crystalline properties due to enhanced polarisation effects[2,3] as well as the dipole moment associated with the Au-X functionality[4,5,6] for complexes **3-9** (L = 4-10-OST). Complexes **1-2** would however not be expected to exhibit mesomorphic behaviour due to the presence of only a polarisable rigid core without flexible 4-alkyl or 4-alkoxy tails to increase molecular anisotropy and facilitate liquid crystalline formation.[7]

Molecular structure plays an important role in mesophase formation. It is thus of particular interest to determine whether ClAu(n-OST) complexes form neutral, ClAuL, or ionic, $[AuCl_2]^-$ $[AuL_2]^+$, species and whether Au...Au bonding interactions result in any interesting dimeric, tetrameric or polymeric supramolecular arrangements. It has been shown that gold(I) pyridine complexes, X = Cl, Br or I, form ionic complexes, $[AuX_2]^-[Au(py)_2]^+$, with chain-like tetrameric[8,9] and polymeric[9] structures (Figure 2.1). Gold(I) complexes with nitrogen-donor

ligands have even been reported to form both neutral and ionic species in the same reaction, with the neutral species having a chain-like polymeric and the ionic species a tetrameric structure.[10]

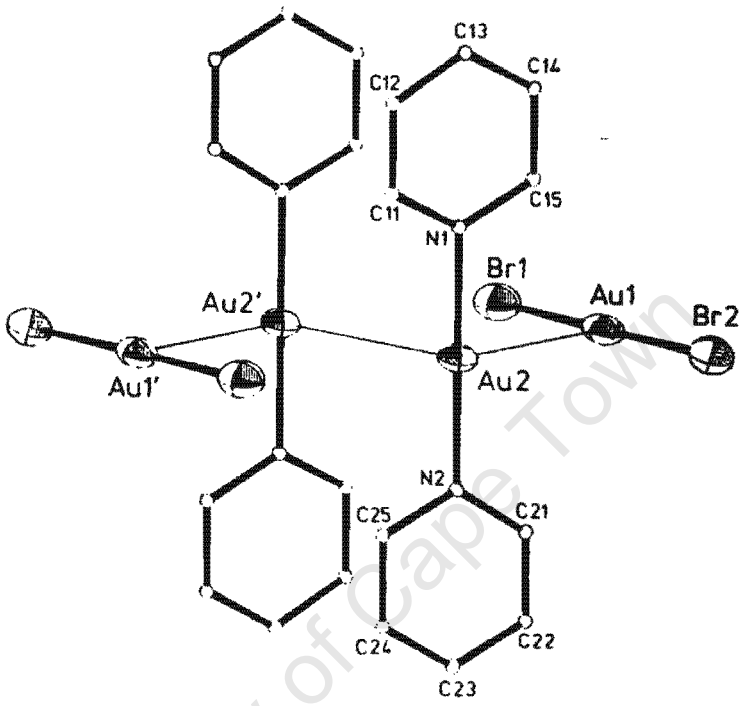

Figure 2.1: Molecular structure of tetrameric $[AuBr_2]^-[Au(py)_2]^+$ with Au...Au bonding interactions

2.2 Synthetic method and characterisation of gold(I) complexes 1-9

2.2.1 Synthesis of n-OST ligands

The n-OST ligands were prepared in a two step process according to literature procedures (Scheme 2.1).[1,11] Firstly, the intermediate 4-alkoxyiodo- or 4-alkoxybromobenzene was formed by refluxing iodo- or bromophenol with the corresponding 1-bromoalkane and potassium carbonate in acetone. This was then refluxed with 4-vinylpyridine in acetonitrile via the palladium acetate catalysed Heck[12] reaction to form the corresponding n-OST ligand. FT-IR,

^{1}H- and ^{13}C-NMR spectroscopic data for the n-OST ligands are reported in Appendix 2A, Tables 2A.1, 2A.3 and 2A.5 and compare well with literature data.[11,24]

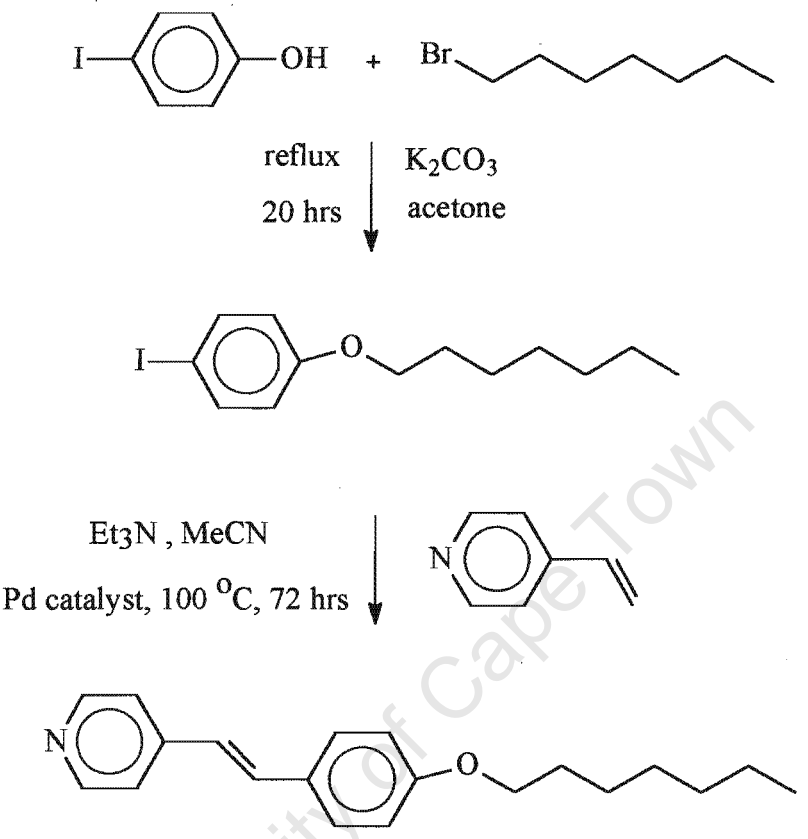

Scheme 2.1: Reaction scheme for the synthesis of 7-OST

2.2.2 Synthesis of gold(I) complexes ***1-9***

Complexes **1** and **2** were formed via displacement of tetrahydrothiophene (tht) from a suspension of ClAu(tht) in toluene by the addition of a large excess of py and vnlpy respectively (Scheme 2.2). The reactions were conducted at about 50 °C with reaction times ranging between 15 to 60 minutes and yields ranging between 50% to 80%. Complex **1** has previously been synthesised via displacement of carbonyl,[13] dimethyl sulphide[14] and di(phenylmethane) sulphide[8] by pyridine. It was reported to be light-sensitive and thermally unstable and although IR spectra and luminescence properties were discussed,[8] no ^{1}H- or ^{13}C-NMR spectroscopic data

were reported.

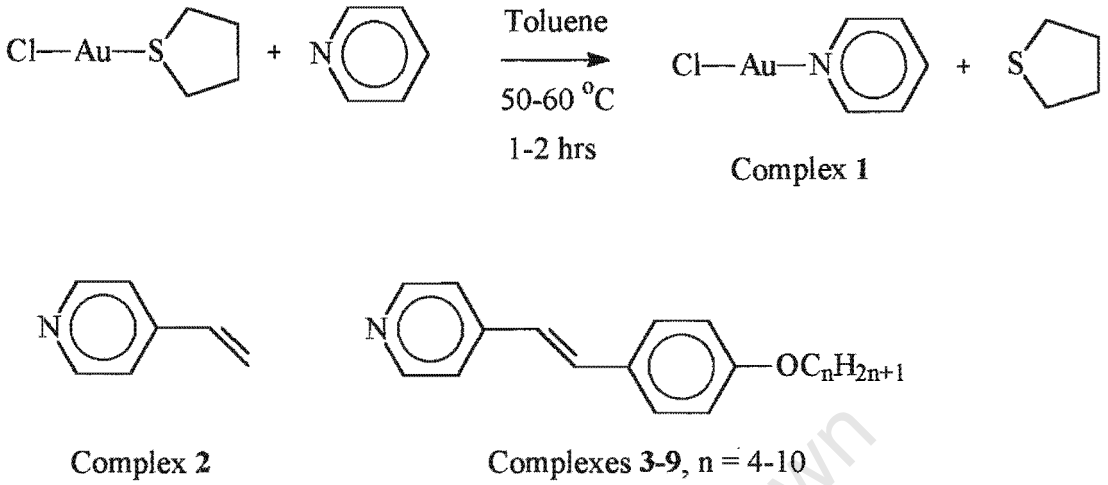

Scheme 2.2: Reaction scheme for the synthesis of complexes **1-9**, L = py, vnlpy and n-OST

Complexes **3-9** were prepared in a similar manner to complexes **1-2** (Scheme 2.2), except that the reactions were conducted at slightly higher temperatures of about 60 °C, for longer time-periods of about 2 hours. Complex **7** has previously been made,[15] but no synthetic details and IR, ^{1}H- or ^{13}C-NMR spectroscopic data have as yet been published. Although the ligands (n-OST) were initially added in excess, it was found that equimolar amount of ClAu(tht) and n-OST resulted in good reaction yields of up to 83%. However, the yields for complexes **3-9** after purification were much lower, about 45%, due in part to inevitable decomposition that occurred during the purification procedures. Complexes **3-9** precipitate from solution as fine yellow powders and are usually recrystallised from dichloromethane/pentane solutions as thin platelets or long (up to 4 cm) thin yellow needles.

2.2.3 Characterisation of gold(I) complexes 1-9

Complexes **1-2** form white crystals that decompose at 109 °C and 117 °C respectively. They are soluble in common organic solvents including dichloromethane, acetone, chloroform, diethyl ether, ethyl acetate and toluene but insoluble in hydrocarbon solvents such as pentane and hexane. Conflicting melting (or decomposition) temperatures of 92 °C[13] and 250-252 °C[14] have been reported for complex **1**. However, these workers only provide microanalysis data in supporting evidence for the structure of their compound. No thermal data were reported in an X-ray crystallographic study[8] of complex **1**. If protected from light, complexes **1-2** can be stored for over six months at -25 °C without decomposition. Complexes **1-2** were characterised via FT-IR, ^{1}H- and ^{13}C-NMR spectroscopy (Appendix 2A, Tables 2A.1-3), elemental analysis (chapter 6) and conductivity in acetone (Table 2.3 in the text). FT-IR, ^{1}H- and ^{13}C-NMR spectroscopic data for the free py and vnlpy ligands are also reported.

Complexes **3-9** are soluble in similar organic solvents compared to complexes **1-2**, except that they are also insoluble in diethyl ether. It is also observed that as n increased, the solubility of the complexes tended to decrease. Complexes **3-9** can be stored unprotected from light at room temperature for more than a year. They are unstable when heated or in solution. Decomposition occurs more rapidly when the solution is exposed to light even for short times. Complexes **3-9** were characterised via FT-IR, ^{1}H- and ^{13}C-NMR spectroscopy (Appendix 2A, Tables 2A.1-2, 2A.4-7), elemental analysis, FAB mass spectrometry (chapter 6) and conductivity in acetone (Table 2.3 in the text).

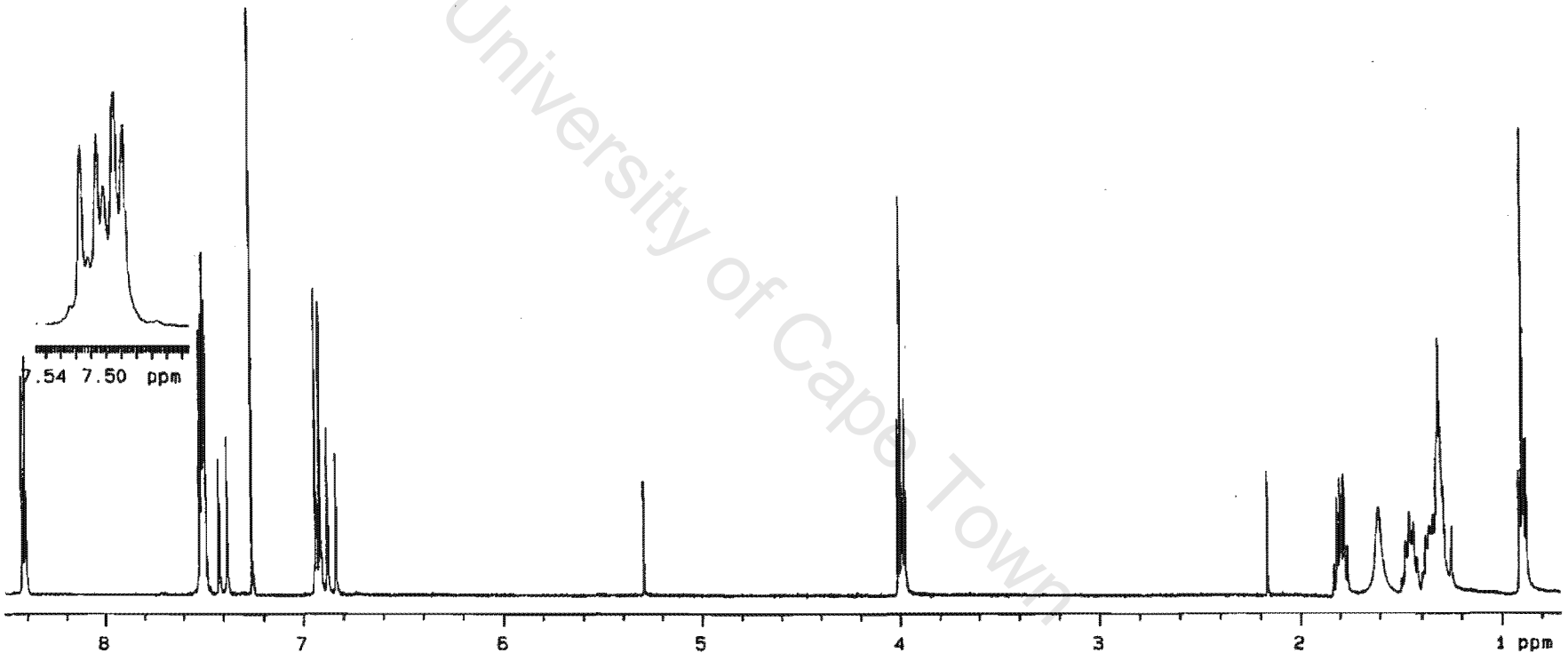

Figure 2.2: ^{1}H-NMR spectrum of complex **6** in $CDCl_3$.

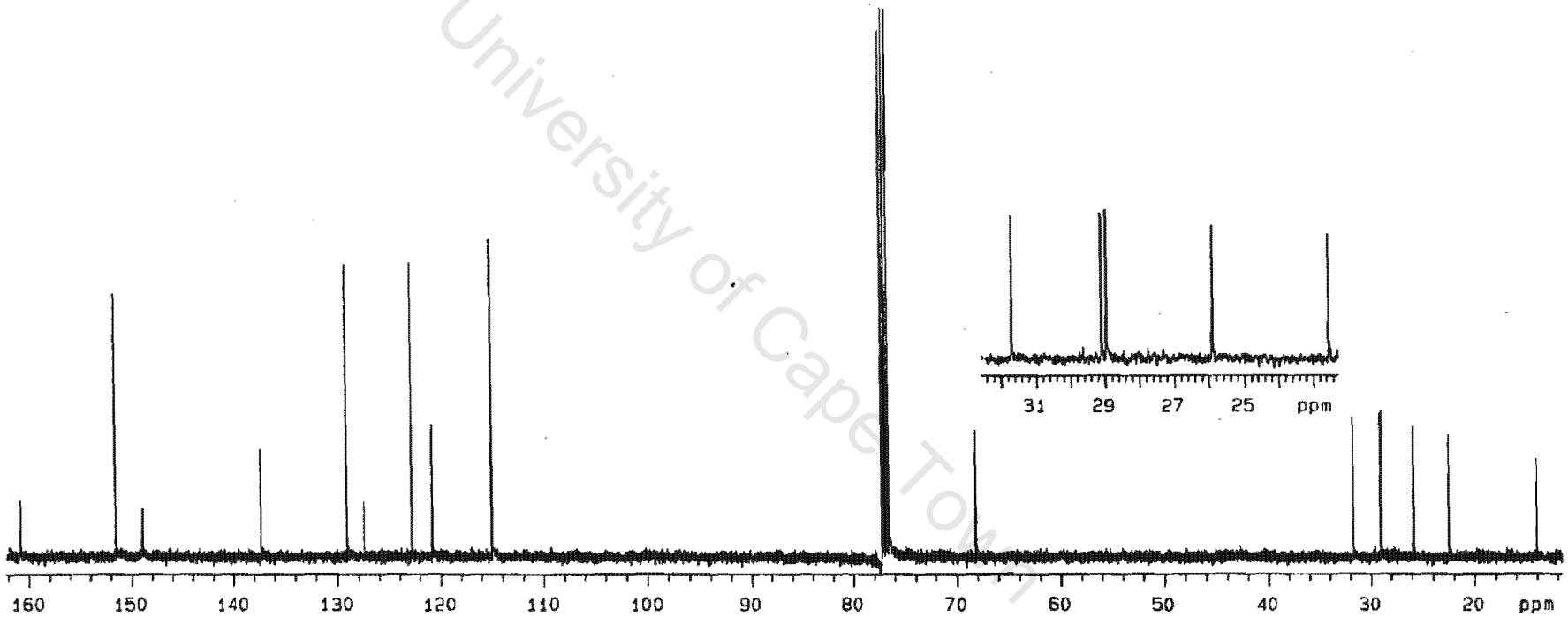

Figure 2.3: ^{13}C-NMR spectrum of complex **6** in $CDCl_3$.

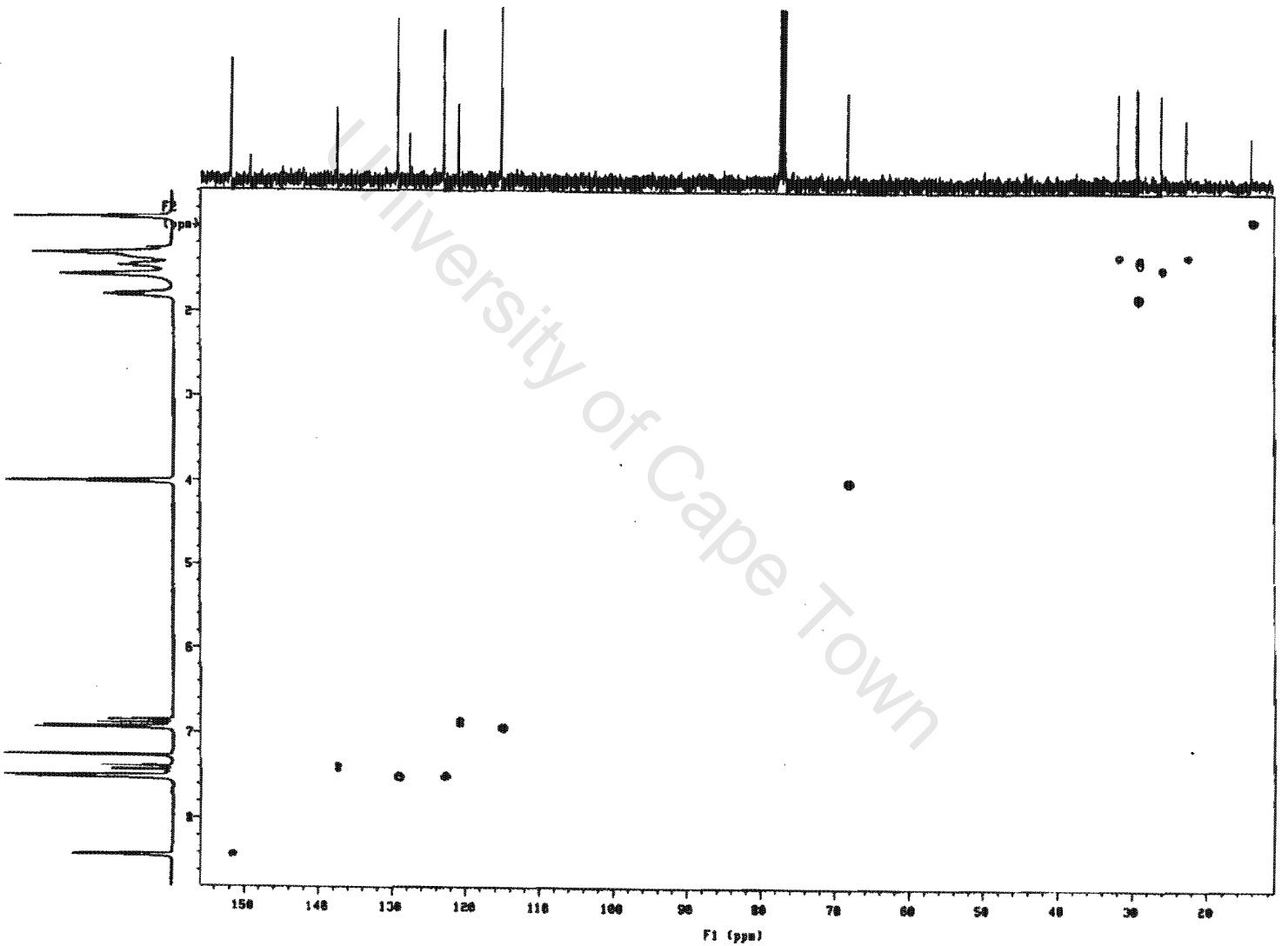

Figure 2.4: HETCOR spectrum of complex **6** in $CDCl_3$.

The assignments for the FT-IR spectra of complexes **1-9** were made by comparison with the free ligands and literature ν(Au-Cl) values.[8] The ^{1}H- and ^{13}C-NMR spectra of complexes **1-9** were assigned by comparison with the free py[23], vnlpy[23] and n-OST[11,24] ligands and two dimensional ^{1}H,^{13}C-NMR spectra (HETCOR). Representative ^{1}H- and ^{13}C-NMR and HETCOR spectra of complex **6** can be seen in Figures 2.2-4. The proton signals for H_b and H_g overlap, but were easily assigned as on the basis that H_b/H_a and H_g/H_h proton pairs would have similar coupling constants. Complexes **3** and **5** were observed to exhibit cis-trans isomerisation and ^{1}H- and ^{13}C-NMR spectroscopic data for complexes **3a** and **5a**, the respective cis isomers, are reported in Appendix 2A, Tables 2A.8-9. The ^{1}H- and ^{13}C-NMR and HETCOR spectra of the mixture of complexes **5/5a** can be seen in Figures 2.11-13. The liquid crystalline properties of complexes **3-9** were evaluated via differential scanning calorimetry (DSC) and optical microscopy techniques. The DSC data are presented in Table 2.4.

2.2.4 Attempted synthesis of complexes of the type IAuL

The nature of the X group has been found to affect the mesomorphic properties. Transition temperatures in gold(I) complexes[4,5,6] have been found to increase in the order Cl < Br < I due to changes in the enhanced polarisation effect or decrease in the order Cl > Br > I due to changes in the Au-X dipole moment. An attempt was made to synthesis the iodo derivatives of complexes **1-9** by reaction with excess potassium iodide in acetone at -72 °C, with no success. In all cases, during extraction with dichloromethane, deep purple solutions (L = py, vnlpy) or brown/orange solutions (L = n-OST) and metallic gold deposition were observed. A small amount of free n-OST was recovered from the brown/orange solutions. This was unexpected behaviour, as tetrameric, ionic IAupy[8] has previously been prepared by reaction of excess py with gold(I)iodide in toluene and is reported to be stable below -30 °C. Schmidbaur and coworkers,[10] while attempting to synthesise iodogold (diphenylmethanimine) complexes, have recently

observed similar unexpected behaviour. In all cases the triiodide (diphenylmethanimine)gold(I) salt was crystallised, according to scheme 2.3 proposed below.

$$3ClAu(Ph_2C{=}NH) + 3KI \rightarrow [Au(Ph_2C{=}NH)_2][I_3] + 2Au + Ph_2C{=}NH + 3KCl$$

$$3AuI + 2Ph_2C{=}NH \rightarrow [Au(Ph_2C{=}NH)_2][I_3] + 2Au$$

Scheme 2.3: Reaction schemes for the synthesis of triiodide (diphenylmethanimine)gold(I) salts[10]

It was suggested by Schmidbaur[10] *et. al.* that the reactions lead to a partial redox process to give Au metal and I_2, the latter reacting with I^- to form the triiodide. Recent work done by Nakao and Sone[31] was quoted to support this conclusion. As IAu(py) can be prepared using toluene,[8] but not acetone/dichloromethane, it is possible that a similar redox process to the one proposed in scheme 2.3 applies for ClAuL complexes, L = py, vnlpy and n-OST, in acetone/dichloromethane but not toluene.

2.3 Discussion of results for gold(I) complexes 1-9

2.3.1 Model of molecular orbital interactions in gold(I) complexes 1-9

Gold(I) has the electron configuration $[Xe]4f^{14}5d^{10}$ and can form linear bonds with hybridisation at the gold(I) atom initially thought to be sp, but involvement of 5d orbitals due to mixing of closely spaced $5d_{z^2}$ and 6s orbitals is also thought to be important.[25] Some studies have suggested that there is very little involvement of the 6p orbitals and molecular orbital calculations have predicted a d-s hybridisation scheme, but the issue has not been conclusively decided.[25] The 5d levels of gold(I) have been interpreted to split into σ ($5d_{z^2}$), π (d_{xz}, d_{yz}) and δ(d_{xy}, $d_{x^2-y^2}$) as expected from crystal field theory.[25] The σ Au^I-L (L = py, vnlpy and n-OST) bonds will be further strengthened by the π-donation of electrons from the filled d_{xz} and d_{yz} orbitals of gold(I) into the empty π^* orbitals of the pyridine (and substituted pyridine) ring

systems. The Au^{I}-Cl bond is not expected to have much π-bond character, although the p-orbitals of the chloride ion would be able to donate π-electrons. This is because as all the d-orbitals of gold(I) are filled and would be more willing to donate rather than accept electrons.

The Au^{I}-py bond will be affected by the bond between gold(I) and the trans ligand, *e.g.* the protons of the pyridine ring in $[(PPh_3)Au(py)]^{+}[ClO_4]^{-}$[26] experiences greater downfield shifts than complex **1**, due to π donation of electrons from filled d_{xz} and d_{yz} orbitals of Au^{I} into corresponding empty dπ orbitals of phosphorous. As the trans ligand remains a chloride group for complexes **1-9**, it will be assumed that changes in the electronic structure (FT-IR, ^{1}H- and ^{13}C-NMR spectra) of the py ring of the L group will be due largely to changes in the Au^{I}-L bonding interaction and enhanced conjugation effects (explained further in section 2.3.3). It should also be noted that the trans ligand would be a chloride group only if complexes **1-9** were neutral species. Although FT-IR, ^{1}H- and ^{13}C-NMR spectroscopy may be useful in indicating whether one or both species are present, these techniques cannot distinguish between the neutral or ionic species.

The ν(Au-Cl) value, which gives an indication of bond strength, ranges between 341 to 361 cm^{-1} for complexes **1-9** (Table 2A.1). This might indicate that the Au^{I}-Cl bond is slightly affected by changes in the L group, but no distinct trends are observed between ν(Au-Cl) and ligand type.

2.3.2 Variation in ν(C=N), ν(C=C) and $\nu(C\text{-}H)_{alkene}$ as L group changes

As L changes from py to vnlpy in both the free ligands and gold(I) complexes, ν(C=N) tends to decrease and some ν(C=C) values increase slightly (Table 2.1). For L = n-OST, then ν(C=N), certain ν(C=C) values and $\nu(C\text{-}H)_{alkene}$ tends to decrease (Table 2.1).

Table 2.1: Selected aromatic FT-IR spectroscopic data (in cm^{-1}) of complexes **1-9** and the free ligands

L	ν(C-H)		ν(C=C)		ν(C=N)	
	Free L	**ClAuL**	**Free L**	**ClAuL**	**Free L**	**ClAuL**
Py	3040 s	3043 m	1599 s	1611 s	1439 vs	1454 vs
			1483 s	1486 m		
Vnlpy	3094 m[a]	3098 m[a]	1597 vs	1620 vs	1409 vs	1433 vs
	3045 s	3048 s	1548 vs[a]	1546 s[a]		1417 vs
			1495 s	1501 s		
4-OST	3071 w[a]	3046 m	1592 vs	1599 vs	1417 s	1436 s
	3034 m		1550 w[a]	1513 s		
			1512 s	1475 m		
			1475 m			

a = alkene, w = weak, m = medium, s = strong, vs = very strong

In particular, ν(C=N) is about 20 to 30 cm^{-1} less when L is vnlpy and n-OST, compared to py. The weaker the C=N bond, the more electron density from the sp^2 hybridised orbitals of the nitrogen atom will be available to bond with gold(I). The Au^{I}-N bond is thus stronger when L corresponds to vnlpy and n-OST, compared to L = py.

2.3.3 Conjugation effects in py, vnlpy and n-OST ligands

The relative stability of complexes **2-9** (L = vnlpy, n-OST) compared to complex **1** (L = py) is most likely due to conjugation effects (Figure 2.5). The introduction of electron-rich groups such as the alkene group (L = vnlpy, n-OST) and an ether linkage and aromatic ring (L = n-OST) results in the formation of conjugated systems with highly delocalised electrons compared to py, reflected in lower ν(C=N) values. From the ^{1}H-and ^{13}C-NMR spectra of the free n-OST ligands and corresponding complexes **3-9** (Tables 2A.4-7), it can be seen that each alternate carbon and its associated proton (i.e. $C(H)_b$, $C(H)_d$, $C(H)_f$, $C(H)_h$) are regions of higher electron density than the adjacent carbon and its associated proton. This has also been observed in similar n-OST metal complexes.[11]

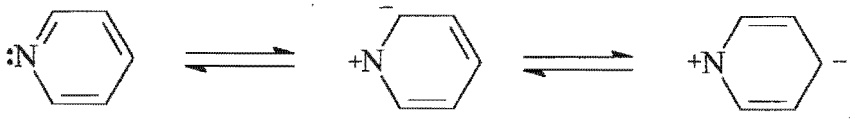

L = py (Complex **1**)

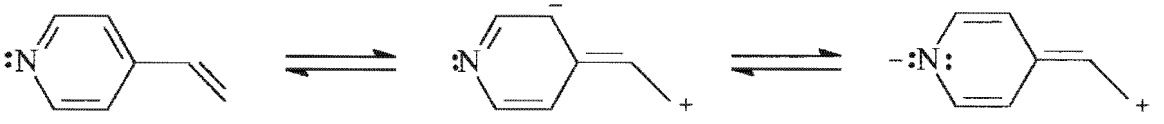

L = vnlpy (Complex **2**)

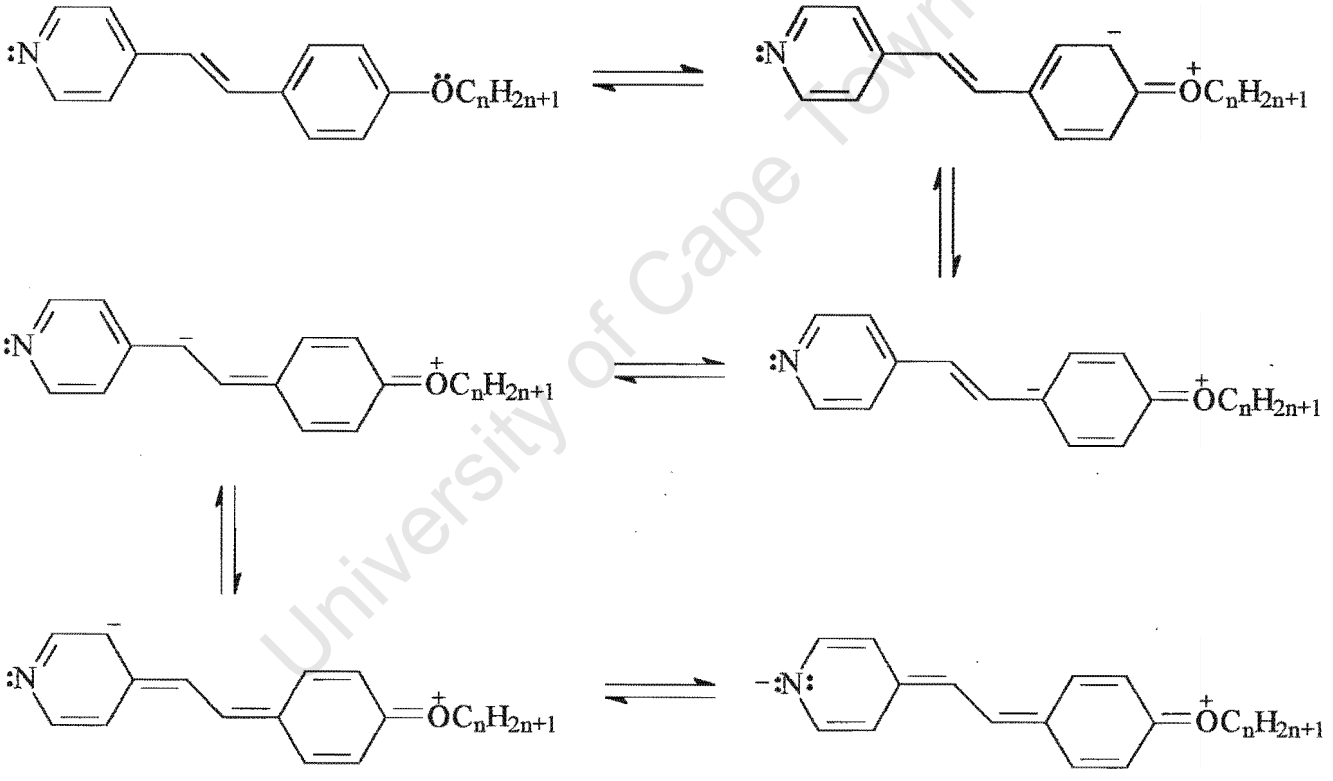

L = n-OST (Complexes **3-9**)

Figure 2.5: Resonance structures for py, vnlpy and n-OST ligands

2.3.4 Variation of $\nu(C\text{-}H)_{alkane}$ and alkane coupling constants in n-OST ligands

As n increases from 4 to 6 for both the free n-OST ligands and complexes **3-9**, the $\nu(C\text{-}H)_{alkane}$ value decreases by about 30 cm^{-1} (Tables 2A.1-2), after which it decreases very gradually by about 6 cm^{-1} as n increases from 6 to 10.

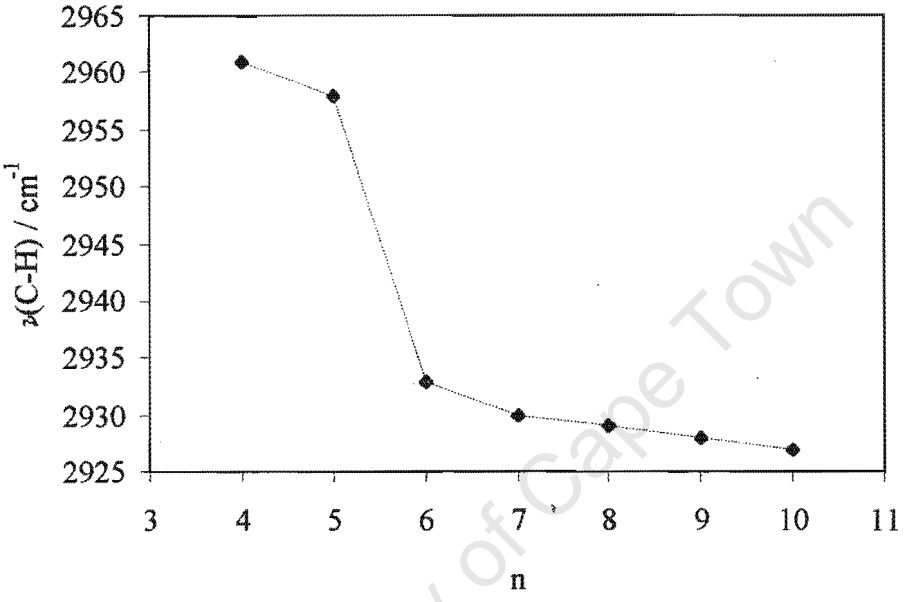

Figure 2.6: Changes in $\nu(C\text{-}H)_{alkane}$ as a function of increasing alkoxy chain length, n.

From the graph (Figure 2.6) it can inferred that for shorter alkoxy chains (n = 4 to 6), the C-H alkane bonds vibrate at slightly higher energies than for longer chains (n = 6 to 10). After n = 6, the contribution of the alkane groups closer to the ether group hardly has any effect on the overall $\nu(C\text{-}H)_{alkane}$ value. The $^3J_{HH}$ coupling constants (Table 2A.5) for the ethylene group, H_j, next to the oxygen atom is less (6.6 Hz) than the ethylene groups, H_k and H_l, further away (7.0 and 7.5 Hz), for both the free ligand and complexes **3-9**. This might indicate shorter C-H bonds for ethylene groups close to the ether group, with corresponding higher energies.

*2.3.5 Variation in FT-IR, ^{1}H- and ^{13}C-NMR spectra of complexes **1-9** compared to free ligands*

It is generally observed that ν(C=N), ν(C=C) and ν(C-H) values (Table 2.2) increased after complexation to gold(I). This could be attributed to the π donation of d_{xz} and d_{yz} electrons from the filled gold(I) d-orbitals or enhanced conjugation effects. When n-OST ligands are complexed to gold(I), the conjugation effect (section 2.3.3) is also magnified, resulting in the atoms which are regions of higher electron density, *e.g.* H_b, H_d, H_f and H_h, experiencing an upfield shift and vice versa for H_a, H_c, H_d and H_g. This sort of behaviour has previously been reported for n-OST ligands complexed to aryl cobaloximes, with H_d (a region of higher electron density) experiencing an upfield shift of 0.26 ppm.[11] Most of the Δδ (ppm) in ^{1}H- and ^{13}C-NMR spectra observed for complexes **1-9** (Table 2.2) are downfield shifts.

Table 2.2: Δδ in ^{1}H- and ^{13}C-NMR spectra of complexes **1-9** compared to the free ligands

Complex	L	Δδ (ppm) in ^{1}H- and ^{13}C-NMR spectra								
		H_a	H_b	H_c	H_d	H_e		H_g	H_h	
1	py	+0.22	+0.53	+0.60						
2	vnlpy	+0.08	+0.36		+0.18	+0.32^{t}				
						+0.41^{c}				
3-9	n-OST	-0.12	+0.18		0.00	+0.17^{t}		+0.06	+0.02	
		C_a	C_b	C_c	C_d	C_e	C_f	C_g	C_h	C_i
1	py	+2.8	+3.4	+4.2						
2	vnlpy	+2.0	-1.7	+3.9	+2.8	+4.7				
3-9	n-OST	+1.6	+2.3	+4.0	-2.7	+4.6	-1.1	+0.8	+0.2	+1.1

t = trans, c = cis.

Before further discussion, it should be noted that the small changes in chemical shift (δ) values for the proton or carbon atoms after the ligands are complexed to gold(I) will be due to small changes in the shielding constant (σ), which are linearly related. The magnitude of σ changes due to changes in the electronic structure near the nucleus of interest and is the sum of contributions from: (i) the electrons of the atom which contains the nucleus of interest, (ii) the groups of atoms that form the rest of the molecule and (iii) the solvent molecules. Thus if the δ

value of the nucleus of interest decreases on complexation to gold(I), then the nucleus experiences an upfield shift and becomes relatively more shielded (i.e. σ has increased). The electron density (from the atom as well as the atoms in the rest of the molecule) around the nucleus has increased (assuming that the electronic contribution from the solvent remains constant). and vice versa. The downfield shifts (Table 2.2) can easily be explained by reduced electron density due to sigma donation of electrons from the sp^2 hybridised nitrogen atom and/or enhanced conjugation effects in regions of relatively lower electron density. All upfield changes, except H_a, can be explained on the basis of enhanced conjugation effects in regions of relatively higher electron density.

What is more difficult to explain with the conjugation model is why H_a, a region of relatively lower electron density, experiences an upfield shift when L = n-OST (-12 ppm), but downfield shifts when L = vnlpy (+0.08 ppm) and py (+0.22 ppm). To a lesser extent, the trend of relatively increased shielding for complexes **1-9** as L changes from py (+2.8 ppm) to vnlpy (+2.0 ppm) to n-OST (+1.6 ppm) for C_a agrees with what is observed for H_a. Another possible source of increased electron density is the π back-donation of electrons from gold(I) into the pyridine ring. One could either say that the conjugation effect becomes less pronounced at H_a as L changes from py to vnlpy, or that the π back-donation from the metal into the pyridine ring has increased from L = py to vnlpy. The upfield shift observed for H_a when L = n-OST though, can only be explained due to the π back-donation of gold(I) into the pyridine ring. If increased π back-donation from gold(I) into the pyridine ring is an indication of increased Au^I-L bond strength, then n-OST ligands form stronger bonds with gold compared to vnlpy and py. Due to uncertainty in the magnitude of the contribution of enhanced conjugation effects to the downfield shifts of H_a, it cannot be said that vnlpy forms a stronger bond with gold(I) compared to py, unless increased conjugation also increases the Au^I-L bond strength.

2.3.6 Neutral or ionic molecular structure of complexes 1-9

The neutral or ionic molecular structure of complexes **1-9** were investigated using molar conductivity measurements, FT-IR, ^{1}H- and ^{13}C-NMR spectroscopy, electron impact (EI) and fast atom bombardment (FAB) mass spectrometry and X-ray photography. The average molar conductivities (Λ) for complexes **1-9** were calculated (Equation 2.1) using specific conductivities (κ) measured as 10^{-3} M acetone solutions and are given in Table 2.3.

$$\Lambda = 1000\ \kappa / c \qquad (2.1)$$

where Λ = molar conductivity ($ohm^{-1}.mol^{-1}.cm^{2}$)

κ = specific conductivity ($S.cm^{-1}$)

c = concentration of electrolyte (M)

Tetrabutylammonium perchlorate is a common 1:1 electrolyte and was used as a reference point. Its Λ value was determined to be 148 $ohm^{-1}.mol^{-1}.cm^{2}$ in10^{-3} M acetone. The measured κ values for each complex did not vary by more than 0.10 $\mu S.cm^{-1}$.

Table 2.3: Molar conductivity values for complexes **1-9** in acetone (10^{-3} M).

Complex	L Group	Λ ($ohm^{-1}.mol^{-1}.cm^{2}$)
1	py	7.24
2	vnlpy	4.15
3	4-OST	5.01
4	5-OST	4.67
5	6-OST	4.63
6	7-OST	7.25
7	8-OST	6.75
8	9-OST	13.77
9	10-OST	7.00

Various types of 1:1 electrolyte gold(I) complexes have been reported to have Λ values (determined in acetone) ranging between 60 to 150 $ohm^{-1}.mol^{-1}.cm^{2}$.[16,17,18] The Λ values from

Table 2.3 indicate that complexes **1-9** are predominantly non-conducting, neutral species when dissolved in acetone. Minor precipitation of a grey solid, which may be indicative of decomposition, was observed during analysis of complex **1**. Therefore, because Λ is concentration dependant, the value quoted in Table 2.3 for complex **1** may be regarded as an underestimation of the true Λ for this complex. Complex **1**, determined to be pure by microanalysis, was observed to decompose even more rapidly in dichloromethane, resulting in a purple solution, gold deposition and the liberation of py. The liberated py was identified on the basis of ν(C=N) in the FT-IR spectra of complex **1** (Figure 2.7) and suggested that about 20 % decomposed while measuring the sample. This provides an indication of decomposition rate, although the Λ value was measured in a different solvent, which would also affect the rate.

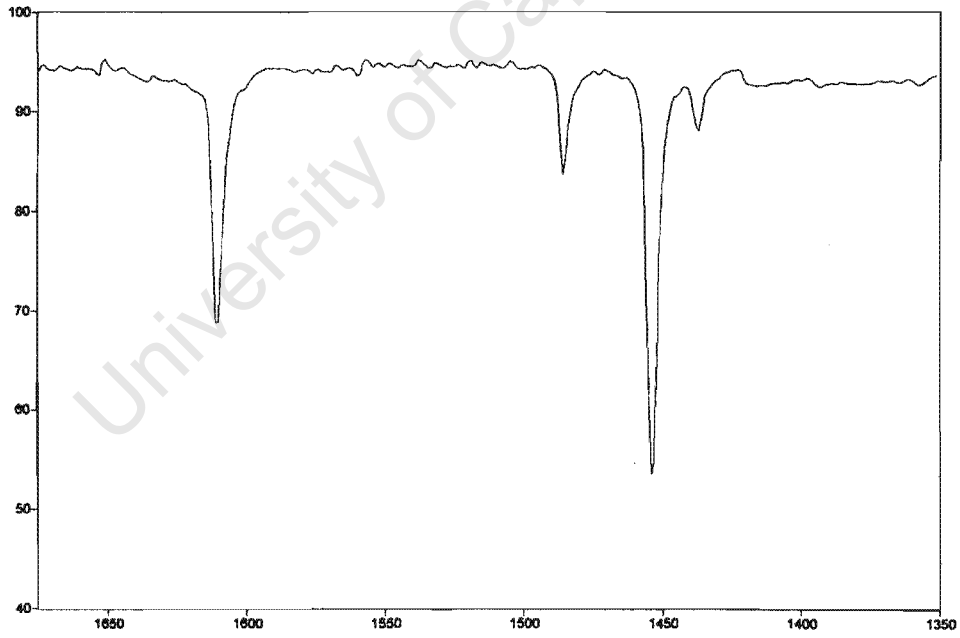

Figure 2.7: FT-IR spectrum of complex **1**

The Λ value for complex **1** (Table 2.3) is about one order of magnitude less than what would be expected for a 1:1 electrolyte (even assuming 20% of the complex decomposed) and indicates

that it is most likely a neutral species. However, Adams *et al*[8], showed that complex **1** crystallises with an ionic structure from ethanol.[8] They did however not provide any Λ value for comparison. This discrepancy may be explained by noting that a complex may crystallise from different solvents with different molecular structures, or have different molecular structures in different solvents, which may or may not differ from the solid state molecular structures. In this study, complex **1** was crystallised from toluene and that the Λ values were determined in acetone. The less polar toluene might promote the formation of the neutral species, with the more polar ethanol promoting the ionic species, or the complexes may prefer to form neutral species in acetone. This type of polymorphic behaviour might explain the differences in melting points (92 °C[13] and 250–252 °C[14]) reported for complex **1**. The ionic bromine derivative[9] of complex **1** was also found to exhibit polymorphic behaviour, crystallising as tetrameric zigzag chains from dichloromethane (Figure 2.1) or infinite polymeric chains from toluene.

Schmidbaur and coworkers[10] have used ν(C=N) of the diphenylmethanimine ligand, which they complexed to gold(I) chloride, to differentiate between neutral and ionic isomers formed in the same reaction. The ionic species had a slightly higher wave number of 1599 cm^{-1} compared to 1592 cm^{-1} for the neutral species. Only one ν(C=N) peak is observed in the FT-IR spectra of complexes **1-9**, indicating that either the neutral or ionic species exists independently in dichloromethane, except for complex **2**. Complex **2** has two ν(C=N) peaks at 1433 and 1417 cm^{-1} (Table 2.1, Figure 2.8), which might indicate the presence of a mixture of a neutral and an ionic isomer in dichloromethane. However, conductivity measurements (Table 2.3) show that complex **2** forms a neutral species in acetone. The nature of the solvent can affect the degree of ionisation of these complexes. Conductivity measurements of complex **2** in dichloromethane would be required to conclusively prove whether an ionic species formed in that solvent. ^{1}H-NMR spectra of complex **2** (Figure 2.9) shows that only a single species forms in

deuterochloroform. Whether this species is ionised or not in deuterochloroform cannot be ascertained from the spectra, as NMR spectroscopy is not a sensitive tool for distinguishing between neutral or ionic species. Complex **2** exists only as the neutral species in acetone and as a single species in deuterochloroform (either neutral or ionic). It may exist as both neutral and ionic species in dichloromethane, but further conductivity measurements in dichloromethane are required to confirm the FT-IR observation.

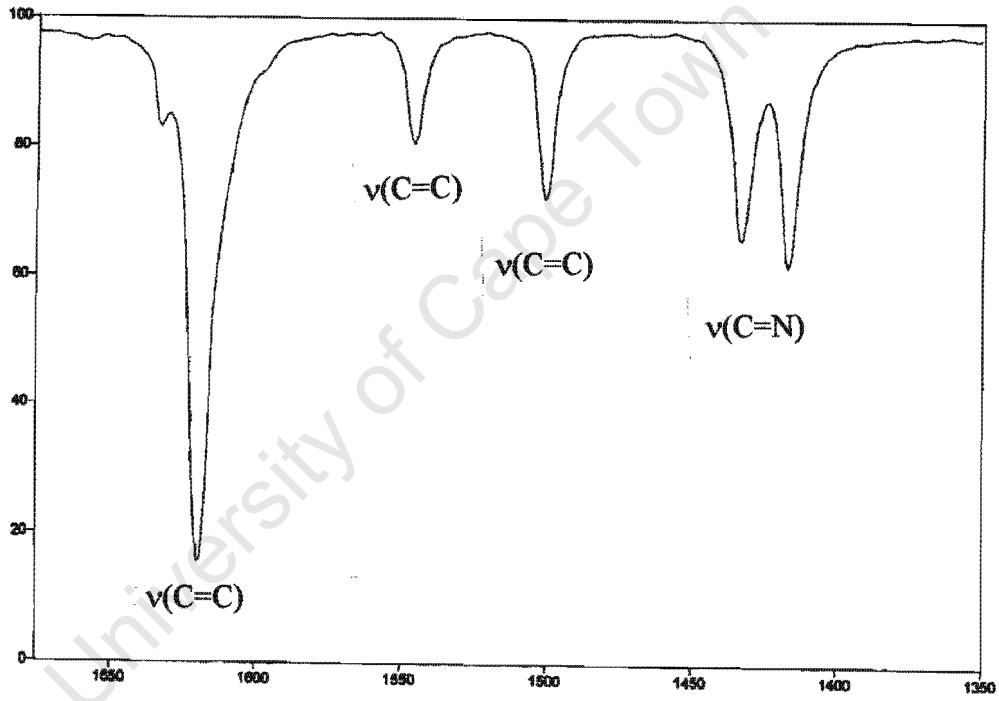

Figure 2.8: FT-IR spectrum of complex **2**

Attempts at obtaining parent ion peaks M^+ using both electron impact (EI) and fast atom bombardment (FAB) mass spectrometry have met with limited success. As this form of analysis depends on the complexes being stable when dissolved in the matrix (2-nitrobenzylalcohol) and heated, the fact that parent ions were not observed may be due to the inherent instability of the

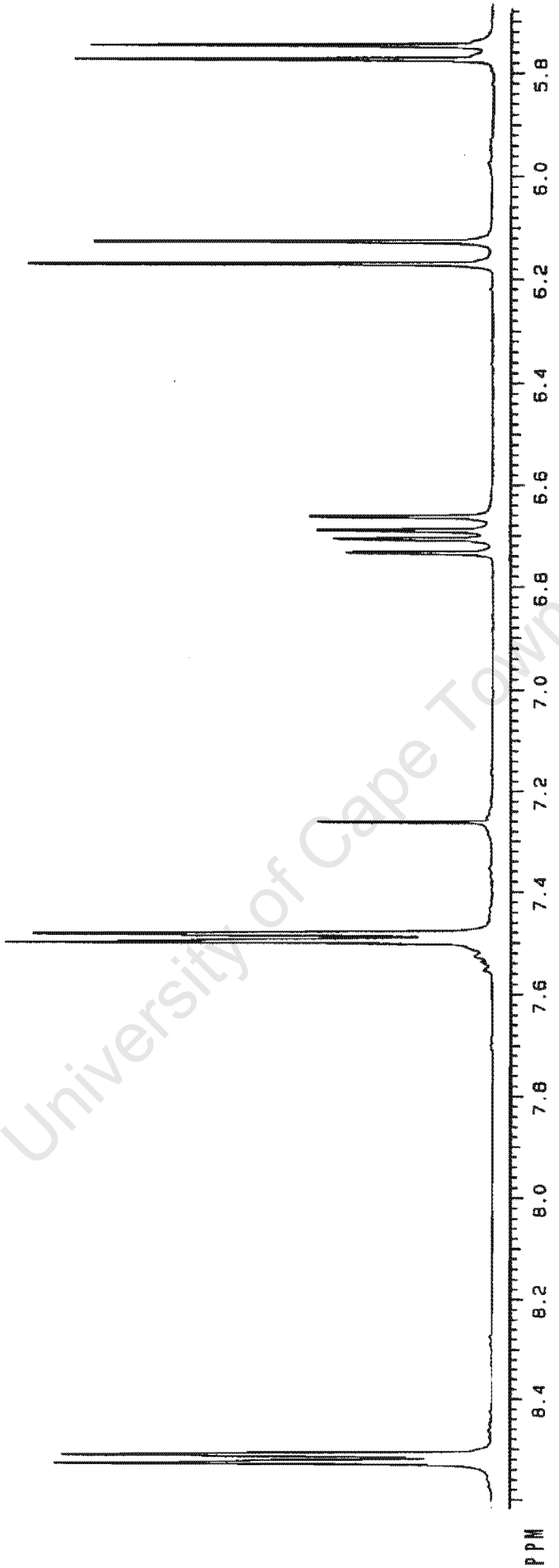

Figure 2.9: ^{1}H-NMR spectrum of complex **2** in $CDCl_3$.

complexes. The parent ion of complex **4**, $[ClAu(5\text{-}OST)]^+$, was eventually observed after addition of rubidium to the complexes before performing the FAB experiment. A very small peak corresponding to the $[Au(n\text{-}OST)_2]^+$ cation was also generally observed, but this could be created during the analysis.

The structural and electronic features of molecules in the liquid crystal phase are studied using X-ray diffraction and extended X-ray adsorption fine structure spectroscopy (EXAFS),[19] but would not be applicable to complexes **3-9**, which decompose in the liquid crystal phase. An idea of how these molecules pack together in the solid phase might also give one insight as to what sort of interactions give rise to the liquid crystal phase. This is because intermolecular packing arrangements are often maintained in the liquid crystal phase.[20,21,22] It would be of particular interest whether complexes **3-9** form neutral or ionic species in the solid state and whether any weak Au...Au bonding interactions occur. Attempts to grow suitable crystals of complexes **3-9** from dichloromethane/pentane solutions resulted in decomposition while in solution. Crystals that were obtained tended to form very long, thin needles or platelets unsuitable for X-ray crystallography. It was possible to perform oscillation and De Jong Bouman photography on one specimen, which yielded Laue symmetry 2/m and indicated that the crystal belonged to the monoclinic system, but unfortunately the crystal decomposed before any more X-ray information could be obtained.

2.3.7 Cis-trans isomerisation of complexes 3, 3a, 5 and 5a

Thermal cis-trans isomerisation (stereomutation) of alkenes in aromatic conjugated systems occurs due to the actual ground state of the molecule being a resonance hybrid with one or more of the ionised canonical hybrid forms having a central double bond with reduced π-bond

character.[27] Indigo, 4-nitro-, 4-amino- and 4-amino-4'-nitrostilbene (Figure 2.10) are typical examples of molecules exhibiting this phenomenon.[28,29] The activation energy for cis-trans isomerisation of 4,4'-aminonitrostilbene has been calculated to be only 17.1 ± 2.5 kcal/mole.[29]

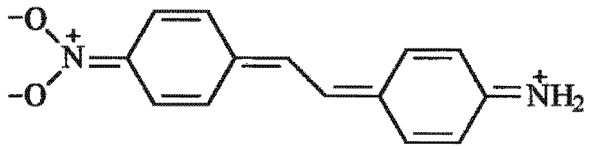

Figure 2.10: Resonance structure of 4,4'aminonitrostilbene with reduced π-bond character

The single bond character in the hybrid canonical forms of these conjugated systems reduces the resistance to rotation about the bond. This resistance could become so low that isomerisation readily occurs at room temperature, resulting in inseparable cis–trans isomers (as has been observed for the indigo molecule).[28] From the resonance structures proposed for the n-OST ligands (Figure 2.5) it can be seen that the alkene bond may also exist with reduced π-bond character and that similar cis-trans isomerisation, as observed for complexes **3, 3a, 5** and **5a**, is possible.

When ^{1}H- and ^{13}C-NMR spectra of complexes **3** and **5** were run immediately after sample preparation, only the trans isomers were observed. Subsequent ^{1}H- and ^{13}C-NMR spectra run after the samples had been kept for, at most, 6 hours at room temperature indicated the presence of another molecular gold(I) species (complexes **3a** and **5a**) coexisting with the previously observed species. Based on proton integration, the ratio of complexes **3:3a** and **5:5a** were 1:1 and 4:1 respectively. Crystallisation of complex **5** from dichloromethane/pentane at -25 °C also

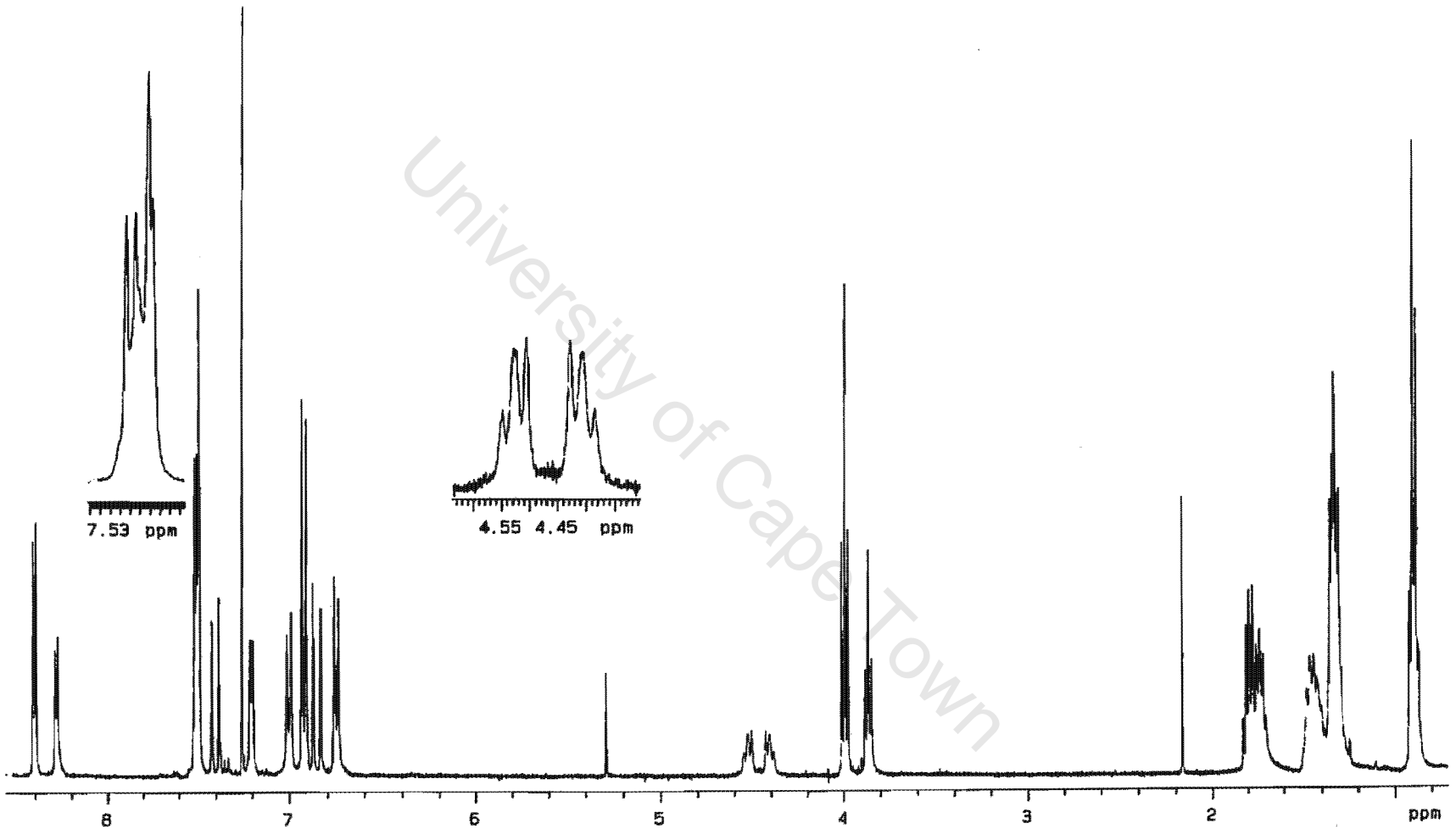

Figure 2.11: ^{1}H-NMR spectrum of complexes **5** and **5a** in $CDCl_3$.

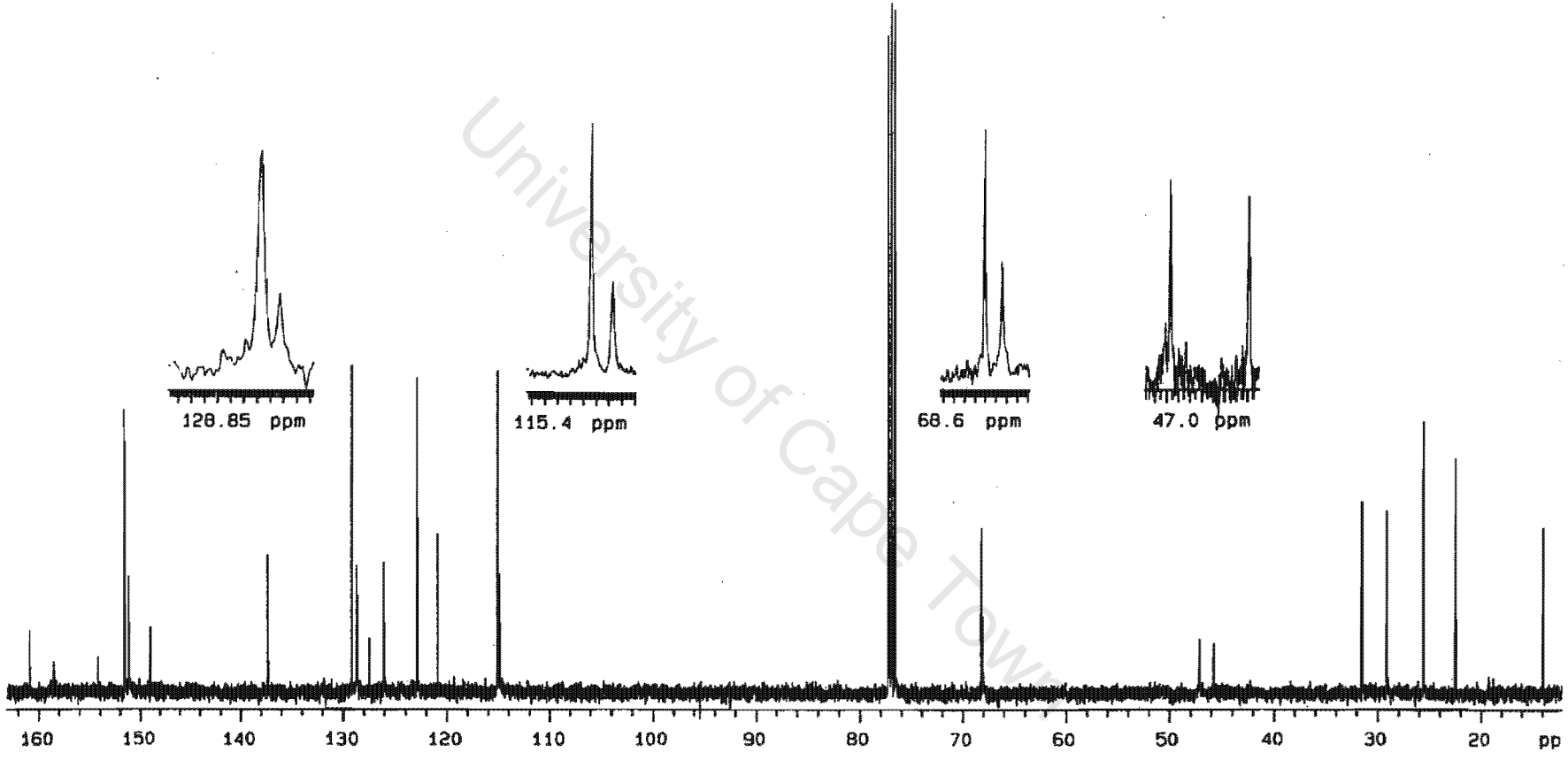

Figure 2.12: ^{13}C-NMR spectrum of complexes **5** and **5a** in $CDCl_3$.

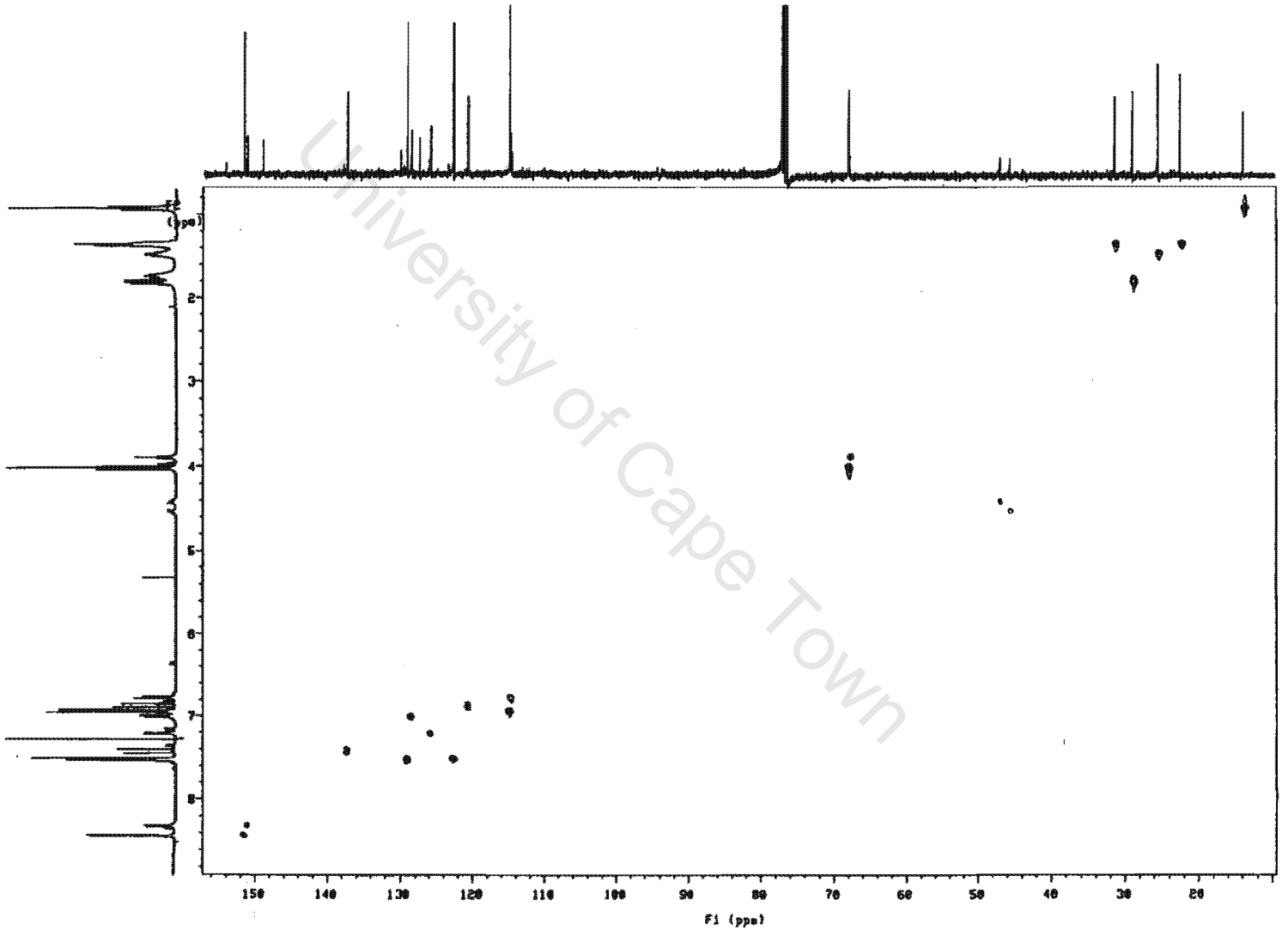

Figure 2.13: HETCOR spectrum of complexes **5** and **5a** in $CDCl_3$.

yielded a yellow powder consisting of a 3:2 mixture of complexes **5:5a**. Attempts to isolate complexes **3a** and **5a** from the mixtures via column chromatography were unsuccessful, as complexes **3a** and **5a** were unstable and decomposed immediately on the silica column.

^{1}H-, ^{13}C-NMR and HETCOR spectra of a mixture of complexes **5** and **5a** are presented in Figures 2.11-13 and the assignments for complexes **3, 3a, 5** and **5a** are presented in Appendix 2A, Tables 2A.8-9. The most significant differences between complexes **3, 5** and **3a, 5a** respectably is observed in the region of the C_d-C_e double bond. The δ values for C_d and C_e decrease dramatically from 120.9 and 137.4 ppm to 47.2 and 45.9 ppm respectively (Table 2A.9). This change provides evidence that the double bond character of the C_d-C_e bond has been replaced with the single bond character of a secondary or tertiary alkane. The integration of H_a vs H_d indicates that only one proton can be bonded to C_d and C_e. Therefore it could be a tertiary alkane group. Interestingly, both the H_d and H_e peak of complexes **3a** and **5a** have two coupling constants (Figure 2.11, Table 2A.8). The smaller coupling constant (7.2 and 8.6 Hz for complexes **3a** and **5a** respectively) could be the $^{3}J_{HH}$ coupling expected for the cis isomer of an alkene or, considering the single bond character of the C_d-C_e bond., a tertiary alkane. The larger coupling constant (17 and 18 Hz for complexes **3a** and **5a** respectively) could only be the $^{3}J_{HH}$ coupling expected for the trans isomer, indicating that some double bond character must still be present in complexes **3a** and **5a**.

According to proposed scheme (Scheme 2.4) the resonance structure for the trans complexes (R_{trans}) have reduced π-bond character and rotation about the C_d-C_e bond results in the formation of the resonance structure for the cis complexes (R_{cis}). The resonance structures with reduced π-bond character, R_{trans} and R_{cis}, for complexes **3, 3a, 5** and **5a** would have a higher electron density in the py ring. Complexes **3a** and **5a** both have upfield shifts of 0.12 and 0.32 ppm for

H_a and H_b respectively, relative to complexes **3** and **5**. This indicates increased shielding in accordance with the resonance model.

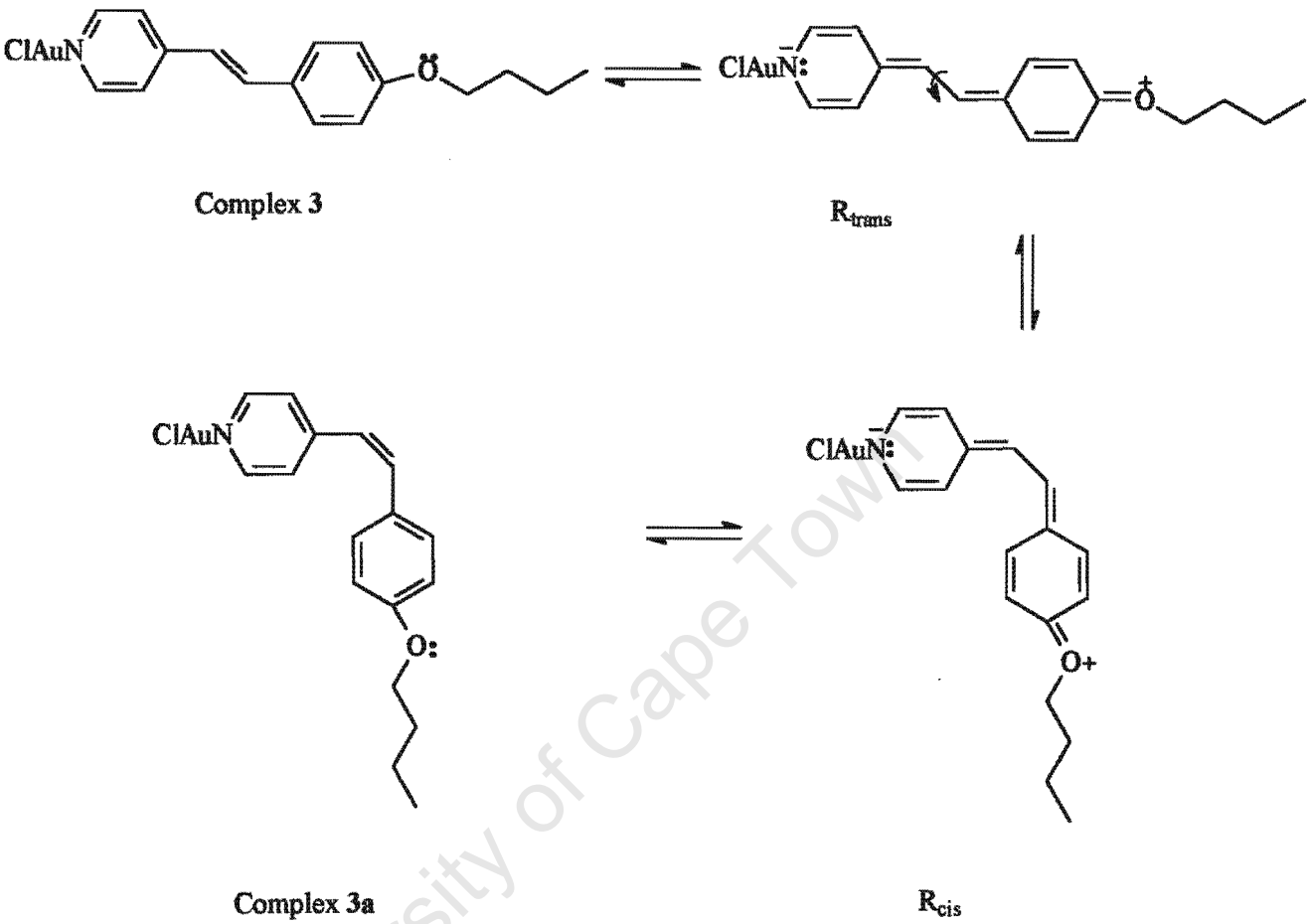

Complex **3** R_{trans}

Complex **3a** R_{cis}

Scheme 2.4: Proposed mechanism for cis-trans isomerisation for complexes **3** and **3a**

There is no conclusive proof that the cis isomer has been formed. Evidence from ^{1}H- and ^{13}C-NMR spectra for complexes **3, 3a, 5** and **5a** indicates the presence of a molecular species with reduced π bond character of the alkene group and increased electron density of the py ring. The fact the both H_d and H_e of complexes **3a** and **5a** have a cis and trans coupling constant might mean that complexes **3a** and **5a** are in fact mixtures of both cis and trans resonance structures.

2.3.8 Thermal behaviour of complexes 3-9.

The liquid crystalline properties of complexes **3-9** were evaluated via differential scanning calorimetry (DSC), thermogravimetric analysis (TG) and optical microscopy techniques. Complexes **3-9** are mesomorphic, exhibiting S_A phases with typical homeotropic textures (Plate 2.1). Although focal conic fan textures were also observed, the interesting texture depicted in Plate 2.2 was a more common occurrence.

A typical DSC thermogram of complex **4** (Figure 2.16) has one broad and one sharp endothermic peak corresponding to a solid state polymorphic transition and the mesophase transition temperature respectively. A broad exothermic peak is observed at the temperature at which the clearing point was optically observed. Clearing point transitions are usually endothermic events and broad exothermic peaks could be an indication of irreversible events such as decomposition[30] The enthalpy contribution of the clearing point transition of complexes **3-9** are therefore much less than the enthalpy contribution associated with decomposition.

A typical TG thermogram of complex **4** indicates a steady mass loss after about 200 °C (Figure 2.17). The extensive decomposition that is observed at the clearing point is a problem experienced when studying the mesomorphic properties of complexes **3-9**. Thus, the transition temperatures and enthalpy values recorded were obtained on the first heating run (Table 2.4) and are graphically represented in Figure 2.16. Thin layer chromatography (TLC) experiments conducted on the samples immediately after heating them to the clearing point indicated that metallic gold and free alkoxystilbazole ligand are products of decomposition.

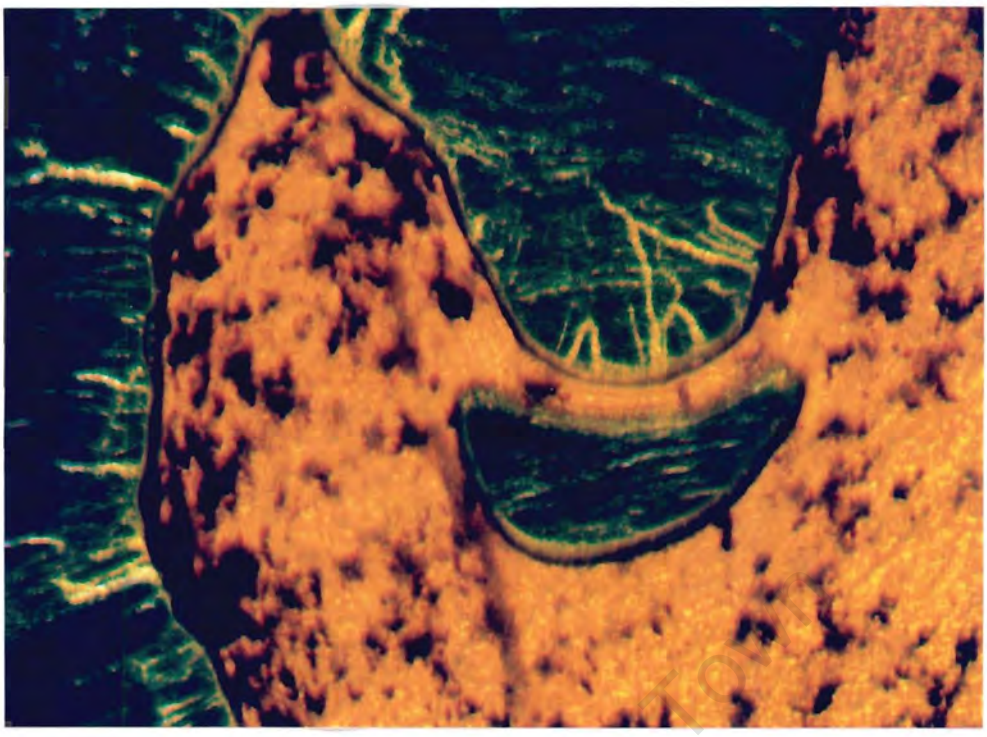

Plate 2.1: Homeotropic S_A texture of complex **9** at 160 °C (1st heating), cross-polarised light, and x10x4x2 magnification.

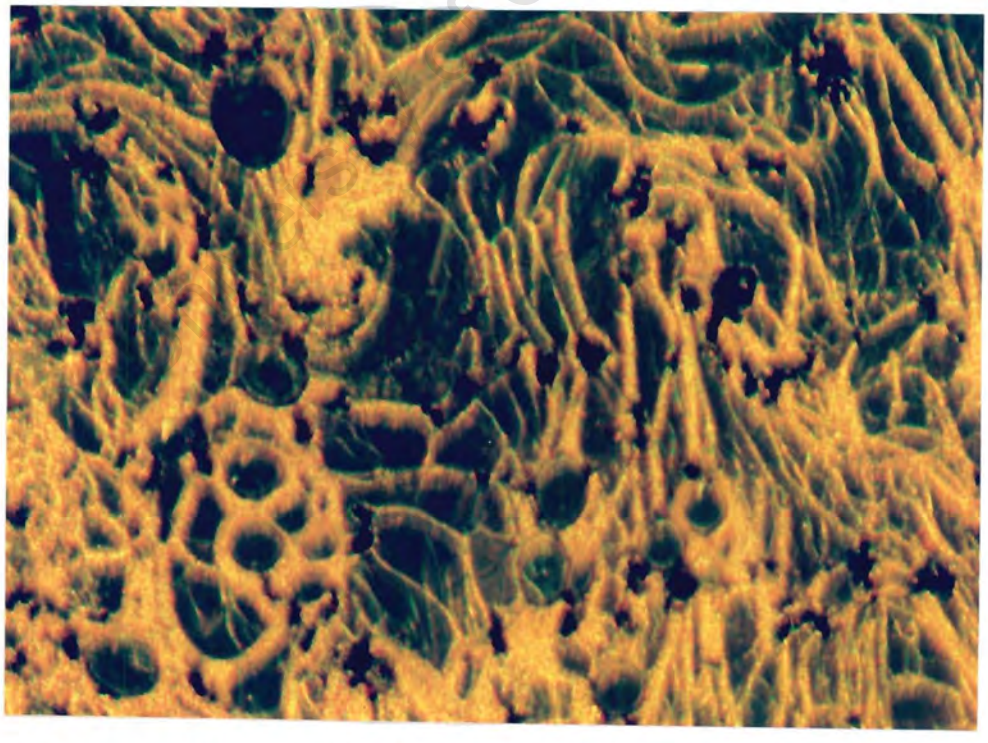

Plate 2.2: S_A texture of complex **4** at 160 °C (1st heating), cross-polarised light, and x10x4x2 magnification.

Table 2.4: DSC data of transitions in (°C) and ΔH (kJ.mol^{-1}) for complexes **3-9**

Complex	n	C-C'	C'-S_A	S_A-I[a]	Decomposition
3	4	130 (9.0)	153 (12.9)	175	168 (-6.9)
4	5	113 (8.9)	152 (11.7)	181	180 (-8.7)
5	6	121 (5.1)	147 (9.9)	182	168 (-18.1)
6	7	88 (7.0)	140 (11.5)	185	180 (-7.2)
7	8	72 (0.3)	139 (10.9)	193	183 (-7.4)
8	9	62 (18.2)	138 (10.1)	185	185 (-3.2)
9	10	60 (3.3)	135 (10.3)	177	182 (-7.6)

a = Clearing point transition temperatures (S_A-I) were determined optically using a Kofler hotstage microscope and are uncorrected. The temperature quoted is the final disappearance of anisotropy.

The polymorphic transition temperatures for complexes **3-9** decrease from 129 (complex **3**) to 60 °C (complex **9**) as n increases. The only anomaly observed is complex **5** (n = 6), where the transition is higher than expected. A possible explanation for the wide range in enthalpy values observed from 0.3 to 18.2 kJ.mol^{-1} (Table 2.4) might be the degree of crystallinity of the samples. In some cases, a highly crystalline sample yielded a large enthalpy value. When the same sample was dissolved and rapidly precipitated, the polymorphic transition was not observed. It is most likely that the sample formed by rapid precipitation was amorphous in nature and thus no structural rearrangement was possible.

The melting point transition temperatures for complexes **3-9** are generally quite high, ranging from 153 to 135 °C (Table 2.4) and decreases as n increases, similar to what was observed for the polymorphic transitions. This trend agrees with what is generally observed in liquid crystal systems. Complex **7** (n = 8) has previously been reported to form an unidentified mesophase at 120 °C,[15] but in this study undergoes melting at 139 °C. Both complexes have a similar clearing point though. The clearing points seem to be independent of alkoxy chain length and occur

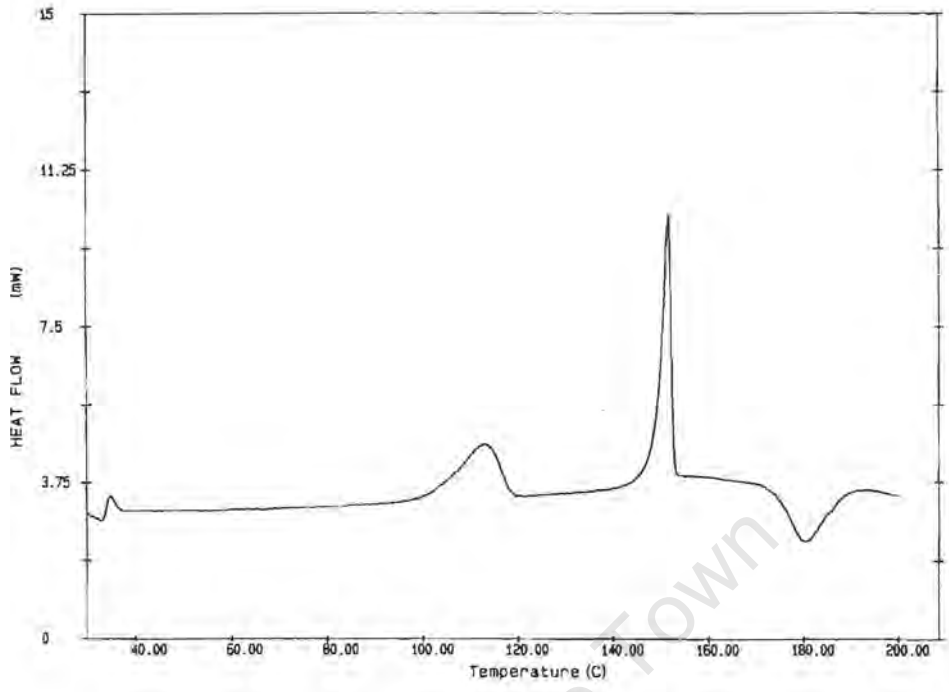

Figure 2.14: DSC thermogram of complex **4** with a 10 °C/min heating rate

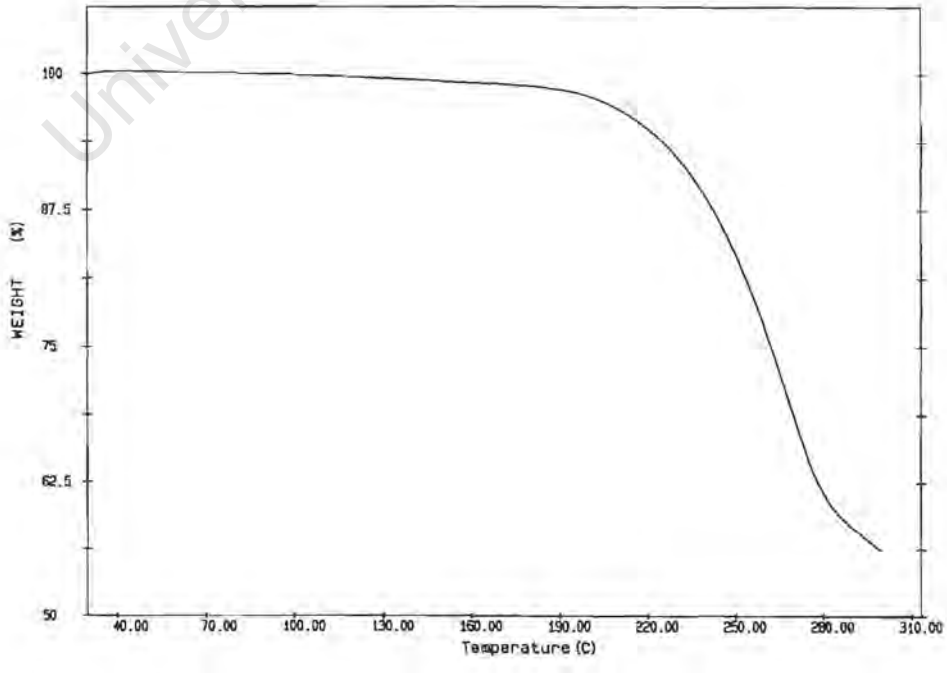

Figure 2.15: TG thermogram of complex **4** with a 10 °C/min heating rate

generally in the region 182 to 185 °C, except for complex **7**, which is slightly higher at 193 °C and complexes **3** or **9**, which are slightly lower at 175 or 177 °C, respectively (Table 2.4, Figure 2.16).

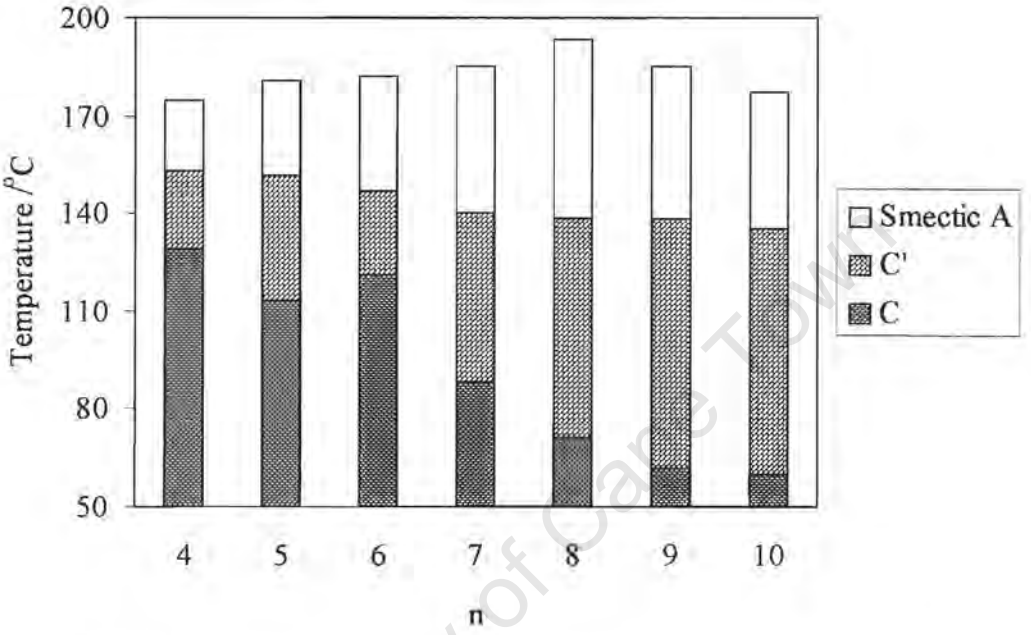

Figure 2.16: Graphical representation of transition temperatures for complexes **3-9**

Compared to the free ligands which are themselves mesomorphic (Figure 2.17),[1] the temperature range over which the mesophase exists in complexes **3-9** increases dramatically, but unfortunately so do the transition temperatures. The type of mesophases observed for complexes **3-9** also differs from the free ligands. The free n-OST ligands form monotropic S_B and S_E phases on supercooling from the isotropic liquid (n = 4) and enantiotropic S_B and S_E phases (n = 5-10) (Figure 2.17) but the gold(I) complexes **3-9** (n = 4-10) form only an enantiotropic, less ordered S_A mesophase. The free n-OST ligands also do not undergo solid state polymorphic transition, as observed for complexes **3-9**.

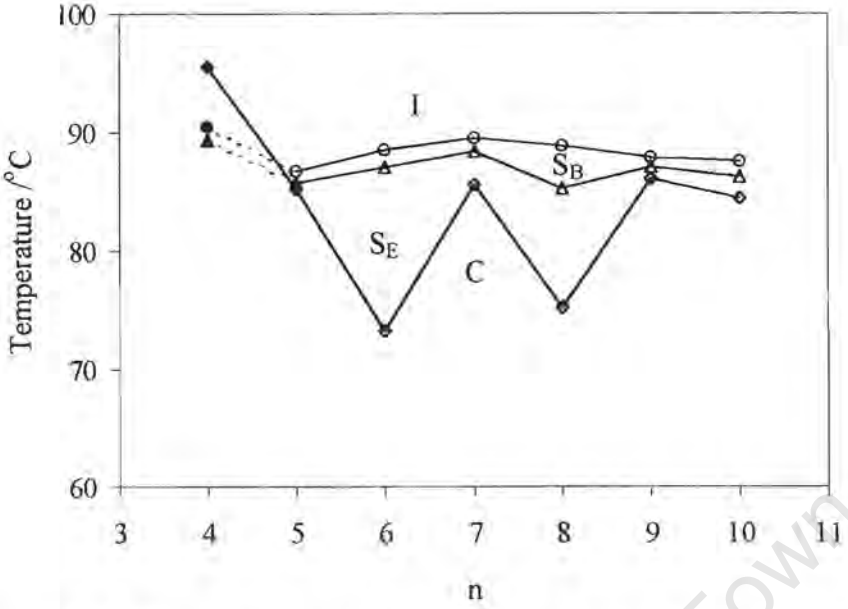

Figure 2.17: Transition temperatures and mesophases observed for n-OST ligands, n = 4-10[1]

It should also be noted that the crystal to S_E transitions of the free n-OST ligands show the odd-even effect, with transition temperatures being lower when the terminal alkyl chain contains an even number of carbon atoms. The effect is more pronounced in the smaller n-OST chain lengths. Although no odd-even effect was observed in the transition temperatures for the gold(I) complexes, the even numbered complexes **3** and **5** do appear to be less thermally stable, undergoing decomposition at lower temperatures than the other homologues (Table 2.4). Complexes **3** and **5** also appear to undergo cis-trans isomerisation more readily. The cis-trans isomerisation might offer a low-energy pathway for decomposition, as the cis isomer was observed to be less stable than the trans isomer (section 2.3.7).

2.4 Summary

In conclusion, the following were established in chapter2:

1. ClAuL complexes are more stable when L is vnlpy and n-OST compared to py, due to conjugation and delocalisation of electrons.

2. Methylene groups next to the ether group in n-OST ligands vibrate at higher energies than methylene groups further away and this is most pronounced when n = 4 to 6.

3. The conjugation is enhanced when the ligands are complexed to gold(I).

4. Trends in $\Delta\delta$ (ppm) of H_a and C_a for complexes **1-9** relative to free ligands could indicate that π back-bonding in Au-L bonds increase in the order py < vnlpy < n-OST. These trends could also mean that the enhanced conjugation effect decreases in the order py > vnlpy when py or vnlpy bonds with gold(I). A positive $\Delta\delta$ (ppm) of H_a for ClAu(7-n-OST) complexes though, cannot be explained on the basis of conjugation effects and unambiguously suggests that increased that π back-bonding occurs for n-OST ligands compared to vnlpy or py.

5. ν(C=N) values suggest that ClAu(vnlpy) and ClAu(n-OST) complexes may have stronger Au-N bonds than ClAu(py).

6. Complexes **1-9** appear to have a neutral monomeric structure in acetone, which may also be monomeric on the basis of the FAB-MS of complex **4**. This is contrary to the fact that complex **1** has been reported to form a tetrameric ionic species in the solid state when crystallised from ethanol. Two ν(C=N) peaks observed in dichloromethane for complex **2** indicates that possibly both the neutral and ionic species of complex **2** coexist in this solvent. Attempts at determining the solid state structure of complexes **3-9** were unsuccessful.

7. ^{1}H- and ^{13}C-NMR spectroscopic data indicate that complexes **3** and **5** undergo thermal cis-trans isomerisation to form complexes **3a** and **5a**, but it was not possible to isolate the cis isomers.

8. Complexes **3-9** form S_A mesophases at much higher temperatures, with much larger ranges of mesophase existence compared to the free n-OST ligands, which form S_B and S_E phases. This is probably a result of stronger intermolecular attractions due to the enhanced polarisation effects and the introduction of the Au-Cl dipole moment when the gold(I) complexes were formed.

Unfortunately, in part due to the higher transition temperatures, complexes **3-9** decompose at the clearing point.

9. The melting point transitions for complexes **3-9** were found to decrease regularly as the alkoxy chain length increased.

2.5 References

1. D. W. Bruce, D. A. Dunmur, E. Lalinde, P. M. Maitlis and P. Styring, *Liquid Crystals*, 1988, **3**, 385.
2. D. W. Bruce, *J. Chem. Soc., Dalton Trans.*, 1993, 2983.
3. M. B. Ros, Other Physical Properties and Possible Applications of Metallomesogens, in *Metallomesogens: Synthesis, Properties, and Applications*, ed. J.L. Serrano, VCH, Weinheim, 1st edn.1996, ch. 11, pp. 419-480.
4. M. Benouazzane, S. Coco, P. Espinet and J.M. Martín-Alvarez, *J. Mater. Chem.*, 1995, **5**, 441.
5. S. Coco, P. Espinet, S. Falagán and J.M. Martín-Alvarez, *New. J. Chem.*, 1995, **19**, 959.
6. S. Coco, P. Espinet, J.M. Martín-Alvarez and A. Levelut, *J. Mater. Chem.*, 1997, **7**, 19.
7. A. Giroud-Godquin and P. M. Maitlis, *Angew. Chem., Int. Ed. Engl.*, 1991, **30**, 375.
8. Von H.-N. Adams, W. Hiller and J. Strähle, *Z. anorg. allg. Chem.*, 1982, **485**, 81.
9. W. Conzelmann, W. Hiller and J. Strähle, *Z. anorg. allg. Chem.*, 1984, **512**, 169.
10. W. Schneider, A Bauer and H. Schmidbaur, *J. Chem. Soc. Dalton Trans.*, 1997, 415.
11. E. J. Starr, Ph.D. Thesis, University of Cape Town, 1997.
12. R. F. Heck, *Palladium Reagents in Organic Synthesis*, Academic Press Ltd., London, 1985, ch. 6, pp. 179-321.
13. M. S. Kharasch and H. S. Isbell, *J. Am. Chem. Soc.*, 1930, **52**, 2919.
14. P. C. Ráy and D. C. Sen, *J. Indian Chem. Soc.*, 1930, **7**, 67.
15. D. W. Bruce, E. Lalinde, P. Styring, D. A. Dunmur and P. Maitlis, *J. Chem. Soc., Chem. Commun.*, 1986, 581.
16. R. Uson, A. Laguna and P. Brun, *J. Organomet. Chem.*, 1979, **182**, 449.
17. R. Uson, A. Laguna and J. Vicente, *J. Organomet. Chem.*, 1977, **131**, 471.
18. R. Uson, A. Laguna, M Laguna, I. Colera and E. de Jesús, *J. Organomet. Chem.*, 1984, **263**,

121.

19. J. Barberá, X-ray Studies of Metallomesogens in *Metallomesogens: Synthesis, Properties and Applications*, eds. J. L. Serrano, VCH, Germany, 1996, ch. 8, pp. 325- 348.

20. M. J. Baena, P. Espinet, M. C. Lequerica and A. M. Levelut, *J. Am. Chem. Soc.*, 1992, **114**, 4182.

21. J. Barberá, A. Elduque, R. Giménez, F. J. Lahoz, J. A. López, L.A. Oro and J.L. Serrano, *Inorg. Chem.*, 1998, **37**, 2960.

22. S. J. Kim, S. H. Kang, K. Park, H. Kim, W. Zin, M. Choi and K. Kim, *Chem. Mater.*, 1998, **10**, 1889.

23. F. A. Bovey, *Nmr data tables for organic compounds*, John Wiley and Sons, USA, 1967, vol. 1, p. 610.

24. D. J. Price, K. Willis, T. Richardson, G. Ungar and D. W. Bruce, *J. Mater. Chem.*, 1997, **7**, 883.

25. R. J. Puddephatt, Gold in *Comprehensive Coordination Chemistry , The Synthesis, Reactions, Properties and Applications of Coordination Compounds*, eds. G. Wilkinson, R. D. Gillard and J. A. McCleverty, Pergamon, England, 1st edn., 1987, vol. 5, ch. 55, pp 861-923.

26. M. Munakata, S. Yan, M. Maekawa, M. Akiyama and S. Kitagawa, *J. Chem. Soc., Dalton Trans.*, 1997, 4257.

27. K. Mackenzie in , The Chemistry of Alkenes, ed. S. Patai, Interscience Publishers, London, 1st edn., 1964, ch. 7, pp. 387-468.

28. M. Calvin and R. E. Buckles, *J. Am. Chem. Soc.*, 1940, **62**, 3324.

29. M. Calvin and H. W. Alter, *J. Chem. Phys.*, 1951, **19**, 765.

30. H. H. Willard, L. L. Meritt, Jr., J. A. Dean and F. A. Settle, Jr., Thermal Analysis in *Instrumental methods of analysis*, Wadsworth Publishing Company, California, 7th edn.,

1988, ch. 25, pp. 761-785.

31. Y. Nakao and K. Sone, *J. Chem. Soc., Chem., Commun.*, 1996, 897.

Appendix 2A

Table 2A.1: FT-IR spectroscopic data (in cm^{-1}) for free py, vnlpy and n-OST ligands[a]

L	ν(C-H)[b]	ν(C-H)[c]	ν(C=C)	ν(C=N)	ν(C-C)	ν(O-C)	ν(C-H)[d]
py	3040 s		1599 s 1483 s	1439 vs			
vnlpy	3094 m[e] 3045 s		1597 vs 1548 vs 1495 s	1409 vs			991 vs 929 vs 1859 m[f]
4-OST	3071 w[e] 3034 m	2961 s 2874 s	1592 vs 1550 w 1512 s 1475 m	1417 s	1252 vs	1193 s 1175 vs	968 s
5-OST	3071 w[e] 3035 m	2958 s 2873 s	1592 vs 1550 w 1512 s 1470 m	1417 s	1253 vs	1193 s 1175 vs	968 s
6-OST	3071 w[e] 3034 m	2932 s 2860 s	1592 vs 1551 w 1512 s 1470 m	1416 s	1249 vs	1193 s 1175 vs	968 s
7-OST	3072 w[e] 3035 m	2931 s 2858 s	1592 vs 1550 w 1512 s 1470 m	1417 s	1253 vs	1193 s 1175 vs	968 s
8-OST	3072 w[e] 3035 m	2929 s 2856 s	1592 vs 1550 w 1512 s 1470 m	1417 s	1253 vs	1193 s 1175 vs	968 s
9-OST	3072 w[e] 3034 m	2928 s 2856 s	1592 vs 1550 w 1512 s 1470 m	1417 s	1253 vs	1193 s 1175 vs	968 s
10-OST	3072 w[e] 3034 m	2927 s 2856 s	1592 vs 1550 w 1512 s 1470 m	1417 s	1252 vs	1193 s 1175 vs	968 s

a = spectra were obtained using dichloromethane solution cells with NaCl windows, b = aromatic stretch, c= alkane stretch, d = alkane out-of-plane bend, e = alkene, f = overtone. w = weak, m = medium, s = strong, vs = very strong.

Table 2A.2: FT-IR spectroscopic data (in cm^{-1}) for ClAu(L) complexes **1-9**[a]

Complex	L	ν(C-H)[b]	ν(C-H)[c]	ν(C=C)	ν(C=N)	ν(C-C)	ν(O-C)	ν(C-H)[d]	ν(Au-Cl)[e]
1	py	3043 m		1611 s 1486 m	1454 vs				349 s
2	vnlpy	3098 m[f] 3048 s		1620 vs 1546 s 1501 s	1433 vs 1417 vs			987 vs 941 vs 1884 m[g]	353 s
3	4-OST	3046 m	2961 s 2874 s	1599 vs 1513 s 1475 m	1436 s	1250 vs	1198 s 1175 vs	969 s	355 s
4	5-OST	3046 m	2958 s 2873 s	1599 vs 1513 s 1470 m	1437 s	1251 vs	1198 s 1175 vs	968 s	361 s
5	6-OST	3044 m	2933 s 2860 s	1599 vs 1513 s 1469 m	1436 s	1250 vs	1198 s 1175 vs	968 s	353 s
6	7-OST	3044 m	2930 s 2858 s	1599 vs 1513 s 1469 m	1437 s	1251 vs	1198 s 1174 vs	968 s	357 s
7	8-OST	3045 m	2929 s 2856 s	1599 vs 1513 s 1469 m	1437 s	1251 vs	1198 s 1174 vs	968 s	341 s
8	9-OST	3045 m	2928 s 2856 s	1599 vs 1513 s 1469 m	1437 s	1254 vs	1198 s 1174 vs	968 s	348 s
9	10-OST	3047 m	2927 s 2855 s	1599 vs 1513 s 1469 m	1437 s	1251 vs	1198 s 1174 vs	968 s	342 s

a = spectra were obtained using dichloromethane solution cells with NaCl windows except ν(Au-Cl), b = aromatic stretch, c= alkane stretch, d = alkane out-of-plane bend, e = obtained as a nujol mull between polyethylene sheets, f = alkene, g = overtone, m = medium, s = strong, vs = very strong.

Table 2A.3: ^{1}H- and ^{13}C-NMR spectroscopic data for complexes **1-2** and their free ligands in $CDCl_3$.

Compound	δ (ppm)					J (Hz)			
	H_a	H_b	H_c			H_a-H_b	H_b-H_c	H_a-$H_{a'}$	H_b-$H_{b'}$
	2H	2H	1H						
py[a]	8.39 td	7.04 dddd	7.43 dtt			4.2	7.6	0.4	1.7
ClAu(py)[a]	8.61 td	7.57 ddd	8.03 tt			4.9	7.8	-	1.6
	H_a	H_b	H_d	H_e^{trans}	H_e^{cis}	H_a-H_b	H_b-$H_{b'}$	H_d-H_e^{trans}	H_d-H_e^{cis}	H_e^{cis}-H_e^{trans}
	2H	2H	1H	1H	1H					
vnlpy[b]	8.44 dd	7.13 dd	6.52 dd	5.83 dd	5.35 dd	4.4	1.7	17.6	10.9	0.6
ClAu(vnlpy)[b]	8.52 dd	7.49 dd	6.70 dd	6.15 d	5.76 d	5.2	1.6	17.4	10.8	-
	δ (ppm)									
	C_a	C_b	C_c	C_d	C_e					
py	149.4	123.4	135.7	-	-					
ClAu(py)	152.2	126.8	139.9	-	-					
vnlpy	150.0	134.6	144.5	120.6	118.5					
ClAu(vnlpy)	152.0	132.9	148.4	123.4	123.2					

a = ABB'XX' spin system, b = AA'XX' and ABC spin systems, d = doublet, t = triplet.

Table 2A.4: ^{1}H-NMR spectroscopic data for n-OST ligands in $CDCl_3$.

n	H_a AA'XX' 2H	H_b AA'BB' 2H	H_d AB 1H	H_e AB 1H	H_g AA'XX' 2H	H_h AA'XX' 2H	H_j t 2H	H_k qn 2H	H_l qn 2H	H_m m	H_n t 3H
4	8.53 (6.4)	7.31 (6.0)	6.85 (16.4)	7.23 (16.0)	7.45 (8.8)	6.90 (8.8)	3.98 (6.6)	1.77 (7.0)	1.50[a] (7.4)	-	0.98 (7.4)
5	8.53 (6.0)	7.32 (6.4)	6.86 (16.4)	7.24 (15.6)	7.46 (8.8)	6.90 (8.8)	4.00 (6.6)	1.80 (7.0)	1.41[b]	1.41[b]	0.94 (7.2)
6	8.54 (6.0)	7.32 (6.0)	6.86 (16.6)	7.25 (16.4)	7.46 (8.8)	6.91 (8.8)	3.98 (6.5)	1.79 (6.7)	1.47 (7.4)	1.34 4H	0.91 (7.1)
7	8.53 (6.2)	7.31 (6.2)	6.85 (16.3)	7.23 (16.3)	7.45 (8.9)	6.89 (8.9)	3.96 (6.5)	1.78 (7.1)	1.46 (7.6)	1.33 6H	0.89 (6.9)
7[c]	8.52 (6.0)	7.34 (6.4)	6.90 (16.0)	7.28 (16.4)	7.49 (8.4)	6.91 (8.8)	3.99 (6.6)	1.80 (7.1)	1.46 (6.7)	1.33 6H	0.91 (7.0)
8	8.53 (6.0)	7.31 (6.0)	6.85 (16.4)	7.24 (16.8)	7.45 (8.8)	6.90 (8.8)	3.97 (6.4)	1.79 (7.2)	1.46 (7.6)	1.29 8H	0.89 (7.0)
9	8.54 (6.0)	7.32 (6.0)	6.86 (16.4)	7.24 (16.0)	7.46 (8.8)	6.90 (8.8)	3.98 (6.6)	1.79 (7.2)	1.46 (7.6)	1.28 10H	0.88 (6.8)
10	8.54 (6.4)	7.32 (6.4)	6.86 (8.8)	7.24 (16.0)	7.46 (9.2)	6.90 (8.8)	3.98 (6.4)	1.79 (7.1)	1.46 (7.6)	1.28 12H	0.88 (7.0)

a = sextet, b = one signal which forms a multiplet intergrating for 4H, c = in CD_2Cl_2, t = triplet, qn = quintet, m = multiplet.

Table 2A.5: ^{1}H-NMR spectroscopic data for ClAu(n-OST) complexes **3-9** in $CDCl_3$.

Complex	n	H_a AA'XX' 2H	H_b AA'BB' 2H	H_d AB 1H	H_e AB 1H	H_g AA'XX' 2H	H_h AA'XX' 2H	H_j t 2H	H_k qn 2H	H_l qn 2H	H_m m	H_n t 3H
3	4	8.41 (6.8)	7.49 (7.0)	6.85 (16.0)	7.40 (16.0)	7.51 (8.9)	6.92 (8.4)	4.00 (6.4)	1.78 (7.0)	1.50[a] (7.5)	-	0.98 (7.4)
4	5	8.41 (6.8)	7.50 (6.8)	6.86 (16.4)	7.40 (16.0)	7.51 (8.8)	6.92 (8.4)	4.00 (6.6)	1.80 (7.0)	1.41[b]	1.41[b]	0.93 (7.0)
5	6	8.41 (6.8)	7.50 (6.8)	6.86 (16.4)	7.40 (16.4)	7.51 (9.2)	6.93 (8.8)	4.00 (6.6)	1.80 (7.2)	1.47 (7.6)	1.34 4H	0.91 (7.0)
6	7	8.41 (6.9)	7.50 (6.8)	6.86 (16.2)	7.40 (16.2)	7.51 (9.2)	6.92 (8.7)	3.99 (6.6)	1.80 (7.0)	1.46 (7.1)	1.32 6H	0.89 (7.0)
7	8	8.41 (6.8)	7.50 (6.8)	6.86 (16.4)	7.40 (16.0)	7.51 (9.2)	6.92 (8.8)	3.99 (6.6)	1.79 (7.1)	1.46 (7.3)	1.31 8H	0.88 (6.8)
8	9	8.41 (6.8)	7.50 (6.8)	6.86 (16.0)	7.40 (16.4)	7.51 (8.8)	6.92 (8.8)	3.99 (6.4)	1.79 (7.1)	1.46 (7.2)	1.28 10H	0.88 (6.8)
9	10	8.42 (6.8)	7.50 (6.8)	6.86 (16.4)	7.40 (16.4)	7.51 (9.2)	6.93 (8.8)	3.99 (6.6)	1.80 (7.0)	1.46 (7.3)	1.27 12H	0.88 (6.8)

a= sextet, b = one signal which forms a multiplet intergrating for 4H, t = triplet, qn = quintet, m = multiplet.

Table 2A. 6: ^{13}C-NMR spectroscopic data for n-OST ligands in $CDCl_3$.

n	C_a	C_b	C_c	C_d	C_e	C_f	C_g	C_h	C_i	C_j	C_l	$C_{k,m}$	C_n
4	150.0	120.5	145.0	123.5	132.7	128.6	128.3	114.8	159.7	67.7	19.2	31.2	13.8
5	150.0	120.5	145.0	123.5	132.7	128.6	128.3	114.8	159.7	68.1	28.1	28.9, 22.4	13.9
6	150.0	120.5	145.0	123.5	132.7	128.6	128.3	114.8	159.7	68.1	25.6	31.5, 29.1, 22.5	14.0
7	150.0	120.5	145.0	123.5	132.7	128.6	128.3	114.8	159.7	68.1	25.9	31.7, 29.2, 29.0, 22.5	14.0
7[a]	140.3	110.7	135.1	113.7	122.8	118.9	118.5	104.9	150.1	58.4	16.2	22.0, 19.4, 19.2, 12.8	4.0
8	150.0	120.5	145.0	123.5	132.7	128.6	128.3	114.8	159.7	68.1	26.0	31.7, 29.4, 29.3, 29.2, 22.6	14.0
9	150.1	120.6	145.0	123.5	132.8	128.7	128.3	114.8	159.8	68.1	26.0	31.8, 29.5, 29.4, 29.3, 29.2, 22.6	14.1
10	150.0	120.5	145.0	123.5	132.8	128.6	128.3	114.8	159.7	68.1	26.0	31.8, 29.5, 29.5, 29.3, 29,2, 29.1, 22.6	14.0

a = in CD_2Cl_2.

Table 2A.7: ^{13}C-NMR spectroscopic data for ClAu(n-OST) complexes **3-9** in $CDCl_3$.

Complex	n	C_a	C_b	C_c	C_d	C_e	C_f	C_g	C_h	C_i	C_j	C_l	$C_{k,m}$	C_n
3	4	151.6	122.8	149.0	120.8	137.3	127.5	129.1	115.0	160.8	67.9	19.1	31.1	13.7
4	5	151.6	122.8	149.0	120.8	137.3	127.5	129.1	115.0	160.8	68.2	28.1	28.8, 22.4	13.9
5	6	151.6	122.8	149.0	120.8	137.4	127.5	129.1	115.0	160.8	68.2	25.6	31.5, 29.1, 22.5	14.0
6	7	151.6	122.8	149.0	120.8	137.3	127.5	129.1	115.0	160.8	68.2	25.9	31.7, 29.1, 29.0, 22.5	14.0
7	8	151.6	122.8	149.0	120.8	137.3	127.5	129.1	115.0	160.8	68.2	25.9	31.7, 29.3, 29.2, 29.1, 22.6	14.0
8	9	151.6	122.8	149.0	120.8	137.3	127.5	129.1	115.0	160.8	68.2	25.9	31.8, 29.4, 29.3, 29.2, 29.1, 22.6	14.0
9	10	151.6	122.8	149.0	120.8	137.3	127.5	129.1	115.0	160.8	68.2	25.9	31.8, 29.5, 29.5, 29.3, 29.2, 29.1, 22.6	14.0

Table 2A.8: ^{1}H-NMR spectroscopic data for ClAu(n-OST) complexes **3/3a** and **5/5a**.

Complex	n	H_a AA'XX' 2H	H_b AA'BB' 2H	H_d AB 1H	H_e AB 1H	H_g AA'XX' 2H	H_h AA'XX' 2H	H_j t 2H	H_k qn 2H	H_l qn 2H	H_m m	H_n t 3H
3	4	8.39 (5.2)	7.49 (5.6)	6.84 (16.4)	7.38 (16.0)	7.48 (6.4)	6.91 (7.6)	3.99 (6.6)	1.77 (6.4)	1.46[a] (7.6)	-	0.97 (7.2)
3a	4	8.27 (4.8)	7.17 (5.6)	4.37 (17.2) (7.6)	4.50 (16.8) (6.8)	6.97 (7.6)	6.74 (7.6)	3.86 (6.4)	1.71 (7.0)	1.46[a] (7.6)	-	0.94 (7.4)
5	6	8.39 (6.7)	7.48 (5.2)	6.84 (16.0)	7.38 (16.0)	7.49 (8.8)	6.91 (8.4)	4.98 (6.6)	1.78 (6.8)	1.45 (7.4)	1.32 4H	0.89 (6.8)
5a	6	8.28 (6.7)	7.18 (6.4)	4.38 (17.6) (8.0)	7.51 (18.4) (9.2)	6.97 (8.4)	6.74 (8.8)	3.85 (6.6)	1.72 (7.2)	1.45 (7.4)	1.32 4H	0.89 (6.8)

a = octet intergrating for 2H, t = triplet, qn = quintet, m = multiplet.

Table 2A.9: ^{13}C-NMR spectroscopic data for ClAu(n-OST) complexes **3/3a** and **5/5a**

Complex	n	C_a	C_b	C_c	C_d	C_e	C_f	C_g	C_h	C_i	C_j	C_l	$C_{k,m}$	C_n
3	4	151.6	122.9	149.1	120.9	137.4	127.6	129.2	115.1	160.9	67.9	19.2	31.2	13.9
3a	4	151.2	126.0	154.2	47.2	45.9	128.6	128.7	115.0	158.6	67.8	19.2	31.2	13.8
5	6	151.6	122.9	149.1	120.9	137.4	127.5	129.2	115.1	160.9	68.3	25.7	31.6, 29.2, 22.6	14.0
5a	6	151.2	126.1	154.2	47.2	45.9	128.6	128.7	114.9	158.6	68.1	25.7	31.5, 29.2, 22.6	14.0

CHAPTER 3. Synthesis, characterisation and mesomorphic behaviour of RAuL complexes, R = perhalophenyl and L = 7-OST

3.1 Introduction

In this chapter, the synthesis and characterisation of complexes of the type RAu(L), L = 7-OST and R = C_6F_5, 2-C_6F_4Br, 4-C_6F_4Br or μ-4,4'-$C_6F_4C_6F_4$ will be discussed. These complexes are all mesomorphic and their liquid crystalline properties are discussed and compared with complex **6**, ClAu(7-OST), discussed in section 2.3.8. As similar RAu(isocyanide) complexes were recently reported by Pablo Espinet and co-workers[1] to exhibit liquid crystalline behaviour, the RAu(n-OST) complexes **11**, **13**, **15** and **18** were contrasted with these complexes. The crystal structure of complex **11** was elucidated and its molecular structure was investigated.

3.1.1 Importance of fluorine in liquid crystalline materials

Fluoro-substitution in organic arene liquid crystalline compounds is commonly used to give liquid-crystals with lower melting points and to give molecules increased positive or negative dielectric anisotropy.[2] The strong dipole moment of the carbon-fluorine bond is responsible for the increased dielectric anisotropy. One disadvantage of adding fluorine substituents though, is a resulting decrease in the clearing temperatures by about 25-30 °C per fluorine substituent.[3] Nonetheless, organic liquid crystals with highly fluorinated aromatic substructures meet most of the criteria required for liquid crystal displays, such as high dielectric anisotropy and low rotational viscosity. They are commonly used as

major components of liquid-crystal mixtures for active matrix displays.[3] Fluorine substituents in metal-containing liquid crystal systems have been found in general to induce properties similar to those observed in conventional organic liquid crystals and have recently also been introduced to gold(I) liquid crystal systems.[1,4]

3.1.2 Arylgold(I) chemistry

The first arylgold(I) complex was synthesised in 1931,[5] but it was only after 1970 that arylgold(I) chemistry matured, with about 495 new compounds being reported by 1985.[6] The recent rapid development is due to the use of perhaloaryl species (*e.g.* C_6F_6, C_6Cl_5, C_6Br_5, $C_6F_3H_2$) in the synthesis and isolation of arylgold(I) complexes.[7,8] The perhaloarylgold(I) complexes have been found to be particularly thermally stable, most probably due to the strong electron-withdrawing nature of the perhaloaryl group.

Organometallic transition-metal complexes with perfluorinated ligands are generally found to be thermally more stable than their hydrocarbon equivalents and this can be attributed to a combination of thermodynamic and kinetic factors.[9] Metal fluorides are the most likely decomposition products and their higher lattice energies suggests that the perfluorinated transition metal complexes should be thermodynamically less stable than the hydrocarbon analogues. Higher thermal stability is thus most likely attributable to the perfluorinated complexes having greater bond dissociation energy. The low-lying π^* molecular orbitals effectively lend themselves to metal-arene backbonding, in the case of perfluoro-substituted arene groups, thereby increasing the metal-carbon bond strength.[9]

Perhalophenyl, as opposed to phenyl groups, were thus chosen because of their relative stabilities[9] and because the electronegative fluorine atom has been shown to impart higher polarisabilities compared to non-fluorinated liquid crystalline compounds.[2,3] These higher polarisabilities have important implications in liquid crystal technologies.

A search of the Cambridge Crystallographic Database, CCD,[10] for linear two-coordinate gold(I) complexes revealed 45 structures where gold is bonded to phenyl (or substituted phenyl) rings and 11 structures where gold is bonded to py (or substituted py) rings (Table 3.1). Weak Au...Au intermolecular bonding interactions (section 1.4.1) were reported for some of the structures, but they were still considered as two-coordinate complexes.

Table 3.1: Results of CCD search (October 1998) for RAuL complexes.

R-group search fragment	Atom of L group which bonds with Au^I	Total number of structures found
	Phenyl	
C_6H_5Au-	P	6
C_6F_5Au-	C (12 structures) P (10 structures) Cl, Se, N or S (1 structure each)	26
C_6Au-[a]	P (9 structures) N, C, Cl or As (1 structure each)	13
	Pyridine	
C_5H_5NAu-	Br (2 structures) Cl, I or C (1structure each)	5
C_5NAu-[b]	P (5 structures) Cl (1 structure)	6

a = other than C_6H_5Au- or C_6F_5Au-. b = other than C_5H_5NAu-

From Table 3.1 it can be seen that no crystal structures of two-coordinate linear arylgold(I) complexes with py ligands and only two structures with other nitrogen-donor

ligands have been reported. The crystal structure of a binuclear mesitylgold(I) complex (Figure 3.1) with a bridging C≡N group has been determined,[11] but the C≡N group was reported to be disordered and the Au^{I}-N bond length was not well determined. The other structure is a C_6F_5gold(diphenyldiazo) complex (Figure 3.2). [12]

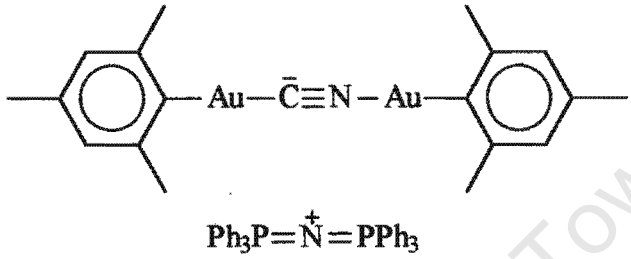

Figure 3.1: Molecular structure of a mesitylgold(isocyanide) complex[11]

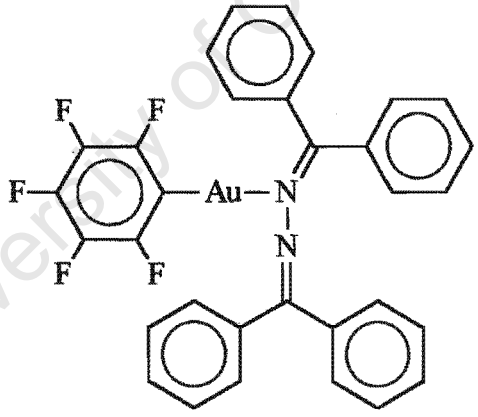

Figure 3.2: Molecular structure of perfluorophenylgold(diphenyldiazo)[12]

In the case of the mesityl arene group, the ortho substituents play a major role in stabilising gold(I) complexes[13] and probably prevents rotation of the aryl group as proposed for square-planar complexes of the type M(mesityl) $_2(PR_3)_2$, M = Ni, Pd and Pt.[14,15] The mesityl group is forced into a conformation that ensures optimal overlap

between the filled π d-orbitals, d_{xz} and d_{yz}, of gold(I) (section 2.3.1) and empty π* orbitals of the aryl group. Based on types of arylgold(I) complexes reported in the literature[6,7,8] and structures obtained from the CCD, $C_6H_5Au^I(L)$ complexes are stable when L is a phosphine or isocyanide ligand. All other types of L groups, even some isocyanide ligands, seem to require ligands with substituted phenyl rings such as mesityl[11] or perhaloaryl groups[6,7,8] to form stable aryl-Au^I bonds. This is due to the large trans effect observed for RAuL complexes (section 4.1).

Although the only reported crystal structure in the CCD of an organometallic $Au^I(py)$ complex is a trinuclear mixed Au^I and Au^{III} complex containing the tridentate bis(diphenylphosphino)methanide ligand,[16] the binuclear μ-4,4'-bipy$(AuC_6F_5)_2$ complex has been prepared as a white air- and moisture-stable solid (Figure 3.3).[17]

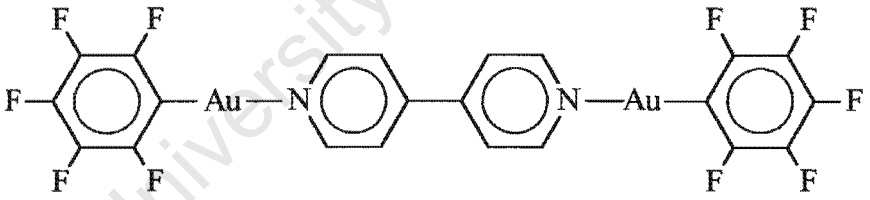

Figure 3.3: Molecular structure of μ-4,4'-bipy$(AuC_6F_5)_2$[17]

3.2 Synthetic Method

3.2.1 Synthesis of RAu(tht) complexes

RAu(tht) complexes **10**, **12**, **14** and **16** were synthesised in a two step reaction (Scheme 3.1). In the first step, the aryllithium reagent was generated at -72 °C by reaction of the appropriate bromoaryl compound in diethyl ether with one molar equivalent of n-

butyllithium for an hour, according to literature procedures.[18,19,20]

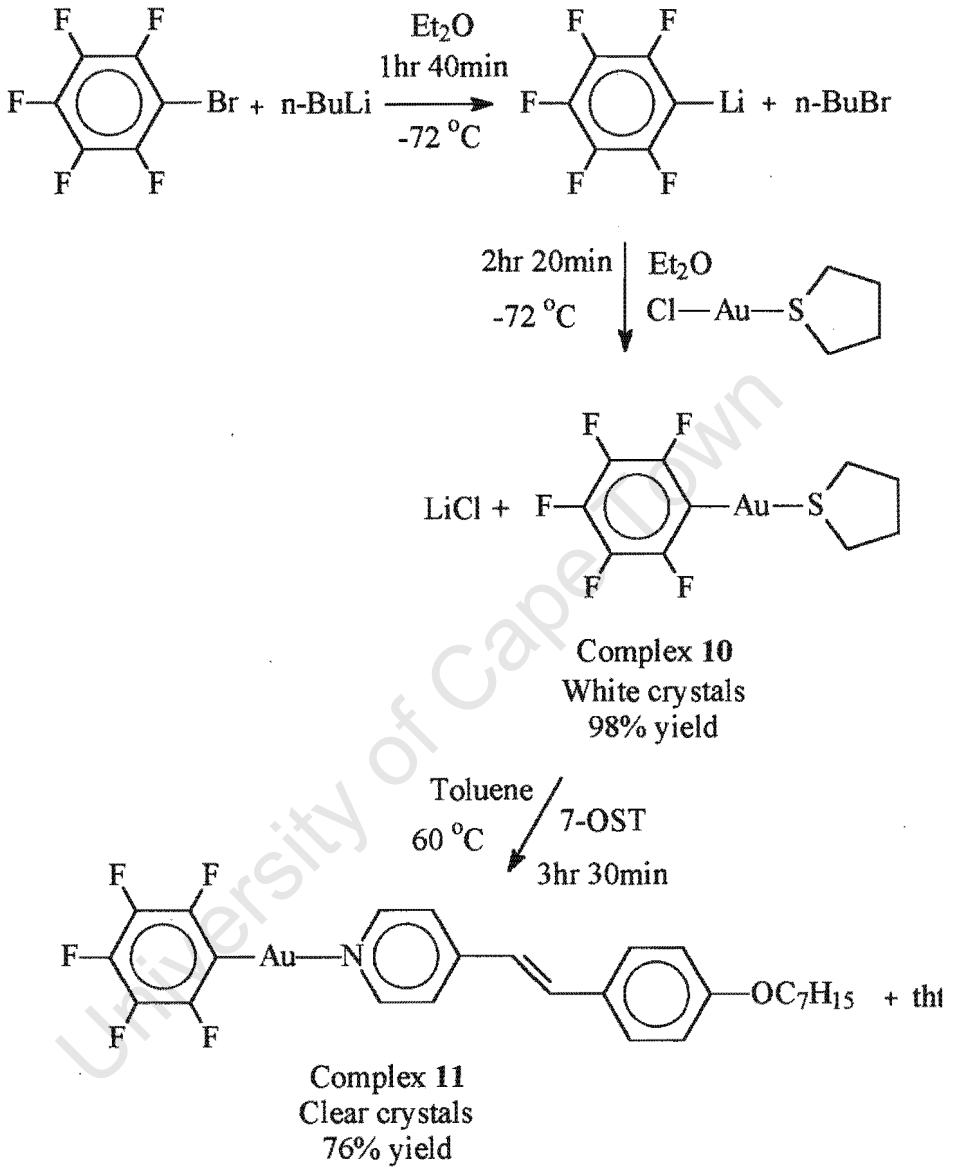

Scheme 3.1: Reaction scheme for the synthesis of RAu(7-OST) complexes from RAu(tht)

The second step involved the reaction of a slight excess of the aryllithium reagents with ClAu(tht) to form the corresponding RAu(tht) complexes, according to literature procedures.[1,20,21] It was generally found best not to allow the reaction mixtures to warm

up above 0 °C and to keep complexes **10, 12, 14** and **16**, which where isolated as white solids, below 0 °C at all times.

The reaction yields for complexes **10, 12** and **14** were quite high, ranging from 86 to 98% and these compared well with literature values.[21] The reason for the lower yield of 34% for complex **16** may be due to the fact that insufficient solvent was used during the reaction. Some product could thus have precipitated from solution when the reaction mixture became saturated and lost with the reaction residue during separation procedures. In support of this explanation is the fact that some of the product was extracted from the reaction residue and recrystallised from dichloromethane/hexane (chapter 6).

When ClAu(tht) reacts with the binuclear aryllithium reagent in the presence of water, both complexes **16** and **17** are formed (Scheme 3.2).[20] As complex **16** was desired, the reaction was conducted under anhydrous conditions, but a small amount of adventitious water present would explain why 5 % of complex **17** was nonetheless isolated as a white solid.

3.2.2 Synthesis of RAu(7-OST) complexes

The RAu(7-OST) complexes **11, 13, 15** and **18** were synthesised in a similar manner to complexes **3-9** (section 2.2.2) by displacement of tht with 7-OST in warm toluene (60 °C), as depicted in scheme 3.1. Due to the thermal instability of ClAu(tht) complexes **10, 12, 14** and **16**, the reagents were initially added at 0 °C to reduce the risk of these complexes decomposing prior to reaction.

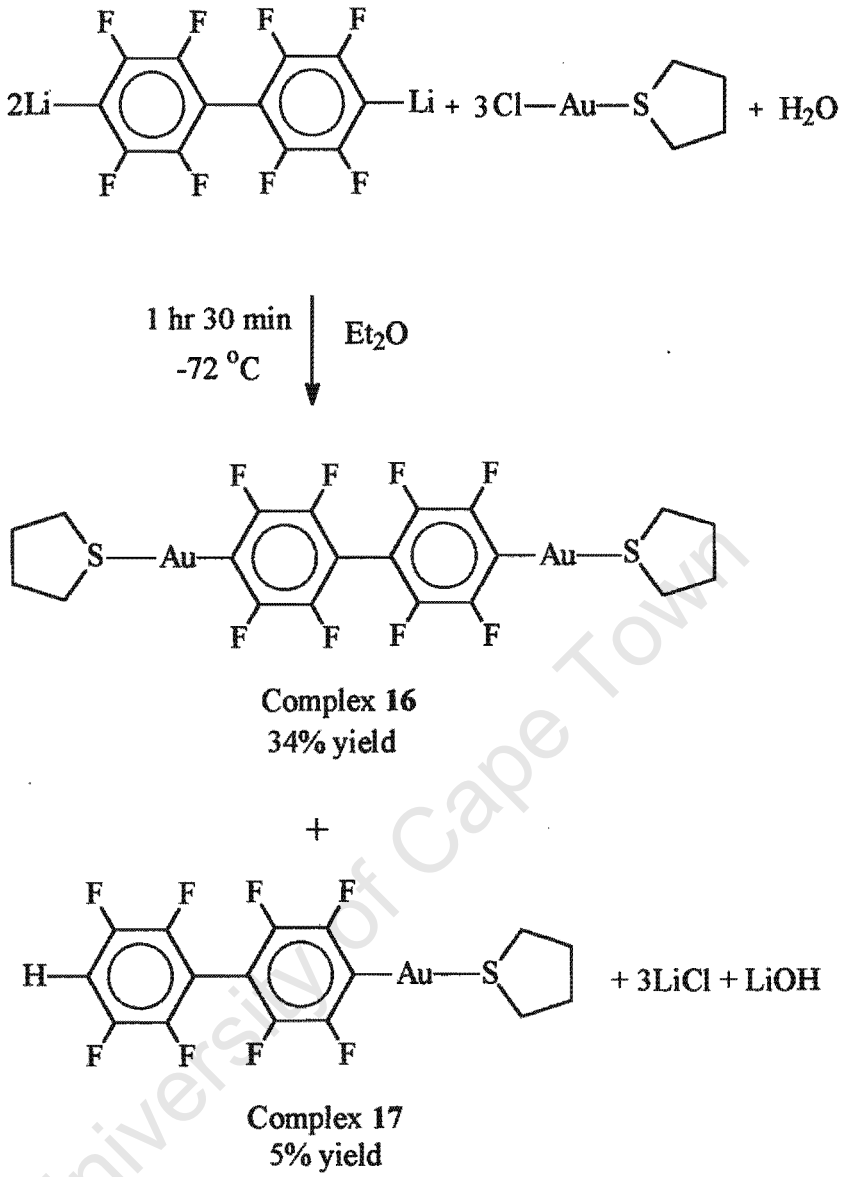

Scheme 3.2: Reaction scheme for the synthesis of complexes **16** and **17**.

RAu(n-OST) complexes form yellow (complex **18**), green-yellow (complexes **11, 15**) or white (complex **13**) air- and moisture-stable crystals with crude yields ranging from 53 % to 76 %. Complexes **11** and **18** were purified by recrystallisation from toluene/pentane or dichloromethane/hexane respectively. Complexes **13** and **15** were passed through a short,

2 cm long, Pasteur pipette column made up of silica gel and with dichloromethane as an eluent. Complexes **11, 13** and **15** are soluble in similar solvents to complexes **3-9** (section 2.2.3) and are similarly unstable when in solution, with decomposition accelerated when the solutions are exposed to light. Complex **18** is not very soluble in most organic solvents, but does dissolved in dichloromethane, deuterochloroform, acetone and DMSO with heating to form very dilute solutions, decomposing rapidly in warm DMSO. It is insoluble in warm methanol and acetronitrile.

3.2.3 Attempted synthesis of $C_6H_5Au(7OST)$

The synthesis of C_6H_5Au(7-OST) was attempted using a method similar to that used for the synthesis of RAu(7-OST) complexes (Section 3.2.2), as well as by reacting C_6H_5Li directly with ClAu(7OST). Both attempts were unsuccessful. Similarly, mesitylgold(I) complexes have been found to form stable compounds with various phosphine ligands, but not with N- or As- or S-donor ligands such as pyridine, $AsPh_3$ or tht.[11] Thus, arylgold(py) complexes with stable C-Au^I bonds are formed when the aryl groups is C_6F_5, but not phenyl or mesityl groups.

3.3 Characterisation of RAu(tht) and RAu(7-OST) complexes

RAu(tht) complexes **10, 12, 14, 16** and **17** were characterised mainly via ν(C-F) and ν(C-Au) (Table 3A.1) and were used in the next step without further purification. RAu(7-OST) complexes **11, 13, 15** and **18** were characterised by elemental analysis and FAB mass spectrometry (Chapter 6), FT-IR, ^{1}H-, ^{13}C- and ^{19}F-NMR spectroscopy (Tables

3A.2-6) and molar conductivities in acetone (Table 3.7). These complexes were also found to exhibit liquid crystalline behaviour and their mesomorphic properties were evaluated via differential scanning calorimetry (DSC) and optical microscopy techniques (Table 3.8). X-ray crystallographic data for complex **11** are presented in Tables 3.3 and 3A.7-11.

3.3.1 Assignments for FT-IR spectra

The ν(Au-C) assignment for complexes **10, 11, 12, 13, 15** and **18** (Table 3A.1) was made on the basis of ν(Au-C) for gold(I) complexes[6] usually occurring in the region of 580-530 cm^{-1}. The strong ν(C-F) bands of the aryl groups were found to be very useful in characterisation and assignments for complexes **10-18** was made by comparison with literature values,[21] as well as comparison with the ν(C-F) of the respective starting bromoaryl compounds (Table 3A.1). The assignments for the FT-IR spectra of the 7-OST ligand of complexes **11, 13, 15** and **18** were made by comparison to the free 7-OST ligand and complexes **3-9** (section 2.2.3).

3.3.2 Assignments for ^{1}H- and ^{13}C-NMR spectra

Assignments for the ^{1}H- and ^{13}C-NMR spectra of the 7-OST ligand of complexes **11, 13, 15** and **18** was made on the basis of HETCOR spectra and comparison with the free 7-OST ligand, similarly to complexes **3-9** (section 2.2.3). Representative ^{1}H- and ^{13}C-NMR and HETCOR spectra of complex **15** are presented in Figures 3.4-6. No peaks were observed in the 150 ppm region of the ^{13}C-NMR spectra of complexes **10-18**, where peaks for the carbon atoms of fluorine-substituted aryl rings would be expected. This is

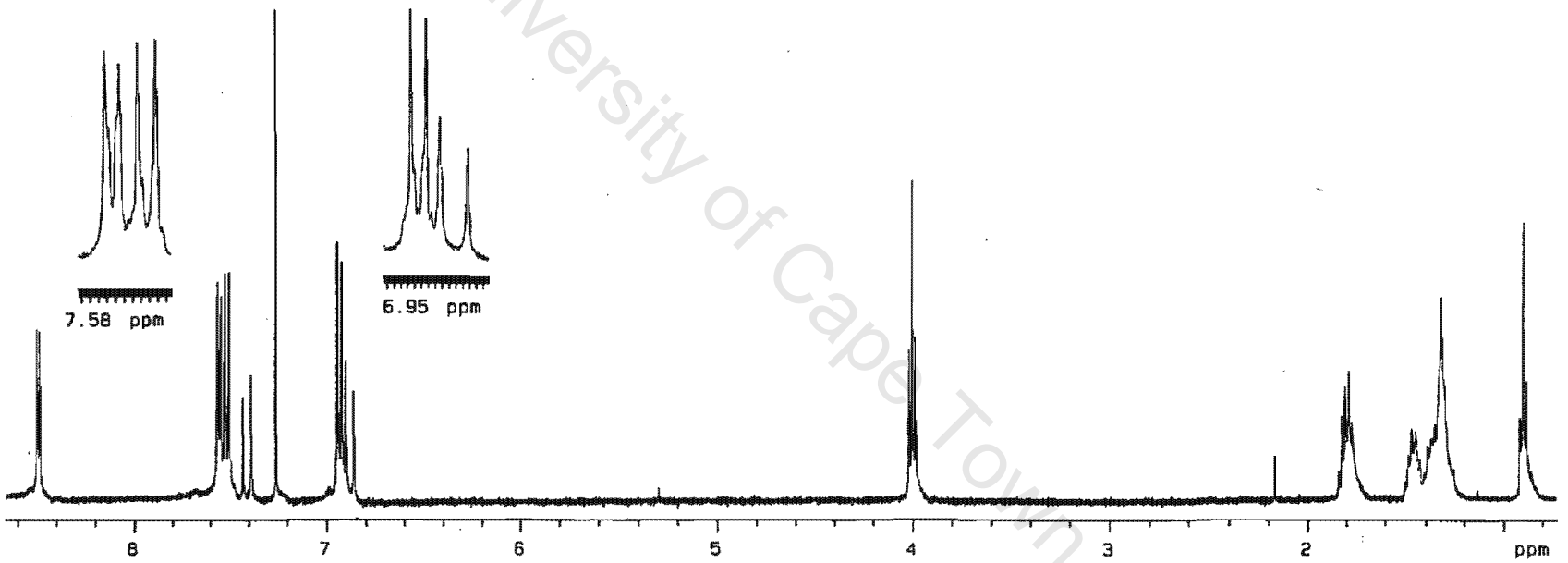

Figure 3.4: ^{1}H-NMR spectrum of complex **15** $CDCl_3$.

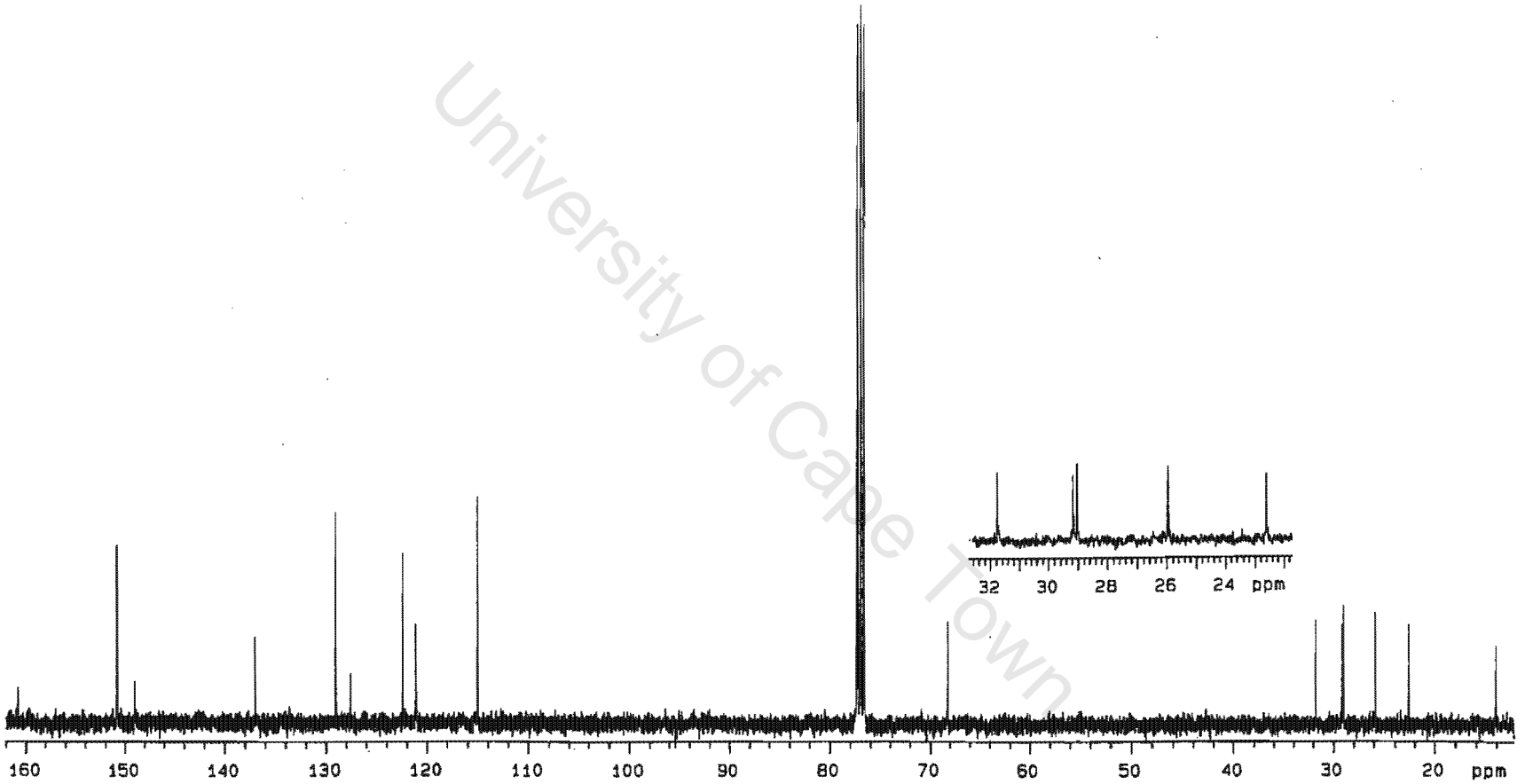

Figure 3.5: ^{13}C-NMR spectrum of complex **15** $CDCl_3$.

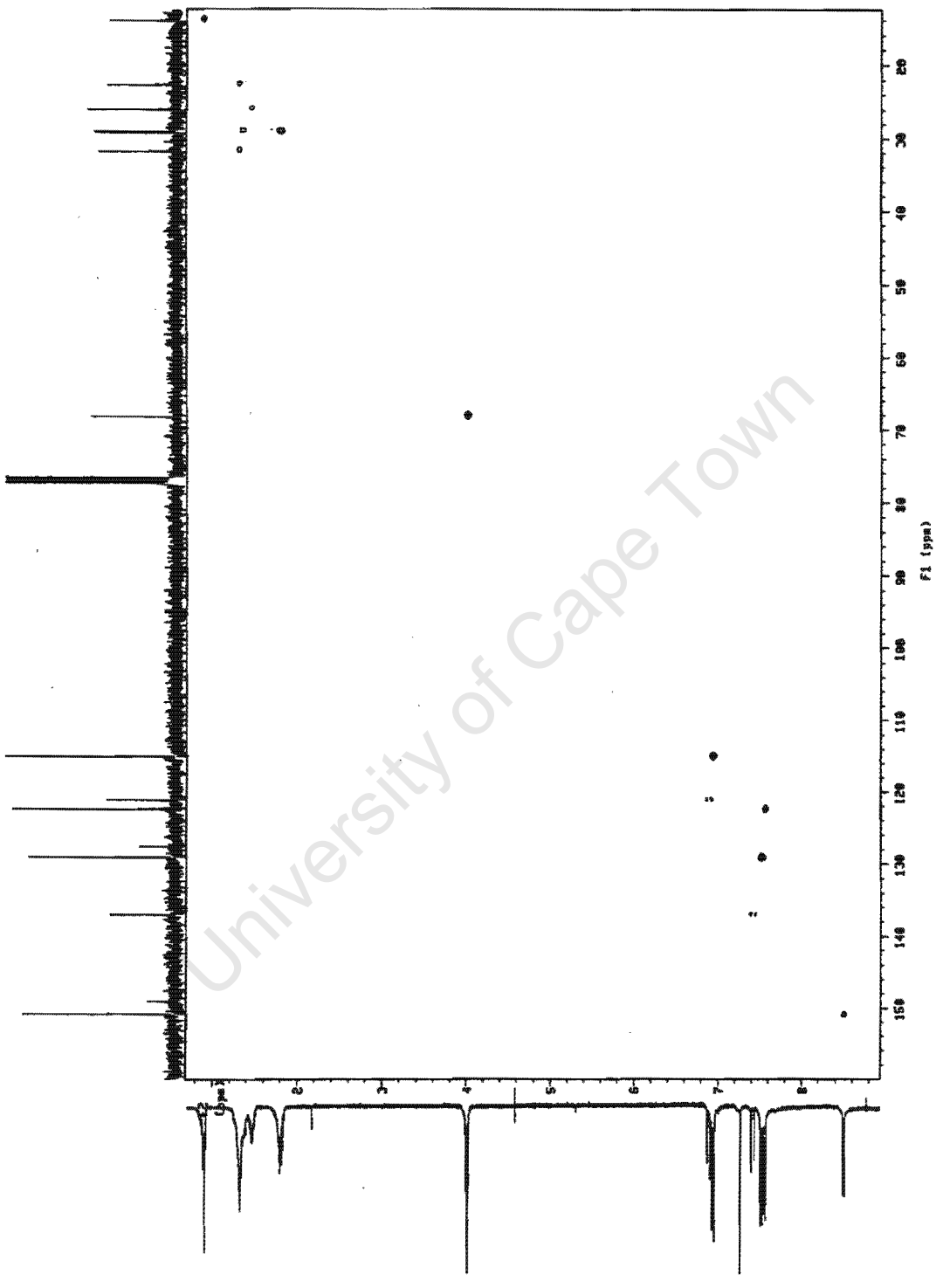

Figure 3.6: HETCOR spectrum of complex **15** $CDCl_3$.

probably due to the carbon nuclei of the perhaloaryl groups having a long relaxation time, resulting in the intensity decreasing below the instrumental detection limits. Solubility problems were experienced for complex **18**, which was sparingly soluble $CDCl_3$. Although it was more soluble in CD_2Cl_2, with a better signal-to-noise ratio, it was required for comparative purposes to collect the ^1H- and ^{13}C-NMR spectra of complex **18** in $CDCl_3$, allowing for longer data collection times of 8.5 and 10.9 hours respectively. As a result of a slight downfield shift of the H_b proton of complexes **11, 13, 15** and **18** relative to the complex **6**, better peak separation between H_b and H_g was observed, with the H_b peak appearing slightly more downfield than H_g

3.3.3 Assignments for ^{19}F-NMR spectra

The ^{19}F-NMR chemical shifts of complexes **10, 11, 13, 15, 16** and **18** are reported relative to $CFCl_3$. Assignments were made by comparison with similar perhalophenylgold(I) complexes[1] and are reported in Tables 3A.5-6. In the cases of complexes **10, 11** and **16**, the spectra were initially measured relative to bromopentafluorobenzene, which has three peaks at 84.01 (F_b), 62.19 (F_c) and 56.14 (F_a) ppm.[22] Bromopentafluorobenzene was subsequently measured relative to $CFCl_3$, with the three peaks appearing at -132.35 (F_b), -154.16 (F_c) and -160.20 (F_a) ppm. The difference of 216.35 ppm was then subtracted from the spectral peaks of complexes **10, 11** and **16** to give values relative to $CFCl_3$. The ^{19}F-NMR spectra of complexes **12** and **14** were not determined, and data was obtained from literature.[1]The patterns for the ^{19}F-NMR spectra of these complexes are typical of what is commonly observed for perhalophenyl containing complexes (Table 3A.5-6).[1] Complexes **10** and **11** have an AA'MXX' spin

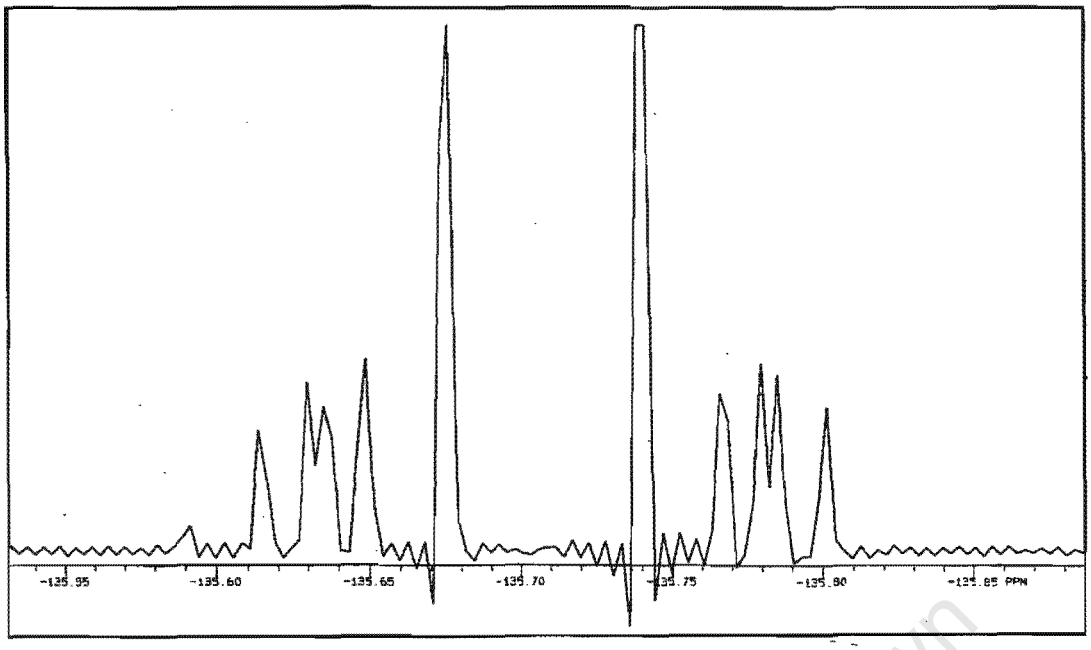

Figure 3.7: ^{19}F-NMR spectrum for F_b of complex **15** $CDCl_3$.

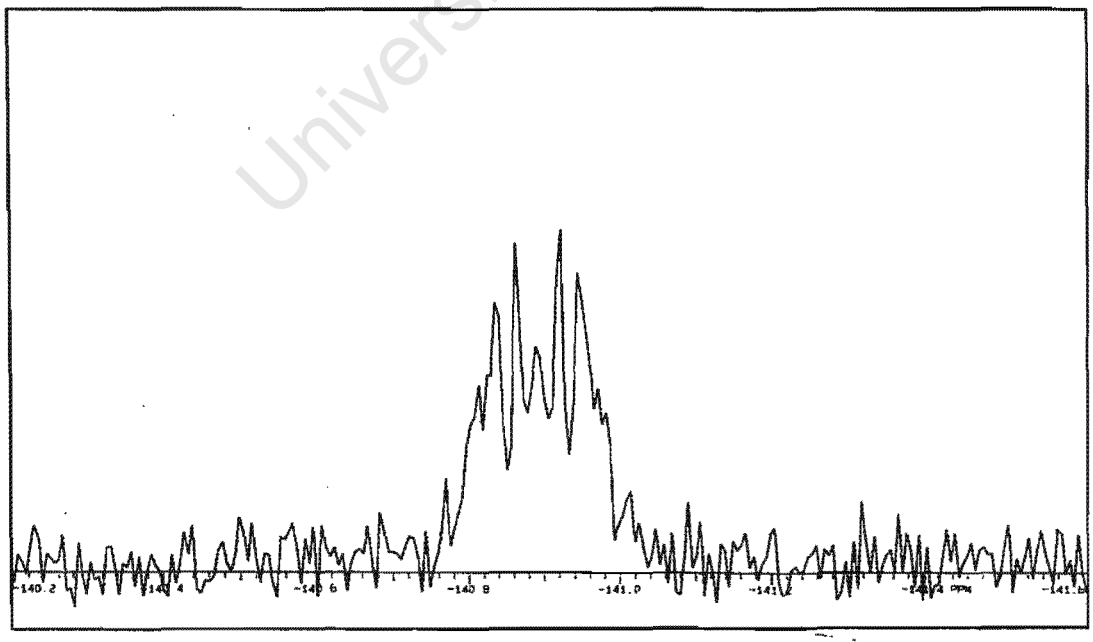

Figure 3.8: ^{19}F-NMR spectrum for F_b of complex **18** $CDCl_3$.

system, complexes **12** and **13** a first order AKRX spin system and complexes **14** and **15** an AA'XX' spin system with $J_{AA'} \approx J_{XX'}$ (Tables 3A.5-6).[1] The ^{19}F-NMR spectrum of complex **15** though, shows that the doublets of F_a and F_b are distorted and are each flanked by two pseudotriplets (Figure 3.7). The triplets probably indicate coupling of F_a and F_b with $F_{a'}$ and $F_{b'}$. The spectra of complexes **16** and **18** also do not reflect a typical AA'XX' spin system, but rather exhibit two complex multiplets (Figure 3.8). Cross-coupling of the fluorine atoms on one tetrafluorophenyl ring with those on the adjacent ring most likely causes this. The afore-mentioned patterns have been observed in similar gold(I) isocyanide complexes.[1]

3.3.4 X-ray photography and intensity data collection for complex 11

Preliminary unit cell parameters and space group data were determined from oscillation and precession photographs taken with CuKα-radiation (λ = 1.5418 Å) on Stoe goniometers. Laue symmetry 2/m was revealed on the photographs, indicating the monoclinic crystal system. The conditions for observed reflections were: hkl none, h0l l = 2n, 0k0 k = 2n, which indicated the space group $P2_1/c$ (No.14) unambiguously.

For intensity data-collection (Table 3.2), a small single crystal was selected and mounted on a glass fibre. Data were collected with the crystal to detector distance fixed at 45 mm and using a strategy based on a series of φ- and ω-scans with rotations of 1° between frames. Data were corrected for absorption[23,24] and Lorentz-polarization effects and reduced to a unique set.[25,26] The structure was solved by the heavy-atom procedure after location of the gold atom from the three-dimensional Patterson function, using the SHELX-86 computer program.[27] All non-hydrogen atoms were revealed in the Fourier

synthesis phased on the gold atom coordinates. The structure was refined using SHELX-93.[28] In the final cycles of refinement, the non-H atoms were treated anisotropically. All hydrogen atoms were included in idealized positions with C-H in the range 0.93-0.97 Å depending on the type (i.e. methyl, phenyl, methylene) using SHELX-93[28] and were treated isotropically with a common free variable U_{iso} which refined to 0.11(1) Å^2.

Table 3.2: Crystal data and structure refinement for complex **11**

Compound	$C_6F_4Au(NC_6H_4CHCHC_6H_4O(CH_2)_6CH_3$
Colour / shape	Colourless / prismatic
Empirical formula	$C_{26}H_{25}AuF_5NO$
Formula weight	659.448
Temperature	293 (1) K
Crystal system	Monoclinic
Space group	$P2_1/c$
Unit cell dimensions	a = 5.744(1) Å, α = 90°
	b = 46. 026(1) Å, β = 103.98(1)°
	c = 9.521(1) Å, δ = 90°
Volume	2442.5(5) Å^3
Z	4
Density (calculated)	1.793 / m^3
Absorption coefficient	6.080 mm^{-1}
Diffractometer	KAPPA CCD area detector
Radiation / wavelength	MoK_α (graphite monochrom.) / 0.71069 Å
F(000)	1280
Crystal size	0.30 x 0.20 x 0.25 mm
2θ range for data collection	2.0-52.61°
Index ranges	$0 \le h \le 7$, $0 \le k \le 52$, $-11 \le l \le 11$
Independent reflections [I > 2σ(I)]	2648
Absorption correction	Semi-empirical (sortav)
Absorption correction factors	0.62-1.12
Refinement method	Full-matrix least-squares
Computing	SHELXL-93
Data / restraints / parameters	2636 / 0 / 309
Goodness-of-fit on F^2	1.032
SHELX-93 weight parameters	0.1037, 14. 925
R index (all data)	R = 0.0626, wR2 = 0.1970
Largest diff. peak and hole	+ 0.48 and -0.97 eÅ^3

3.4 Discussion of results

3.4.1. 7-OST ligand spectroscopic data for RAu(7-OST) complexes and comparison with ClAu(7-OST)

The 7-OST ligands were investigated using FT-IR, ^{1}H- and ^{13}C-NMR spectroscopy. It can be seen from ν(Au-C) and ν(Au-Cl) values (Table3.3) that the energy of the Au-C bonds of complexes **11, 13, 15** and **18** are quite similar to each other and significantly higher than the Au-Cl bond of complex **6**. This would indicate that the Au-C bond is stronger than the Au-Cl bond. This may or may not have an affect on the Au-N bond strength, which could result in changes in the electronic structure of the highly conjugated 7-OST ligands.

Table 3.3: Selected FT-IR bands of RAu(7-OST) complexes **6, 11, 13, 15** and **18**

Complex	R group	ν(Au-R) cm^{-1}	ν(C=N) cm^{-1}	$\nu(C{=}C)_{aromatic}$ cm^{-1}	$\nu(C\text{-}H)_{aromatic}$ cm^{-1}
6	Cl	357 m	1437 s	1469 m	3044 m
11	C_6F_5	600 m	1445 s	1460 m	3031 m
13	2-C_6F_4Br	580 m	1426 s	1465 m	3039 m
15	4-C_6F_4Br	594 m	1435 s	1458 m	3039 m
18	μ-4,4'-$C_6F_4C_6F_4$	580 m	1435 s	1463 m	3039 m

m = medium, s = strong

The variance in ν(C=N) as the R group changes for these complexes (Table 3.3) ranges from 1426 to 1445 cm^{-1}. ν(C=N) does not change significantly as R changes from a halide (complex **6**) to an aryl group (complexes **11, 13, 15** and **18**). It can be assumed then that the Au-N bond strength remains reasonably constant regardless of whether Au^{I} is bonded to a perhaloaryl group with one aromatic ring or a halide. The FT-IR, ^{1}H- and ^{13}C-NMR spectra of the 7-OST ligand when R = Cl (complex **6**) is remarkably similar to

when R = perhaloaryl (complexes **11, 13, 15** and **18**), again indicating that the Au^{I}-N bond is not affected by the nature of the R group. Their FT-IR spectra (Tables 2A.2 and 3A.2) are almost identical except for small changes in ν(C=N), $\nu(C{=}C)_{aromatic}$ and $\nu(C{-}H)_{aromatic}$ reported in Table 3.3. Similarly, their ^{1}H- and ^{13}C-NMR spectra were found to be almost identical (Tables 2A.5, 2A.7, 3A.3-4), with slight differences noted for complex **18**.

The protons of complex **18**, where the aryl group has two aromatic rings, are slightly more shielded compared to complexes **6, 11, 13** and **15**, with the most noticeable difference observed for H_a of the py ring, which has a Δδ (ppm) of -0.34. The py ring C_c nucleus of complex **18** is also more shielded (Δδ = -5.4 ppm) compared to complexes **6, 11, 13** and **15**, but most of the other carbon nuclei of complex **18** are relatively more deshielded. For example, the C_j to C_n atoms of the alkoxy chain become deshielded with Δδ values of about +1.9 ppm relative to complexes **6, 11, 13** and **15**.

These changes in the ^{1}H- and ^{13}C-NMR spectra of complex **18** cannot be explained on the basis of enhanced conjugation effects (section 2.3.5). The increased electron density of the py ring of complex **18** could indicate that the μ-4,4'-$C_6F_4C_6F_4$ group increased the stability of the Au-N bond, relative to complexes **6, 11, 13** and **15**, by promoting π-back-bonding of Au^{I} d-orbitals into π* orbitals of the 7-OST ligand (section 2.3.1). Complex **18** is thermally more stable and has much higher transition temperatures than complexes **6, 11, 13** and **15** (section 3.3.6) and this may reflect an increase in Au-N bond strength.

3.4.2 Spectroscopic changes in R groups between RAu(tht) and RAu(7-OST) complexes

The R groups of complexes **10-18** were investigated with FT-IR (ν(C-F) and ν(Au-C) bands) and ^{19}F-NMR spectroscopy. The ν(Au-C) for RAu(tht) complexes **10** and **12** were found to be about 10 cm^{-1} lower than corresponding RAu(7-OST) complexes **11** and **13** (Table 3A.1). The Au-C bond is thus slightly stronger for the 7-OST ligand compared to the more labile tht ligand, but does not seem to change for different R groups of the same ligand. This may indicate that 7-OST is more electron-donating than tht.

RAu(tht) and RAu(7-OST) complexes **10-18** has lower ν(C-F) values compared to their corresponding free bromoaryl compounds (Table 3A.1). The symmetry of the R group affects changes in ν(C-F), with ν(C-F) values of the more symmetrical para-substituted RAu(tht) and RAu(7-OST) complexes **14, 15, 16** and **18** remaining constant irrespective of whether the ligand is tht or 7-OST. For the less symmetrical R groups, ν(C-F) of RAu(7-OST) complexes **11** and **13** were found to increase by about 9 to 18 cm^{-1}compared to RAu(tht) complexes **10** and **12**, but a decrease of about by 8 $cm^{-1}$was also observed for one peak. ν(C-F) values for complexes **10-18** thus varies according to the L group, tht or 7-OST, as well as the symmetry of the R groups.

The Δδ (ppm), and hence electron density, experienced by the fluorine nuclei of complexes **11, 13, 15** and **18** (Table 3.4) when tht is replaced by 7-OST indicates that the nature of the L group (tht or 7-OST) not only affects to nature of the Au-C bond, but also the electronic environment of the F atoms in the R group. This is also supported by changes in ν(C-F) observed when tht is replaced with 7-OST.

Table 3.4: Δδ values for ^{19}F-NMR spectra of RAu(7-OST) complexes **11, 13, 15** and **18** relative to the corresponding RAu(tht) complexes **10, 12, 14** and **16**

Complex	R group	Δδ (ppm)			
		F_a (ortho)	F_b (meta)	F_c (para)	$F_{b'}$ (meta)
11	C_6F_5	-0.49	+0.12	-0.91	
13	2-C_6F_4Br	+0.49	-0.32	-0.75	+0.13
15	4-C_6F_4Br	+0.39	-0.41		
18	μ-4,4'-$C_6F_4C_6F_4$	-0.20	-0.67		

3.4.3. Spectroscopic changes between R groups for RAu(tht) and RAu(n-OST) complexes

Considering the electron-withdrawing properties of a bromine substituent on a phenyl ring, the F_a and F_c nuclei of RAu(tht) and RAu(7-OST) complexes **12-15**, which have bromine substituents, would be expected to shift upfield relative to complexes **10-11**, and downfield in the case of the F_b nucleus. The F_a atom of complexes **12-15** experience a significant upfield shift of about +52ppm (Tables 3A.5-6). To a lesser extent, F_c of complexes **12-13** is also shifted by +5ppm. Conversely, F_b experiences a downfield shift, which is greater for complexes **12-13** (–37ppm) compared to complexes **14-15** (–15ppm). As similar changes in F_a and F_b is observed (Tables 3A.5-6) for complexes **16** and **18** as for complexes **14-15**, the –C_6F_4AuL (L = tht or 7-OST) fragment can also be viewed as behaving in a similar manner to the –Br fragment as an electron-withdrawing substituent in the para position.

3.4.4 Crystal and molecular structure of complex 11

The conformation of a molecule of complex **11** with the atomic numbering scheme can be seen in Figure 3.9. A complete list of the atomic coordinates, thermal displacement

parameters, bond lengths, bond angles and torsion angles for complex **11** is given in Tables 3A.7-11. The Au-N1 bond length (Table 3.5) compares well with Au-N bond lengths reported for various py (or substituted py) linear gold(I) complexes with halide[29], phosphine[30,31,32] organic[16] or other N-donor ligands.[12,33]

Table 3.5: Selected bond lengths,[a] bond angles[b] and torsion angles[b] for complex **11**

Gold atom bond lengths and angle		**Alkene bond lengths and torsion angle**	
Au-N1	2.06(1)	C9-C12	1.42(2)
Au-C1	1.99(1)	C12-C13	1.28(2)
N1-Au-C1	179(1)	C13-C14	1.47(2)
		C9-C12-C13-C14	178(1)
Alkoxy chain torsion angles		**Alkene/py ring torsion angles**	
O1-C20-C21-C22	-174(1)	C8-C9-C12-C13	0(3)
C20-C21-C22-C23	-179(1)	C10-C9-C12-C13	179(2)
C21-C22-C23-C24	-179(1)	**Alkene/phenyl ring torsion angles**	
C22-C23-C24-C25	178(1)	C12-C13-C14-C15	-166(2)
C23-C24-C25-C26	180(1)	C12-C13-C14-C19	15(2)

a = Angström, b = degrees

The Au-C1 bond length (Table 3.5) is comparable to the only reported Au-C bond length of 1.992(6) Å for a linear C_6F_5AuL complex bonded to a N-donor ligand.[12] These values are in agreement with reported Au-C bond lengths for linear gold(I) complexes with pentafluorophenyl[34,35,36,37] and other aryl ligands.[11,38,39] The C1-Au-N1 bond angle is almost linear at 179(1)°.

The alkene C12-C13 bond length of 1.28(2) Å is shorter than the adjacent C9-C12 and C13-C14 bond lengths (Table 3.5) and confirms the double bond character of the C12-C13 bond. The C9-C12-C13-C14 torsion angle (Table 3.5) confirms that the alkene bond of complex **11** is in the trans conformation. By looking at the torsion angles about the C9-C12 and C13-C14 bonds (Table 3.5), it can be seen that the alkene bond is co-planar with

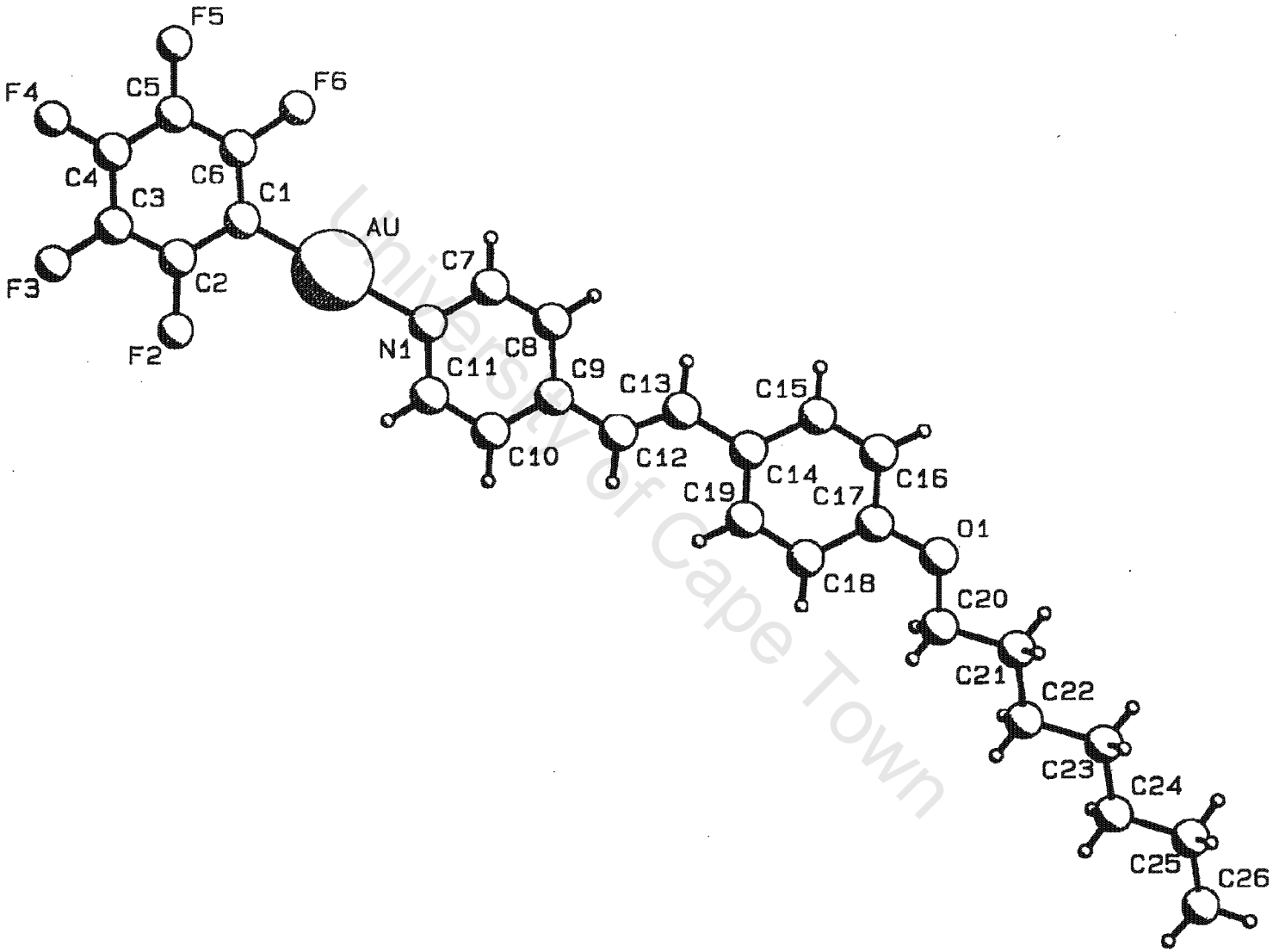

Figure 3.9: Molecular structure of complex **11**.

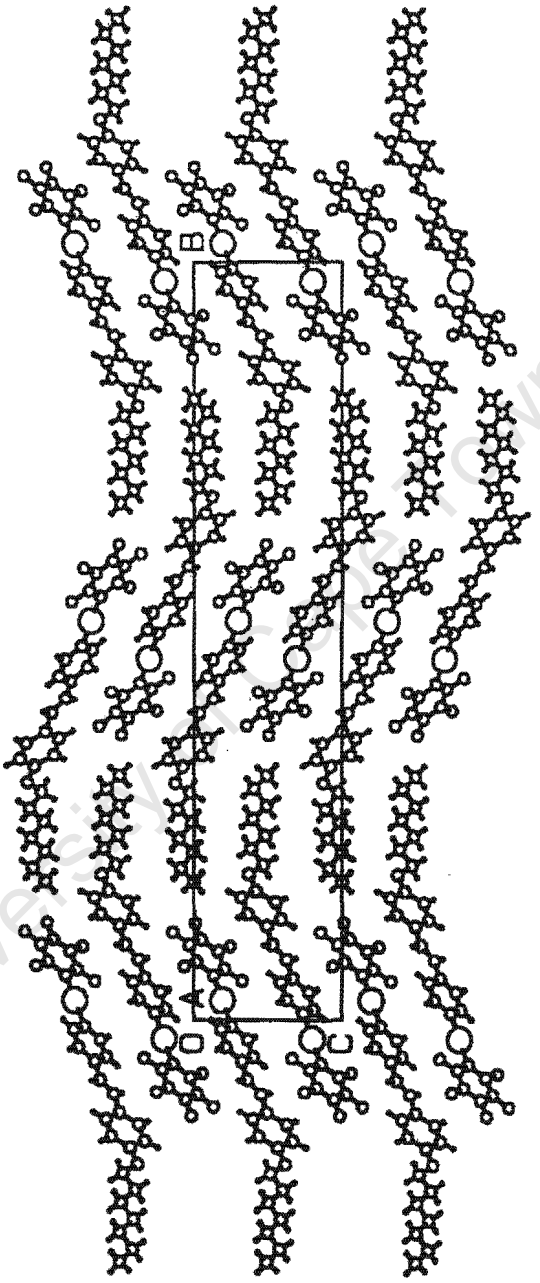

Figure 3.10: Packing of molecules of complex 11 down the C axis.

the py ring, but deviates slightly (about 15°) from co-planarity with the phenyl ring, C14 to C19. From the torsion angles about the carbon atoms in the alkoxy chain (Table 3.5), it can be seen that the alkoxy chain does not deviate much from planarity, except for the O1-C20-C21-C22 torsion angle of -174(1)°, which indicates that the alkoxy chain is slightly bent (about 6°) at the oxygen atom relative to the phenyl ring, C14 to C19.

The weighted least-squares planes for the groups of atoms defined by the pentafluorophenyl, C1 to C6, pyridine, N1, C7 to C11, and phenyl rings, C14 to C19, were calculated (Tables 3A.12-14). The sum of the squared relative standard deviations of the atoms in the respective rings from their calculated planes were 2.626 $x10^{-2}$, 4.566 $x10^{-2}$ and 4.681 $x10^{-2}$ and indicate that all three rings are planar. The dihedral angles between the planes were also calculated and the results indicate that the C_6F_5, py and phenyl rings are almost co-planar (Table 3.6).

Table 3.6: Dihedral angles between the planes defined by the C_6F_5 (C1 to C6), py (N1, C7 to C11) and phenyl (C14 to C19) rings for complex **11**

Plane 1	Plane 2	Dihedral angle (e.s.d.)	Tilt direction[a]
C_6F_5	py	4.0 (4)°	anti-clockwise
py	phenyl	13.6 (4)°	clockwise
C_6F_5	phenyl	9.6 (4)°	clockwise

a = plane 2 tilted relative to plane 1 looking towards N1 down the C1-Au-N1 bond axis

The tilt directions were determined by the relative displacements of the C7 and C11 atoms of the py ring to the plane defined by the C_6F_5 ring and the C15 and C19 atoms of the phenyl ring to the plane defined by the py ring. The C7 and C11 atoms were displaced 0.05 above and 0.12 Å below the C_6F_5 ring respectively (Table 3A.12) and the C15 and C19 atoms of the phenyl ring 0.17 below and 0.37 Å above the py ring respectively

(Table 3A.13). The magnitude of the dihedral angle between the py and phenyl rings agrees with the torsion angles between the alkene group and the py and phenyl rings (Table 3.5). As the relative standard deviation of the torsion angles about the Au-N1 and Au-C1 bonds (Table 3A.11) were very large (about 38 °), the dihedral angle of 4.0 (4)° between the C_6F_5 and py rings is a better indication of their co-planarity.

Intermolecular atomic distances between all atoms of complex **11** up to 4.00Å were evaluated, but no significant contacts were found. This confirms that complex **11** has no Au...Au intermolecular bonding interactions (typically between 2.75-3.4 Å) and has a neutral and monomeric structure (section 1.4). Figure 3.10 shows the packing of the molecules as viewed down the A axis. Although the molecules pack with the aromatic groups stacked below each other, various stereograms (Figures 3.11) reveal that no π---π stacking effects occur.

A search of the CCD[10] for stilbazole fragments resulted in five structures, three of which were various n-methyl-stilbazolium cations[40,41] and one was 4-octyloxystilbazole with hydrogen bonding to 4-cyanophenol.[42] The other crystal structure of dimeric bis[4-(4-methyloxystilbazole)]silver(I) octyl sulfate hemihydrate[43] is the only reported example of a metal-containing alkoxystilbazole complex. The structure of the stilbazole ligand of the latter complex is similar to that of complex **11**, with the planar py and phenyl rings of the four stilbazole ligands also twisted relative to the ethane planes by 2.5 and 14.0; 10.6 and 15.0; 2.3 and 4.5; 12.5 and 17.5° respectively.[43]

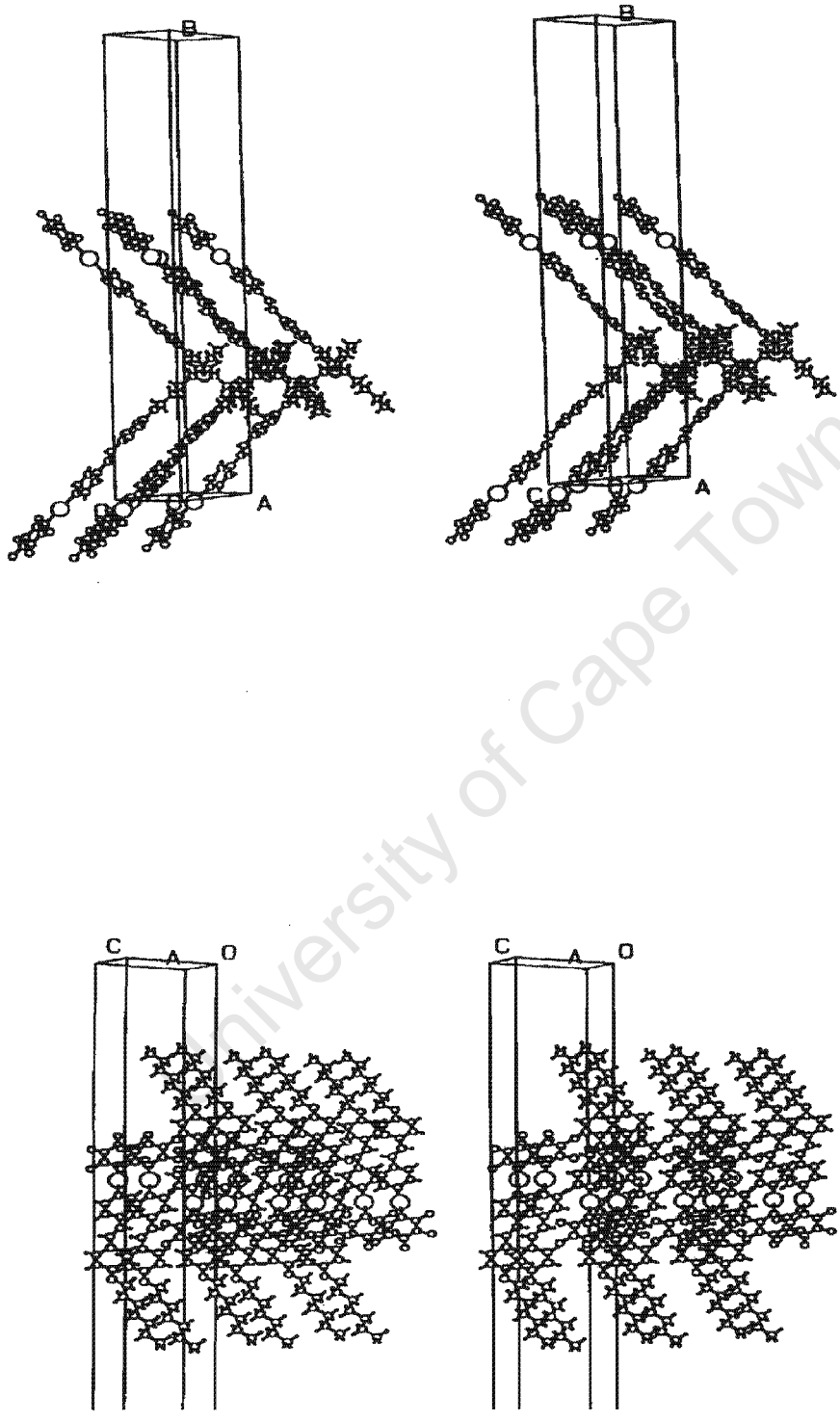

Figure 3.11 Stereograms of complex **11** illustrating molecular packing arrangements

3.4.5 Neutral or ionic molecular structure of complexes 11, 13, 15 and 18

As with ClAu(n-OST) complexes **3-9** (section 2.3.6), the neutral or ionic molecular structure of RAu(7-OST) complexes were investigated using molar conductivity measurements, FT-IR, ^{1}H- and ^{13}C-NMR spectroscopy, FAB mass spectrometry and X-ray crystallography. One ν(C=N) peak in FT-IR spectra indicated that only one species (either neutral or ionic) exists when complexes **11, 13** and **15** are dissolved in dichloromethane or when complex **18** is crystallised from dichloromethane/hexane (KBr disc). ^{1}H-, ^{13}C- and ^{19}F-NMR spectra also indicate that only one species is observed when complexes **11, 13, 15** and **18** are dissolved in deuterochloroform. The molar conductivities of complexes **11, 13** and **15** (Table 3.7) in acetone were found to be very small and similar to those obtained for complexes **3-9** (section 2.3.6, Table 2.3). Complexes **11, 13** and **15** were thus also found to exist as the neutral species in acetone.

Table 3.7: Molar conductivities (Λ) for RAu(7-OST) complexes in acetone

Complex	R group	Λ (ohm^{-1}.mol^{-1}.cm^{2})
11	C_6F_5	1.46
13	2-C_6F_4Br	1.31
15	4-C_6F_4Br	0.45
18	μ-4,4'-$C_6F_4C_6F_4$[a]	-

a = complex **18** is only partially soluble in acetone at the concentration levels of 10^{-3} M required for Λ measurements.

Only the parent ion of complex **11** $[C_6F_5Au(7\text{-OST})]^{+}$, was detected by FAB mass spectrometry techniques. As mentioned in section 2.3.6, samples are dissolved in a matrix (2-nitrobenzylalcohol). Complexes **13, 15** and **18** may have been less stable in the matrix or decomposed thermally during analysis. All the RAu(7-OST) complexes were found to

be unstable thermally (section 3.3.6) and when in solution (section 3.2.2). The parent ion of complex **11** indicated that the RAu(7-OST) complexes may exist as the neutral monomeric species when dissolved in the 2-nitrobenzylalcohol matrix. A small peak corresponding to the $[Au(7\text{-}OST)_2]^+$ cation was again generally observed, but as stated in section 2.3.6 could have been created during the analysis.

An X-ray crystallographic study of complex **11** crystallised from toluene/pentane (section 3.3.4) confirms that the complex is a neutral species in the solid state This is similar to what was observed by FAB-MS when complex **11** was dissolved in the 2-nitrobenzylalcohol matrix. Its molecular structure is monomeric when crystallised from toluene/pentane, as no intermolecular Au...Au bonding interactions (section 3.3.4) were detected. Conductivity measurements confirm that a neutral species also exists in acetone. FT-IR and ^{1}H-, ^{13}C- and ^{19}F-NMR spectra merely indicate that both the neutral and ionic species do not coexist in dichloromethane or deuterochloroform, but cannot differentiate between the two.

3.4.6 Mesomorphic properties and decomposition of RAu(7-OST) complexes and comparison with ClAu(7-OST)

The transition temperatures and enthalpy of transitions for complexes **11, 13, 15** and **18** were recorded on the first DSC scan cycle (Table 3.8) and DSC thermograms of complexes **11, 13** and **15** are presented in Figures 3.12-14. Two structural rearrangements in the solid state are observed for complexes **11** and **13**, one for complex **15** and none for complex **18** before they melt into the liquid crystal phase (Table 3.8, Figure 3.16).

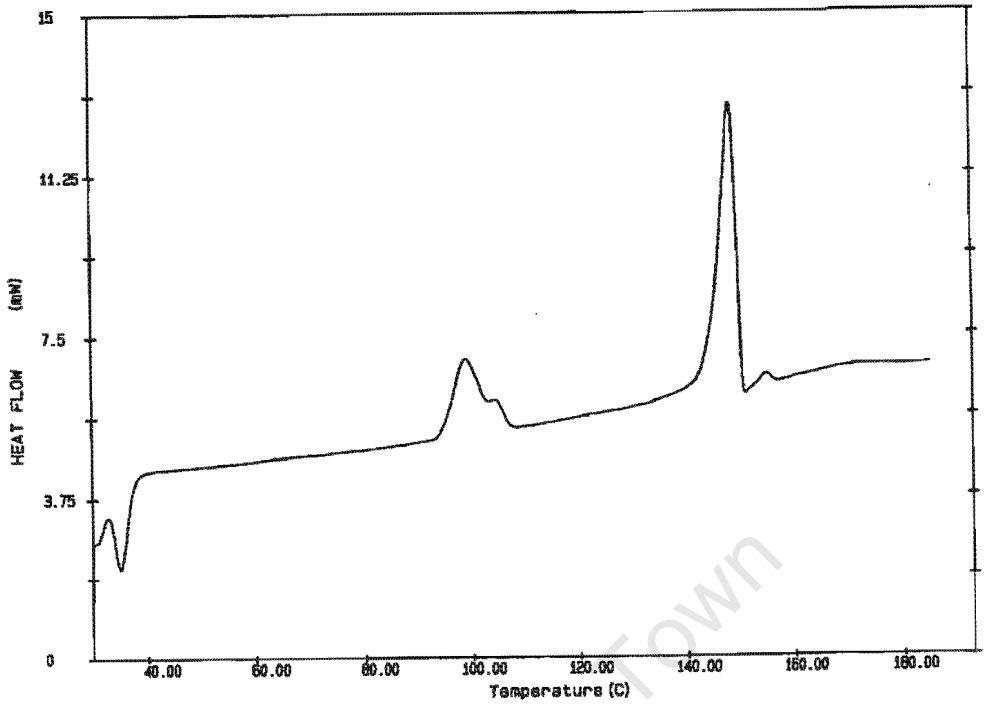

Figure 3.12: DSC thermogram of complex **11** with a 10 °C/min heating rate.

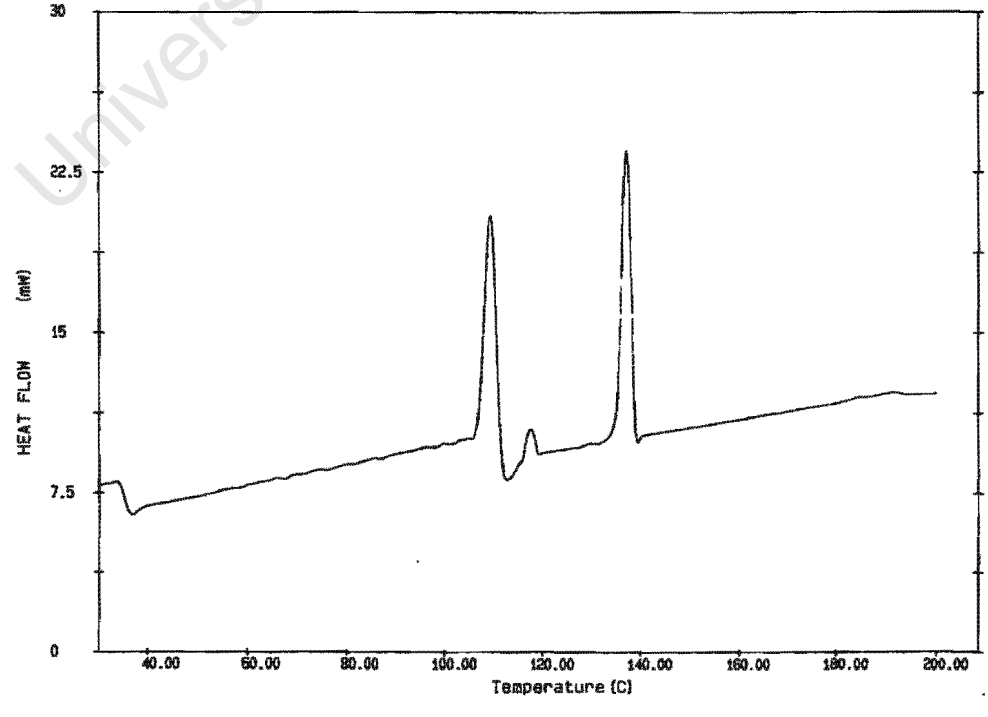

Figure 3.13: DSC thermogram of complex **13** with a 10 °C/min heating rate.

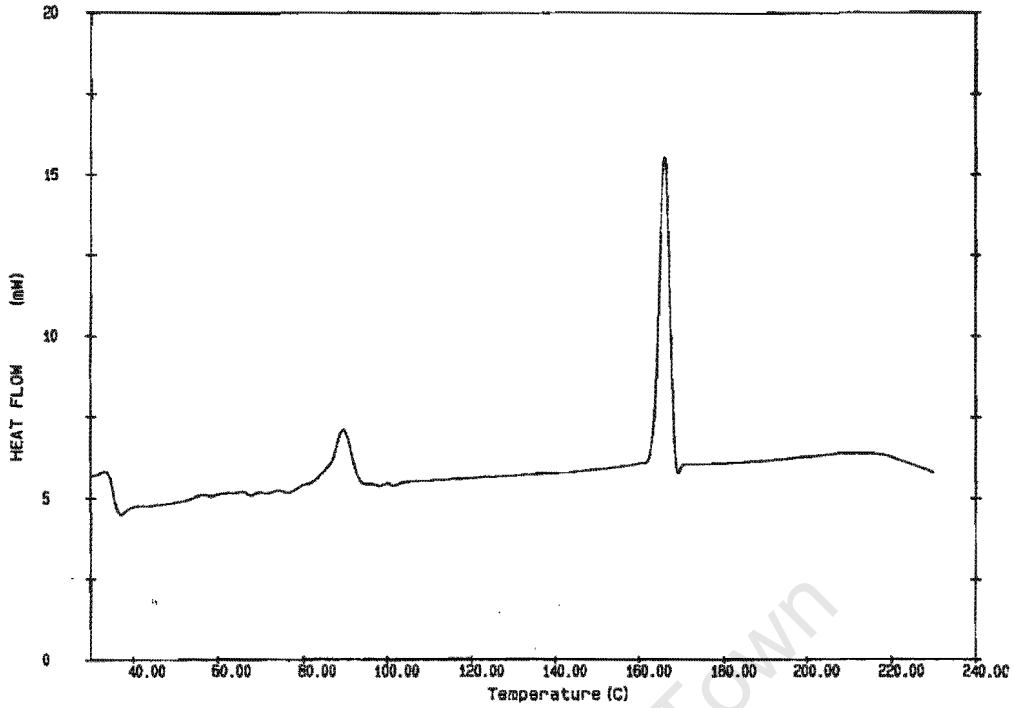

Figure 3.14: DSC thermogram of complex **15** with a 10 °C/min heating rate.

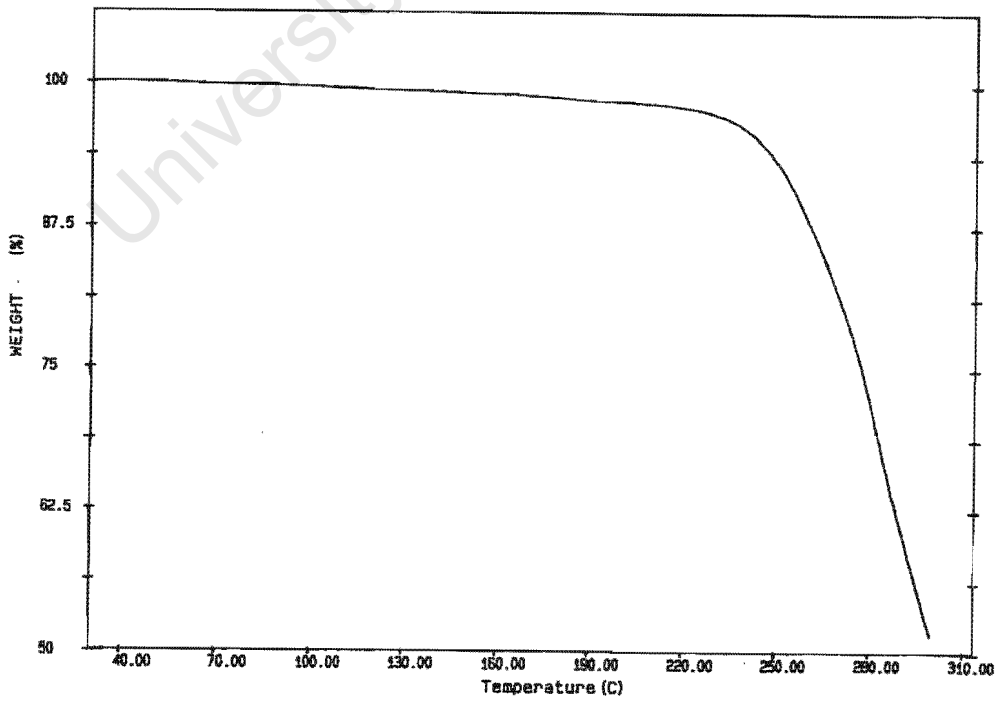

Figure 3.15: TG thermogram of complex **15** with a 10 °C/min heating rate.

Table 3.8: DSC thermal data of transition temperatures (°C) and ΔH (kJ.mol^{-1}) for RAu(7-OST) complexes

Complex	R group	C-C′	C′-C″	S_A	N	I[a]
11	C_6F_5	99 (12.6)[b]	105 (12.6)[b]	148 (25.9)	155 (0.7)	179
13	2-C_6F_4Br	109 (32.9)	118 (2.8)	-	137 (30.2)	185
15	4-C_6F_4Br	89 (9.1)	-	-	166 (31.4)	222
18	μ-4-4'-$C_6F_4C_6F_4$[1]	-	-	-	206 (15.4)	246

a = clearing point transition temperatures were determined optically using a Kofler hotstage microscope and are uncorrected. The temperature quoted is the final disappearance of anisotropy. b = the C-C′ and C′-C″ transitions of complex **11** are reported with the combined ΔH value of 12.6 kJ.mol^{-1} as the transitions occur close together.

As previously observed for ClAu(7-OST) complexes **3-9** (section 2.3.8), no solid state transitions were observed when the samples were rapidly precipitated. Complex **18** always precipitated rapidly from solution and this may explain the absence of such transitions. Compared to ClAu(7-OST) complex **6**, which only exhibits a S_A mesophase, all RAu(7-OST) complexes **11, 13, 15** and **18** exhibit predominantly nematic phases. Only complex **11** forms a S_A phase with a narrow temperature range before forming the nematic phase (Figure3.6). The S_A phase of complex **11** has a similar texture to the S_A phases of complexes **3-9** (section 2.3.8). The nematic phase was more fluid than the S_A phase and typical schlieren (Plate 3.1) and marbled (Plate 3.1) textures were observed. Application of slight pressure to the microscope cover slip resulted in the observation of emission of light flashes, also characteristic of the nematic phase.

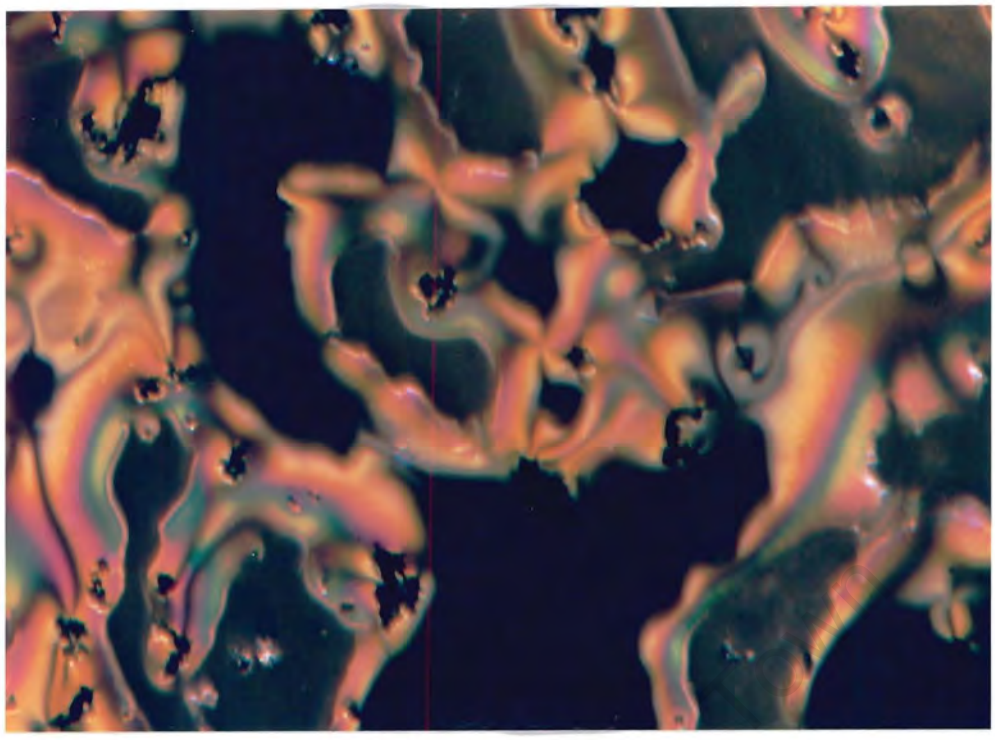

Plate 3.1: Schlieren N texture of complex **13** at 164 °C (1st cooling), crossed polarised light, and x10x4x2 magnification.

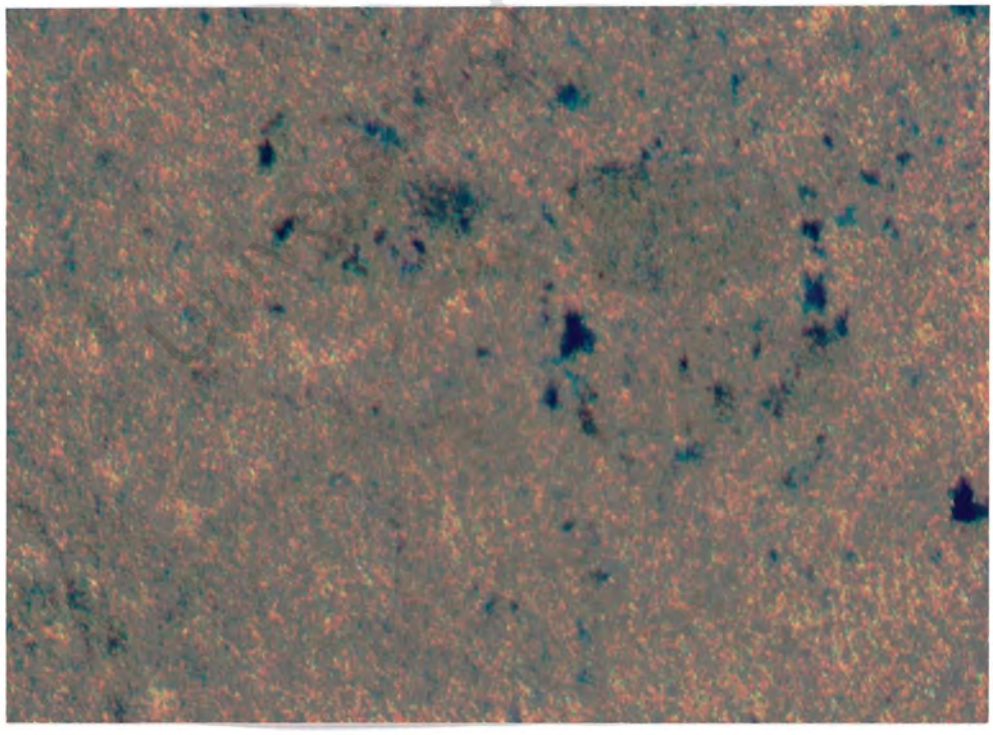

Plate 3.1: Marbled N texture of complex **13** at 145 °C (1st heating), crossed polarised light, and x10x4x2 magnification.

As with complexes **3-9**, no endothermic peak was observed in the DSC thermogram of complexes **11, 13, 15** and **18** at the temperature at which an optical observation of the clearing point transition was made. The clearing point transition temperature is thus only optically observed and is recorded as the final disappearance of the nematic phase. Unlike ClAu(n-OST) complexes **3-9**, RAu(7-OST) complexes **11, 13, 15** and **18** do not have a broad exothermic peak accompanying the clearing point, although accelerated mass loss and partial decomposition do occur. Even at a lower scan rate of 2 °C/min, the DSC thermogram of complex **13** seemed to indicate that the energy required at the clearing point transition for the RAu(7-OST) complexes is below detection limits, with no corresponding change in heat flow at that point. A sharp decrease in heat flow in the DSC thermogram, often observed during decomposition processes, was however obtained in the case of complex **18**, which decomposed completely at the clearing point. TLCs run on these complexes immediately after formation of the isotropic liquid state also confirm that partial decomposition has occurred, accompanied with the release of some stilbazole from the complexes. The accelerated mass loss at the optically observed clearing points for RAu(7-OST) complexes can clearly be seen from an example of a typical TG thermogram (Figures 3.15). This is due to very gradual thermal decomposition on heating, which accelerates markedly when the complexes pass from the liquid crystalline into the isotropic liquid phase. Although the complexes **3-9, 11, 13** and **15** partially decompose at the clearing point, liberating stilbazole, it is observed that some of the complexes still exhibit their liquid crystal phases during the second heating run, but at lower transition temperatures.

In any event, an orange liquid usually forms at the clearing point after the first or second heating run of the sample. On cooling, this orange isotropic liquid forms a very viscous, highly birefringent liquid crystal phase at about 155 °C for complex **6** and 135 to 138 °C for complexes **11, 13** and **15**. This viscous mesophase crystallised at about 60 to 69 °C with further cooling, and melted with subsequent heating at about 65 to 78 °C. The first cooling scan of a DSC thermogram of complex **11** showed two small exothermic peaks at 128 °C and 67 °C and the second heating scan has an endothermic transition at 71 °C, which corresponds to the above observations for the orange fluid. From the above information, it should be clear that the mesomorphic properties of these complexes should only be observed on the first heating run, as these complexes are thermally unstable.

3.4.7 Changes in mesomorphic properties of RAu(n-OST) complexes and comparison with RAu(isocyanide) complexes[1]

By comparing complex **6** (X = Cl) with complexes **11, 13** and **15** (R = C_6F_5, 2-C_6F_4Br, 4-C_6F_4Br) it can be seen that the more bulky perhalophenyl groups do not result in lower transition temperatures or shorter mesophase ranges, as observed in the isocyanide system.[1] The R groups are more bulky than the chloride group and it may be expected that they lower transition temperatures due to reduced lateral intermolecular interactions. Electronic factors such as the polarisability of the R groups however, may result in

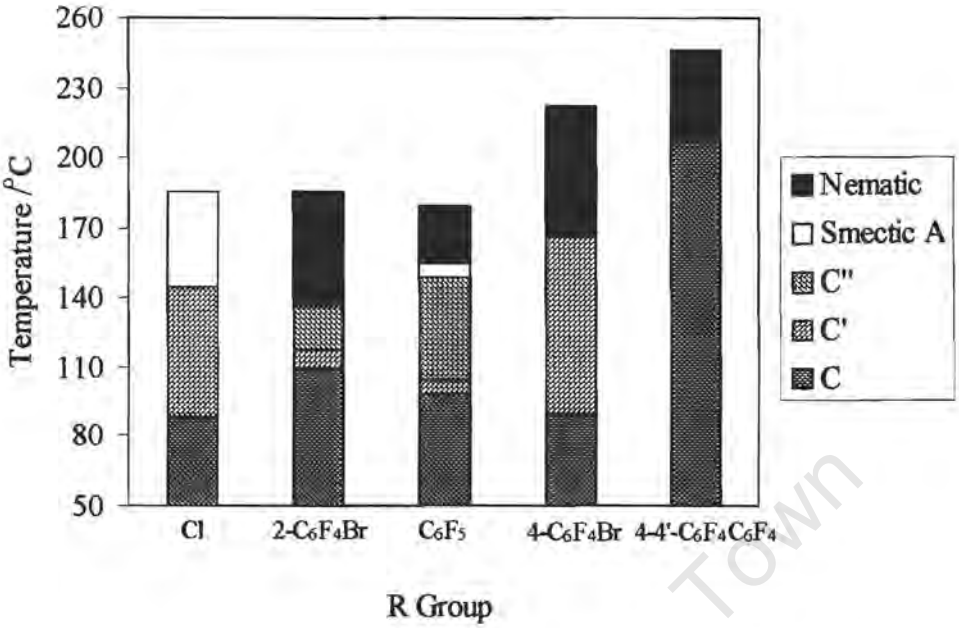

Figure 3.16: Graphical illustration of transition temperatures for RAu(7-OST) complexes

increased intermolecular attractive forces and conversely increased transition temperatures. The observed transition temperatures of RAu(7-OST) complexes compared with ClAu(7-OST) is probably a result of a balance between these steric and electronic factors.

The R groups formed RAu(n-OST) complexes exhibiting predominantly nematic phases whereas the chloride group resulted in S_A phase formation (Figure 3.16). A similar preference of the R groups for forming nematic phases was observed for the gold(I)isocyanide complexes.[1] This implies that the complexes with bulky R groups have less-ordered intermolecular arrangements in the mesophase compared with the chloride group.

The smectic (S_A) to nematic phase transition involves the slip of molecules from a structure with discreet aromatic and aliphatic regions to a structure where the aromatic and aliphatic regions are mixed.[1] Figure 3.17 (a) depicts a simple model of the aromatic interactions that favours the adoption of a smectic arrangement.

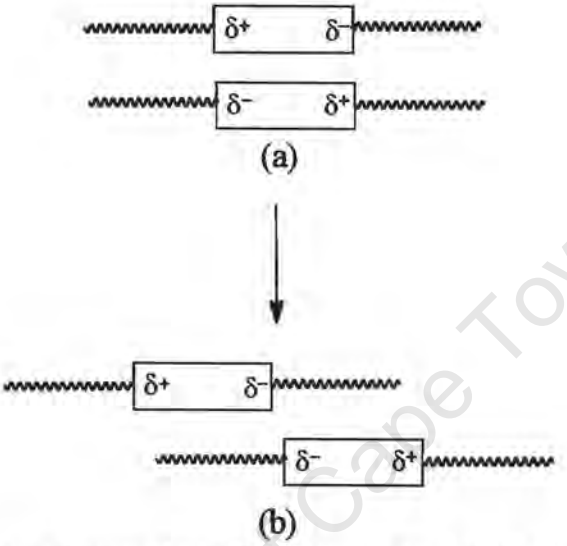

Figure 3.17: Schematic representation of electronic interactions for the smectic (a) and nematic (b) molecular arrangements of a rod-shaped dipolar mesogen[1]

These electronic interactions have to be overcome to achieve mixing of aromatic and aliphatic regions (b) characteristic of the nematic phase of a dipolar molecule.[1] For complex **11**, this slip occurs soon after melting, indicating the existence of ordered discrete aromatic and aliphatic regions in the solid phase, but complexes **13** and **15** melt directly into the nematic phase, indicating the presence of a less-ordered solid phase structure at or before melting. The R group of complex **11** does not contain a bromine atom and is slightly less bulky, which may explain why the more ordered S_A phase initially formed. For complex **6** (and other ClAu(n-OST) complexes), the electronic interactions are much greater and this slip does not occur at all.

The melting point transitions of RAu(7-OST) complexes **11**, **13**, **15** and **18** increase in the following order: 2-C_6F_4Br < C_6F_5 < 4- C_6F_4Br << μ-4-4'-$C_6F_4C_6F_4$ (Figure 3.16). The clearing point transitions behave similarly, except for C_6F_5, where it is slightly lower than 2-C_6F_4Br. The effects which bromine substituents on the perhaloaryl group may have on the mesophase transition temperatures can be explained by considering the following simple electronic and bulk effects:

(i) Electronic effect: Irrespective of its position, the introduction of a bromine substituent would lead to higher values for the molecular polarisability as the bromine atom is more polarisable than the fluorine atom. This leads to increased intermolecular interactions which in turn leads to higher transition temperatures.[1]

(ii) Bulk effect: The bromine atom in the *para* position produces only a small change in the total length of the molecule, whereas in the *ortho* position it causes a noticeable increase in the width of the molecule. This leads to a reduction in the intermolecular attractions and lower transition temperature.[1]

It has been observed for similar RAu(alkoxybiphenylisocyanide) complexes[1] that for chain lengths n ≥ 8 (Figure 3.19), electronic effects dominate the liquid crystal behaviour and melting and transition temperatures increasing in the following R group order of C_6F_5 < 2-C_6F_4Br < 4-C_6F_4Br. For smaller chain lengths n ≤ 6 though (Figure 3.20), it was found that bulk effects become more dominant, with the transition temperatures increasing in the following order of 2-C_6F_4Br < C_6F_5 < 4- C_6F_4Br.[1]

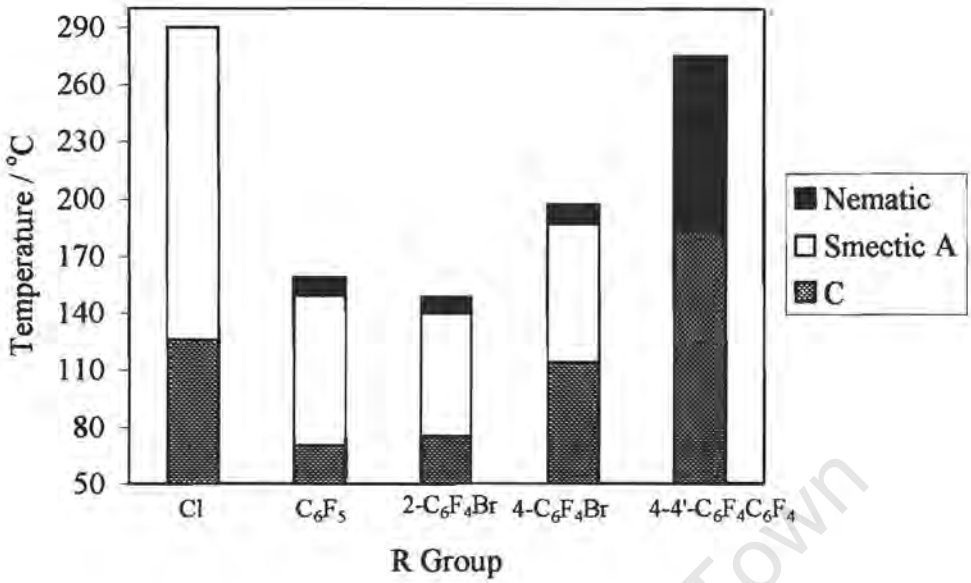

Figure 3.19: Graphical illustration of transition temperatures for RAu(isocyanide) complexes, m = 2, n = 8.[1]

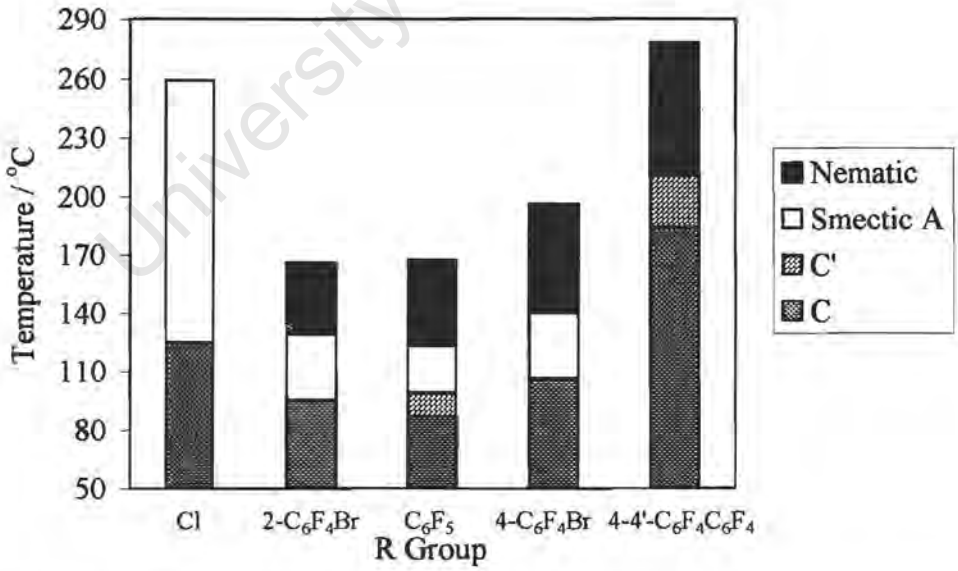

Figure 3.20: Graphical illustration of transition temperatures for RAu(isocyanide) complexes, m = 2, n = 6.[1]

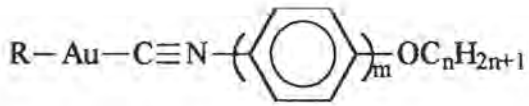

Figure 3.18: Schematic molecular structure of analogous RAu(isocyanide) complexes, m = 1,2, n = 4, 6, 8, 10, 12[1]

The trend in transition temperatures for complexes **11, 13** and **15** is similar to the one observed for analogues alkoxybiphenylisocyanide complexes with smaller chain lengths $n \leq 6$[1] and although the 2-C_6F_4Br group is more polarisable than the C_6F_5 group, complex **13** has lower transition temperatures due to the 2-C_6F_4Br group being more bulky.

The significantly higher transition temperatures of the binuclear complex **18** (Figure 3.16) suggests that much stronger intermolecular attractions must exist when R = μ-4,4'-$C_6F_4C_6F_4$. It is well-known that the steric and electronic repulsions between fluorine atoms produce large twist angles (about 53°) between the two rings of the octafluorobiphenyl group, as found crystallographically for nickel complexes.[1] This reduces the π-conjugation between the phenyl rings of the R group of complex **18** to a very small value.[1] Thus polarisability, which is associated with the π-conjugation, will be very limited between these phenyl rings.[1] It is probably best to consider complex **18** to behave as a symmetric dimer with two separate monomeric molecules linked head-to-head (Figure 3.21). The dimer has no net dipole moment but possesses a complex multipolar structure.[1] It has been proposed that a combination of the non-planar nature of the octafluorobiphenyl group (which hinders the adoption of a planar shape for a more efficient stacking of molecules) and the high melting temperatures helps to promote the

appearance of the entropically favoured nematic phase in gold(I) isocyanide derivatives.[1]

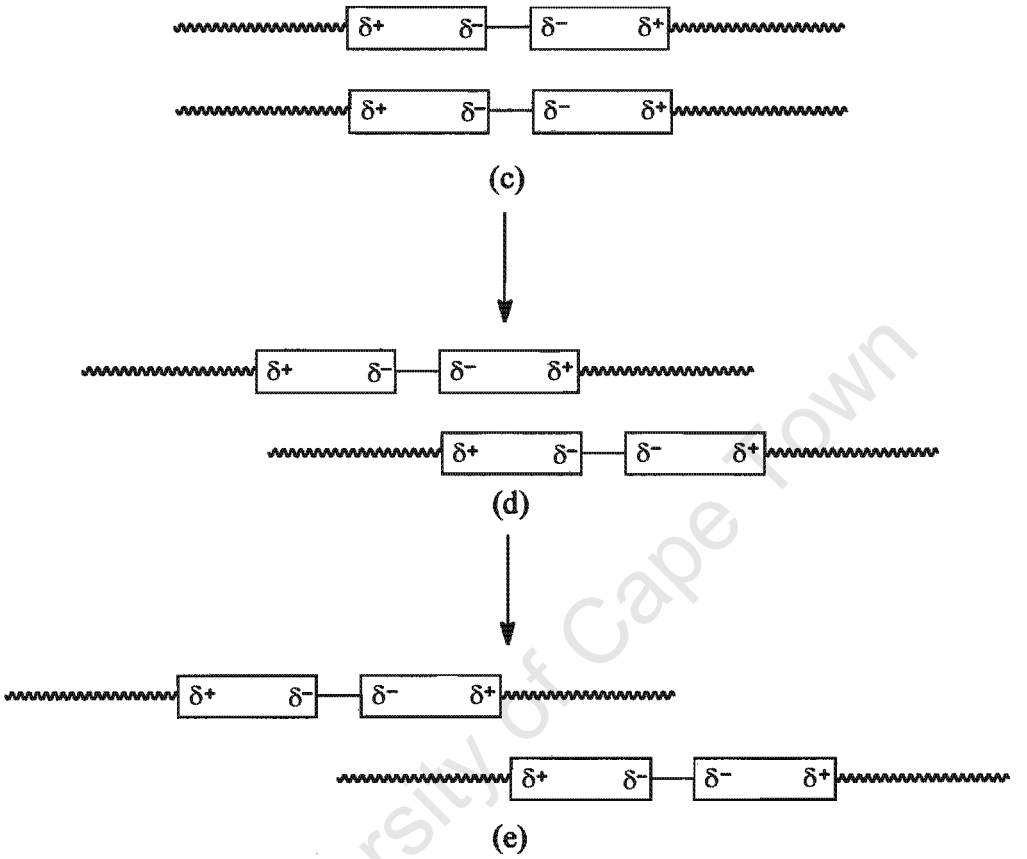

Figure 3.21: Schematic representation of electronic interactions for smectic (c), (d) and nematic (e) molecular arrangements of a symmetric multipolar rod-shaped mesogen[1]

The same probably holds true for the complex **18**, which also contains an octafluorobiphenyl group. According to the model for symmetric dimers (Figure 3.21), the most favoured electronic multipole-multipole interactions are probably represented by (d) rather than (c), so that some mixing of aromatic and aliphatic regions has already occurred.[1] The slip giving rise to the complete mixing of regions of the nematic phase (e)

thus becomes thermally more accessible.[1]

The isocyanide gold(I) complexes are thermally more stable, as most of the data for the transitions were collected on the second heating scan, compared to the stilbazole complexes, which partially decomposed at the clearing point. The deshielding experienced by the fluorine atoms in the *para* position of the R = C_6F_5 or 2-C_6F_4Br groups on displacement of tht indicates that isocyanide is a good π-acceptor ligand,[1] whereas in the 7-OST complexes the increased shielding observed on displacement of tht indicates that the 7-OST ligand is not such a good π-acceptor ligand as the isocyanide ligand, resulting in weaker gold-ligand bonds.

Gold(I)isocyanide complexes have much lower melting points and larger mesophase ranges than the analogous gold(I)(n-OST) complexes. RAu(isocyanide) complexes, R = C_6F_5, 2-C_6F_4Br and 4-C_6F_4Br, also exhibits both S_A and nematic phases, whereas the nematic phase is predominantly observed in the RAu(n-OST) complexes (Figures 3.16, 3.19-20). The isocyanide ligands thus tend to form gold(I) complexes with mesophases having weaker intermolecular attractive forces (*i.e.* lower melting temperatures) and a more ordered arrangement of molecules (initial formation of the S_A phase) compared to analogous gold(I)(n-OST) complexes.

3.5 Summary

1. When tht of RAu(tht) complexes **10, 12, 14** and **16** were replaced with 7-OST to form RAu(7-OST) complexes **11, 13, 15** and **18**, changes in ν(C-F) and Δδ (ppm) of ^{19}F-NMR spectra suggest that the 7-OST ligand induces changes in the electronic environment of atoms in the R groups. ν(Au-C) also indicates that the strength of the Au-C bond is greater for RAu(7-OST) complexes.

2. As ν(Au-C) values for RAu(tht) or RAu(7-OST) complexes remained constant and independent of the nature of the R group, the Au-C bond strength was not affected by changes in the R group.

3. The Δδ (ppm) of F_a, F_b and F_c for the R groups of complexes **12, 13, 14** and **15** are consistent with the electron-withdrawing properties of the Br atom. As similar changes were observed for complexes **16** and **18**, the $-C_6F_4AuL$ (L = tht or 7-OST) fragment can also be considered to behave as an electron-withdrawing group.

4. The symmetry of the R group was found to affect ν(C-F) values.

5.The electronic environment of the 7-OST ligands of RAu(7-OST) and ClAu(7-OST) complexes **6, 11, 13** and **15** seems to be independent of the nature of the trans ligand (R or Cl) except for complex **18**, when R = μ-4,4'-$C_6F_4C_6F_4$, even though the Au-C bond is significantly stronger than the Au-Cl bond. The FT-IR, ^{1}H- and ^{13}C-NMR spectra of complexes **6, 11, 13** and **15** were almost identical, however, very slight changes were observed in ν(C=N) values might imply slight changes in the Au-N bonds.

6. Changes in the ^{1}H- and ^{13}C-NMR spectra of the 7-OST ligand of complex **18**, especially the increased electron density of the py ring, as well as much higher transition temperatures, suggests that the R group μ-4,4'-$C_6F_4C_6F_4$ increases the stability of the Au-N

bond.

7. X-ray crystallography studies indicate that complex **11** crystallise in the monoclinic system from toluene/pentane as a neutral and monomeric species. The gold(I) atom is linearly coordinated with no intermolecular Au...Au bonding interactions. π---π stacking was not observed to play any role in the packing of the molecules in the crystal lattice.

8. Calculated dihedral angles between C_6F_5, py and phenyl rings of complex **11** indicate that they are relatively co-planar, with the C_6F_5 and py rings being more co-planar (about 4.1 °) than the py and phenyl rings (about 13.6 °). Torsion angles indicate that the ethane group is relatively co-planar with the py and phenyl rings, with the phenyl ring deviating slightly from planarity by about 15 °.

9. Compared to ClAu(n-OST) complexes, RAu(7-OST) complexes have similar mesomorphic transition temperatures, except for the more stable binuclear complex **18**, and this is attributed to electronic effects being more important than bulk effects. RAu(isocyanide) complexes have lower melting points than ClAu(isocyanide) complexes, indicating that the more bulky R group reduced the intermolecular attractions.

10. RAu (7-OST) complexes, as apposed to S_A phases formed by the ClAu (7-OST) complexes favour the nematic phase. This is due to weaker electronic interactions, which promote the slip of molecules into mixed aromatic/aliphatic regions indicative of the nematic state.

11. Bulk and electronic effects of the bromine atom compared to fluorine are important in explaining changes in mesomorphic properties for complexes **11, 13** and **15** and these changes have previously been observed in similar RAu(isocyanide) complexes.

12. RAu(isocyanide) complexes have lower melting points which favours the appearance

of the S_A phase compared to analogous RAu(7-OST) complexes.

3.6 References

1. R. Bayón, S. Coco, P. Espinet, C. Fernández-Mayordomo and J. M. Martín-Alvarez, *Inorg. Chem.*, 1997, **36**, 2329.
2. A. J. Seed, K. J. Toyne and J. W. Goodby, *J. Mater. Chem.*, 1995, **5**, 2201.
3. P. Kirsch and K. Tarumi, *Angew. Chem. Int. Ed.*, 1998, **37**, 484.
4. S.Coco, P. Espinet, J. M. Martín-Alvarez and A. Levelut, *J. Mater. Chem.*, 1997, **7** 19.
5. M. S. Kharasch and H. S. Isbell, *J. Am. Chem. Soc.*, 1931, **53**, 3053.
6. R. Usón and A. Laguna, *Coord. Chem. Rev.*, 1986, **70**, 1.
7. R. J. Puddephatt, in *Comprehensive Organometallic Chemistry: The synthesis, reactions and structures of organometallic compounds,* eds. E. W. Abel, F. G. A. Stone and G. Wilkinson, Pergamon Press, Oxford, 1st edn., 1982, vol. 2, ch. 15, pp. 765-821.
8. A. Grohmann and H. Schmidbaur in *Comprehensive Organometallic Chemistry II: a review of the literature 1982-1994*, eds. E. W. Abel, F. G. A. Stone and G. Wilkinson, Pergamon Press, Oxford, 1st edn., 1994, vol. 3, ch. 1, pp. 1-56.
9. C. Elschenbroich and A. Salzer, *Organometallics A Concise Introduction,* VCH,, Weinheim, 1st edn., 1989, ch. 13, pp 193-205.
10. Cambridge Structural Database and Cambridge Structural Database System, version 5.16, October 1998, Cambridge Crystallographic Data Centre, University Chemical Laboratory, Cambridge, England.
11. R. Usón, A. Laguna. E. J. Fernández, M. E. Ruiz-Romero, P. J. Jones and J. Lautner, *J. Chem. Soc., Dalton Trans.*, 1989, 2127.

12. S. Bordoni, L. Busetto, M. C. Cassani, V. G. Albano and P. Sabatino, *Inorg. Chim. Acta,* 1994, 267.

13. G. van Koten, C. A. Schaap, J. T. B. H. Jastrzebski and J. G. Noltes, *J. Organomet. Chem.*, 1980, **186**, 427.

14. C. Elschenbroich and A. Salzer, *Organometallics A Concise Introduction*, VCH,, Weinheim, 1st edn., 1989, ch. 14, pp 206-251.

15. J. R. Moss and B. L. Shaw, *J Chem Soc A*, 1966, 1793.

16. R. Usón, A. Laguna, M. Laguna, B. Manzano, P. G. Jones and G. M. Sheldrick, *J. Chem. Soc, Dalton Trans.*, 1985, 2417.

17. R. Usón, A. Laguna and M. D. Villacampa, *Inorg. Chim. Acta,* 1984, **81**, 25.

18. R. Usón and A. Laguna, *Inorg. Synth.,* 1982, **21**, 71.

19. A. C. Albéniz, A. L. Casado and P. Espinet, *Organometallics*, 1997, **16**, 5416.

20. R. Usón, A. Laguna, M. Laguna, I. Colera and E. de Jesús, *J. Organomet. Chem.*, 1984, **263**, 121.

21. R. Usón, A. Laguna and M. Laguna, *Inorg. Synth.,* 1989, **26**, 85.

22. R. Fields, J. Lee and D. J. Mowthorpe, *J. Chem. Soc. (B)*, 1968, 308.

23. R. H. Blessing, *Acta Cryst.*, 1995, **A51**, 33.

24. R. H. Blessing, *J. Appl. Cryst.*, 1997, **30**, 421.

25. Z. Otwinowski and W. Minor, "Processing of X-ray Diffraction Data Collected in Oscillation Mode", *Methods in Enzymology, Volume 276: Macromolecular Crystallography, part A*, eds. C. W. Carter, Jr. and R. M. Sweet, Academic Press, 1997, pp. 307-327.

26. S. Mackay, C. J. Gilmore, C. Edwards, M. Tremayne, N. Stewart and K Shankland,

"maXus: a computer program for the solution and refinement of crystal structures from diffraction data", University of Glasgow, Scotland, UK, Nonius BV, Delft, The Netherlands and MacScience Co. Ltd., Yokohama, Japan, 1998.

27. G. M. Sheldrick, *Acta Cryst.*, 1990, **A46**, 467.
28. G. M. Sheldrick, SHELXL-93, Program for the Refinement of Crystal Structures, University of Göttingen, Germany, 1993.
29. W. Conzelmann, W. Hiller and J. Strähle, *Z. anorg. allg. Chem.*, 1984, **512**, 169.
30. M. J. Irwin, J. J. Vittal, G. P. A. Yap and R. J. Puddephatt, *J. Am. Chem. Soc.*, 1996, **118**, 13101.
31. Y. Inoguchi, B. Milewski-Mahrla and H. Schmidbaur, *Chem. Ber.*, 1982, **115**, 3085.
32. A. Kolb, P. Bissinger and H. Schmidbaur, *Inorg. Chem.*, 1993, **32**, 5132.
33. P. G. Jones, *Gold Bulletin*, 1981, **14**, 102.
34. E. J. Fernández, M. C. Gimeno, P. G. Jones, A. Laguna, J. M. López-de-Luzuriaga and E. Olmos, *Chem. Ber.*, 1997, **130**, 1513.
35. R. W. Baker and P. J. Pauling, *J. Chem. Soc, Dalton Trans.*, 1972, 2264.
36. R. Usón, A. Laguna, J. Vicente, J. Garcia, P. G. Jones and G. M. Sheldrick, *J. Chem. Soc, Dalton Trans.*, 1981, 655.
37. J. Vicente, M. Chicote, P. González-Herrero and C. Grünwald, *Organometallics*, 1997, **16**, 3381.
38. X. Hong, K. Cheung, C. Guo and C. Che, *J. Chem. Soc, Dalton Trans.*, 1994, 1867.
39. T. V. Baukova, L. G. Kuz'mina, N. A. Oleinikova, D. A. Lemenovskii and A. L. Blumenfel'd, *J. Organomet. Chem.*, 1997, **530**, 27.
40. S. R. Marder, J. W. Perry and C. P. Yakymyshyn, *Chemistry of Materials*, 1994, **6**,

1137.

41. D. Zhang, T. Zhang, Y. Zhang, L. Ge and K. Yu, *Acta Crystallogr., Sect. C. (C.Str.Comm.)*, 1998, **54**, 138.

42. K. Willis, D. J. Price, H. Adams, G. Ungar and D. W. Bruce, *J. Mater. Chem.*, 1995, **5**, 2195.

43. H. Adams, N. A. Bailey, D. W. Bruce, S. C. Davis, D. A. Dunmur, P. D. Hempstead, S. A. Hudson and S. Thorpe, *J. Mater. Chem.*, 1992, **2**, 395.

Appendix 3A

Table 3A.1: FT-IR spectroscopic data (in cm^{-1}) of R groups for RAu(tht) and RAu(7-OST) complexes and precursor perfluorobromoaryl compounds.

Complex	R group	L group	ν(C-F)[a]	ν(C-Au)[b]
	BrC_6F_5		1510, 1066, 979, 835	
	2-$Br_2C_6F_4$		1502, 1117, 1036, 848	
	4-$Br_2C_6F_4$		1490, 957	
	μ-4,4'-$Br_2C_6F_4C_6F_4$		1476, 961	
10	C_6F_5	tht	1505 s, 1072 s, 959 s, 792 s	532 m
12	2-C_6F_4Br	tht	1483 s, 1080 s, 1007 s, 821 s	534 m
14	4-C_6F_4Br	tht	1446 s, 936 s	-
16	μ-4,4'-$C_6F_4C_6F_4$	tht	1445 s, 934 s	-
17	$HC_6F_4C_6F_4$	tht	1500 s, 1443 s, 926 s	-
11	C_6F_5	7-OST	1505 s, 1064 s, 958 s, 808 s	600 m
13	2-C_6F_4Br	7-OST	1488 s, 1087 s, 1013 s, 830 s	580 m
15	4-C_6F_4Br	7-OST	1447 s, 937 s	594 m
18[c]	μ-4,4'-$C_6F_4C_6F_4$[3]	7-OST	1446 s, 932 s	580 m

a = spectra were obtained in dichloromethane solution cells with NaCl windows, b = obtained as a nujol mull between polyethylene sheets, c = obtained as a KBr disc, m = medium, s = strong..

Table 3A.2: FT-IR spectroscopic data[a] (in cm^{-1})of 7-OST ligands for RAu(7-OST) complexes.

Complex	R Group	ν(C-H)[b]	ν(C-H)[c]	ν(C=C)	ν(C=N)	ν(C-C)	ν(O-C)	ν(C-H)[d]
11	C_6F_5	3031 m	2930 s 2857 s	1599 vs 1513 s 1460 m	1445 s	1249 vs	1198 s 1174 vs	968 s
13	2-C_6F_4Br	3039 m	2930 s 2858 s	1599 vs 1513 s 1465 m	1426 s	1251 vs	1198 s 1174 vs	968 s
15	4-C_6F_4Br	3039 m	2930 s 2858 s	1599 vs 1513 s 1458 m	1435 s	1250 vs	1198 s 1174 vs	969 s
18[e]	μ-4,4'- $C_6F_4C_6F_4$	3039 m	2930 s 2854 s	1594 vs 1511 s 1463 m	1435 s	1249 vs	1198 s 1172 vs	961 s

a = spectra were obtained using dichloromethane solution cells with NaCl windows, b = aromatic stretch, c= alkane stretch, d = alkane out-of-plane bend, e = obtained as a KBr disc, m = medium, s = strong, vs = very strong.

Table 3A.3: ^{1}H-NMR spectroscopic data for RAu(7-OST) complexes in $CDCl_3$.

Complex	R group	H_a AA'XX' 2H	H_b AA'XX' 2H	H_d AB 1H	H_e AB 1H	H_g AA'XX' 2H	H_h AA'XX' 2H	H_j t 2H	H_k qn 2H	H_l qn 2H	H_m m 6H	H_n t 3H
11	C_6F_5	8.49 (6.8)	7.56 (6.8)	6.88 (16.3)	7.41 (16.3)	7.52 (8.8)	6.93 (8.8)	4.00 (6.6)	1.81 (7.0)	1.46 (7.2)	1.32	0.90 (6.9)
13	2-C_6F_4Br	8.48 (6.8)	7.53 (6.8)	6.87 (16.0)	7.39 (16.4)	7.51 (9.2)	6.93 (8.8)	4.00 (6.4)	1.81 (7.0)	1.47 (7.6)	1.32	0.90 (6.8)
15	4-C_6F_4Br	8.49 (6.8)	7.55 (6.4)	6.88 (16.0)	7.41 (16.0)	7.51 (8.8)	6.93 (8.5)	4.00 (6.6)	1.81 (7.2)	1.47 (7.6)	1.32	0.90 (6.8)
18	μ-4,4'-$C_6F_4C_6F_4$	8.07, 4H (7.2)	7.49, 4H (9.2)	6.86, 2H (14.8)[a]	7.33, 2H (17.2)	7.46, 4H (8.8)	6.89, 4H (8.8)	3.97, 4H (6.6)	1.76, 4H (7.2)	1.39, 4H (7.6)	1.29, 12H	0.88, 6H (7.6)
18[b]	μ-4,4'-$C_6F_4C_6F_4$	8.55, 4H (6.8)	7.64, 4H (7.2)	6.97, 2H (16.0)	7.48, 2H (16.0)	7.57, 4H (8.4)	6.96, 4H (8.8)	4.02, 4H (6.4)	1.81. 4H (6.9)	1.48, 4H (7.2)	1.34, 12H	0.91, 6H (6.8)

a = Poor resolution of coupling constant due to overlapping H_d and H_h peaks, b = measured in CD_2Cl_2, t = triplet, qn = quintet and m = multiplet.

Table 3A.4: ^{13}C-NMR spectroscopic data for RAu(7-OST) complexes in $CDCl_3$.

Complex	R group	C_a	C_b	C_c	C_d	C_e	C_f	C_g	C_h	C_i	C_j	C_l	$C_{k,m}$	C_n
11	C_6F_5	150.9	122.5	149.0	121.1	137.0	127.6	129.1	115.1	160.8	68.2	26.0	31.8, 29.2, 29.0, 22.6	14.1
13	2-C_6F_4Br	150.8	122.4	148.9	121.1	136.9	127.6	129.0	115.0	160.7	68.2	25.9	31.7, 29.0, 29.1, 22.5	14.0
15	4-C_6F_4Br	150.9	122.4	149.1	121.1	137.0	127.6	129.1	115.1	160.8	68.2	26.0	31.8, 29.2, 29.0, 22.6	14.1
18	μ-4,4'-$C_6F_4C_6F_4$	152.8	124.4	143.6	123.2	138.6	127.5	130.9	116.8	155.9	70.1	27.8	33.6, 31.0, 30.9, 24.4	15.7

Table 3A.5: ^{19}F-NMR spectroscopic data for RAu(tht) complexes in $CDCl_3$.

Complex	R Group	L Group	F_a (ortha)		F_b (meta)		F_c (para)		F_d (meta)	
			δ (ppm)	J (Hz)	δ (ppm)	J (Hz)	δ (ppm)	J (Hz)	δ (ppm)	J (Hz)
10	C_6F_5	tht	-166.63	-	-120.39	-	-162.70	$^3J_{2,3}$ = 20.1		
			m		m		t			
12[a]	o-C_6F_4Br	tht	-116.19	$^3J_{1,2}$ = 30.5	-157.08	$^3J_{1,2}$ = 30.5	-157.80	$^3J_{3,4}$ = 21.2	-127.10	$^3J_{3,4}$ = 21.2
			dd	$^5J_{1,4}$ = 11.9	ddd	$^3J_{2,3}$ = 19.5	dd	$^3J_{2,3}$ = 19.5	ddd	$^5J_{1,4}$ = 11.9
						$^4J_{2,4}$ = 1.4				$^4J_{2,4}$ = 1.4
14[a]	p-C_6F_4Br	tht	-115.50	$^3J_{1,2}$+ $^5J_{1,2'}$ = 18.3	-135.30	$^3J_{1,2}$+$^5J_{1,2'}$ = 18.3				
			m	$^4J_{1,1'}$+$^4J_{2,2'}$ = 10.0		$^4J_{1,1'}$+$^4J_{2,2'}$ = 10.0				
				$^3J_{1,2}$–$^5J_{1,2'}$ = 42.5		$^3J_{1,2}$–$^5J_{1,2'}$ = 42.5				
16	μ-4-4'-$C_6F_4C_6F_4$	tht	-117.51	-	-140.22	-				
			m		m					

a = data obtained from literature[1], d = doublet, t = triplet, m = multiplet.

Table 3A.6: ^{19}F-NMR spectroscopic data for complexes RAu(7-OST) in $CDCl_3$.

Complex	R Group	L Group	F_a (ortha)		F_b (meta)		F_c (para)		F_d (meta)	
			δ (ppm)	J (Hz)	δ (ppm)	J (Hz)	δ (ppm)	J (Hz)	δ (ppm)	J (Hz)
11	C_6F_5	7-OST	-167.12	-	-120.27	-	-163.61	$^3J_{2,3}$ = 20.1		
			m		m		t			
13	2-C_6F_4Br	7-OST	-115.70	$^3J_{1,2}$ = 30.3	-157.40	$^3J_{1,2}$ = 30.0	-158.55	$^3J_{3,4}$ = 21.2	-126.97	$^3J_{3,4}$ = 21.3
			dddd	$^5J_{1,4}$ = 11.5	ddd	$^3J_{2,3}$ = 19.5	dd	$^3J_{2,3}$ = 19.6	tdd	$^5J_{1,4}$ = 11.5
				$^5J_{1,2'}$ = 6.0		$^4J_{2,4}$ = 1.3				$^4J_{2,4}$ = 1.2
				$^4J_{1,3}$ = 1.4						
15	4-C_6F_4Br	7-OST	-115.11	$^3J_{1,2}$+ $^5J_{1,2'}$ = 18.3	-135.71	$^3J_{1,2}$+$^5J_{1,2'}$ = 18.2				
			m	$^4J_{1,1'}$+$^4J_{2,2'}$ = 9.5	m	$^4J_{1,1'}$+$^4J_{2,2'}$ = 9.5				
				$^3J_{1,2}$–$^5J_{1,2'}$ = 41.8		$^3J_{1,2}$–$^5J_{1,2'}$ = 41.8				
17	μ-4,4'-$C_6F_4C_6F_4$[3]	7-OST	-117.71	-	-140.89	-				
			m		m					

d = doublet, t = triplet, m = multiplet.

Table 3A.7 Atomic coordinates for complex **11**.

Atom	X/a (e.s.d.)	Y/b (e.s.d.)	Z/c (e.s.d.)
Au	0.1228(1)	0.0252(0)	0.1977(1)
F2	-0.0203(13)	0.0695(2)	-0.0639(8)
F3	0.2231(16))	0.1141(2)	-0.1460(8)
F4	0.6797(17)	0.1260(2)	0.0070(11)
F5	0.8817(13)	0.0948(2)	0.2453(12)
F6	0.6419(13)	0.0502(2)	0.3295(8)
O1	-0.9413(17)	-0.1900(2)	0.6238(9)
N1	-0.0692(16))	-0.0083(3)	0.2586(10)
C1	0.3049(21)	0.0576(3)	0.1365(12)
C2	0.2064(21)	0.0751(3)	0.0172(13)
C3	0.3270(25)	0.0975(4)	-0.0297(13)
C4	0.5592(25)	0.1044(4)	0.0486(16))
C5	0.6580(21)	0.0883(4)	0.1672(14)
C6	0.5290(24)	0.0652(3)	0.2088(13)
C7	0.0259(24)	-0.0258(3)	0.3693(15)
C8	-0.0973(22)	-0.0485(4)	0.4091(13)
C9	-0.3370(20)	-0.0545(3)	0.3337(13)
C10	-0.4296(23)	-0.0358(4)	0.2215(14)
C11	-0.2964(25)	-0.0128(4)	0.1890(13)
C12	-0.4667(28)	-0.0785(4)	0.3701(15)
C13	-0.4085(24)	-0.0982(4)	0.4678(14)
C14	-0.5513(24)	-0.1223(3)	0.5040(13)
C15	-0.4705(24)	-0.1377(4)	0.6348(13)
C16	-0.6067(24)	-0.1592(4)	0.6710(14)
C17	-0.8210(26)	-0.1682(4)	0.5766(12)
C18	-0.8988(25)	-0.1533(4)	0.4439(13)
C19	-0.7616(27)	-0.1310(4)	0.4125(14)
C20	-1.1474(24)	-0.2020(4)	0.5273(13)
C21	-1.2532(24)	-0.2242(3)	0.6102(13)
C22	-1.4591(26)	-0.2406(4)	0.5155(13)
C23	-1.5715(27)	-0.2627(4)	0.5992(13)
C24	-1.7745(25)	-0.2799(4)	0.5074(14)
C25	-1.8802(28)	-0.3025(4)	0.5908(17)
C26	-2.0796(31)	-0.3194(4)	0.5035(18)

Table 3A.8: Thermal displacement parameters (x 10^3) for complex **11**, $\exp(-2\pi^2(U_{11}h^2a^{*2}+\ldots 2U_{12}hka^*b^*+\ldots)$.

Atom	U_{11} (e.s.d.)	U_{22} (e.s.d.)	U_{33} (e.s.d.)	U_{23} (e.s.d.)	U_{13} (e.s.d.)	U_{12} (e.s.d.)
Au[a]	562(4)	565(6)	671(4)	20(3)	171(3)	-4(3)
F2	64(5)	86(8)	77(5)	-2(4)	-8(4)	-2(5)
F3	110(6)	71(8)	74(5)	18(5)	28(4)	13(5)
F4	94(6)	71(9)	124(7)	-10(6)	42(5)	-23(6)
F5	47(5)	81(9)	153(8)	-17(6)	4(5)	-9(4)
F6	71(5)	83(8)	70(5)	9(4)	1(4)	17(5)
O1	76(6))	73(9)	63(5)	2(5)	13(5)	-23(6)
N1	44(6)	67(10)	54(5)	4(6)	14(4)	-4(6)
C1	48(7)	74(13)	48(6)	-2(6)	17(5)	1(7)
C2	47(7)	55(12)	67(8)	-14(7)	23(6)	-6(7)
C3	75(9)	61(13)	51(7)	10(7)	20(6)	15(8)
C4	64(9)	57(13)	82(9)	-2(8)	30(7)	-6(8)
C5	39(7)	76(14)	69(8)	-12(8)	16(6)	3(7)
C6	63(8)	48(11)	59(7)	1(6)	17(6)	17(8)
C7	49(7)	61(13)	71(8)	-4(7)	14(6)	-8(7)
C8	54(8)	82(14)	58(7)	21(7)	4(6)	-6(8)
C9	46(7)	38(11)	73(8)	11(7)	17(6)	5(6)
C10	50(7)	42(11)	71(8)	-3(7)	4(6)	0(7)
C11	64(8)	60(12)	52(7)	2(7)	5(6)	5(9)
C12	89(10)	56(13)	66(8)	14(8)	50(7)	17(9)
C13	66(8)	47(12)	62(8)	-5(1	39(6)	1(8)
C14	75(9)	45(11)	57(7)	4(6)	15(6)	-4(8)
C15	65(8)	59(13)	57(7)	-4(7)	-12(6)	-1(8)
C16	67(8)	63(13)	61(7)	5(7)	11(6)	2(8)
C17	86(10)	71(14)	43(6)	3(7)	5(6)	-12(9)
C18	69(9)	77(15)	57(7)	6(7)	-3(6)	-16(9)
C19	86(10)	66(14)	58(7)	7(7)	1(7)	-11(9)
C20	61(8)	87(14)	56(7)	6(7)	11(6)	-10(8)
C21	75(8)	55(12)	54(7)	-4(6)	7(6)	-8(8)
C22	90(10)	66(14)	59(7)	8(7)	26(7)	-10(9)
C23	99(11)	94(15)	45(7)	3(7)	18(7)	-29(10)
C24	73(9)	101(17)	62(8)	-2(8)	23(7)	-9(9)
C25	85(11)	73(16))	93(11)	9(9)	-5(8)	-17(10)
C26	109(13)	97(18)	86(10)	-4(10)	23(9)	-26(12)

a = x 10^4

Table 3A.9: Bond lengths (Å) for complex **11**.

Bond	Bond length (e.s.d.)[a]
Au-N1	2.06(1)
Au-C1	1.99(1)
F2-C2	1.37(1)
F3-C3	1.36(2)
F4-C4	1.32(2)
F5-C5	1.35(1)
F6-C6	1.36(1)
O1-C17	1.36(2)
O1-C20	1.42(2)
N1-C7	1.34(2)
N1-C11	1.33(2)
C1-C2	1.40(2)
C1-C6	1.35(2)
C2-C3	1.37(2)
C3-C4	1.40(2)
C4-C5	1.36(2)
C5-C6	1.41(2)
C7-C8	1.36(2)
C8-C9	1.42(2)
C9-C10	1.37(2)
C9-C12	1.42(2)
C10-C11	1.39(2)
C12-C13	1.28(2)
C13-C14	1.47(2)
C14-C15	1.41(2)
C14-C19	1.37(2)
C15-C16	1.36(2)
C16-C17	1.40(2)
C17-C18	1.41(2)
C18-C19	1.37(2)
C20-C21	1.50(2)
C21-C22	1.51(2)
C22-C23	1.53(2)
C23-C24	1.50(2)
C24-C25	1.52(2)
C25-C26	1.47(2)

a = uncorrected

Table 3A.10: Bond angles (degrees) for complex 11.

Atoms	Angle (e.s.d.)
N1-Au-C1	179(1)
C17-O1-C20	119(1)
Au-N1-C11	120(1)
Au-N1-C7	122(1)
C7-N1-C11	118(1)
Au-C(1)-C6	123(1)
Au-C1-C2	122(1)
C2-C1-C6	114(1)
F2-C2-C1	120(1)
C1-C2-C3	124(1)
F2-C2-C3	116(1)
F3-C3-C2	122(1)
C2-C3-C4	119(1)
F3-C3-C4	119(1)
F4-C4-C3	121(1)
C3-C4-C5	118(1)
F4-C4-C5	121(1)
F5-C5-C4	119(1)
C4-C5-C6	120(1)
F5-C5-C6	121(1)
C1-C6-C5	124(1)
F6-C6-C5	116(1)
F6-C6-C1	120(1)
N1-C7-C8	123(1)
C7-C8-C9	121(1)
C8-C9-C12	122(1)
C8-C9-C10	115(1)
C10-C9-C12	123(1)
C9-C10-C11	121(1)
N1-C11-C10	122(1)
C9-C12-C13	132(1)
C12-C13-C14	130(1)
C13-C14-C19	122(1)
C13-C14-C15	120(1)
C15-C14-C19	118(1)
C14-C15-C16	120(1)
C15-C16-C17	121(1)
O1-C17-C16	116(1)
C16-C17-C18	118(1)
O1-C17-C18	125(1)
C17-C18-C19	119(1)
C14-C19-C18	123(1)
O1-C20-C21	108(1)
C20-C21-C22	113(1)
C21-C22-C23	113(1)
C22-C23-C24	114(1)
C23-C24-C25	114(1)
C24-C25-C26	115(1)

Table 3A.11: Torsion angles (degrees) for complex **11**.

Atoms	Angle (e.s.d.)
N1-Au-C1-C2	13(38)
N1-Au-C1-C6	-170(37)
C1-Au-N1-C11	-16(38)
C1-Au-N1-C7	165(37)
C17-O1-C20-C21	-176(1)
C20-O1-C17-C16	-174(1)
C20-O1-C17-C18	9(2)
Au-N1-C11-C10	177(1)
Au-N1-C7-C8	-179(1)
C7-N1-C11-C10	-4(2)
C11-N1-C7-C8	3(2)
Au-C1-C2-F2	-2(2)
Au-C1-C6-F6	1(2)
C2-C1-C6-F6	178(1)
Au-C1-C6-C5	-179(1)
Au-C1-C2-C3	-179(1)
C6-C1-C2-F2	-180(1)
C2-C1-C6-C5	-2(2)
C6-C1-C2-C3	3(2)
F2-C2-C3-F3	3(2)
C1-C2-C3-F3	-180(1)
C1-C2-C3-C4	-3(2)
F2-C2-C3-C4	180(1)
F3-C3-C4-F4	-3(2)
C2-C3-C4-F4	-180(1)
C2-C3-C4-C5	1(2)
F3-C3-C4-C5	178(1)
F4-C4-C5-F5	1(2)
C3-C4-C5-F5	-179(1)
C3-C4-C5-C6	0(2)
F4-C4-C5-C6	-179(1)
F5-C5-C6-C1	180(1)
F5-C5-C6-F6	0(2)
C4-C5-C6-C1	0(2)
C4-C5-C6-F6	-180(1)
N1-C7-C8-C9	0(2)
C7-C8-C9-C10	0(2)
C7-C8-C9-C12	178(1)
C8-C9-C12-C13	0(3)
C8-C9-C10-C11	-1(2)
C10-C9-C12-C13	179(2)
C12-C9-C10-C11	-180(1)
C9-C10-C11-N1	4(2)
C9-C12-C13-C14	178(1)
C12-C13-C14-C15	-166(2)
C12-C13-C14-C19	15(2)
C13-C14-C19-C18	-180(1)
C13-C14-C15-C16	177(1)
C15-C14-C19-C18	2(2)
C19-C14-C15-C16	-4(2)
C14-C15-C16-C17	5(2)
C15-C16-C17-O1	180(1)

C15-C16-C17-C18	-3(2)
C16-C17-C18-C19	0(2)
O1-C17-C18-C19	178(1)
C17-C18-C19-C14	0(2)
O1-C20-C21-C22	-174(1)
C20-C21-C22-C23	-179(1)
C21-C22-C23-C24	-179(1)
C22-C23-C24-C25	178(1)
C23-C24-C25-C26	180(1)

Table 3A.12: Least squares plane through C1 to C6 atoms of complex **11**.

Atom	d	s	d/s	d/s^2
*C1	0.0109	0.0133	0.819	0.671
*C2	-0.0155	0.0137	-1.135	1.289
*C3	0.0101	0.0145	0.693	0.481
*C4	0.0020	0.0155	0.129	0.017
*C5	-0.0059	0.0149	-0.393	0.155
*C6	-0.0016	0.0140	-0.117	0.014
C7	0.0536	0.0146	3.681	13.549
C11	-0.1224	0.0152	-8.032	64.520
C15	0.0469	0.0148	3.179	10.104
C19	0.4225	0.0156	27.117	735.359

* = atoms used for plane calculation, d = displacement of atom from the calculated plane, s = standard deviation.

Table 3A.13: Least squares plane through N1, C7 to C11 atoms of complex **11**.

Atom	d	s	d/s	d/s^2
*N1	0.0116	0.0108	1.070	1.144
*C7	-0.0056	0.0145	-0.389	0.151
*C8	-0.0067	0.0140	-0.476	0.227
*C9	0.0043	0.0128	0.333	0.111
*C10	0.0091	0.0146	0.625	0.391
*C11	-0.0238	0.0149	-1.594	2.541
C15	-0.1724	0.0145	-11.864	140.755
C19	0.3655	0.0153	23.842	568.447

* = atoms used for plane calculation, d = displacement of atom from the calculated plane, s = standard deviation.

Table 3A.14: Least squares plane through C14 to C19 atoms of complex **11**.

Atom	d	s	d/s	d/s^2
*C14	-0.0129	0.0142	-0.907	0.823
*C15	0.0233	0.0151	1.541	2.375
*C16	-0.0172	0.0151	-1.139	1.297
*C17	0.0025	0.0156	0.160	0.026
*C18	0.0063	0.0157	0.399	0.159
*C19	0.0005	0.0160	0.030	0.001

* = atoms used for plane calculation, d = displacement of atom from the calculated plane, s = standard deviation.

CHAPTER 4. Synthesis and characterisation of RAuL complexes, R = alkyl, L = PPh_3 and n-OST

4.1 Introduction

This chapter will deal with the synthesis and characterisation of RAuL complexes, R = linear alkyl group and L = PPh_3, n-OST. Although various aryl-, acetylide- and isonitrilegold(I) complexes have been found to form liquid-crystal phases (section 1.4), no alkylgold(I) complexes have yet been reported to have such properties. It is however not unusual for transition metal complexes containing linear carbon chains to exhibit mesomorphism, since the linear arrangement of the carbon atoms favours alignment in a specific direction. If alignment persists beyond the melting point, then the liquid crystal state will be achieved. Silver thiolate alkyl complexes $[AgSC_nH_{2n+1}]_x$, n = 4, 6, 8, 10, 12, 16 and 18, (Figure 4.1) afford a typical example of such behaviour, where the alignment of the linear alkyl thiolate chains in the liquid crystal phase has been found by X-ray diffraction studies to be similar to that in the solid state.[1]

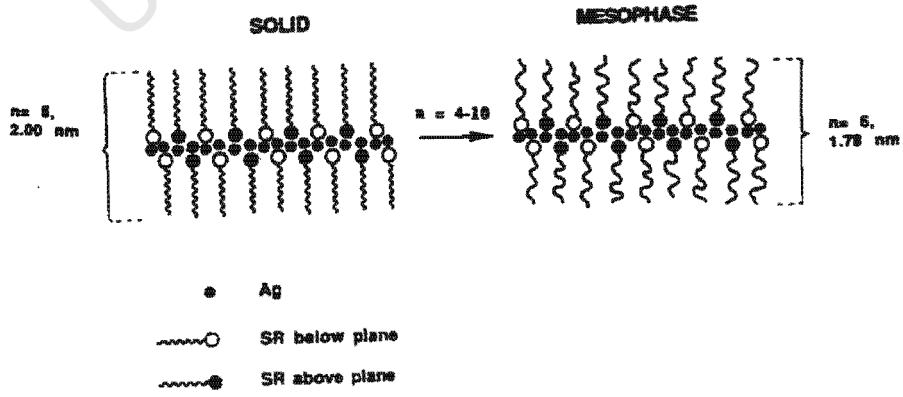

Figure 4.1: Schematic representation of silver thiolate mesogens

Although RAuL complexes, R = alkyl, with a very wide range of organic groups exist, the neutral ligand, L, is usually confined to tertiary phosphine or isocyanide ligands.[2,3] This limitation is probably a result of σ-bonded R groups in general exerting a high *trans* influence.[2,3] This creates an easy dissociation pathway to the reactive RAu^{I} species if the ligand L does not have a particularly high affinity for gold, so that the complex has a low stability constant and decomposition to metallic gold occurs readiliy.[2,3] This might explain why only aryl- and acetylidegold(isocyanide) complexes have thus far been prepared with mesomorphic properties (section 1.4). Corresponding alkylgold(isocyanide) [4] complexes are volatile and have more potential as chemical vapour deposition agents than as liquid crystals. Although acetylidegold(PR_3) complexes were not found to be mesomorphic as a result of steric hindrance of the bulky PR_3 ligands,[5,6] the possibility of alkylgold(PPh_3) complexes exhibiting mesomorphic behaviour were investigated. These alkylgold(I) complexes with PPh_3 ligands would be stable, but the bulky PPh_3 group would also inhibit linear alignment and greatly reduce the intermolecular attractions necessary to allow the molecules to maintain an ordered arrangement after melting. RAu(PR_3) complexes, R = linear alkyl group, were first synthesised in 1959.[7] Since then, complexes of up to four carbon atoms in an alkyl chain have been synthesised, but in most cases characterisation information has been limited to microanalysis, IR and sometimes ^{1}H-NMR spectroscopy.[7-15]

Due to n-OST ligands already possessing liquid crystalline properties compared to the bulky PPh_3 ligands, it is more likely for RAu(n-OST) complexes, R = alkyl, to be mesomorphic. RAu(n-OST) complexes are likely to be less stable than RAu(PPh_3)

complexes though, as a result of the large *trans* effect for RAuL complexes with ligands other than isocyanide or PR_3. These alkylAu(n-OST) complexes are also expected to have lower transition temperatures than the ClAu(n-OST) complexes and to favour smectic phases compared to the nematic phases favoured by the arylAu(n-OST) complexes.

4.2 Synthesis of RAu(PPh_3) complexes 19-24

4.2.1 General synthetic method for alkylithium reagents

The *n*-alkyllithium reagents used in the synthesis of complexes **19-24** were either freshly prepared by reaction of the appropriate *n*-alkylhalide with lithium metal, according to literature procedures,[18,19,20] or commercially available (MeLi and *n*-BuLi). The concentration of the *n*-alkyllithium reagent was determined immediately prior to use via:

(i) An indirect method,[21] involving a double titration of a hydrolysed sample and a hydrolysed sample to which dry allyl bromide had been added, with dilute hydrochloric acid, using phenolphthalein as an indicator,

(ii) A direct titration[22] of a sample with 2-butanol in xylene, using 2,2'-biquinoline as an indicator.

An alternative and more convenient method for synthesis of *n*-alkyllithium reagents[23] involving lithium-iodide exchange between *n*-iodoalkanes and *t*-BuLi at low temperature (–72 °C) was also employed. This method proved to be especially useful for the synthesis of the *n*-perfluorododecyllithium reagent (section 4.2.3).

*4.2.2 General synthetic method for RAu(PPh_3) complexes **19-24***

Complexes **19-24** was synthesised by reaction of the corresponding alkyllithium reagent RLi with ClAu(PPh_3) according to the procedure described in literature (Scheme 4.1).[8,10]

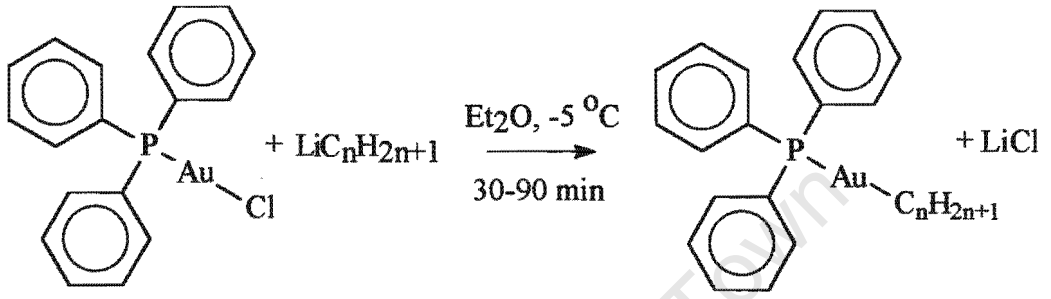

Complexes **19-23** (n = 1-5), **24** (n = 7)

Scheme 4.1: Reaction scheme for the synthesis of RAu(PPh_3) complexes **19-14**

The reactions were conducted in dry diethyl ether at about -5 °C and the products were either recrystallised from diethyl ether/hexane or toluene as white crystals (complexes **19-21, 24**) or recovered from diethyl ether as clear oils (complexes **22-23**). The complexes were found to be stable when exposed to air and water, but were thermally unstable and light-sensitive. Unfortunately, these complexes were not found to exhibit liquid-crystalline behaviour, most likely due to the fact that the bulky PPh_3 group prevents the molecules from forming linear structures.

4.2.3 Attempted synthesis of RAu(7-OST) complexes

We attempted to synthesise RAu(7-OST), R = CH_3 either by addition of MeLi at -72 °C to ClAu(tht) to form the intermediate RAu(tht) complex or directly to complex **6**

(Scheme 4.2). These reactions were unsuccessful, resulting in the formation of a black precipitate and deposition of metallic gold immediately after MeLi addition.

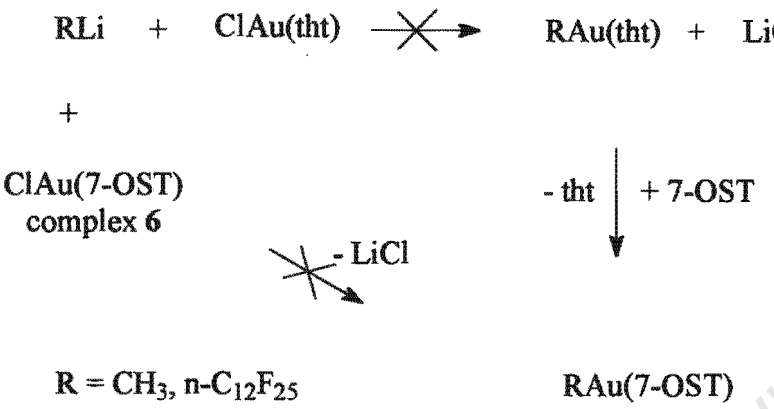

Scheme 4.2: Reaction scheme for the attempted synthesis of RAu(7-OST) complexes

Transition metal complexes with perfluorinated ligands often show increased thermal stability compared to the hydrocarbon analogues (section 3.1.2).[32] For example, although $CH_3Co(CO)_4$ decomposes at -30 °C, $CF_3Co(CO)_4$ can be distilled at 91 °C without decomposition.[32] The more electronegative perfluoroalkyl group results in the metal having a higher partial positive charge.[31] This generates contracted metal orbitals and the metal-carbon overlap is increased. Perfluoroalkyl groups have also been reported to enhance the thermal stability of smectic A and C phases of liquid crystals due to the increased rigidity around the perfluoroalkyl moiety.[33,34,35] *n*-PerfluoroalkylAu(n-OST) complexes were thus considered for investigated as the perfluoroalkyl group may result in more stable alkylAu(n-OST) complexes and would not inhibit mesophase formation.

$RAu(PPh_3)$ complexes, R = *n*-perfluoroalkyl have previously been reported, with $CF_3Au(PPh_3)$ being isolated as a by-product from the reaction of PPh_3 with $Re_2(HgCF_3)(AuPPh_3)(\mu\text{-}OC\text{-}C_4H_9)$[36] and $CH_3(CF_2)_2Au(PPh_3)$ being formed by insertion

of tetrafluoroethylene into the C-Au bond of complex **19**.[37]

An attempt was made to synthesise the RAu(tht) complex, R = $C_{12}F_{25}$, in a similar method described for the synthesis of RAu(tht) complexes, R = perhalophenyl (section 3.2.1), with the aim of later displacing the tht with 7-OST to make the corresponding RAu(7-OST) complex (Scheme 4.2). The $C_{12}F_{25}$ lithium reagent (section 4.2.1) was reacted with ClAu(tht) at –72 °C. Unlike in the attempted synthesis of the R = CH_3 complex (Scheme 4.2), immediate decomposition did not occur. The RAu(tht) complex, R = $C_{12}F_{25}$, appeared to be stable below -30 °C, but started decomposing while warming up to 0 °C, being completely unstable above 0 °C. It was not possible to confirm that this complex had been formed, except for tenuous TLC evidence indicating the presence of a complex that had a similar R_f value to the perfluorophenylgold(tht) complexes **10, 12** and **14.** Further work on this system was not carried out. Considering that the RAu(7-OST) complexes **11, 13, 15** and **18** were thermally far more stable than the analogous RAu(tht) complexes (chapter 3), it is probable that the displacement of tht by 7-OST of the unstable $C_{12}F_{25}$Au(tht) complex, if carried out below -30 °C, might lead to the isolation of the more stable $C_{12}F_{25}$Au(7-OST) complex.

4.3 Characterisation of RAu(PPh_3) complexes 19-24

RAu(PPh_3) complexes **19-24** were characterised by means of microanalysis (chapter 6), FT-IR (Table 4.1) and ^{1}H- and ^{13}C-NMR spectroscopy (Appendix4A, Tables 4A.1-2). FT-IR spectroscopy proved to be a very useful characterisation tool in confirming that the gold-carbon bond had been formed. A single strong absorption band at 532 cm^{-1} has

previously been attributed to ν(Au-C) for complex **19**[7] and the ν(Au-C) assignments for complexes **19-24** were made by comparison to this reference value (Table 4.1).

Table 4.1: ν(Au-C), melting points and yields for $RAu(PPh_3)$ complexes **19-24**

Complex	n	ν(Au-C) in cm^{-1}	m.p. in °C	Yield in %
19	1	533.4[a]	176	58
20	2	532.5[a]	148	42
21	3	530.5[a]	77-78	40
22	4	531.1[b]	oil	88
23	5	530.6[b]	oil	85
24	7	532.3[a]	64	83

a = nujol mull between CsCl plates, b = neat

Elemental analysis of complexes **23-24** was hampered by their thermal instability (section 4.3.4). Complex **23** is clear oil and complex **24** forms white crystals, both of which decompose to brown viscous oils while drying under high vacuum even at 0 °C. ^{1}H-NMR integration for the methylene protons (Figure 4.2) and recalculated elemental analysis (chapter 6) for the brown oil sample of complex **23**, suggested that *n*-decane is present in a proportion of about 10% for that particular sample. This type of unstable behaviour is not uncommon for $RAu(PPh_3)$ complexes, as *s*-butylgold(PPh_3) was reported to form off-white crystals which turned brown overnight at 0 °C or when allowed to warm to room temperature, turning dark-brown and sticky in half an hour at room temperature.[10]

4.3.1 Reaction yields for $RAuPPh_3$ complexes

Reaction yields for the synthesis of complexes **19-24**, ranged from 40 to 88%. It has been shown that complex **19** reacts with one molar equivalent of MeLi in diethyl ether solutions to form the corresponding $[RAuR(PPh_3)]^-Li^+$ complex and subsequently $[RAuR]^-Li^+$ on removal of PPh_3 (Scheme 4.3).[24,25] A possible reason for lower yields in .

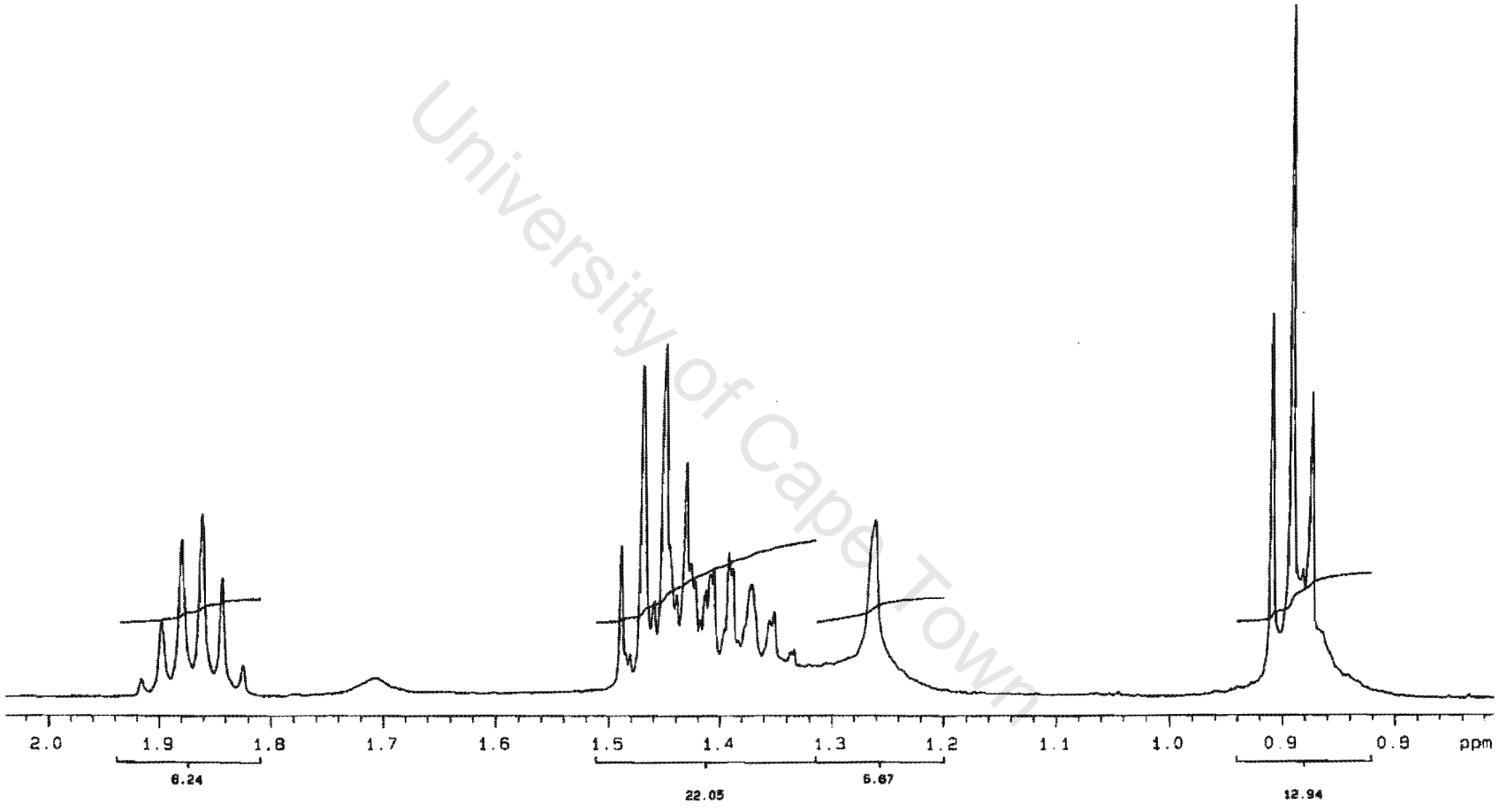

Figure 4.2: ^{1}H-NMR spectrum of complex **23** and *n*-decane in $CDCl_3$.

some cases may be the formation of competing $[RAuR(PPh_3)]^{-1}Li^+$ complexes during the reaction, as an excess of the *n*-alkyllithium reagents were used. These type of complexes have been found to undergo oxidative decomposition (with oxygen and methyl iodide), thermal decomposition and hydrolysis reactions, forming metallic gold and black precipitates.[26] A black precipitate was occasionally observed during the hydrolysis and two-phase separation steps, suggesting that the undesired $[RAuR(PPh_3)]^{-1}Li^+$ complexes may have formed.

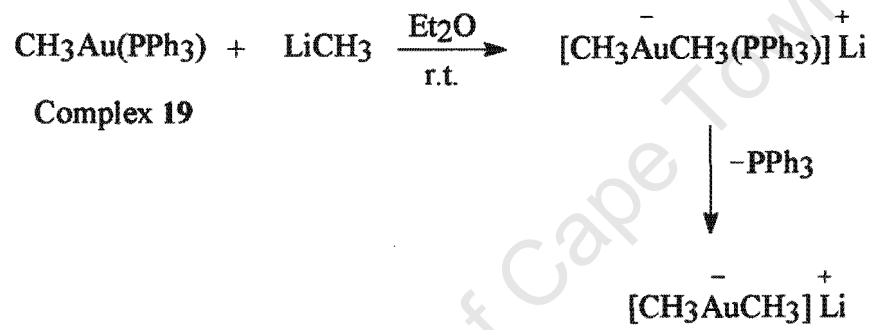

Scheme 4.3: Reaction scheme for the synthesis of $[RAuR(PPh_3)]^{-1}Li^+$ complexes

4.3.2 ^{1}H- and ^{13}C-NMR spectroscopic data for complexes 19-24

Some methylene signals in the ^{1}H-NMR spectra of $RAu(PPh_3)$ complexes dissolved in $CDCl_3$ were superimposed, but better peak separations were obtained when C_6D_6 was used, *e.g.* complex **20** (Figures 4.3-4). Although the three-bond $^3J_{PH}$ coupling constants reported for complexes **19-21** and **23** have previously been reported for complex **19**[11,12,13] and similar $RAu(PMe_3)$ complexes,[27] it is interesting to note that four-bond $^4J_{PH}$ coupling constants are also observed for complexes **20-24** (Table 4A.1). The $^3J_{PH}$ coupling of the α-proton of complex **20** (Figure 4.4) is indicated by the signal for the methylene group forming a slightly distorted quintet and the $^4J_{PH}$ coupling to the β-proton by the signal for the methyl protons forming a quartet. In both cases, it is difficult to distinguish between

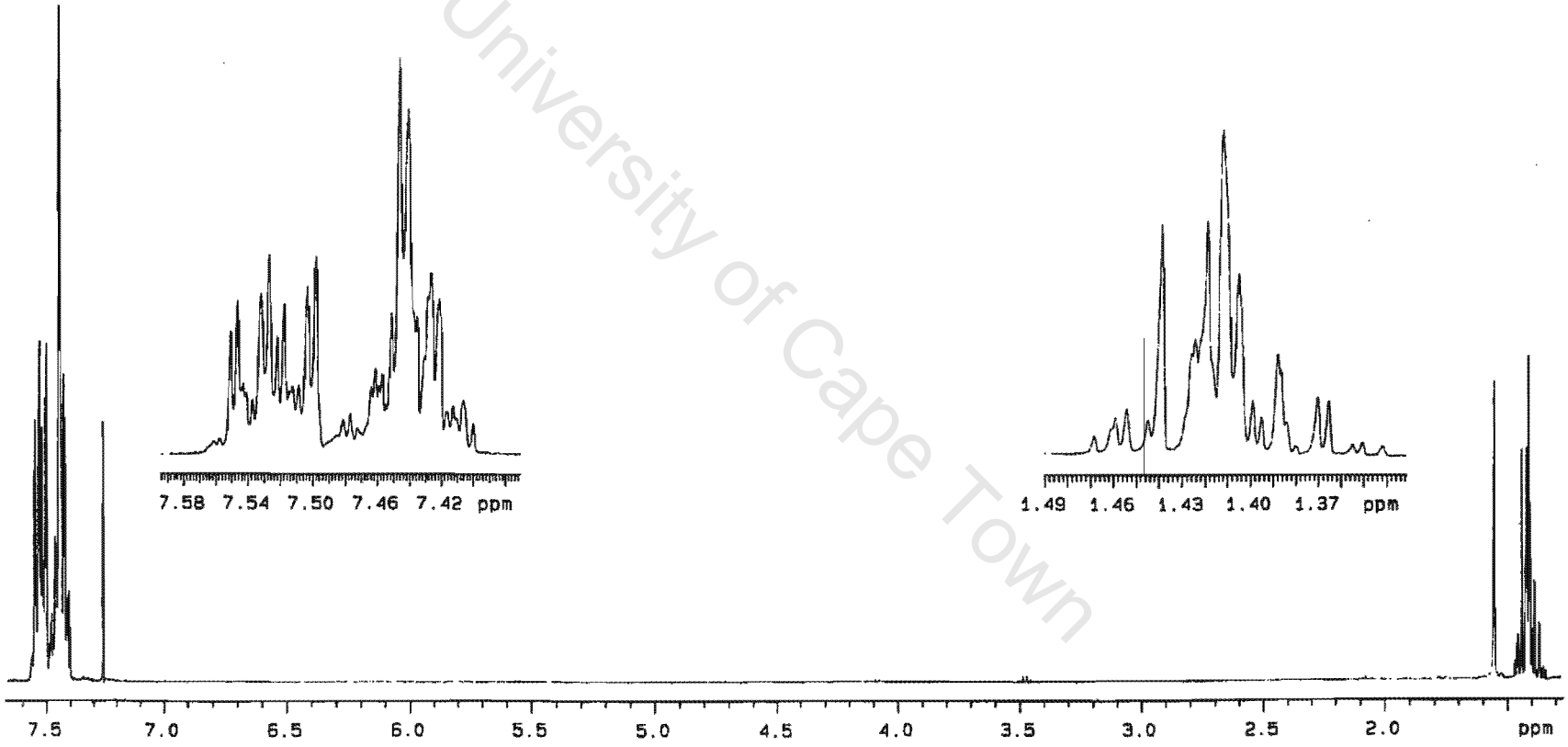

Figure 4.3: ^{1}H-NMR spectrum of complex **20** in $CDCl_3$.

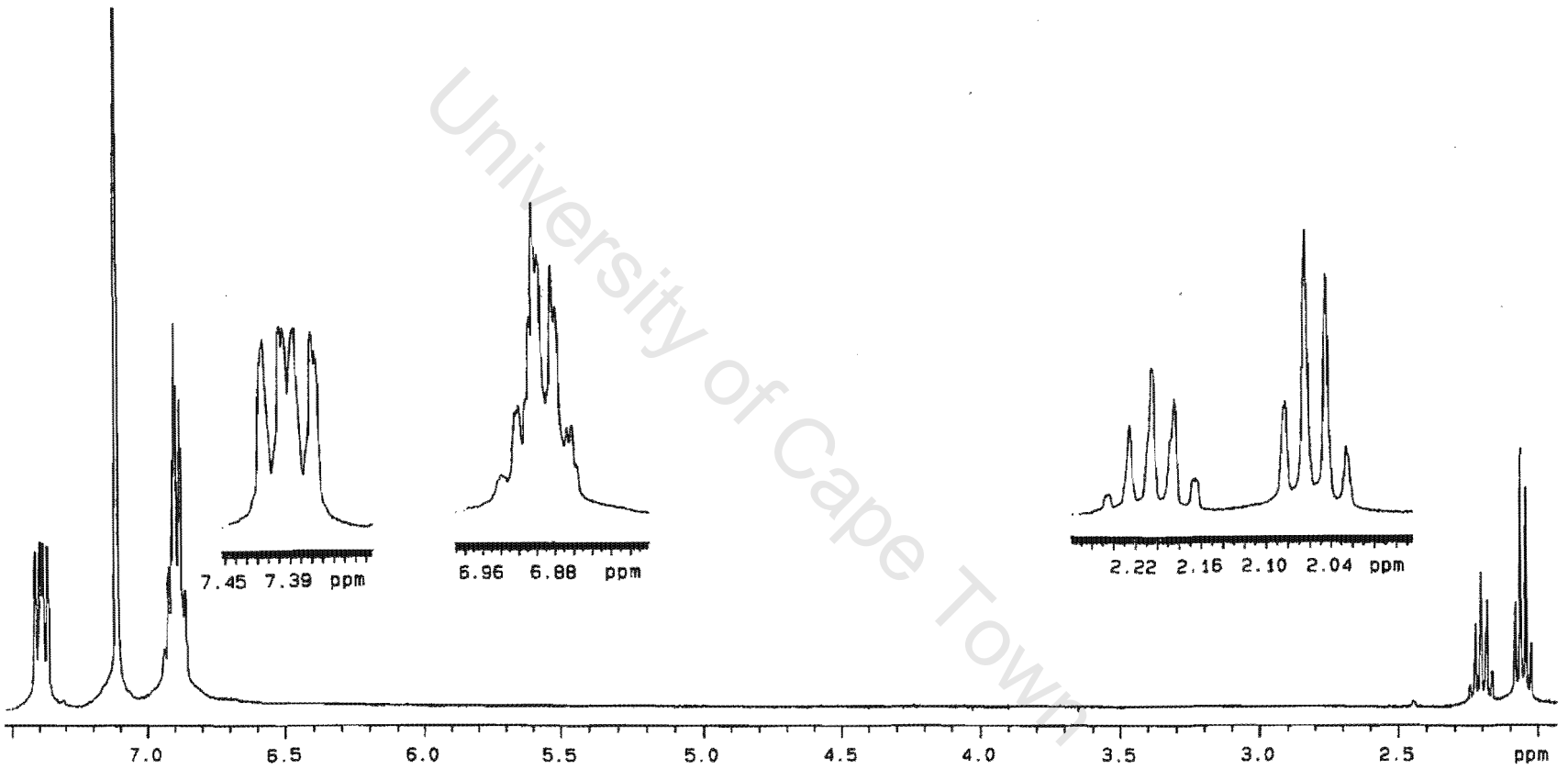

Figure 4.4: ^{1}H-NMR spectrum of complex **20** in C_6D_6.

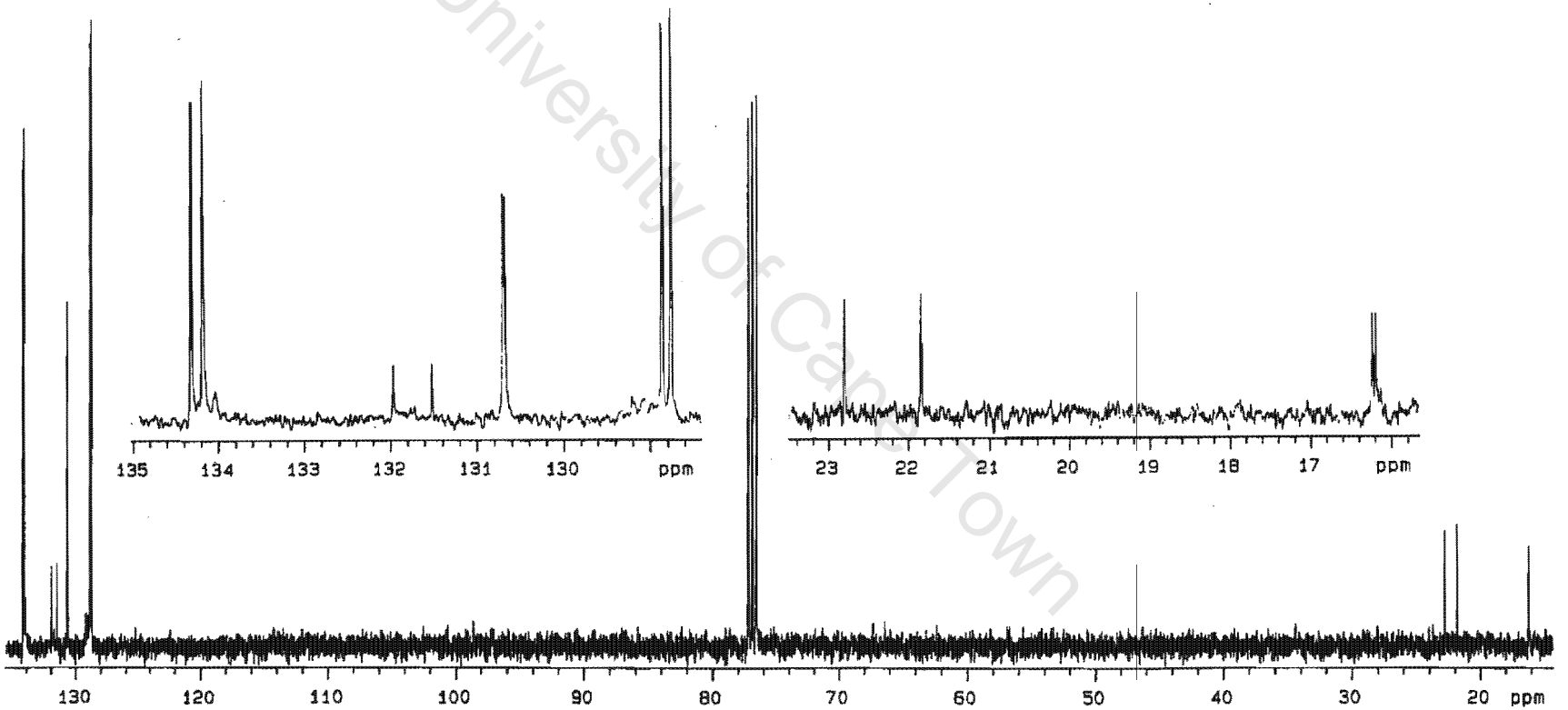

Figure 4.5: ^{13}C-NMR spectrum of complex **20** in $CDCl_3$.

the phosphorus-proton and proton-proton coupling constants, as they are of a similar order.

No ^{13}C-NMR spectroscopic data have been reported previously for RAu(PPh_3) complexes. A two-bond $^2J_{PC}$ coupling with a magnitude of about 95 Hz (Table 4A.2, Figure 4.5) is observed for the α-carbon atoms (C_g for complex **19** and C_a for complexes **20-24**). This value agrees with the $^2J_{PC}$ coupling constant of about 94 Hz reported for the α-carbon trans to PPh_3 in cis-[$PtBu_2(PPh_3)_2$].[28] No appreciable $^3J_{PC}$ coupling to the β-carbon (C_g for complex **20** and C_b for complexes **21-24**) occurs, although a fine splitting of about 4.2 Hz is observed for the β-carbon peak (Figure 4.5). The rest of the methylene carbon atoms, C_c to C_f, were assigned on the basis of increased shielding with distance to the gold atom, as was observed for the methylene protons, H_c to H_f.

The α-protons (H_g for complex **19** and H_a for complexes **20-24**) are relatively shielded due to their close proximity to the high electron density of the gold atom. α-H_g of complex **19** has a significantly lower δ value (0.55 ppm) compared to the CH_3 groups of complexes **20-24** (Table 4.2). The δ values for α-H_a of complexes **20-24** occur upfield relative to β-H_b, in the limited range of 1.41 to 1.49 ppm, and seem to be independent of chain length.

The β-protons (H_g for complex **20** and H_b for complexes **21-24**) conversely experiences a large degree of deshielding. Consequently, β-H_g of complex **20** (Table 4.2) has a much higher δ value (1.42 ppm) compared to the CH_3 groups of complexes **21-24** (about 1.0

ppm). The δ values for β-H_b of complexes **21-24** also occur furthest downfield in the region of 1.87 to 1.91 ppm, seemingly independent of the length of the alkyl chain. Increased shielding of the α-protons by the metal, with significantly deshielded β-protons, have also been reported for other σ-bonded metal-alkyl complexes.[29]

Table 4.2: Selected ^{1}H-NMR δ (ppm) values for $RAu(PPh_3)$ complexes in $CDCl_3$.

Complex	n	δ (CH_2 groups)		δ (CH_3 groups)
		α-H_a	β-H_b	H_g
19	1	-	-	0.55 (α-H_g)
20	2	1.42	-	1.42 (β-H_g)
21	3	1.49	1.91	1.08
22	4	1.49	1.91	0.96
23	5	1.41	1.87	0.89
24	7	1.46	1.91	0.87

As observed earlier for the proton nuclei, the β-carbon atoms (C_g for complex **20** and C_b for complexes **21-24**) occur furthest downfield and are the most deshielded and the α-carbon atoms (C_g for complex **19** and C_a for complexes **20-24**) are relatively more shielded (Table 4.3). Again, this trend is typical of what is observed in other σ-bonded metal-alkyl systems.[29] The only exception is in the case of complex **21**, where the δ value of β-C_b (25.1 ppm) is significantly more shielded than even α-C_a (33.8 ppm) and the methyl group C_g (21.0 ppm) is significantly deshielded (Table 4.3).

Table 4.3: Selected ^{13}C-NMR δ values (ppm) for $RAu(PPh_3)$ complexes in $CDCl_3$.

Complex	n	δ (CH_2 groups)		δ (CH_3 groups)
		α-C_a	β-C_b	C_g
19	1	-	-	7.1 (α-C_g)
20	2	22.4	-	16.2 (β C_g)
21	3	33.8	25.1	21.0
22	4	30.8	34.1	14.2
23	5	30.9	38.9	14.4
24	7	30.8	36.5	14.0

*4.3.3 Thermal Decomposition of complexes **19-24***

Unlike many alkyl transition metal systems, $RAu(PPh_3)$ complexes do not undergo β-elimination pathways to produce an alkene. This can be attributed to the reluctance of gold to form hydride complexes.[31] When heated in the solid state or in solution, $RAu(PPh_3)$ complexes **19** and **20** have been shown to decompose to metallic gold, free PPh_3 and coupled R-R organic fragments (Scheme 4.4).[12] The decomposition for complex **19** in decalin at 100 °C has been found to follow first-order reaction kinetics and a mechanism involving initial release of PPh_3 as the rate-limiting step has been suggested by Tamaki and Kochi (Scheme 4.4).[12] The intermediate CH_3Au^I species was not detected by these authors.[12]

$$2RAu(PPh_3) \xrightarrow{heat} R\text{-}R + 2Au + 2PPh_3$$

Mechanism

$$CH_3Au(PPh_3) \underset{}{\overset{k_1}{\rightleftharpoons}} CH_3Au + PPh_3$$

$$CH_3Au + CH_3Au(PPh_3) \longrightarrow CH_3\text{-}CH_3 + 2Au + PPh_3$$

Scheme 4.4: Proposed mechanism for thermal decomposition of complex **19**

In the present study, the decomposition of complex **23** in C_6D_6 was conducted in a sealed NMR tube protected from light and investigated via ^{1}H- and ^{13}C-NMR spectroscopy. Complex **23** was generated *in situ* in the NMR tube (chapter 6) and ^{1}H- and ^{13}C-NMR spectra (Figures 4.6-8) of the mixture was run;

(i) immediately after sealing the NMR tube

(ii) after leaving the NMR tube for 24 hrs at room temperature

(iii) after allowing the NMR tube to stand for an additional 24 hrs at 50 °C

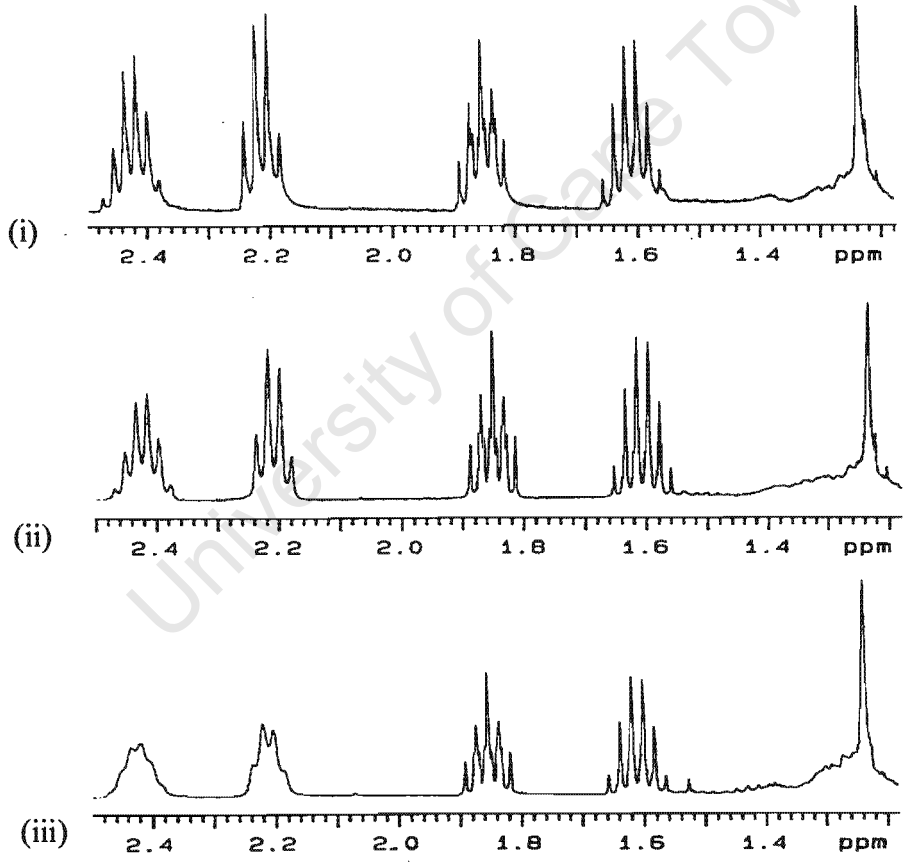

Figure 4.6: ^{1}H-NMR spectra (i), (ii) and (iii) for the $-CH_2$ peaks of complex **23** and *n*-decane in C_6D_6

The peak at 1.24 ppm observed even in spectrum (i) can be attributed to the methylene protons of the expected *n*-decane decomposition product for complex **23**[12] (Figure 4.6)

and is a reflection of its thermal instability. From the ^{1}H-NMR spectra (i), (ii) and (iii) it can be seen that the coupling of α-H_a and β-H_b protons become perturbed, especially in spectrum (iii), but the integration for the methylene protons of complex **23** remains unchanged (Figure 4.6). The integration for the *n*-decane peak (at 1.24 ppm) relative to the methylene protons of complex **23** in spectrum (iii) increased slightly (Figure 4.6) compared to spectra (i) and (ii), indicating that some *n*-decane was produced when heating the sample to 50 °C. The *n*-pentyl group of complex **23** remained bonded to gold(I) in spectrum (iii), as the δ values of the methylene protons has not changed. The phenyl signals for the PPh_3 group of complex **23** in the ^{1}H-NMR spectra (i), (ii) and (iii) indicate that changes occurred to the PPh_3 group (Figure 4.7).

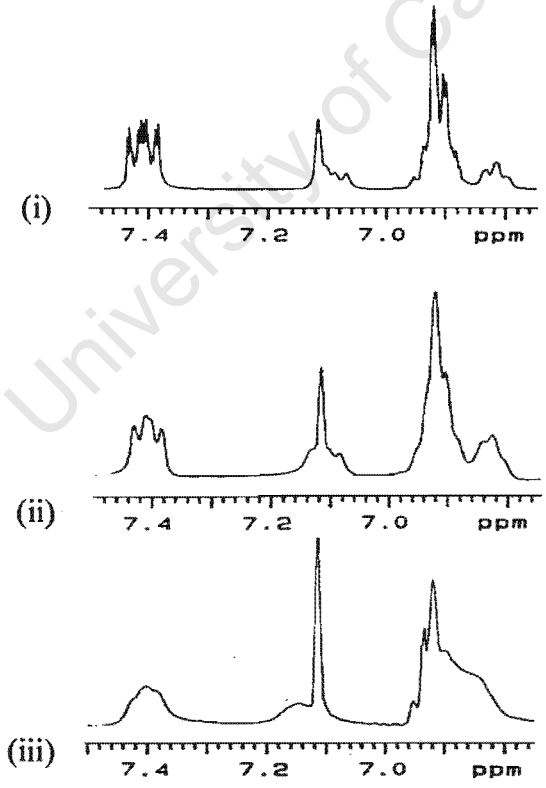

Figure 4.7: ^{1}H-NMR spectra (i), (ii) and (iii) for the phenyl peaks of complex **23** in C_6D_6

The ^{13}C-NMR spectra (Figure 4.8) offers the most convincing evidence that the RAu^{I} intermediated of complex **23** may have been isolated in spectrum (iii). The C_a ($^2J_{PC}$ = 96 Hz) and C_c peaks of complex **23**, both having a δ value of 32 ppm (Table 2A.1), are clearly visible in spectra (i) and (ii). No $^2J_{PC}$ coupling is observed in spectrum (iii) after the sample was heated at 50 °C for 24 hrs.

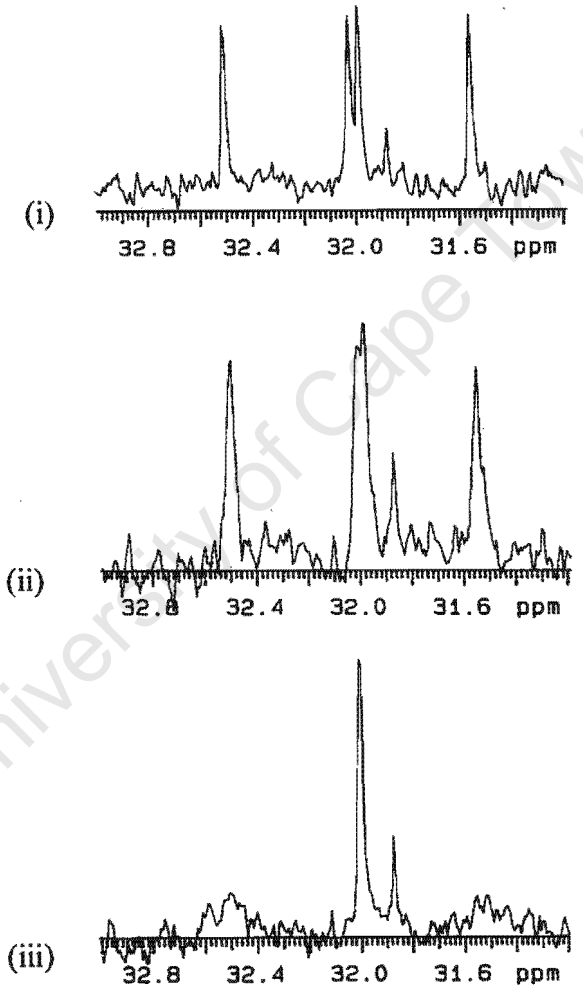

Figure 4.8: ^{13}C-NMR spectra (i), (ii) and (iii) for the $-CH_2$ peaks of complex **23** and *n*-decane in C_6D_6

The absence of $^2J_{PC}$ coupling to the α-C_a (Figure 4.8), a corresponding perturbation in the $^3J_{PH}$ and $^4J_{PH}$ coupling (Figure 4.6) and Au-PPh_3 bond (Figure 4.7) and the generation of

n-decane (Figure 4.6) in spectra (iii) strongly suggests that complex **23** decomposed while heating the sample at 50 °C. PPh_3 was released from complex **23**, resulting in the formation of the intermediate RAu^I complex, R = *n*-pentane, and some *n*-decane, according to the mechanism proposed by Tamaki and Kochi (Scheme 4.4).[12] It should be noted that strong peaks at 3.31 ppm and 1.16 ppm were observed the ^{1}H-NMR spectra (i), (ii) and (iii) due to the presence of some diethyl ether in the NMR tube. The intermediate RAu^I species was most likely stabilised by coordination to diethyl ether.

*4.3.4 Photochemical decomposition of complexes **19-24***

$RAu(PPh_3)$ complexes **19-24** are also light-sensitive and were protected at all times with aluminium foil. The photolysis of complex **19** in $CDCl_3$ has been found to involve the generation of singlet and triplet excited states (Scheme 4.5).[30] The latter react with $CDCl_3$ to produce $ClAu(PPh_3)$ and methyl radicals, which produce several species including CH_3CDCl_2, CH_3CCl_3, C_2H_6 and CH_3D.[30]

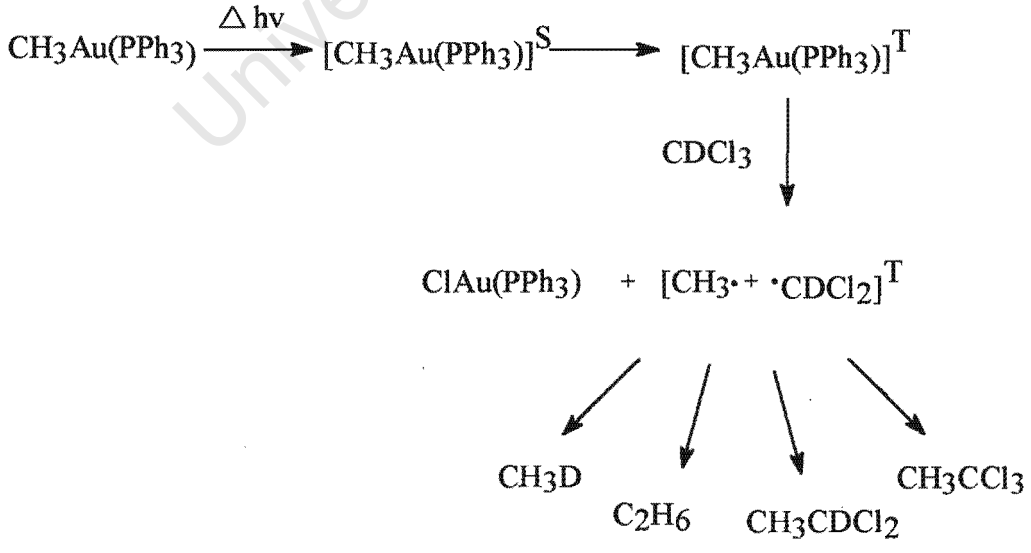

Scheme 4.5: Photochemical decomposition of complex **19**[30]

4.3.5 Catalytic activity of $RAuPPR_3$ complexes

Many transition metal alkyl species are catalytically active[16] and it has recently been shown that methylgold(PR_3) complexes catalyse the addition of alcohols to alkynes under mild conditions (T = 20-50 °C), with H^+ as a cocatalyst.[17] In all cases the *in situ* protonolysis of the methylgold(PR_3) complex generates the cationic $[Au^I(PR_3)]^+$ catalyst (Figure 4.9), which does not exist in the free form.[17] The catalysts achieve total turnover numbers of up to 10^5 moles of product per mole of catalyst, with turnover frequencies of up to 5,400 per hour.[17]

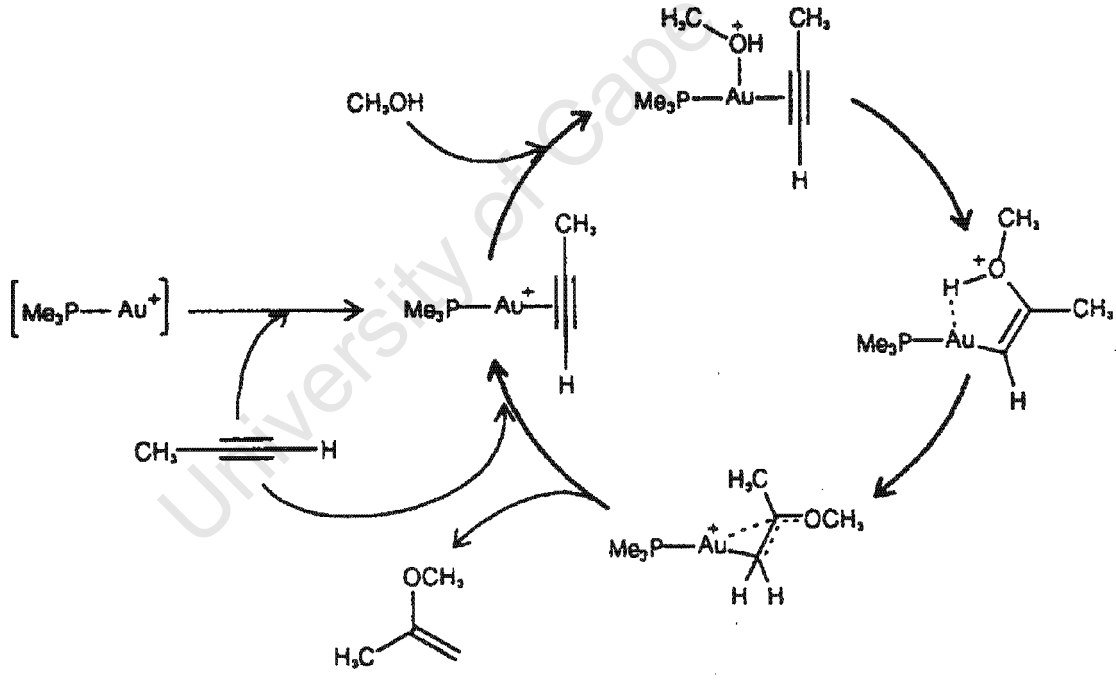

Figure 4.9: The proposed mechanism for the addition of methanol to propyne, catalysed by the $[Au^I(PMe_3)]^+$ cation.[17]

4.4 Summary

1. A series of $RAu(PPh_3)$ complexes **19-24**, which undergo thermal and photochemical decomposition, were found not to exhibit liquid crystalline behaviour, possibly due to the bulky PPh_3 ligand inhibiting linear arrangements of molecules. These complexes have however recently been found to have applications in catalysis.

2. ^1H- and ^{13}C-NMR spectra reveal that phosphorus-proton ($^3J_{PH}$ and $^3J_{PH}$) and phosphorus-carbon ($^2J_{PC}$) occur in $RAu(PPh_3)$ complexes **19-24**. The α-atoms of the alkyl fragments of complexes **19-24** are relatively shielded by the Au^I atom and the β-atoms are relatively shielded, except for the carbon atoms of complex **21**.

3. $RAu(PPh_3)$ complexes undergo thermal decomposition and an undetected RAu^I species has been proposed to be an intermediate decomposition product. ^1H- and ^{13}C-NMR spectra provide evidence for the existence of this RAu^I species, formed during the decomposition of complex **23** in a sealed NMR tube.

4. Due to a large trans effect, the L group required to form stable RAuL complexes, R = alkyl, are limited to PR_3 and isocyanide ligands. Attempts to synthesis RAu(7-OST) complexes were unsuccessful and presumably perfluoroalkyl R groups may result in more stable complexes.

4.5 References

1. M. J. Baena, P. Espinet, M. C. Lequerica and A. M. Levelut, *J. Am. Chem. Soc.*, 1992, **114**, 4182.
2. R. J. Puddephatt, in *Comprehensive Organometallic Chemistry: the synthesis, reactions and structures of organometallic compounds,* eds. E. W. Abel, F. G. A. Stone and G. Wilkinson, Pergamon Press, Oxford, 1st edn., 1892, vol. 2, ch. 15, pp. 765-821.
3. A. Grohmann and H. Schmidbaur in *Comprehensive Organometallic Chemistry II: a review of the literature 1982-1994*, eds. E. W. Abel, F. G. A. Stone and G. Wilkinson, Pergamon Press, Oxford, 1st edn., vol. 3, ch. 1, pp. 1-56.
4. R. J. Puddephatt and I. Treurnicht, *J Organomet. Chem.*, 1987, **317**, 129.
5. T. Kaharu, R. Ishii, T. Adachi, T. Yoshida and S. Takahashi, *J. Mater. Chem.*, 1995, **5**, 687.
6. P. Alejos, S. Coco and P. Espinet, *New J. Chem.*, 1995, **19**, 799.
7. G. Calvin, G. E. Coates and P. S. Dixon, *Chemistry and Industry*, 1959, 1628.
8. G. E. Coates and C. Parkin, *J. Chem. Soc.*, 1962, 3220.
9. G. E. Coates and C. Parkin, *J. Chem. Soc.*, 1963, 421.
10. B. J. Gregory and C. K. Ingold, *J. Chem. Soc. (B),* 1969, 276.
11. H. Schmidbaur and A. Shiotani, *Chem. Ber.*, 1971, **104**, 2821.
12. A. Tamaki and J. K. Kochi, *J Organomet. Chem.*, 1973, **61**, 441.
13. A. Tamaki and J. K. Kochi, *J Organomet. Chem.*, 1974, **64,** 411.
14. A. Tamaki, S. A. Magennis and J. K. Kochi, *J. Am. Chem. Soc.*, 1974, 6140.
15. A. N. Nesmeyanov, E. G. perevalova, K. I. Grandberg and D. A. Lemenovskii, *Izv.*

Akad. Nauk SSSR, Ser. Khim., 1974, 1068.

16. J. R. Moss, Trends in Organomet. Chem., 1994, **1**, 211.
17. J. H. Teles, S. Brode and M. Chabanas, *Angew. Chem., Int. Ed. Engl.*, 1998, **37**, 1415.
18. B.S. Furniss, A.J. Hannaford, P.W.G. Smith and A.R. Tatchell, *Vogel's Textbook of Practical Organic Chemistry*, Longman Scientific & Technical, England, 5th edn., 1989, ch. 4, pp. 442-445.
19. D. Bryce-Smith and E. E. Turner, *J. Chem. Soc.*, 1953, 861.
20. E. H. Amonoo-Neizer, R. A. Shaw, D. O. Skovlin and B. C. Smith, *Inorg. Synth.*, 1966, **8**, 19.
21. H. Gilman and F. K. Cartledge, *J Organomet. Chem.*, 1964, **2**, 447.
22. S. C. Watson and J. F. Eastham, *J Organomet. Chem.*, 1967, **9**, 165.
23. W. F. Bailey and E. R. Punzalan, *J. Org. Chem.*, 1990, **55**, 5404.
24. A. Tamaki and J. K. Kochi, *J Organomet. Chem.*, 1973, **51**, C39.
25. A. Tamaki and J. K. Kochi, *J. Chem. Soc. Dalton Trans.*, 1973, 2620.
26. S. Komiya, T. A. Albright, R. Hoffmann and J. K. Kochi, *J. Am. Chem. Soc.*, 1977, **99**, 8440.
27. H. Schmidbaur, A. Shiotani and H. F. Klein, *J. Am. Chem. Soc.*, 1971, **93**, 1555.
28. X. Yin, Ph.D. Thesis, University of Cape Town, 1997.
29. J. M. Andersen and J. R. Moss, *J Organomet. Chem.*, 1995, **494**, 105.
30. P. W. N. M. Van Leeuwen, R. Kaptein, R. Huis and C. F. Roobeek, *J Organomet. Chem.*, 1976, **104**, C44.
31. R. V. Parish, *Gold Bulletin*, 1997, **30**, 55.
32. C. Elschenbroich and A. Salzer, *Organometallics A Concise Introduction*, VCH,

Weinheim, 1st edn., 1989, ch. 13, pp 193-205.

33. S. Takenaka, *J. Chem. Soc. Chem. Commun.*, 1992, 1748.

34. S. Pensec and F. Tournilhac, *J. Chem. Soc. Chem. Commun.*, 1997, 441.

35. T. Thiele, D. Prescher, R. Ruhmann and D. Wolff, *J. Fluorine Chem.*, 1997, **85**, 155.

36. U. Flörke, H. Haupt and P. G. Jones, *Acta Cryst.*, 1996, **C52**, 609.

37. A. Johnson, R. J. Puddephatt and J. L. Quirk, *J. Chem. Soc. Chem. Commun.*, 1972, 938.

Appendix 4A

Table 4A.1: ^{1}H-NMR spectroscopic data for RAu(PPh_3) complexes.

Complex	n	Solvent	δ (ppm)	δ (ppm) / CH_2					δ (ppm) / CH_3
			PPh_3 15H	H_a ($^3J_{PH} \approx {}^3J_{HH}$) 2H	H_b ($^4J_{PH} \approx {}^3J_{HH}$) 2H	H_c ($^3J_{HH}$) 2H	H_d ($^3J_{HH}$) 2H	H_e 2H	H_f 2H	H_g ($^3J_{HH}$) 3H
19	1	$CDCl_3$	7.54, m 7.44, m							0.55, d (7.9Hz)[a]
20	2	$CDCl_3$	7.52, m 7.44, m	1.42, m[b]						1.42, m[b]
20	2	C_6D_6[h]	7.44, m 6.94, m	2.25, qn (7.9Hz)						2.10, qt (7.5Hz)[c]
21	3	$CDCl_3$	7.53, m 7.44, m	1.49, qt (7.6Hz)	1.91, hp (7.2Hz)					1.08, tr (7.2Hz)
22	4	$CDCl_3$	7.53, m 7.44, m	1.49, sx[d]	1.91, sx (7.2Hz)	1.49, sx[d] (7.3Hz)				0.96, tr (7.2Hz)
23	5	$CDCl_3$	7.53, m 7.44, m	1.41, m[e]	1.87, sx (7.3Hz)	1.41, m[e]	1.41, m[e]			0.89, tr (7.2Hz)
23	5	C_6D_6[h]	7.46, m 6.96, m	2.26, qt (7.6Hz)	2.48, sx (7.4Hz)	1.90, qn (7.5Hz)	1.66, sx (7.4Hz)			1.05, tr (7.4Hz)
24	7	$CDCl_3$	7.53, m 7.43, m	1.46, m[f]	1.91, sx (7.3Hz)	1.46, m[f]	1.37, qn (7.1Hz)	1.29, m[g]	1.29, m[g]	0.87, tr (7.0Hz)

a = $^3J_{PH}$, b = H_a and H_g form one multiplet which integrates for 5H, c = $^4J_{PH} \approx {}^3J_{HH}$, d = the quartet for H_a is exactly overlain by the sextet for H_c. H_a and H_c thus form one sextet which integrates for 4H, e = H_a, H_c and H_d form one multiplet integrating for 6H, f = H_a and H_c form one multiplet integrating for 4H, g = H_e and H_f form one multiplet integrating for 4H, h = The C_6D_6 solvent peak shifted slightly during analysis and δ values for complexes **20** and **23** were corrected relative to the standard reference value, d = doublet, tr = triplet, qt = quartet, qn = quintet, s = sextet, hp = heptet, m = multiplet.

Table 4A.2: ^{13}C-NMR spectroscopic data for RAu(PPh_3) complexes.

Complex	n	Solvent	δ (ppm) / PPh_3					δ (ppm) / CH_2					δ (ppm) / CH_3
			C_{ipso} ($^1J_{PC}$)	C_{ortha} ($^2J_{PC}$)	C_{meta} ($^3J_{PC}$)	C_{para}	C_a ($^2J_{PC}$)	C_b	C_c	C_d	C_e	C_f	C_g
19	1	$CDCl_3$	131.6, d (47Hz)	134.2, d (13Hz)	128.8, d (10Hz)	130.8							7.1, d (95Hz)[a]
20	2	$CDCl_3$	131.7, d (45Hz)	134.3, d (14Hz)	128.8, d (11Hz)	131.1	22.4, d (97Hz)						16.2
20	2	C_6D_6[b]	133.1, d (44Hz)	134.2, d (14Hz)	129.7, d (10Hz)	131.3	24.7, d (98Hz)						18.1
21	3	$CDCl_3$	131.8, d (45Hz)	134.2, d (14Hz)	128.8, d (10Hz)	130.7	33.8, d (95Hz)	25.1					21.0
22	4	$CDCl_3$	131.8, d (45Hz)	134.8, d (13Hz)	128.8, d (10Hz)	130.7	30.8, d (95Hz)	34.1	29.5				14.2
23	5	$CDCl_3$	131.8, d (45Hz)	134.2, d (13Hz)	128.8, d (10 Hz)	130.7	30.9, d (95Hz)	38.9	31.3	22.6			14.4
23	5	C_6D_6[b]	132.5, d (44Hz)	134.6, d (13Hz)	129.0, d (9Hz)	130.7	32.4, d (96Hz)	39.5	32.4	23.3			15.5
24	7	$CDCl_3$	131.7, d (45Hz)	134.1, d (14Hz)	128.7, d (11Hz)	130.6	30.8, d (95Hz)	36.5	32.1	31.6	29.2	22.6	14.0

a = $^2J_{PC}$, b = The C_6D_6 solvent peak shifted slightly during analysis and δ values for complexes **20** and **23** were corrected relative to the standard reference value, d = doublet.

CHAPTER 5. Conclusion

ClAu(n-OST) and ClAu(vnlpy) complexes were found to be more stable than ClAu(py), in part due to stronger Au-N bonds with increased π back-bonding and the presence of electron-rich alkene and ether centres which resulted in highly conjugated aromatic ligand systems. This conjugation was enhanced when the ligands were bonded with gold(I).

ClAu(n-OST) complexes **3-9** formed S_A mesophases at much higher transition temperatures over a much larger temperature range than the free n-OST ligands, which formed S_B and S_E phases. These changes are indicative of stronger intermolecular forces caused by the gold(I) atom increasing the polarisability of the n-OST ligand and the strong Au-Cl dipole interaction. The expected trend of decreasing melting point with increasing alkoxy chain length is also observed. These complexes were thermally unstable and decomposed at the clearing points.

It was not possible to synthesise iodo, phenyl or alkyl derivatives of RAu(n-OST) complexes, but perhalophenyl derivatives formed stable complexes. They formed almost exclusively nematic mesophases with similar transition temperatures to the analogous chloro derivative (complex **6**) for the mononuclear complexes **11, 13** and **15**, but at much higher temperatures for the binuclear complex **18**. Electronic rather than bulk effects were thus more important in determining the transition temperatures, as the more bulky perhaloaryl groups did not result in the reduced intermolecular interactions and subsequently lower transition temperatures, previously reported for

analogous RAu(isocyanide) complexes. The intermolecular attractions created by the Au-Cl dipole of complex **6** is probably of a similar magnitude to those created by the introduction of the polarisable perhaloaryl groups. The binuclear complex **18** has one more polarisable aromatic ring compared to complexes **11, 13** and **15** and as expected has higher transition temperatures.

The nature of the electronic interactions between molecules of the RAu(n-OST) complexes promote the slip of molecules into mixed aromatic/aliphatic regions indicative of the nematic state compared to the ClAu(n-OST) complexes. This slip occurs even before melting into the liquid crystal state, except for complex **11**, which exhibits a short-lived S_A mesophase after melting before forming the nematic phase. Conversely, this slip occurs mostly in the liquid crystal state for the RAu(isocyanide) complexes, as they have much lower melting points compared to the RAu(n-OST) complexes.

The transition temperatures of the RAu(7-OST) complexes **11, 13** and **15** increase in the following R group order of 2-C_6F_4Br < C_6F_5 < 4-C_6F_4Br. As the bromine atom is more polarisable than fluorine, both complexes with bromine atoms are expected to have higher transition temperatures. The bromine atom is more bulky than fluorine and increases the breadth of the molecule in the *ortha* position and the length in the *para* position. The increased width of the molecule for the 2-C_6F_4Br group reduces the strength of the lateral interactions and results in lower transition temperatures. A similar trend was observed for RAu(isocyanide) complexes when $n \leq 6$, but when chain lengths $n \geq 8$ for the isocyanide ligands, the bulk effect of the bromine atom was less

pronounced, resulting in the following order C_6F_5 < 2-C_6F_4Br< 4-C_6F_4Br. Presumably, similar behaviour may be expected for ClAu(n-OST) complexes with longer chains.

Although XAu(py) complexes grown from ethanol or toluene crystallise as ionic $[AuX_2]^-[Au(py)_2]^+$ species, conductivity measurements (in acetone), FAB-MS experiments (2-nitrobenzylalcohol matrix) and an X-ray crystallographic of complex **11** (grown from toluene/pentane) indicate that the XAuL and RAuL complexes investigated in this study form neutral species which have a monomeric structure. The only indication that an ionic and neutral species may coexist is two ν(C=N) peaks in the FT-IR spectrum of ClAu(vnlpy) in dichloromethane. Otherwise the FT-IR and ^{1}H-^{13}C- and ^{19}F-NMR spectra indicated that only one species is formed, but cannot be used to distinguish which species. Solvent effects may explain why ClAu(py) crystallises from ethanol as an ionic species, but forms a neutral species in acetone and why ClAu(vnlpy) may exists as two species in dichloromethane, but not acetone. No Au...Au bonding interactions and π-stacking were observed for the RAu(n-OST) complex **11** and are not important in liquid crystal formation. The molecules are arranged according to van der Waals interactions and electronic interactions between the rigid core of the molecules give rise to the liquid crystal phases. It was however not possible to obtain suitable crystals of ClAu(n-OST) complexes for comparison.

As with other gold(I) and transition metal systems, ClAu(n-OST) metallomesogens suffered the problem of higher transition temperatures and associated decomposition. Attempts at reducing the transition temperatures by replacing the chloride group with other halogen atoms or organometallic aryl or alkyl fragments were hampered by

lability of the RAuL system. Due to a high *trans* effect present in gold(I) complexes, stable organometallic complexes have almost exclusively isocyanide or PR_3 ligands. Halogen substituents on the organic fragment result in more stable Au^I-L bonds and this made it possible to form stable arylgold(I) complexes. It was similarly observed that the perhaloalkylgold(tht) complexes were stable below -30 °C where the alkylgold(tht) failed to form at -72 °C. As alkylgold(isocyanide) complexes have previously been reported to be quite volatile and the alkylgold(PR_3) complexes in this study are too bulky to form liquid crystal phases, perhaloalkyl rather than alkyl fragments may be important in reducing the *trans* effect in gold(I) complexes and increase the possibility of forming stable alkyl complexes with ligands other than isocyanide or PR_3.

Future suggestions in attempting to overcome the high transition temperatures and thermal instability of RAu(n-OST) complexes include (i) the synthesis of perfluoroalkylgold(n-OST) complexes which are likely to be more stable than the tht precursors and would promote S_A or S_C mesophases at lower temperatures than the ClAu(n-OST) complexes. (ii) the introduction of lateral or terminal alkoxy chains to the n-OST ligands, which have been found to lower transition temperatures by reducing intermolecular attractions and form more stable Ag^I, Pd^{II} and Pt^{II} complexes.[1] These substituted n-OST ligands were also found to promote the formation of nematic, S_A or columnar mesophases, depending on the position of the substituents. (iii) the mixing of two mesogenic RAu(n-OST) complexes would reduce the melting point of the mixture relative to the pure components and has been found to reduce transition temperatures for n-OST derivatives of Pt^{II}.[2] (iv) the synthesis of [(PPh_3)Au(n-

OST)]$^{+}$[ClO_4]$^{-}$ complexes similar to the py derivative mentioned in section 2.3.1. The strong dipolar interaction created by the Au-Cl bond will be replaced by Au-PPh_3, which has greater π bond character. This may affect how the Au^I atom increases the polarisability of the n-OST ligand and hence transition temperatures. The bulky PPh_3 ligand would also on a steric basis be expected to reduce the lateral intermolecular attractions.

Although the $RAu(PPh_3)$ complexes were not found to be mesogenic, they have recently been reported to have catalytic activity. The RAu^I species, which has up till now only been surmised to exist as an intermediate in the thermal decomposition of $RAu(PPh_3)$ complexes, has been observed in this study via ^1H- and ^{13}C-NMR spectroscopy.

5.1 References

1. B. Donnio and D. W. Bruce, *J. Chem. Soc., Dalton Trans.*, 1997, 2745.
2. J. P. Rourke, F. P. Fanizzi, D. W. Bruce, D. A. Dunmur and P. M. Maitlis, *J. Chem. Soc., Dalton Trans.*, 1992, 3009.

CHAPTER 6. Experimental Details

All experiments were performed under nitrogen using standard Schlenk techniques, except where stated otherwise. Tetrachloroauric acid was purchased from BDH Chemicals Ltd. Sodium tetrachloroaurate was either obtained from BDH Chemicals Ltd. or loaned from Johnson Matthey. Palladium(II) acetate was loaned from Johnson Matthey. Lithium metal, methyllithium, *n*-butyllithium, *t*-butyllithium, phenyllithium, pyridine, 4-vinyl-pyridine, 4-iodophenol, 4-bromophenol, *n*-haloalkanes, perfluorododecyl, bromopentafluorobenzene, 2-dibromotetrafluorobenzene, 4-dibromotetrafluorobenzene, μ-4,4'-dibromooctafluorobi-phenyl, tetrahydothiophene, triphenylphosphine, allyl bromide, triethylamine, anhydrous potassium carbonate, potassium iodide, anhydrous magnesium sulfate, sodium chloride, 2,2'-biquinolene, 18-crown-6 and 0.1M hydrochloric acid were purchased from Merck or Aldrich Chemical Co. The molarity of the lithium reagents were determined prior to use according to literature methods.[1-3] $ClAuPPh_3$ was prepared by literature methods from sodium tetrachloroaurate,[4] or tetrachloroauric acid.[5,6] ClAu(tht) was prepared from sodium tetrachloroaurate or tetrachloroauric acid.[7] Solvents were distilled from the appropriate drying agents under nitrogen[3,8] and *n*-haloalkanes were dried over molecular sieves and stored under nitrogen.[8] All other chemicals were used without further purification. Thin layer chromatography (TLC) was performed on aluminium sheets pre-coated with Merck silica gel 60 F_{254}. Column chromatography was performed using Merck silica gel 60, particle size 0.063-0.200 mm (70-230 mesh ASTM).

^{1}H- and ^{13}C-NMR spectra were recorded on a Varian Unity-400 (^{1}H: 399.952 MHz; ^{13}C:100.577 MHz) spectrometer at the University of Cape Town at ambient temperature. ^{19}F-NMR spectra were recorded on a Varian Unity-300 (^{19}F: 282 MHz) spectrometer at the

University of Stellenbosch at ambient temperature. Chemical shifts for ^{1}H- and ^{13}C-NMR spectra are referenced internally to residual solvent resonances and are reported relative to tetramethylsilane (δ 0.00 ppm, ^{1}H, ^{13}C). Chemical shifts for ^{19}F-NMR spectra are reported relative to $CFCl_3$. Infrared spectra were recorded on a Perkin-Elmer Paragon 1000 FT-IR spectrophotometer in CH_2Cl_2 solution cells with NaCl windows, as Nujol mulls between CsCl plates or as a potassium bromide disc. The following abbreviations have been used to describe the intensity of the peaks in the infrared spectra: w = weak, m = medium, s = strong and vs = very strong. Melting points and transition temperatures were determined on a Kofler hotstage microscope (Reichert Thermovar) and are uncorrected. The thermodynamic information on the transitions were obtained from DSC and TG measurements made on a Perkin-Elmer PC Series 7 thermal station under a nitrogen atmosphere, with a heating rate of 10 °C per minute. Elemental analysis was performed in the University of Cape Town micro analytical laboratory, using a Carlo Erba AE1108 elemental analyser. FAB and EI mass spectrometry analysis were obtained from the Mass Spectrometry Unit at the Cape Technicon Laboratories. A VG-70SEQ mass spectrometer with a MaspecII data-system was used and the samples were analysed under xenon in a 3-nitrobenzylalcohol matrix.

6.1 Synthesis of ClAuL complexes 1-2

Synthesis of ClAu(py),[9-11] complex 1

Method 1:

White ClAu(tht) (326 mg, 0.736 mmol) was suspended in dry toluene(4 cm^3) in a Schlenk tube under a N_2 atmosphere. Pyridine (1.0 cm^3, 12 mmol), which was degassed with N_2, was added to the mixture via a syringe and the reaction was stirred for 2.5 hrs at room temperature, during which time the product precipitated as a fine white powder. The white product (78 mg) is visually indistinguishable from ClAu(tht) and was collected on a Hirsch funnel and washed with

toluene (3 x 5 cm^3) to remove excess pyridine and tht. On removal of solvent from the filtrate under reduced pressure some more of the white product (76 mg) was precipitated and was collected in the same manner as the first fraction. Both fractions were dried for 2hrs under high vacuum and were analytically pure without further purification. Cumulative yield (154 mg, 67 %).

Method 2:

White ClAu(tht) (202 mg, 0.630 mmol) was suspended in 3 cm^3 dry toluene in a Schlenk tube under a N_2 atmosphere. Pyridine (1.0 cm^3, 12 mmol), which was degassed with N_2, was added to the mixture at 50 °C via a syringe and the reaction was stirred for 1hr at that temperature, during which time the white product formed. The mixture was cooled down to 0 °C to promote further precipitation of the product. The product (139 mg) was collected on a Hirsch funnel and washed with chloroform (3 x 5 cm^3), diethyl ether (3 x 5 cm^3) and hexane (3 x 5 cm^3). On reduction of volume and addition of hexane to the filtrate, more product (22 mg) was precipitated. Both fractions were dried for 2hrs under high vacuum and were analytically pure without further purification. Cumulative yield (161 mg, 82 %). The product was protected from sunlight throughout the reaction using aluminium foil and stored in a freezer (-25 °C) as the Au-N bond is light-sensitive and thermally unstable. Found m.p. 109 °C (dec.). Literature m.p. 92 °C (dec.)[9] and 250-252 °C(dec.).[10] (Found: C, 18.9; H, 1.5; N, 4.4 %.C_5H_5AuClN requires C, 19.3; H, 1.6; N, 4.4 %). FT-IR, ^1H- and ^{13}C-NMR spectroscopic and conductivity data are presented in Tables 2A.2-3 and 2.3 respectively.

Synthesis of ClAu(vnlpy), complex 2

White ClAu(tht) (606 mg, 1.890 mmol) was suspended in dry toluene (9 cm^3) in a Schlenk tube under a N_2 atmosphere. 4-Vinylpyridine (5.0 cm^3, 46 mmol), which was degassed with N_2, was added to the mixture at 55 °C via a syringe and the reaction was stirred for 15 min at that

temperature during which time a slightly purple solid was precipitated. The reaction progress was monitored by TLC (50 % ethyl acetate / 50 % hexane eluent). The mixture was cooled to -25 °C (ethanol/N_2) to promote further precipitation. The purple solid (280 mg) was collected on a Hirsch funnel and washed with chloroform (3 x 5 cm^3), diethyl ether (3 x 5 cm^3) and pentane (3 x 5 cm^3). The purple solid is totally insoluble normal organic solvents such as chloroform, toluene and benzene as well as water and was not analysed any further. On further addition of pentane to the filtrate, a white product (201 mg) precipitated out of solution. The white product was collected on a Hirsch funnel and washed with (3 x 5 cm^3) pentane. On further addition of pentane to the mother liquor, more product was precipitated (141 mg) and this was also collected on a Hirsch funnel. Both fractions were dried under high vacuum for 10 hrs and were analytically pure without further purification. Cumulative yield (342 mg, 54 % yield). The product was protected from sunlight throughout the reaction using aluminium foil and stored in freezer (-25 °C) as the Au-N bond is light sensitive and thermally unstable. Found m.p. 117 °C (dec.). (Found: C, 25.1; H, 2.0; N, 4.1 %. C_7H_7AuClN requires C, 24.9; H, 2.1; N, 4.1 %). FT-IR, ^1H- and ^{13}C-NMR spectroscopic and conductivity data are presented in Tables 2A.2-3 and 2.3 respectively.

6.2 Representative synthesis of n-OST ligands

Synthesis of 4-heptyloxyiodobenzene[12,13]

4-Iodophenol (3.435 g, 15.613 mmol), 1-bromoheptane (2.5 cm^3, 15 mmol), anhydrous potassium carbonate (2.216 mg, 16.034 mmol) and 18-crown-6 (*ca* 2 mg) was placed in a dry Schlenk tube under a N_2 atmosphere. Dry acetone (20 cm^3) was added from a syringe and refluxed for 20 hrs. After cooling, water (25 cm^3) was added and the organic fraction was extracted with diethyl ether (1 x 50 cm^3, 2 x 25 cm^3). The combined organic fractions were washed with a saturated sodium chloride solution (2 x 25 cm^3) and water (3 x 25 cm^3) and then

dried over magnesium sulfate. After filtration, the solvent was removed under reduced pressure, to give a brown oil. TLC (50% dichloromethane / 50% hexane) indicated that the oil was a mixture of the desired product, 4-iodophenol and an unidentified impurity which could easily be separated by column chromatography (silica gel). Hexane was used to make the silica gel slurry and the polarity of the eluent was gradually increased by adding 25 cm^3 fractions of 10%, 20%, 30%, 40% dichloromethane in hexane followed by a 50 cm^3 fraction of 50% dichloromethane in hexane. A clear oil of 4-heptyloxyiodobenzene (4. 045 g, 81% yield), an unidentified brown oil (10 mg) and white flakes of 4-iodophenol (112 mg, 0.509 mmol) were successively separated in this way. ^1H (400 MHz, $CDCl_3$), δ (ppm) 0.93 (t, $^3J_{HH}$ = 7.0 Hz, 3H, H_i), 1.34 (m, 6H, H_h), 1.47 (q, $^3J_{HH}$ = 7.6 Hz, 2H, H_g), 1.79 (q, $^3J_{HH}$ = 7.1 Hz, 2H, H_f), 3.94 (t, $^3J_{HH}$ = 6.4 Hz, 2H, H_e), 6.70 (AA'XX', J = 9.2 Hz, 2H, H_c) and 7.56 (AA'XX', J = 8.8 Hz, 2H, H_b). ^{13}C, δ 14.0 (C_i), 22.5, 25.9, 29.0 (C_h), 29.1 (C_g), 31.7 (C_f), 68.1 (C_e), 82.3 (C_a), 116.8 (C_c), 138.1 (C_b) and 159.0 (C_d).

Synthesis of 7-OST[12,13]

4-heptyloxyiodobenzene (4.045 g, 12.712 mmol), 4-vinylpyridine (1.8 cm^3, 16 mmol), triethylamine (2.1 cm^3, 15 mmol) and palladium acetate (14 mg, 0.062 mmol) were added dry acetonitrile (13 cm^3) to in a thick-walled pyrex tube with a teflon tap under N_2 and the mixture was refluxed with stirring for 72 hrs. The tube was covered with aluminium foil during the reaction to protect the palladium catalyst from light. On cooling, a green solid precipitated from the green solution. The solid was dissolved in neutralised dichloromethane (10 cm^3), which had been neutralised by stirring overnight with anhydrous potassium carbonate. The solution was washed with saturated sodium chloride solution (3 x 20 cm^3), and the aqueous fraction was then washed with neutralised dichloromethane (3 x 20 cm^3). The combined organic fractions were washed with water (3 x 50 cm^3), dried with magnesium sulfate, filtered, and the solvent was removed under reduced pressure, leaving behind a green/brown residue (2.685 g, 72% crude

yield). TLC (50% ethyl acetate / 50% hexane) indicated a mixture of the product and two unidentified side-products. The product was extracted from the residue using a Soxhlet apparatus with hot hexane. The hexane was removed under reduced pressure, leaving behind a white solid (1.721 g, 46% crude yield) which was still a mixture of the product and one of the side products. The pure product was recrystallised from cold acetone as white flakes (1.298 g, 35% purified yield). FT-IR, ^{1}H- and ^{13}C-NMR spectroscopic data compare well with literature[13,14] and are reported in Tables 2A.1, 2A.4 and 2A.6.

Synthesis of 4-octyloxybromobenzene[12,13]

4-Bromophenol (4.000g, 23.120 mmol), 1-bromooctane (4,0 cm^3, 23 mmol), anhydrous potassium carbonate (3.244 g, 23. 816 mmol) and 18-crown-6 (*ca* 2 mg) were placed in a dry Schlenk tube under a N_2 atmosphere. Dry acetone (25 cm^3) was added via a syringe and the reaction mixture was refluxed with stirring for 23 hrs. After cooling the same work-up procedure was followed as for 4-heptyloxyiodobenzene, resulting in a clear oil (5.503 g, 83% crude yield). The oil was passed through a silica gel column (eluent 50% dichloromethane / 50% hexane) in order to remove unreacted 4-bromophenol, resulting in a clear oil (4.737 g, 72% crude yield) which was confirmed by ^{1}H-NMR to be a mixture of 85% 4-octyloxybromobenzene and 15% 1-bromooctane. The oil was dissolved in the minimum volume of acetone and white crystals formed at -25 °C. 1-Bromooctane (m.p. -55 °C) was easily removed by washing the crystals at -25 °C, resulting in the pure product (3.023 g, 46% purified yield), which is a colourless oil at room temperature. ^{1}H (400 MHz, $CDCl_3$), δ (ppm) 0.89 (t, $^{3}J_{HH}$ = 7.0 Hz, 3H, H_i), 1.32 (m, 8H, H_h), 1.44 (q, $^{3}J_{HH}$ = 7.6 Hz, 2H, H_g), 1.77 (q, $^{3}J_{HH}$ = 7.0 Hz, 2H, H_f), 3.91 (t, $^{3}J_{HH}$ = 6.6 Hz, 2H, H_e), 6.77 (AA'XX', J = 9.2 Hz, 2H, H_c) and 7.35 (AA'XX', J = 8.8 Hz, 2H, H_b). ^{13}C, δ 14.0 (C_i), 22.6, 26.0, 29.1, 29.2 (C_h), 29.3 (C_g), 31.8 (C_f), 68.2 (C_e), 112.5 (C_a), 116.3 (C_c), 132.1 (C_b) and 158.2 (C_d).

Synthesis of 8-OST[12,13]

4-Octyloxybromobenzene (2.993 g, 10.493 mmol), 4-vinyl pyridine (1.4 cm^3, 12 mmol), triethylamine (1.8 cm^3, 12.914 mmol), palladium acetate (25 mg, 0.111 mmol) and triphenylphosphine (55 mg, 0.210 mmol) were added to dry acetonitrile (10 cm^3) in a thick-walled Pyrex tube with a teflon tap under N_2 and the mixture was refluxed with stirring for 77 hr 20 min. The tube was covered with aluminium foil during the reaction to protect the palladium catalyst. On cooling some long needles of the product crystallised from the green solution. Neutralised dichloromethane (10 cm^3) was added to the product mixture and the same work-up procedure as for 7-OST was followed, resulting in a green oil which was dried for 6 hrs on a high vacuum pump to give a green/brown residue (6.942 g). TLC (50% ethyl acetate / 50% hexane) indicated a mixture of the product and three unidentified side-products. The product was extracted from the residue using a Soxhlet apparatus with hot hexane. The hexane was removed under reduced pressure, leaving behind a cream solid (2.420 g, 75% crude yield) which still was a mixture of the product and two of the side products (TLC evidence). The pure product was precipitated from cold acetone/hexane at -40 °C (dry ice / ethanol) as a cream solid (517 mg, 16% purified yield). FT-IR, ^{1}H- and ^{13}C-NMR spectroscopic data compare well with literature[13,14] and are reported in Tables 2A.1, 2A.4 and 2A.6.

6.3 Synthesis of ClAu(n-OST) complexes 3-9

Synthesis of ClAu(4-OST) complexes 3 and 3a

Dry toluene (3 cm^3) was added via a syringe to a dry, empty Schlenk tube under a N_2 atmosphere and heated slightly to 69 °C. White ClAu(tht) (152 mg, 0.474 mmol) and yellow 4-OST (120 mg 0.474 mmol) were added and the mixture was stirred at that temperature for 2hr 17min, during which time a yellow precipitate was formed. The reaction was monitored by TLC

(100 % dichloromethane and 50 % ethyl acetate / 50 % hexane eluents). The crude product was collected on a Hirsch funnel (187 mg, 81 % crude yield), washed with hexane (3 x 5 cm^3) and dried under high vacuum for 1 hr. It was further purified using column chromatography techniques. Dichloromethane was used as the eluent and the silica gel was packed in a Pasteur pipette to a length of *ca* 4 cm^3. Although protected from sunlight by wrapping in aluminium foil, some decomposition still occurred while the product was passing through the microcolumn. The solvent was reduced *in vacuo* and hexane was added to the dichloromethane solution to precipitate the pure yellow powder (105 mg, 46 % purified yield), which was collected on a Hirsch funnel and dried under high vacuum for 4 hrs. The product, complex **3**, is stable in the solid phase at room temperature, even when unprotected from sunlight, but decomposes in solution, more rapidly when exposed to sunlight. A sample of complex **3** (purity confirmed with ^{1}H- and ^{13}C-NMR spectra) which was left protected from light at room temperature in an NMR tube for a few hours yielded 53 % of the cis isomer, complex **3a**. FAB-MS: m/z 254 (4-OST^+ + H), 198 (Au^+ + H). (Found: C, 41.9; H, 4.0; N, 3.0 %. $C_{17}H_{19}AuClNO$ requires C, 42.2; H, 4.0; N, 2.9 %) FT-IR, ^{1}H-and ^{13}C-NMR spectroscopic, conductivity and DSC data are presented in Tables 2A.2, 2A.5, 2A.7, 2.3 and 2.4 for complex **3** and ^{1}H-and ^{13}C-NMR spectroscopic data in Tables 2A.8-9 for complex **3** and **3a** mixtures.

Synthesis of ClAu(5-OST), complex 4

Dry toluene (5 cm^3) was added via a syringe to a dry, empty Schlenk tube under a N_2 atmosphere and heated slightly to 50 °C. White ClAu(tht) (201 mg, 0.627 mmol) and yellow 5-OST (167 mg 0.625 mmol) was added and the mixture was stirred at that temperature for 2hrs, during which time a yellow precipitate (275 mg, 88 % crude yield) was formed. Complex **4** was purified and dried in an analogous manner to complex **3** to yield a pure yellow powder (140 mg, 45 % purified yield). FAB-MS: m/z 501 (ClAu(5-$OST)^+$ + H), 268 (5-OST^+ + H), 198 (Au^+ +

H). (Found: C, 43.4; H, 4.2; N, 3.0 %. $C_{18}H_{21}AuClNO$ requires C, 43.3; H, 4.2; N, 2.8 %) FT-IR, ^{1}H-and ^{13}C-NMR spectroscopic, conductivity and DSC data are presented in Tables 2A.2, 2A.5, 2A.7, 2.3 and 2.4.

*Synthesis of ClAu(6-OST), complexes **5** and **5a***

Method 1

Dry toluene (4 cm^3) was added via a syringe to a dry, empty Schlenk tube under a N_2 atmosphere and warmed slightly to 56 °C. White ClAu(tht) (111 mg, 0.348 mmol) and yellow 6-OST (97 mg 0.345 mmol) were added and the mixture was stirred at that temperature for 2hr 13min, during which time a yellow precipitate (145 mg, 81 % crude yield) was formed. Complex **5** was purified and dried in an analogous manner to complex **3** to yield a pure yellow powder (92 mg, 51 % purified yield). A sample of complex **5** (purity confirmed with ^{1}H- and ^{13}C-NMR spectra) which was left protected from light at room temperature in an NMR tube for a few hours yielded 21 % of the cis isomer, complex **3a**.

Method 2

Dry toluene (10 cm^3) was added via a syringe to a dry, empty Schlenk tube under a N_2 atmosphere and warmed slightly to 56 °C. White ClAu(tht) (298 mg, 0.930 mmol) and yellow 6-OST (408 mg 1.430 mmol) were added and the mixture was stirred at that temperature for 4hr 40 min during which time a yellow precipitate was formed. The mixture was cooled *in vacuo* to 0 °C to promote precipitation of product. The yellow product (342 mg, 72 % crude yield) was collected on a Hirsch funnel, washed with cold toluene (2 cm^3) and pentane (3 x 5 cm^3) and dried for 5 hrs under high vacuum. Recrystallisation of the crude product from dichloromethane/hexane at -25 °C yielded 200 mg of a yellow product, with a further 77 mg recrystallised from the mother liquor. TLC of the recrystallised product indicated that a mixture

of two products was present and ^{1}H-NMR spectra confirm that 12 % of the first batch and 42 % of the second batch consisted of complex **5a** the balance being complex **5**. Only complex **5** was isolated from these mixtures, as complex **5a** decomposed during column chromatography separation procedures. FAB-MS: m/z 282 (6-OST^{+} + H), 198 (Au^{+} + H). (Found: C, 44.3; H, 4.5; N, 2.7 %. $C_{19}H_{23}AuClNO$ requires C, 44.4; H, 4.5; N, 2.7 %) FT-IR, ^{1}H-and ^{13}C-NMR spectroscopic, conductivity and DSC data are presented in Tables 2A.2, 2A.5, 2A.7-9, 2.3 and 2.4 for complex **5** and ^{1}H-and ^{13}C-NMR spectroscopic data in Tables 2A.8-9 for complex **5** and **5a** mixtures.

Synthesis of ClAu(7-OST), complex 6

Dry toluene (4 cm^{3}) was added via a syringe to a dry, empty Schlenk tube under a N_2 atmosphere and warmed slightly to 50 °C. White ClAu(tht) (360 mg, 1.123 mmol) and yellow 7-OST (371 mg 1.256 mmol) were added and the mixture was stirred at that temperature for 1hr during which time a yellow precipitate was formed. The mixture was placed in the freezer overnight (-25 °C) to promote precipitation of product. The yellow product (516 mg, 87 % crude yield) was collected on a Hirsch funnel, washed with cold toluene (2 cm^{3}) and pentane (3 x 5 cm^{3}) and dried for 5 hrs under high vacuum. Some of the product (345 mg, 0.654 mmol) was further purified by washing with a mixture of 50 % ethyl acetate in hexane and recrystallising from minimum dichloromethane at -25 °C to form yellow needles (153 mg, 44 % purified yield). FAB-MS: m/z 296 (7-OST^{+} + H), 198 (Au^{+} + H). (Found: C, 45.4; H, 4.9; N, 2.7 %. $C_{20}H_{25}AuClNO$ requires C, 45.5; H, 4.8; N, 2.6 %) FT-IR, ^{1}H-and ^{13}C-NMR spectroscopic, conductivity and DSC data are presented in Tables 2A.2, 2A.5, 2A.7, 2.3 and 2.4.

Synthesis of ClAu(8-OST), complex 7

Dry toluene (5 cm^{3}) was added via a syringe to a dry, empty Schlenk tube under a N_2

atmosphere and warmed slightly to 58 °C. White ClAu(tht) (150 mg, 0.468 mmol) and yellow 8-OST (145 mg 0.469 mmol) were added and the mixture was stirred at that temperature for 2hr 10min. The resulting clear solution was cooled to 0 °C (with addition of hexane) to form a green precipitate (175 mg, 69 % crude yield). Complex **7** was purified and dried in an analogous manner to complex **3** to yield a pure yellow powder (100 mg, 39 % purified yield). FAB-MS: m/z 310 (8-OST$^+$ + H), 198 (Au$^+$ + H). (Found: C, 46.2; H, 5.1; N, 2.8 %. $C_{21}H_{27}AuClNO$ requires C, 46.5; H, 5.0; N, 2.6 %) FT-IR, ^{1}H-and ^{13}C-NMR spectroscopic, conductivity and DSC data are presented in Tables 2A.2, 2A.5, 2A.7, 2.3 and 2.4.

Synthesis of ClAu(9-OST), complex 8

Dry toluene (3 cm^3) was added via a syringe to a dry, empty Schlenk tube under a N_2 atmosphere and heated to 80 °C. White ClAu(tht) (111 mg, 0.348 mmol) and yellow 9-OST (117 mg 0.362 mmol) were added and the mixture was stirred at that temperature for 2hrs, during which time a yellow precipitate was formed. The yellow precipitate (161 mg, 84 % crude yield) was collected on a Hirsch funnel and washed with pentane (3 x 5 cm^3). The complex was recrystallised from dichloromethane / pentane to form a fine yellow powder (91 mg, 50 % purified yield). FAB-MS: m/z 324 (9-OST$^+$ + H), 198 (Au$^+$ + H). (Found: C, 47.7; H, 5.3; N, 2.6 %. $C_{22}H_{29}AuClNO$ requires C, 47.5; H, 5.3; N, 2.5 %) FT-IR, ^{1}H-and ^{13}C-NMR spectroscopic, conductivity and DSC data are presented in Tables 2A.2, 2A.5, 2A.7, 2.3 and 2.4.

Synthesis of ClAu(10-OST), complex 9

Dry toluene (3 cm^3) was added via a syringe to a dry, empty Schlenk tube under a N_2 atmosphere and heated slightly to 62 °C. White ClAu(tht) (130 mg, 0.406 mmol) and yellow 10-OST (136 mg 0.403 mmol) was added and the mixture was stirred at that temperature for 2hr 14min during which time a yellow precipitate (210 mg, 91 % crude yield) was formed. Complex

9 was purified and dried in an analogous manner to complex **3** to yield a pure yellow powder (91 mg, 39 % purified yield). FAB-MS: m/z 338 (10-OST$^+$ + H), 198 (Au^+ + H). (Found: C, 48.2; H, 5.5; N, 2.7 %. $C_{23}H_{31}AuClNO$ requires C, 48.5; H, 5.5; N, 2.5 %) FT-IR, ^{1}H-and ^{13}C-NMR spectroscopic, conductivity and DSC data are presented in Tables 2A.2, 2A.5, 2A.7, 2.3 and 2.4.

6.4 Synthesis of RAu(tht) and RAu(n-OST) complexes 10-18

*Synthesis of pentafluorophenylgold(tht), complex **10***[15-19]

Bromopentafluorobenzene (0.10 cm^3, 0.80 mmol) was dissolved in dry diethyl ether (15 cm^3) in a 50 cm^3 dry, two-necked, round-bottomed flask, which was fitted with a rubber septum and connected to a nitrogen inlet. 1.6 M n-Butyllithium (0.50 cm^3, 0.80 mmol) was added dropwise via a syringe after cooling the solution to -72 °C (dry ice/ethanol slurry). The reaction was stirred for 1hr 40min at that temperature. The rubber septum was replaced with a dry dropping funnel and dry ClAu(tht) (180 mg, 0.562 mmol), suspended in diethyl ether (15 cm^3), was added via dropping funnel. The reaction was stirred for 2hr 20min at -72 °C, and then warmed up gradually to room temperature over 1 hr, with continued stirring. The reaction mixture was then stirred at room temperature for an additional 30 min before quenching the reaction with a few drops of water. Reaction progress was monitored via TLC with dichloromethane used as an eluent. Anhydrous magnesium sulfate was added and the solution was then filtered. The solvent was removed *in vacuo* at 0 °C, leaving behind the white product (249 mg, 98 % yield), which was dried under high vacuum for 4 hrs at 0 °C and used without further purification to make complex **11**. Found m.p. 105 °C (dec.). Literature m.p. 109 °C (dec.).[18] ^{1}H (400 MHz, $CDCl_3$), δ (ppm) 3.44 (s, H_a) and 2.22 (s, H_b). ^{13}C, δ 38.6 (C_a) and 30.7 (C_b). FT-IR and ^{19}F - NMR spectroscopic data are presented in Tables 3A.1 and 3A.5 and compare well with literature values.[18-20]

Synthesis of pentafluorophenylgold(7-OST), complex 11

Complex **10** (139 mg, 0.307 mmol) and yellow 7-OST (114 mg, 0.386 mmol) were added to a dry, empty Schlenk tube under a N_2 atmosphere. Dry toluene (3 cm^3) was added via a syringe. The mixture was warmed slightly to 60 °C and then stirred at that temperature for 3hr 30min, during which time the solution remained yellow and clear. Reaction progress was monitored via TLC, using 50 % ethyl acetate / 50 % hexane as the eluent. On cooling the solution to 0 °C, clear crystals with a slight green tinge, (86 mg), formed from the solution. With the addition of pentane another 68 mg crystallised from the mother liquor. Cumulative yield (154 mg, 76%). The crystals were collected on a Hirsch funnel and washed with cold toluene (2 cm^3) and pentane (3 x 5 cm^3) and dried under high vacuum with slight heating. The product was recrystallised from toluene / pentane and some clear rod-shaped single crystals were grown at room temperature via vapour diffusion of pentane into a saturated toluene solution. FAB-MS: m/z 660 $[C_6F_5Au(7\text{-OST}) + H]^+$, 493 $[Au(7\text{-OST}) + H]^+$, 365 $[C_6F_5Au + H]^+$, 297 $[7\text{-OST} + 2H]^+$, 198 $[Au + H]^+$. (Found: C, 47.3; H, 3.6; N, 2.3 %. $C_{26}H_{25}Au\ F_5NO$ requires C, 47.4; H, 3.8; N, 2.1 %). FT-IR, ^1H-, ^{13}C- and ^{19}F-NMR spectroscopic, conductivity and DSC data are presented in Tables 3A.1-4, 3A.6, 3.7 and 3.8.

Synthesis of 2-Bromotetrafluorophenylgold(tht), complex 12[15-19]

1,2-Dibromotetrafluorobenzene (0.09 cm^3, 0.65 mmol) was dissolved in dry diethyl ether (15 cm^3) in a 50 cm^3 dry, two-necked, round-bottomed flask, which was fitted with a rubber septum and connected to a nitrogen inlet. 1.6 M n-Butyllithium (0.40 cm^3, 0.64 mmol) was added dropwise via a syringe after cooling the solution to -83.6 °C (ethyl acetate/N_2 cryostat). The reaction was stirred for 1hr 05min at that temperature. The rubber septum was replaced with a dry dropping funnel and dry ClAu(tht) (190 mg, 0.593 mmol), suspended in diethyl ether (15 cm^3), was added via dropping funnel. The reaction was stirred for 45 min at -72 °C,

and then warmed up gradually to -30 °C over 45 min, with continued stirring at that temperature for 15 min. The reaction mixture was then warmed up to 0 °C over 10 min and stirred at that temperature for an additional 35 min before quenching the reaction with a few drops of water. Reaction progress was monitored via TLC, using dichloromethane as the eluent. Anhydrous magnesium sulfate was added and the solution was then filtered. The solvent was removed *in vacuo* at 0 °C, leaving behind the white product (262 mg, 86 % yield), which was dried under high vacuum for 2 hrs at 0 °C and used without further purification to make complex **13**. FT-IR spectroscopic data is presented in Table 3A.1 and compares well with literature values.[18,20]

Synthesis of 2-Bromotetrafluorophenylgold(7-OST), complex 13

Complex **12** (190 mg, 0.370 mmol) and yellow 7-OST (110 mg, 0.372 mmol) were added to a dry, empty Schlenk tube under a N_2 atmosphere. Dry toluene (5 cm^3) was added via a syringe at 0 °C. The mixture was warmed slightly to 54 °C and then stirred at that temperature for 30 min. Reaction progress was monitored via TLC, using 50 % ethyl acetate / 50 % hexane as the eluent. On cooling the solution to 0 °C, a light yellow solid crystallised from the solution. The mixture was further cooled in the freezer to -25 °C, with the addition of hexane to promote further crystallisation. The light yellow solid (157 mg, 59 % yield) was collected on a Hirsch funnel and washed with cold toluene (2 cm^3) and pentane (3 x 5 cm^3). The product was further purified by column chromatography analogous to complex **3**. Some decomposition still occurred while passing product through the column. The solvent was reduced in vacuo and cooled to 0 °C with addition of hexane to form white crystals (104 mg, 39 % purified yield), which was collected on a Hirsch funnel, washed with pentane (3 x 5 cm °C) and dried for 4 hrs under high vacuum. FAB-MS: m/z 296 $[7\text{-OST} + H]^+$, 197 $[Au]^+$. (Found: C, 43.5; H, 3.4; N, 2.0 %. $C_{26}H_{25}AuBrF_4NO$ requires C, 43.4; H, 3.5; N, 1.9 %). FT-

IR, ^{1}H-, ^{13}C- and ^{19}F-NMR spectroscopic, conductivity and DSC data are presented in Tables 3A.1-4, 3A.6, 3.7 and 3.8.

*Synthesis of 4-Bromotetrafluorophenylgold(tht), complex **14***

1,4-Dibromotetrafluorobenzene (248 mg, 0.806 mmol) was dissolved in dry diethyl ether (15 cm^3) in a 50 cm^3 dry, two-necked, round-bottomed flask, which was fitted with a rubber septum and connected to a nitrogen inlet. 1.6 M n-Butyllithium (0.50 cm^3, 0.80 mmol) was added dropwise via a syringe after cooling the solution to -72 °C (ethanol / dry ice slurry). The reaction was stirred for 1hr 40min at that temperature. The rubber septum was replaced with a dry dropping funnel and dry ClAu(tht) (180 mg, 0.562 mmol), suspended in diethyl ether (15 cm^3), was added via dropping funnel. The reaction was stirred for 2 hrs at -72 °C, and then warmed up gradually to room temperature over 1 hr, with continued stirring. The reaction mixture was then stirred at room temperature for an additional 10 min before quenching the reaction with a few drops of water. Reaction progress was monitored via TLC, using dichloromethane as the eluent. Anhydrous magnesium sulfate was added and the solution was then filtered. The solvent was removed *in vacuo* at 0 °C, leaving behind the white product (268 mg, 93 % yield), which was dried under high vacuum for 3 hrs at 0 °C and used without further purification to make complex **15**. Found m.p. 103 °C (dec.). FT-IR spectroscopic data is presented in Table 3A.1 and compares well with literature values.[18,20]

*Synthesis of 4-Bromotetrafluorophenylgold(7-OST), complex **15***

Complex **14** (119 mg, 0.232 mmol) and yellow 7-OST (69 mg, 0.234 mmol) were added to a dry, empty Schlenk tube under a N_2 atmosphere. Dry toluene (3 cm^3) was added via a syringe at 0 °C. The mixture was warmed slightly to 56 °C and then stirred at that temperature for 1 hr. Reaction progress was monitored via TLC, using 50 % ethyl acetate / 50 % hexane as the

eluent. On cooling the clear solution to 0 °C, white crystals formed from the solution. The mixture was further cooled in the freezer to -25 °C to promote further crystallisation. The white crystals (120 mg, 72 % yield) was collected on a Hirsch funnel and washed with cold toluene (2 cm^3) and pentane (3 x 5 cm^3). Complex **15** was purified and dried in an analogous manner to complex **13**, yielding yellow crystals (76 mg, 45 % purified yield). FAB-MS: m/z 296 [7-OST + H]$^+$, 197 [Au]$^+$. (Found: C, 43.3; H, 3.5; N, 2.2 %. $C_{26}H_{25}AuBr\ F_4NO$ requires C, 43.4; H, 3.5; N, 1.9 %). FT-IR, ^{1}H-, ^{13}C- and ^{19}F-NMR spectroscopic, conductivity and DSC data are presented in Tables 3A.1-4, 3A.6, 3.7 and 3.8.

*Synthesis of μ-4,4'-octafluorobiphenylgold(tht), complexes **16** and **17***

4,4'-Dibromooctafluorobiphenyl (208mg, 0.456 mmol) was dissolved in dry diethyl ether (30 cm^3) in a 50 cm^3 dry, two-necked, round-bottomed flask, which was fitted with a rubber septum and connected to a nitrogen inlet. 1.6 M n-Butyllithium (0.60 cm^3, 0.96 mmol) was added dropwise via a syringe after cooling the solution to -72 °C (dry ice/ethanol slurry). The reaction was stirred for 1hr 05min at that temperature. The rubber septum was replaced with a dry dropping funnel and dry ClAu(tht) (300 mg, 0.936 mmol), suspended in diethyl ether (15 cm^3), was added via dropping funnel. The reaction was stirred for 30 min at -72 °C, and then warmed up gradually to 0 °C over 1hr 10min, with continued stirring. The reaction was quenched with a few drops of water. Reaction progress was monitored via TLC with 50 % ethyl acetate / 50 % hexane used as an eluent. Anhydrous magnesium sulfate was added and the diethyl ether solution was then filtered into a Schlenk tube. The solvent was reduced *in vacuo* at 0 °C to 1.5 cm^3, 7.5 cm^3 hexane was added and the mixture was cooled to -25 °C overnight, resulting in the crystallisation of a white product (46 mg), complex **16**. The mother liquor was removed via a syringe and placed in another Schlenk tube. The solvent was again reduced *in vacuo* at 0 °C to 1.5 cm^3, 7.5 cm^3 hexane was added and the mixture was cooled to

-25 °C overnight, resulting in the crystallisation of a yellow product (12 mg), complex **17**. The reaction residue was suspended in dichloromethane and filtered. The solvent volume was reduced and on addition of hexane, a light yellow solid (88 mg) crystallised, complex **16**. Complex **16** was dried under high vacuum for 4 hrs at 0 °C (134 mg, 34 % cumulative yield) and used without further purification to make complex **18**. Complex **17** (12 mg, 5 % yield) was formed due to the introduction of some water during addition of ClAu(tht). Found m.p. 128 °C (dec.) for complex **16**. Literature m.p. 135 °C (dec.).[17] FT-IR and ^{19}F-NMR spectroscopic data for complex **16** are presented in Tables 3A.1 and 3A.5 and compare well with literature values.[18-20] FT-IR spectroscopic data for complex **17** is presented in Table 3A.1.

*Synthesis of μ-4,4'-octafluorobiphenylgold(7-OST), complex **18***

Complex **16** (88 mg, 0.102 mmol) and yellow 7-OST (66 mg, 0.223 mmol) were added to a dry, empty Schlenk tube under a N_2 atmosphere. Dry toluene (5 cm^3) was added via a syringe at 0 °C. The mixture was warmed slightly to 40 °C and then stirred at that temperature for 1 hr. 7 cm^3 Dry toluene was then added via a syringe at that temperature. The mixture was further heated to 75 °C and then stirred at that temperature for 30 min. Reaction progress was monitored via TLC, using 50 % ethyl acetate / 50 % hexane as the eluent. A yellow precipitate was formed and the reaction mixture was cooled to –25 °C overnight to complete precipitation. The toluene solution was removed via a syringe and the yellow solid (69 mg, 53 % yield) was dissolved, with slight heating, in dichloromethane, filtered, and cooled to –25 °C with the addition of hexane. A yellow solid (53 mg, 40 % yield) was crystallised, collected on a Hirsch funnel, washed with hexane (3 x 5 cm °C) and dried for 4 hrs under high vacuum. EI-MS: m/z 296 $[7\text{-OST} + H]^+$, 198 $[Au + H]^+$. (Found: C, 48.9; H, 3.9; N, 2.4 %. $C_{26}H_{25}AuBr\ F_4NO$ requires C, 48.8; H, 3.9; N, 2.2 %). FT-IR, ^{1}H-, ^{13}C- and ^{19}F-NMR

spectroscopic and DSC data are presented in Tables 3A.1-4, 3A.6 and 3.8.

6.5 Synthesis of $RAuPPh_3$ complexes 19-24

Synthesis of methylgold(PPh_3), complex ***19***[21-27]

White $ClAu(PPh_3)$ (0.200 g, 0.400 mmol) was suspended in dry diethyl ether (3 cm^3) in a Schlenk tube wrapped in aluminium foil under N_2 and cooled to -10 °C (ice / methanol slurry). 1.0M Methyllithium in diethyl ether (0.60 cm^3, 0.60 mmol) was added via a syringe. The reaction mixture was stirred for 35 min at that temperature, with reaction progress being monitored via TLC (30% ethyl acetate/70% hexane). The excess methyllithium was hydrolysed by addition of water (3 cm^3). The diethyl ether and water layers were separated and the water layer was washed with diethyl ether (3 x 3cm^3). The combined organic fractions were dried over anhydrous magnesium sulfate. The solution was filtered through celite and the solvent was evaporated *in vacuo* to give a white solid (0.109 g, 58 % yield). The product was recrystallised from diethyl ether/hexane at -20 °C as colourless cubic crystals and from toluene via slow evaporation at room temperature as colourless rectangular plates. Found m.p. 176 °C (dec.) with an exothermic peak of -32.7 $kJ.mol^{-1}$ reflected in a DSC thermogram. Literature m.p. 175 °C (dec.) from acetone or xylene,[21-23] 173-175 °C (dec.) from benzene/pentane,[24] 172-174 °C (dec.) from benzene/petroleum ether[25] and 167-168 °C (dec.) from diethyl ether/pentane.[26,27] (Found: C, 48.2; H, 3.7 %. $C_{19}H_{18}AuP$ requires C, 48.1; H, 3.8 %). FT-IR, ^1H- and ^{13}C-NMR spectroscopic data are presented in Tables 4.1 and 4A.1-2.

Synthesis of ethylgold(PPh_3), complex ***20***[21,26,28]

White $ClAu(PPh_3)$ (0.199 g, 0.401 mmol) was suspended in dry diethyl ether (3 cm^3) in a Schlenk tube wrapped in aluminium foil under N_2 and cooled to -10 °C (ice / methanol

slurry). 0.15M Ethyllithium in hexane (4.00 cm^3, 0.60 mmol) was added via a syringe. The reaction mixture was stirred for 30 min at that temperature. A cream solid (0.209 g) which contained some impurities was obtained following a similar work-up procedure as used for complex **19**. The product was crystallised from diethyl ether/hexane at -20 °C, forming colourless crystals (0.082 g, 42% yield). Found m.p. 148 °C (dec.). Literature m.p. 150-152 °C (dec.) from diethyl ether/hexane,[28] 134.5-135.5 °C (dec.) from diethyl ether/pentane[26] to 130 °C (dec.) from diethyl ether.[21] (Found: C, 49.0; H, 4.1 %. $C_{20}H_{20}AuP$ requires C, 49.2; H, 4.1 %). IR, ^1H- and ^{13}C-NMR spectroscopic data are presented in Tables 4.1 and 4A.1-2.

Synthesis of n-propylgold(PPh_3), complex 21[26,27]

White $ClAu(PPh_3)$ (0.233 g, 0.471 mmol) was suspended in dry diethyl ether (3 cm^3) in a Schlenk tube wrapped in aluminium foil under N_2 and cooled to -6 °C (ice / ethanol slurry). 0.45M *n*-Propyllithium in diethyl ether (1.6 cm^3, 0.72 mmol) was added via a syringe. The reaction mixture was stirred for 1hr 35min at that temperature. A white solid (0.094 g, 40 % yield) which was analytically pure without further recrystallisation was obtained following a similar work-up procedure as used for complex **19**. Found m.p. 77-78 °C (dec.). Literature m.p. 77.5-79 °C (dec.) from diethyl ether/pentane.[26,27] (Found: C, 50.5; H, 4.5 %. $C_{19}H_{18}AuP$ requires C, 50.2; H, 4.4 %). IR, ^1H- and ^{13}C-NMR spectroscopic data are presented in Tables 4.1 and 4A.1-2.

Synthesis of n-butylgold(PPh_3), complex 22[28]

White $ClAu(PPh_3)$ (0.202 g, 0.407 mmol) was suspended in dry diethyl ether (3 cm^3) in a Schlenk tube wrapped in aluminium foil under N_2 and cooled to -12 °C (ice / ethanol slurry). 2.5M *n*-Butyllithium in hexane (0.24 cm^3, 0.60 mmol) was added via a syringe. The reaction mixture was stirred for 30 min at that temperature. A clear oil (0.173 g, 88 % yield) which

was dried at 0 °C was obtained following a similar work-up procedure as used for complex **19**. Reported as an oil in literature.[28] (Found: C, 50.8; H, 5.0 %. $C_{19}H_{18}AuP$ requires C, 51.2; H, 4.7 %). IR, ^{1}H- and ^{13}C-NMR spectroscopic data are presented in Tables 4.1 and 4A.1-2.

Synthesis of n-pentylgold(PPh_3), complex 23

Method 1

White $ClAu(PPh_3)$ (0.168 g, 0.362 mmol) was suspended in dry diethyl ether (3 cm^3) in a Schlenk tube wrapped in aluminium foil under N_2 and cooled to -4 °C (ice / ethanol slurry). 2.5M *n*-Pentyllithium in diethyl ether (1.00 cm^3, 0.510 mmol) was added via a syringe. The reaction mixture was stirred for 1hr 25min at that temperature. A clear oil (0.163 g, 85 % yield) which became light brown while being dried at 0 °C was obtained following a similar work-up procedure as used for complex **19**. Elemental analysis was recalculated on the basis of *n*-decane being present in a proportion of 10% for the sample (section 4.3). (Found: C, 52.9; H, 5.5 %. $0.9C_{19}H_{18}AuP{\cdot}0.1C_{10}H_{22}$ requires C, 52.9; H, 5.2 %). IR, ^{1}H- and ^{13}C-NMR spectroscopic data are presented in Tables 4.1 and 4A.1-2.

Method 2

White $ClAu(PPh_3)$ (0.039 mg, 0.074 mmol) was suspended in diethyl ether (0.7 cm^3) in an NMR tube wrapped in aluminium foil under N_2. 0.88M *n*-Pentyllithium in diethyl ether (80 μdm^3 , 0.070 mmol) was added by syringe. The NMR tube was shaken occasionally over a period of 2hr 30min. The diethyl ether was removed *in vacuo* to give a white solid and C_6D_6 (0.5 cm^3) was added via a syringe. The NMR tube was sealed under vacuum. The solution was then submitted for ^{1}H-NMR and ^{13}C-NMR spectroscopic analysis (qualitative yield based on ^{1}H-NMR spectrum). The solution was subsequently kept at room temperature for 24 hrs and then heated at 50 °C for 24 hrs, with ^{1}H-NMR and ^{13}C-NMR spectra being obtained

after each interval (section 4.3.3).

Synthesis of n-heptlygold(PPh_3), complex 24

White $ClAu(PPh_3)$ (0.208 g, 0.420 mmol) was suspended in dry diethyl ether (3 cm^3) in a Schlenk tube wrapped in aluminium foil under N_2 and cooled to -7 °C (ice / ethanol slurry). 0.29 M *n*-Heptyllithium in diethyl ether (2.00 cm^3, 0.58 mmol) was added via a syringe. The reaction mixture was stirred for 1hr 05min at that temperature. A cream solid (0.184 g, 83 % yield) which was washed with pentane (3 x 5 cm^3) was obtained following a similar work-up procedure as used for complex **19**. Complex **24** was recrystallised from diethyl ether/hexane as colourless crystals, but decomposed to a viscous brown oil while being dried on high vacuum for 2 hrs. Found m.p. 64 °C. IR, ^1H- and ^{13}C-NMR spectroscopic data are presented in Tables 4.1 and 4A.1-2.

6.6 Unsuccessful syntheses

Attempted synthesis of IAu(vnlpy)

Dry acetone (5 cm^3) was cooled to -40 °C (ethanol / dry ice bath) in a Schlenk tube under a N_2 atmosphere. Complex **2** (37 mg, 0.110 mmol) and white KI (99 mg, 0.498 mmol) were added and the reaction mixture was stirred for 1hr 30min at that temperature. The acetone was removed *in vacuo* (ensuring that the temperature did not go above -10 °C) leaving behind a white residue. When dichloromethane (5 cm^3), cooled to -14 °C, was added in order to extract the product, the solution immediately discoloured to a deep purple. After filtration, the solution was yellow in colour. The dichloromethane was removed *in vacuo*, leaving behind trace amounts (*ca* 2-3 mg) of a white solid, which immediately became brown on removal from the cooling bath in order to run a FT-IR spectrum.

Attempted synthesis of IAu(7-OST)

Complex **6** (50 mg 0.095 mmol) and white KI (80 mg, 0.482 mmol) were placed in a dry Schlenk tube under a N_2 atmosphere. Dry acetone (10 cm^3) was added via a syringe and the reaction was stirred at room temperature for 40 min. The acetone was removed *in vacuo* leaving behind a yellow residue. When dichloromethane (10 cm^3) was added some dissolution of the residue resulted in a brown solution with a grey suspension, which was removed via filtration. After filtration, the solvent was orange in colour and was removed *in vacuo*, resulting in a yellow solid (18 mg), which was dried under high vacuum. ^{1}H-NMR confirmed that the yellow solid was 7-OST.

Attempted synthesis of phenylgold(tht)

Dry diethyl ether (15 cm^3) was added via a syringe to a three-necked round-bottomed flask fitted with a dropping funnel and condenser under a N_2 atmosphere. Lithium metal (413 mg, 0.059 mol) was added as thin plates with shiny surfaces to the diethyl ether. Bromobenzene (3.4 cm^3, 0.027 mol) was dissolved in diethyl ether (10 cm^3) in the dropping funnel and the solution was added dropwise at room temperature to the lithium mixture over a 30 min period. The reaction was cooled to 0 °C and stirred at the temperature for 15 min. The mixture was warmed up to room temperature and filtered under a N_2 atmosphere. The molarity of the phenyllithium solution was determined to be 0.85 M.[1-3] White ClAu(tht) (146 mg, 0,456 mmol) was suspended in dry diethyl (3 cm^3) diethyl ether in a Schlenk tube under a N_2 atmosphere. The mixture was cooled to 0 °C and 0.85M phenyllithium (0,60 cm^3, 0.51 mmol) was added. The solution immediately turned deep purple and metallic gold was deposited on the sides of the Schlenk tube.

Attempted synthesis of phenylgold(7-OST)

Complex **6** (98 mg, 0.186 mmol) was dissolved in dry tetrahydrofuran (4 cm^3) in a Schlenk tube under a N_2 atmosphere and cooled to –72 °C (dry ice / ethanol slurry). 1.8 M Phenyllithium in cyclohexane / diethyl ether (0,15 cm^3, 0.27 mmol) was added to the solution via a syringe and the reaction was stirred at that temperature for 1 hr. While warming the mixture up to room temperature, the solution became purple and metallic gold was deposited on the walls of the Schlenk tube.

Attempted synthesis of methylgold(tht)

White ClAu(tht) (0.214g, 0.668 mmol) was suspended in dry diethyl ether (4 cm^3) in a Schlenk tube wrapped in aluminium foil under N_2 and cooled to -72 °C (dry ice / ethanol slurry). 1.3M Metyllithium in diethyl ether (1.00 cm^3, 1.30 mmol) was added via a syringe and the reaction mixture was stirred for 30 min, resulting in the formation of a black precipitate and metallic gold.

Attempted synthesis of methylgold(n-OST)

White ClAu(tht) (0.103 g, 0.321 mmol) was suspended in dry diethyl ether (10 cm^3) in a Schlenk tube wrapped in aluminium foil under N_2 and cooled to -72 °C (dry ice / ethanol slurry). 1.6M Metyllithium in diethyl ether (0.60 cm^3, 0.96 mmol) was added via a syringe, followed immediately by yellow 7-OST (0.164 g, 0.555 mmol). The reaction mixture was allowed to gradually warm up to room temperature over a period of 1 hr. During the course of the reaction, a black precipitate was observed and metallic gold was deposited on the sides of the Schlenk tube. The excess metyllithium was hydrolysed by addition of saturated ammonium chloride solution (3 cm^3). A yellow solid (0.080 g) was obtained following a similar work-up procedure as used for complex **19** The m.p. and FT-IR, ^1H- and ^{13}C-NMR

spectra confirmed that the yellow solid was unreacted 7-OST.

Attempted synthesis of perfluorododecylgold(tht)

White perfluorododecyl iodide (0.401 g, 0.538 mmol) was dissolved in 15 cm^3 dry diethyl ether in a 50 cm^3 dry, two-necked, round-bottomed flask, which was fitted with a rubber septum and connected to a nitrogen inlet. 1.6M *t*-Butyllithium in hexane (1.80 cm^3, 1.12 mmol) was added dropwise via a syringe after cooling the solution to -72 °C (dry ice/ethanol slurry). The reaction was stirred for 1hr at that temperature. On addition of *t*-butyllithium, the clear solution become brown in colour. The rubber septum was replaced with a dry dropping funnel and dry ClAu(tht) (180 mg, 0.474 mmol), suspended in diethyl ether (15 cm^3), was added via dropping funnel. The reaction was stirred for 15 min at -72 °C, and then warmed up gradually to -30 °C over 1hr 05min, with continued stirring. The reaction mixture was then stirred at that temperature for an additional 15 min. The cooling system was then replaced with ice and the reaction mixture was stirred at 0 °C over a period of 30 min before quenching the reaction with a few drops of water. The brown solution became progressively black and purple in colour while stirring at 0 °C, with some metallic gold being deposited on the sides of the reaction vessel. Anhydrous magnesium sulfate was added and the solution was then filtered, resulting in a clear yellow solution. The solvent was removed *in vacuo* at 0 °C, leaving behind a brown solid (338 mg) which was dried under high vacuum for 2 hrs at 0 °C. Reaction progress was monitored via TLC with dichloromethane used as an eluent and indicates that the brown solid consists of the desired product (similar R_f value to the perfluorophenylgold(tht) complexes **10, 12** and **14**) as well as two other decomposition products. Unfortunately the brown solid decomposed spontaneously on being removed from 0 °C, making purification and further analysis difficult.

6.7 References

1. H. Gilman and F. K. Cartledge, *J Organomet. Chem.*, 1964, **2**, 447.
2. S. C. Watson and J. F. Eastham, *J Organomet. Chem.*, 1967, **9**, 165.
3. B.S. Furniss, A.J. Hannaford, P.W.G. Smith, A.R. Tatchell, *Vogel's Textbook of Practical Organic Chemistry*, Longman Scientific & Technical, England, 5th edn., 1989, ch. 4, pp.442-445.
4. C. A. McAuliffe, R. V. Parish and P. D. Randall, *J. Chem. Soc., Dalton Trans.*, 1979, 1730.
5. M.I. Bruce, B.K. Nicholson, O.B. Shawkataly, J.R. Sharply and T. Henly, *Inorg. Synth.*, 1989, **26**, 324.
6. P. Braunstein, H. Lehner, D. Matt, K. Burgess and M.J. Ohlmeyer, *Inorg. Synth.*, 1990, **27**, 218.
7. R. Uson, A. Laguna, M. Laguna, D.A. Briggs, H.M. Murray and J.P. Fackler, *Inorg. Synth.*, 1989, **26**, 85.
8. D.D. Perrin and W.L.F. Armarego, *Purification of laboratory chemicals*, Pergamon Press, New York, 3rd edn.,1988, p. 391.
9. M. S. Kharasch and H. S. Isbell, *J. Am. Chem. Soc.*, 1930, **52**, 2919.
10. P. C. Ráy and D. C. Sen, *J. Indian Chem. Soc.*, 1930, **7**, 67.
11. Von H.-N. Adams, W. Hiller and J. Strähle, *Z. anorg. allg. Chem.*, 1982, **485**, 81.
12. D. W. Bruce, D. A. Dunmur, E. Lalinde, P. M. Maitlis and P. Styring, *Liquid Crystals*, 1988, **3**, 385.
13. E. J. Starr, Ph.D. Thesis, University of Cape Town, 1997.
14. D. J. Price, K. Willis, T. Richardson, G. Ungar and D. W. Bruce, *J. Mater. Chem.*, 1997, **7**, 883.
15. R. Usón and A. Laguna, *Inorg. Synth.*, 1982, **21**, 71.

16. A. C. Albéniz, A. L. Casado and P. Espinet, *Organometallics*, 1997, **16**, 5416.

17. R. Usón, A. Laguna, M. Laguna, I. Colera and E. de Jesús, *J. Organomet. Chem.*, 1984, **263**, 121.

18. R. Usón, A. Laguna and M. Laguna, *Inorg. Synth.*, 1989, **26**, 85.

19. R. Bayón, S. Coco, P. Espinet, C. Fernández-Mayordomo and J. M. Martín-Alvarez, *Inorg. Chem.*, 1997, **36**, 2329.

20. R. Usón and A. Laguna, *Coord. Chem. Rev.*, 1986, **70**, 1.

21. G. E. Coates and C. Parkin, *J. Chem. Soc.*, 1962, 3220.

22. G. E. Coates and C. Parkin, *J. Chem. Soc.*, 1963, 421.

23. G. Calvin, G. E. Coates and P. S. Dixon, *Chemistry and Industry*, 1959, 1628.

24. B. J. Gregory and C. K. Ingold, *J. Chem. Soc. (B)*, 1969, 276.

25. H. Schmidbaur and A. Shiotani, *Chem. Ber.*, 1971, **104**, 2821.

26. A. Tamaki and J. K. Kochi, *J Organomet. Chem.*, 1973, **61**, 441.

27. A. Tamaki, S. A. Magennis and J. K. Kochi, *J. Am. Chem. Soc.*, 1974, 6140.

28. A. Tamaki and J. K. Kochi, *J Organomet. Chem.*, 1974, **64,** 411.

29. A. N. Nesmeyanov, E. G. Perevalova, K. I. Grandberg and D. A. Lemenovskii, *Izv. Akad. Nauk SSSR, Ser. Khim.*, 1974, 1068.